PERFORMANCE COMPARISONS BETWEEN GROOVED

AND UNGROOVED SQUEEZE-FILM GAS BEARINGS

by

David D. Cooke

Being a thesis submitted for the

Degree of

Master of Philosophy

April 1974

Department of Mechanical Engineering

University of Southampton

CONTENTS

ABSTRACT·

FACULTY OF ENGINEERING AND APPLIED SCIENCE

MECHANICAL ENGINEERING

Master of Philosophy

PERFORMANCE COMPARISONS BETWEEN GROOVED AND

UNGROOVED SQUEEZE-FILM GAS BEARINGS

David Desmond Cooke.

Squeeze-film gas bearings are investigated from the point
of view of determining the effect of extra ambient pressure
boundaries taking the form of deep, narrow grooves and, in
order to accommodate all the bearing geometries normally
encountered, the governing equations are set up in terms of
generalised curvilinear co-ordinates. The possibility of
slip-flow conditions is allowed for, as is vibratory
excitation at a frequency small compared with that assocc-
iated with the squeeze motion.

If conditions are such that slip-flow occurs, it is shown
that the load capacity suffers typically to the extent of
about 5% in thrust bearings and about 10% in journal
bearings.

It is found that the steady state static bearing force in
journal bearings can be considerably improved by the presence
of ambient boundaries, because circumferential leakage flow
is reduced. The steady state dynamic response to forced
vibration in both thrust and journal bearings is strongly
dependent on the number of grooves, which can be used to
advantage in suppressing otherwise large dynamic compliance
resonance peaks which might occur.

Experimental work is suggested for testing the validity
of the theoretical results, and for exploring the effect on
bearing performance of the groove cross-sectional geometry.

ACKNOWLEDGEMENTS

1. INTRODUCTION

Unlike the better known classes of gas bearings, externally-pressurised and self-acting, the squeeze-film gas bearing relies for its load carrying capacity on the vibratory squeezing action of one surface relative to another. The compressibility of the gas film is essential as it is responsible for the non-linearity in the pressure-volume relationship which leads to a net film pressure being developed in excess of the ambient which can then be used to support a load.

This class of gas bearing has not received much attention commercially, possibly because of the low load carrying capacity and the small number of applications where the same job cannot be adequately performed by a suitably designed externally-pressurised bearing with its reduced number of manufacturing tolerance problems. The squeeze-film bearing really comes into its own when there is insufficient room to accommodate the ancillary equipment required by the externally-pressurised bearing, or where turbine torques are prohibited, such as in inertial navigation instruments. Because the load carrying capacity is low, comparatively large projected areas of bearing surface are required to support a given load, leading in turn to relatively large transducer systems to provide the necessary vibratory motion. In aircraft instrument applications especially it is of the utmost importance to keep the instrument bulk to a minimum, so it is highly desirable to improve the load carrying capacity as much as possible to reduce both bearing and transducer size, and in

turn to reduce the power requirement.

This study was stimulated by Beck and Strodtman's[26] conclusion that the very short squeeze-film journal bearing has a much greater load carrying capacity per unit length than the very long journal. This immediately suggested a way of improving the load capacity of cylindrical bearings by segmenting them by means of narrow, deep circumferential grooves held at ambient pressure, and as grooves running axially from end to end of the bearing appeared easier to manufacture in certain instances it was wondered whether the same sort of effect on load capacity would also be achieved in this case.

A further possible advantage of grooving is that it should improve the performance of bearings where the squeeze vibration amplitude is non-uniform. This especially covers all of the present cylindrical transducer designs, and is an area in which the practical benefits are likely to be felt most.

The object of this study is to investigate thoroughly the effect of introducing grooves into bearings of the various geometries commonly encountered, taking into account both static and dynamic behaviour. Because of the writer's interest in small bearings aimed at inertial navigation instruments where the film-thicknesses tend to be reduced as the design work develops, it is felt that slip flow effects might become appreciable some day, so this has been built into the governing equations so that it can be included if required in future work, and estimates have been made for the magnitude of the loss in load capacity

to be expected in two typical cases where analytic solutions can be obtained.

The layout of the thesis is quite straightforward, starting with a survey of the literature in approximately chronological order to give some feel for the way the field has developed and to provide a background for the subsequent sections. Then comes an extended discussion on squeeze-film bearings in general in which the concept of 'local flat thrust plate' behaviour is developed and used repeatedly to obtain simple analytic solutions for various bearing configurations, leading up to the idea of placing grooves in one of the bearing surfaces. Once the concept of grooving has been justified by simple analyses, the dynamic behaviour is discussed, and local squeeze effects in the grooves and bearing segments investigated. In order to perform more rigorous analyses the governing equations are then set up in terms of generalised curvi-linear co-ordinates so that smooth and grooved bearings can be compared, taking into account slip flow and dynamic behaviour, and discussing assumptions made and methods of solution. Slip-flow is briefly considered in terms of simple thrust and journal bearings where analytic solutions are possible, providing estimates of how important the effect is likely to be in reducing load capacity. This is followed by a long section in which the main bearing geometries, grooved and ungrooved, are analysed and typical performance curves presented for their static and forced dynamic behaviour, and we end with some suggestions for experimental work followed by a discussion of the main conclusions to arise out of the theoretical treatment.

To avoid confusion it may perhaps be advisable to point out that in this thesis the term 'damping' is used in a rather unorthodox manner. One normally thinks of damping as referring to a 'force per unit velocity'; in other words, as being the coefficient of the velocity term appearing in the equation of motion. In this report, for brevity, 'damping' will often refer to the quadrature component of the dynamic stiffness, and so will be taken to mean the 'dynamic resistive force per unit deflection' of the system.

It may also avoid confusion if the expressions 'circumferential' and 'axial' are defined in their context with grooving. In cylindrical journal bearings a circumferential groove is taken to be a rotationally symmetric groove passing around the circumference of the bearing at a particular axial location. In other words, the plane containing a very narrow groove is orthogonal to the bearing axis of symmetry. An axial groove, on the other hand, extends from end to end of the cylinder along a generator at a particular orientation of the circumferential co-ordinate θ. In conical and hemispherical bearings an axial groove lies parallel to a generator, while a circumferential groove lies at right angles to this direction. In thrust bearings we will refer to concentric annular segments, being the axial projection of a circumferentially grooved conical bearing.

2. SURVEY OF THE LITERATURE .

Squeeze-film gas bearings in their own right have been studied in depth for the relatively short period of about twelve years, apart from some isolated papers which appeared in the 1950's. The lack of interest, compared with that shown in externally-pressurised and self-acting gas bearings, can probably be attributed to the fact that only a limited number of applications have come to light where the pure squeeze-film bearing can be used to advantage. It becomes an attractive alternative to the externally-pressurised bearing in situations where relative tangential motion of surfaces is too small to provide an acceptable bearing force by self-acting or hydrodynamic means, and where the necessary vibratory drive for the squeeze-film can be accommodated in preference to the rather bulky compression equipment and plumbing required for the externally-pressurised bearing. Examples are journal bearings for the support of low speed rotors, slider bearings operating at low speeds, and bearings for reciprocating devices. Smooth surfaced hemispherical, conical, or parallel flat plate thrust bearings cannot support a thrust load by self-acting means, so squeeze-film support would be an alternative to external pressurisation under suitable conditions. Examples of where only squeeze-films appear to be capable of providing the necessary support are to be found in inertial navigation equipment, in the gimbal bearings of gyroscopes, and in the support of the proof mass in accelerometers. This is because there is no rotation to

enable a self-acting bearing to be used, and externally-pressurised bearings would almost certainly introduce spurious flow effects in sensitive directions which would appear directly as errors in the outputs of the instruments. It is not surprising, therefore, that the main workers in the field of squeeze-film bearings have been associated with the development of inertial navigation sensors, although much of the early work was in connection with slider bearings aimed at the computer industry.

Two centres in the USA are closely associated with work on squeeze-film lubrication:

(i)   MTI (New York), where Pan and his co-workers have exhaustively covered theoretical and practical problems associated predominantly with the application of squeeze-film support to gimbal bearings for inertial navigation gyroscopes, mainly on the strength of NASA contracts.

(ii) Strodtman et al of Lear Siegler (Michigan) have contributed much to the theory of squeeze-films, and have been concerned in practice with the development of inertial quality accelerometers of various types, employing squeeze-film bearings for the support of the proof mass. Another branch of Lear siegler (California) has developed a gyro-compass for the US Army which uses an almost flat squeeze-film thrust bearing (14 inch radius of curvature) to support the sensitive element.

In the UK there are also two centres actively engaged in squeeze-film bearing studies:

(i)   RAE (Farnborough), where the present writer is working in connection with gyro gimbal and accelerometer

proof mass support for inertial navigation instruments used in military aircraft.

(ii) ACO (Slough), who are interested mainly in the possibilities of using a squeeze-film to reduce the starting friction in the rotor of the relatively massive SINS gyroscopes used by the Royal Navy.

In this section it is proposed to outline, in approximately chronological order, the known literature on compressible squeeze-film lubrication. This will show how the subject has developed, provide a background for the present study, and indicate how some of the conclusions have led to the concept of placing grooves in squeeze-film gas bearing surfaces in order to improve the load capacity.

2.1 Historical survey

Although the present author has not seen a translation, other workers[1,2] indicate that the first reference to squeeze-film gas bearings appears to be in a paper by Tipei[3] in 1954. It was not until 1957 that the next relevent paper was published, by Taylor and Saffman[4]. This was not specifically concerned with the lubrication aspect of a squeeze-film, but was motivated by an attempt to explain the result of a controversial experiment, purporting to indicate non-Newtonian properties of air, demonstrated by Professor Reiner[5] at the Applied Mechanics Conference held in Brussels in 1956. The apparatus consisted of a disc 67mm in diameter spinning at 7000 rpm opposite a fixed stator disc, such that the nominal separation between the discs was 20 microns. Taylor and Saffman performed a third order perturbation

analysis on the effects of misalignment and relative normal motion between the discs and showed that the normal motion could account for the effect which had been attributed to non-Newtonian behaviour. Their conclusion was that relative normal motion between surfaces could lead to a time averaged pressure in excess of that of the ambient, so inherent in their analysis was the possibility of a gas bearing operating in a pure squeeze mode, without the necessity for relative sliding motion of the surfaces or external pressurisation. Marsh, in a verbal communication, has since indicated that Reiner carefully repeated his experiment and again observed an effect which this time could not be satisfactorily explained by the Taylor and Saffman analysis, so Reiner remains convinced that he observed a non-Newtonian phenomenon.

Five years elapsed before a further spate of papers appeared, this time specifically concerned with the lubrication aspect of a squeeze-film, and instigated primarily by IBM's interest in the dynamic behaviour of self-acting slider bearings used in the computer industry. For instance, using a numerical method, Gross[7] investigated the growth and decay of pressure in both incompressible and compressible films between parallel flat surfaces following normal impulsive motions. Langlois[1] gave a detailed derivation of the equations governing the pressure distribution in a parallel flat squeeze-film thrust bearing under isothermal conditions using a first order perturbation technique similar to that employed by Elrod[6] in the study of a self-acting journal bearing operating with a constant viscosity incompressible fluid. This approach is convincing in that

it avoids the necessity for many of the ad hoc order of magnitude assumptions usually employed in the derivation of Reynolds' equation. Although the governing equations were set up with both normal and tangential motion in mind, the pressure distribution was obtained for pure squeeze motion. Michael, another member of the IBM team, applied a finite difference method[8] to the time dependent slider bearing problem. In another paper[9] he employed a perturbation analysis similar to that used by Langlois[1], enabling non-periodic as well as periodic solutions to be obtained for the parallel flat plate squeeze-film bearing, and he also allowed for the possibility of flexible surfaces. Out of this paper comes an estimate for the characteristic time associated with transient effects; typically, for a rectangular parallel flat thrust bearing of length L, breadth B, nominal clearance h_o, operating in an ambient pressure p_a with a fluid of viscosity μ, a transient disturbance in the film following a relative normal impulsive motion of the surfaces will decay to 1/e of its initial magnitude in time

$$\frac{12\mu}{p_a(L^2+B^2)} \cdot \left(\frac{LB}{\pi h_o}\right)^2 . \tag{2.1}$$

This theoretical work was backed up experimentally by Salbu[2], demonstrating the feasibility of practical hemispherical, cylindrical journal, and flat thrust squeeze-film bearings driven by piezoelectric and electromagnetic devices. He compared experimentally and theoretically derived results of forces present in a parallel flat disc bearing, using a finite difference method suggested by

Michael[8]. Rotational speeds of up to 50,000 rpm did not
appear to change the bearing characteristics. Generally,
agreement between theory and experiment was within 20%, and
Salbu attributed the discrepancy primarily to experimental
errors. On the dynamic behaviour of the parallel disc
thrust bearing an analogue computer simulation was used,
and there were four main conclusions (see also section 3.3.1):

(i)   failure of the bearing will occur if the squeeze
frequency drops below a critical value, and this critical
frequency decreases as the nominal clearance increases;

(ii) the bearing becomes unstable when the load reaches
a certain value, but can be restabilised by a change in the
excursion amplitude;

(iii) at large mean clearances, a gradual reduction in
operating frequency will cause a progressive increase in
the response amplitude of the supported mass compared with
the squeeze amplitude;

(iv) at small clearances failure will be sudden,
preceded by small changes in the response amplitude of the
supported mass compared with the squeeze amplitude.

In an extended discussion on Salbu's paper, Malanoski
and Pan[10] employed a mass content rule, similar to that set
up by Elrod and Burgdorfer[11] for the self-acting journal
bearing, to remove the ambiguity of the unspecified initial
condition which was built into Salbu's simplified Boyle's
Law approach. A constant which occurs frequently in the
compressible squeeze-film literature is the "squeeze number"
σ given by

$$\sigma = \frac{12\mu\omega}{P_a}\left(\frac{R}{C}\right)^2 \tag{2.2}$$

where μ is the viscosity, ω the angular frequency of the
squeeze motion, p_a the ambient pressure, C the nominal film
thickness, and R is some typical bearing dimension (such as
the radius of the disc in the circular flat plate bearing).
The squeeze number is analogous to the compressibility
number used in self-acting bearing theory, so that the film
behaves incompressibly as $\sigma \rightarrow 0$, and more and more compress-
ibly as $\sigma \rightarrow \infty$. Malanoski and Pan[10] showed that an
asymptotic approach $(\sigma \rightarrow \infty)$ can be used to advantage in
studying the steady state behaviour of the flat disc bearing,
using the property that under suitable combinations of
viscosity, high drive frequency, and compressibility,
lateral flow in the bearing film is inhibited so that the
system behaves very nearly like a nonlinear spring with no
damping. This theory could be used to provide a good
engineering estimate for the time averaged bearing force
for squeeze numbers $\sigma \gtrsim 0$.

Lear Siegler's early interest in the possibilities of
squeeze-films for gyroscope gimbal suspension is indicated
in a paper by Liebler[12], presented at an ultrasonics
symposium, in which he describes experiments to measure
the spurious torques in a squeeze-film journal bearing
generated within the bearing itself and arising from geo-
metrical inaccuracies. In a bearing with length 36mm,
diameter 33mm, nominal clearance 6.25 microns, and journal
out of roundness approximated by an ellipticity of 1.0000169
(major axis/minor axis), he found that oscillatory bearing
torques occurred, decaying under the influence of a film
damping coefficient of estimated magnitude 7.8×10^{-6}Nm per
rad/s.

At the same time MTI was actively concerned with the practical problems associated with designing a transducer suitable for producing the squeeze-film motion in a gyroscope gimbal application. Chiang and Pan[13] studied the longitudinal resonant modes of three transducer configurations, consisting basically of a driving section and a driven extension on which the squeeze-film bearing member was mounted. The extended section was designed to provide a mechanical amplification of the excursion amplitude occurring at the end of the driver, so reducing the power requirements. General and simplified analyses were presented, together with design data, showing that a mechanical amplification factor of about five could typically be attained with this type of transducer.

In a design report for a gyroscope employing squeeze-film bearings, Pan[14] laid down the following guidelines:

(i) the squeeze number should be in the range $\sigma > 100$ to avoid deterioration in load capacity (the asymptotic theory being fairly accurate above this limit);

(ii) the sum of the excursion ratio and maximum steady state displacement ratio (eccentricity, or axial displacement) should not exceed 0.9, to ensure that the minimum instantaneous film thickness is always greater than 0.1 in order to allow for reasonable tolerances in practical bearings;

(iii) given this limitation, the maximum load capacity will be achieved if the excursion amplitude is approximately equal to half the nominal clearance.

Orcutt, Kissinger and Pan[15], following on from the work

of reference 13, investigated an experimental axial

excursion transducer system in which a tubular piezoelectric

driver section was connected to conical bearing pieces

through flexures in the form of flat annular washers. With

a power consumption of 9 watts, a peak to peak axial

excursion of 17.5 microns was achieved (representing a

12.5 micron peak to peak excursion measured normal to the

bearing surfaces, as the cone semi-angle was 45°). The

flexure in this case provided an amplification factor of

about 6 over the motion of the piezoelectric driver, which

was excited at a frequency of 11.1 kHz. One of the

practical difficulties which appeared out of this work was

that the bearing cones moved in a non-rigid manner owing to

the influence of the flexures, causing an undesirable non-

uniform excursion.

Pan, Malanoski, Broussard and Burch[16] formulated the

asymptotic analysis for the cylindrical squeeze-film journal

bearing, obtaining an analytic solution for the radial

stiffness in the case of small eccentricity and uniform

excursion. They also established the equations in terms

of an axially symmetric parabolic excursion distribution,

such that the excursion amplitude is largest at the mid-

plane and decreases towards the ends. This was for effective

comparison with experiment as the piezoelectric tubular

transducers in use tend to have this sort of non-uniform

vibratory motion. Experiments were performed on a double

squeeze-film journal bearing, where a piezoelectric tube

supported both itself and a sleeve by using both of its

vibrating surfaces to form squeeze-films. Curves of load

against eccentricity were obtained and agreement with theory was found within 10% for most loads. However, under very small net loads the agreement was only within 19%, nearer the accuracy Salbu[2] observed. An important conclusion was that the load capacity is significantly reduced by the axial non-uniformity of the squeeze motion.

In 1966 Pan[17] presented a more general asymptotic theory than that suggested in reference 10, applicable to arbitrary bearing shapes, arbitrary modes of oscillation, and for hybrid bearings provided the compressibility number remains finite, and this has formed the basis for most of the more recent papers on the steady state performance of squeeze-film bearings. As an illustration he applied the theory to the conical squeeze-film bearing, obtaining various design curves. Basically, he showed that at high frequencies, the squeeze-film could be considered to consist of two regions:

(i) the internal region, where Boyle's Law is obeyed subject to appropriate initial conditions;

(ii) the edge regions, where the governing equation is of a diffusion type, similar to that discussed by Elrod and Malanoski[18] for the self-acting journal bearing. Where time averaged forces are concerned, the edge region contribution is $0\left\{\dfrac{1}{\sqrt{\sigma}}\right\}$ compared with that of the internal region, so for large σ the effects of the edge region can be neglected and the film considered to behave like a perfect non-linear spring. This theory was applied to the case of a rotating spherical squeeze-film bearing[20], and showed that the squeeze-film and self-acting effects on the pressure distribution are superimposable. Also, to first

order in eccentricity, the axial load capacity and stiffness are independent of eccentricity.

Beck and Strodtman[20] used the asymptotic theory to investigate the stability of an infinite length squeeze-film journal bearing, solving the dynamic equation by both variational and numerical methods. The dynamics equations were arranged in the standard form of the Mathieu equation, which appears frequently in physics and engineering and has well known stability characteristics, and this linked to the variational analysis enabled stability maps to be presented.

At the Southampton Symposium in 1967, Elrod[21] derived governing equations for the dynamic performance of squeeze-film bearings. He showed that for cases where the character-istic frequency of the external disturbance is small compared with that of the squeeze motion itself, the effect of the squeeze motion can be "smoothed out", enabling the asymptotic theory to be extended to cover dynamic conditions. Pan and Chiang[22] applied this to the spherical squeeze-film hybrid bearing, and their methods will be used in the present work. In their paper the boundary conditions are derived by boundary layer considerations, following Di Prima[23], rather than by the mass content rule approach of reference 17.

In discussing a survey of squeeze-film lubrication given by Pan and Broussard[50] at the 1967 Southampton Gas Bearing Symposium, Muijderman[51] referred to some work carried out on spiral grooved self-acting flat thrust bearings subjected to small axial vibrations[52]. This

indicated that the damping component of the dynamic force could be increased by splitting a flat thrust bearing up into a number of segments separated by ambient pressure boundaries. The stiffness component of the dynamic force would be reduced, so the net effect is a smaller amplitude response than would be the case with the unsegmented bearing, fitting in with results given by Langlois[1] and Ausman[37].

At the same meeting, Pan[53] discussed the validity of the assumptions that the squeeze-film behaves isothermally and remains in a state of thermodynamic equilibrium at high squeeze frequencies, concluding that this is indeed the case for all situations likely to be encountered.

In 1968, Strodtman presented several papers with various co-authors. Beck and Strodtman[24] considered steady-state operation with a spherically symmetric (radial) excursion. They showed that the latter case produces considerably more load capacity than the axial excursion case, and they also showed that venting an hemispherical bearing near the pole can increase the load capacity by about 50%. Beck, Holliday and Strodtman[25] described an experiment in which the motion of the supported mass was the main contributor to the generation of the squeeze-film. They performed a perturbation analysis and obtained good agreement with the experimental results. Investigating the steady state behaviour of the finite length journal bearing, Beck and Strodtman[26] found the lift per unit length to be strongly dependent on the length to diameter (L/D) ratio of the bearing. In fact, the very short bearing is 2.5 times

better than the very long bearing with respect to lift per unit length. This conclusion, reached independently by Pan[27,28], is really the starting point of the present work.

An interesting paper from the point of view of the design of gyroscope gimbal bearings is that of Pan and Chiang[29], who theoretically analysed the bearing torques arising from geometric and material imperfections. In a discussion of this paper, Strodtman[30] estimated that a typical journal bearing for gimbal support might produce an error torque as large as 4×10^{-6} Nm. For the gyro to behave sufficiently accurately for inertial navigation purposes, the error torque should typically not exceed 1.2×10^{-9} Nm, which is about 3000 times below that present in the bearing. However, as Pan pointed out in reply, gyroscope gimbals are normally maintained within a few minutes of arc of a fixed orientation and the error torque can be nulled by the application of a bias torque. The effect of bearing torques would become more important in applications where the bearing movement is not so restrained.

Also in reference 27, Pan and Chiang discussed the possibility that supported mass response might explain discrepancies between theory and experiment. More recently, Chiang, Pan and Elrod[31] followed this line of enquiry further by studying the motion of a mass supported between two opposed squeeze-film thrust bearings, and found that the time averaged load capacity can differ considerably from the steady state case. The stability of the system was investigated using the same Mathieu equation approach as Beck and Strodtman[20].

At the 1969 Southampton Gas Bearing Symposium, Constantinescu[34] studied the influence of inertia forces in squeeze-films. He showed that inertia effects can lead to cross-film pressure gradients if the frequency of the squeeze motion is very high, and he derived a validity criterion for neglecting the effect.

Pan[32] extended the asymptotic theory to include the $O\left\{\frac{1}{\sqrt{\sigma}}\right\}$ edge effects which had hitherto been ignored, using singular perturbation techniques as discussed by Di Prima[23], and he identified three edge-interior interaction effects related to

(i)   mean-gap taper,

(ii) squeeze taper,

(iii) cross-edge sliding,

which are analogous to the boundary layer displacement effects in aerodynamics. With reference to the work of Constantinescu[33,34] he also discussed criteria for the validity of isothermal gas lubrication theory in terms of the magnitude of σ.

Finally, Strodtman[35] used a series expansion in terms of ascending powers of eccentricity for a journal bearing, obtaining an analytic solution agreeing well with numerical procedures for large values of eccentricity. Various non-uniform excursion modes were treated, and the same configuration was considered in terms of optimising the clearance in another paper[36]. However, the optimisation of clearance tends to be at the expense of stiffness, and this restricts the usefulness of such an approach.

2.2 Conclusions

These references provide a background for the present study and lead to ways of improving the performance of squeeze-film gas bearings.

Of especial interest is the result indicated in references 25 and 28, that the journal bearing has a lift per unit length which is strongly dependent on L/D, and that in particular the very small L/D bearing has a lift per unit length 2.5 times as great as that having a very big L/D. This suggests, though to the present writer's knowledge it has never been hinted at anywhere else in the literature, that a bearing composed of a number of small L/D segments separated by ambient pressure boundaries will have a considerably greater lift per unit length than a smooth bearing with the same overall value of L/D.

Because the average path lengths of the flow are reduced, it is also felt that the dynamic performance of squeeze-film bearings of arbitrary geometry should be improved by the presence of extra ambient boundaries. A larger region of the film will experience incompressible flow where the forces will contribute to damping, and the region where compressibility occurs will be reduced, so the net effect should be increased dynamic damping with a reduction in dynamic stiffness. This intuitive conclusion is backed up by the work on flat thrust bearings reported in references 1, 37 and 51.

The improvement in static forces obtained by venting the polar region in hemispherical bearings[24] is another pointer to the desirability of suitably increasing the total

ambient boundary length.

Several reports on experimental work have mentioned the non-uniformity of excursion arising from the stress distribution in the transducer used to drive the squeeze motion. In particular, reference 16 noted that in a cylindrical transducer employing a piezoelectric tube, the axial non-uniformity in the excursion could typically lead to a loss in load capacity by a factor of 2.6 . Since the bearing force depends largely on the excursion amplitude at an ambient edge[26], it again appears that improvements should be brought about by placing extra boundaries in regions of more favourable excursion.

For various reasons, therefore, an investigation into the effects of incorporating grooves in squeeze-film gas bearing surfaces is needed as it promises to enable bearings to be designed with a performance superior to that attainable at present.

3. <u>GENERAL DISCUSSION ON GROOVED SQUEEZE-FILM GAS</u>
   <u>BEARINGS</u>

This section takes the form of an extended discussion in which simple analyses will be carried out to justify an interest in the grooving of squeeze-film bearings, and to indicate what might be expected in the more rigorous analysis to be described in section 6.

Firstly, an interpretation will be given of how the "simple" thrust bearing works, labouring the point a little because it will be shown later that the grooved journal bearing in its limiting form behaves locally just like a flat thrust bearing. Apart from Salbu's[2], most of the papers concerned with squeeze-films tend to immerse themselves very rapidly in mathematics and it is difficult to extract in an easy way what is happening in the film, so it is hoped that it will be clear from this discussion how the asymptotic theory fits into the picture in simple terms. It will be shown that the thrust bearing finds an analogy in the externally pressurised thrust bearing, and this may be helpful in determining the dynamic performance of grooved squeeze-film bearings.

The discussion then moves on to consider the cylindrical journal bearing, extending Beck and Strodtman's result[26], and investigating the pressure distribution and flow patterns, leading up to the idea of segmentation by circumferential grooving. The localised link with the flat thrust pad pressure distribution in the limiting case then leads to the suggestion of axial grooving which may have certain manufacturing advantages. Again, an analogy can be found

with externally pressurised bearings.

The dynamic behaviour of squeeze-film bearings is then considered, defining two areas of interest:

(i) what will be referred to as "self-induced response", arising from the forcing action of the squeeze motion itself;

(ii) The "forced response", arising from external disturbances superimposed upon the squeeze motion.

3.1 Steady state behaviour of the squeeze-film thrust bearing

3.1.1 Simple Boyle's Law model

Consider a parallel flat disc thrust bearing of radius R where the lower surface vibrates sinusoidally about the mean clearance C with an amplitude $e_1 C$ as indicated in Fig.1. The instantaneous film thickness is

$$h = C \left(1 + e_1 \cos \omega t \right)$$

(3.1)

where ω is the angular frequency of the squeeze motion, e_1 the excursion ratio, and t is the time. At low frequencies, the gas is alternately squeezed out and sucked into the film as the gap varies, so the system behaves like a viscous damper with a damping force proportional to the velocity of the moving surface, $\dot{h}$. As the frequency is raised, some of the gas near the centre of the film is "trapped by its own viscosity" as the viscous shearing forces preventing flow begin to become appreciable. Consequently, in the central region the gas is alternately compressed and expanded by the squeeze motion, while

nearer the ambient boundary flow in and out of the film takes place incompressibly as before. The film begins to stiffen because of the increased compressibility, while the damping decreases. At high frequencies, the restrictive viscous shearing forces are considerable and virtually the whole film is compressed and expanded, while viscous damping is confined to a very narrow region near the ambient boundary still experiencing incompressible flow. Under these circumstances the film behaves like an almost perfect non-linear spring. It can be shown that the film in general remains isothermal[53], so if the effect of the edge region is ignored, the interior compressibility region can be expected to obey Boyle's Law,

$$p h A = \text{constant} = p_a C A \qquad (3.2)$$

where p is the instantaneous pressure, p_a the ambient pressure, and A the area of the bearing disc. Normalising as follows, pressure $P = p/p_a$, film thickness $H = h/C$, time $\tau = \omega t$, we obtain

$$P = \frac{1}{(1 + e_1 \cos \tau)} . \qquad (3.3)$$

The time averaged film pressure, averaging over a cycle of the squeeze motion, is then[54]

$$\bar{P} = \frac{1}{2\pi} \int_0^{2\pi} P \, d\tau = \frac{1}{\sqrt{1 - e_1^2}} \qquad (3.4)$$

so that the bearing force is given in non-dimensional

terms by

$$F = \frac{F'}{p_a \pi R^2} = \int_0^1 2\bar{r}(\bar{P}-1)\,d\bar{r} = \frac{1}{\sqrt{1-e_1^2}} - 1 \qquad (3.5)$$

where $\bar{r} = r/R$ is the normalised radial co-ordinate. For small values of the excursion ratio,

$$\bar{P} = 1 + \frac{1}{2}e_1^2 + O\{e_1^4\} \qquad (3.6)$$

and

$$F \simeq \frac{1}{2}e_1^2 \qquad (3.7)$$

showing that the load supported is proportional to the square of the excursion ratio.

The non-linear behaviour of the pressure indicated by equation (3.3) can be demonstrated with the aid of Fig. 2. The full curves show how Boyle's Law curvature reflects an asymmetric pressure change following a symmetric volume change, so that the mean pressure during a squeeze cycle is greater than ambient by an amount ΔP which can be used to support a load. This simple model is not valid as $e_1 \rightarrow 1$, where an infinite film pressure is predicted, because other effects occur to prevent this happening, but it does serve to indicate the essential behaviour of the high frequency squeeze-film even though the edge region had been ignored.

3.1.2 Inward pumping edge effect

Salbu[2] observed experimentally that Boyle's Law is a

good approximation to what happens in practice, but the film behaves as if the external pressure were p_1 rather than p_a, where $p_1 > p_a$. In other words, Boyle's Law is obeyed in the form

$$p h A = p_1 C A \qquad (3.8)$$

or

$$P = \frac{P_1}{(1 + e_1 \cos \tau)} \qquad (3.9)$$

where $P_1 = p_1/p_a$. The effect of this is indicated by the broken line curves in Fig. 2, and results in a higher time averaged pressure distribution,

$$\bar{P} = \frac{P_1}{\sqrt{1 - e_1^2}} \qquad (3.10)$$

than was the case with the true ambient pressure initial condition. Salbu estimated that P_1 has a value of 1.15 for $e_1 = 0.5$.

The implication is that, in order to sustain an interior pressure higher than the ambient edge pressure, there must be a transient inward pumping action through the edge region until the interior compressibility forces create a balanced steady state situation. Such an effect can be discussed qualitatively in terms of Fig. 3 where the phase relationships are shown schematically for the compressible interior region pressure, the incompressible edge region pressure, and the film thickness during a cycle of the

squeeze motion.

At $\tau = 0$, the gap is a maximum so gas flows relatively easily into the film because the edge pressure exceeds that of the interior. As the gap closes, increasing the resistance to flow, the interior pressure increases above that of the edge and flow into the film stops. By the time the interior pressure has reached its maximum value above the edge pressure, the gap is a minimum at $\tau = \pi$ and presents a considerable resistance to flow, so that there is little leakage of gas out of the film. Soon after the gap begins to open again the interior pressure drops below that of the edge and once again there is a relatively easy path for gas to flow into the film. In other words, gas flows into the film when there is relatively little restriction to flow, and out when the restriction is considerable. The net effect is a transient flow into the film which pressurises the interior until a time averaged flow balance is achieved.

3.1.3 The asymptotic theory and mass content rule

The asymptotic theory developed by Pan[18], upon which most squeeze-film analyses are based, consists basically of setting up boundary conditions to evaluate the (at present) ambiguous P_1 in such a way that Boyle's Law in the form of equation (3.10) remains a fair description of the bearing film behaviour. To do this use is made of a mass content rule similar to that applied to self-acting bearings[11].

Defining the squeeze number σ for the parallel flat

disc thrust bearing,

$$\sigma = \frac{12\mu\omega}{p_a}\left(\frac{R}{C}\right)^2 \qquad (3.11)$$

where μ is the viscosity, the governing Reynolds' equation for the film pressure in non-dimensional quantities is[2],

$$\frac{H^3}{\bar{r}}\frac{\partial}{\partial\bar{r}}\left(\bar{r}P\frac{\partial P}{\partial\bar{r}}\right) = \sigma\frac{\partial}{\partial\tau}(PH) . \qquad (3.12)$$

In the limit $\sigma \to \infty$,

$$\frac{\partial}{\partial\tau}(PH) = 0 \qquad (3.13)$$

implying that PH = constant, the familiar Boyle's Law. A dilemma now presents itself. If Boyle's Law holds, then the pressure $P \propto 1/H$ is time dependent, in which case it cannot satisfy the true boundary condition ($P = 1$ at $\bar{r} = 1$) which is time independent, so some more suitable boundary condition has to be found.

The derivation of such a boundary condition, using the mass content rule approach, follows on from equations (3.12) and (3.13),

$$\frac{H^3}{\bar{r}}\frac{\partial}{\partial\bar{r}}\left(\frac{\bar{r}}{2}\frac{\partial P^2}{\partial\bar{r}}\right) = 0 . \qquad (3.14)$$

Remembering that this is the radial flow component of the continuity equation modified by the equation of state for a perfect gas, a measure of the radial mass flow rate of

gas into the film is obtained by integrating with respect
to $\bar{r}$ and rearranging, namely

$$\frac{H^3}{2}\frac{\partial P^2}{\partial \bar{r}} = \frac{constant}{\bar{r}} \; . \tag{3.15}$$

The pressure must change smoothly from one ambient edge
to the other across a diameter through the film, so the
pressure gradient at the centre will vanish. Consequently
$\frac{\partial P^2}{\partial \bar{r}} = 0$ at $\bar{r} = 0$, the constant becomes zero, and

$$H^3\frac{\partial P^2}{\partial \bar{r}} = 0 \; . \tag{3.16}$$

Integrating this over one cycle of the squeeze motion
yields a measure of the mass of gas stored in the film
during the cycle as a result of the inward pumping action
at the ambient edge,

$$\int_{0}^{2\pi} H^3\frac{\partial P^2}{\partial \bar{r}}\,d\tau = 0 \tag{3.17}$$

which is zero under steady state conditions because film
equilibrium exists. As no net flow is entering or leaving,
there must be a constant mass of gas contained in the film.
If film equilibrium is disturbed for some reason; for
example, the mean gap might change as a result of a change
in the load supported by the bearing; the right hand side
of equation (3.17) will no longer vanish, but will acquire
a positive or negative value indicating a net transfer of
gas across the ambient boundary until film equilibrium is
restored under the new conditions. Under dynamic conditions

film equilibrium might never be established, and the continual transfer of gas in and out of the film will contribute to the dynamic damping of the system and detract from the dynamic stiffness.

To obtain useful boundary conditions for the asymptotic theory ($\sigma \rightarrow \infty$), equation (3.17) is integrated once more with respect to $\bar{r}$ from a position $\bar{r} = (1-\delta)$ just inside the interior region adjacent to the incompressible edge region, to the ambient boundary at $\bar{r} = 1$ where $P = 1$, giving

$$\int_0^{2\pi} H^3 (P^2 - 1) \, d\tau = 0 \qquad (3.18)$$

or

$$\int_0^{2\pi} (PH)^2 H \, d\tau - \int_0^{2\pi} H^3 d\tau = 0 \qquad (3.19)$$

Now PH = constant (independent of τ), so $(PH)^2$ can be taken outside the integration sign of the first term and, since δ can be made very small if $\sigma \rightarrow \infty$, equation (3.19) provides a pseudo-boundary condition for PH in that it is really for a "boundary" an infinitesimal distance δ inside the true boundary at $\bar{r} = 1$. We obtain

$$(PH)^2 = \frac{\overline{H^3}}{\overline{H}} \qquad at \quad \bar{r} = 1 \qquad (3.20)$$

where

$$\overline{H^3} = \frac{1}{2\pi} \int_0^{2\pi} H^3 d\tau \qquad (3.21)$$

and

$$\bar{H} = \frac{1}{2\pi} \int_0^{2\pi} H \, d\tau \qquad (3.22)$$

are time averaged values. Remembering equation (3.1), it can then be shown that

$$(PH)^2 = 1 + \frac{3}{2} e_i^2 \qquad at \quad \bar{F} = 1 . \qquad (3.23)$$

When H = 1 (squeeze motion passing through the mean gap position), equation (3.9) indicates that

$$P = P_1 = \sqrt{1 + \frac{3}{2} e_i^2} \qquad (3.24)$$

so the time averaged pressure distribution, equation (3.10), for the parallel flat disc thrust bearing becomes

$$\bar{P} = \sqrt{\frac{1 + \frac{3}{2} e_i^2}{1 - e_i^2}} \qquad (3.25)$$

and the load supported, equation (3.5) is

$$F = \frac{F'}{p_a \pi R^2} = \sqrt{\frac{1 + \frac{3}{2} e_i^2}{1 - e_i^2}} - 1 \qquad (3.26)$$

which for small excursion ratios becomes

$$F = \frac{5}{4} e_i^2 + O\{e_i^4\} . \qquad (3.27)$$

Comparing this with the unmodified Boyle's Law model, equation (3.7), it can be seen that the bearing with edge

effect included has 2.5 times the load capacity of the bearing without the edge-pumping effect. This will have important consequences when grooved bearings are discussed at a later stage.

3.1.4 Analogy with externally pressurised thrust bearings

Apart from the basic pressure rise above ambient due to the Boyle's Law behaviour in the interior, the squeeze-film bearing behaves somewhat like an externally-pressurised bearing with pressure sources distributed evenly around the ambient boundary, so in this respect there is a direct analogy with that region of the externally pressurised thrust bearing contained by a circular feeding groove, where the pressure distribution is constant and equal to some value lying between that of the supply and that of the ambient (see Fig.4). In the squeeze-film the pressure must drop sharply from its interior value given by equation (3.25) to the ambient through the edge region, which on the basis of the asymptotic theory can be shown to be of non-dimensional width $O\left\{\dfrac{1}{\sqrt{\sigma}}\right\}$. This analogy may be useful in indicating what might be expected under dynamic conditions.

3.2 Steady state behaviour of the squeeze-film journal bearing

Beck and Strodtman[26] showed that for a small eccentricity e_2 and small e_1^2 the non-dimensionalised lift per unit length of a squeeze-film journal bearing depends on the L/D ratio as follows

$$W_L = \frac{W_L'}{p_a D} = -\frac{\pi}{2} e_1^2 e_2 \left(1 + \frac{3D}{2L} \tanh \frac{L}{D} \right) \qquad (3.28)$$

where the non-dimensionalised film thickness is assumed to have an instantaneous value

$$H = \frac{h}{C} = 1 - e_2 \cos\theta + e_1 \cos\tau \qquad (3.29)$$

such that a negative value of eccentricity e_2 results in a positive bearing force in the direction $\theta = 0$ as indicated in Fig.5 . From the structure of equation (3.28) it can be seen that for long bearings the second term in the parentheses becomes negligible, so that

$$W_L \left(\frac{L}{D} \to \infty\right) \simeq -\frac{\pi}{2} e_1^2 e_2 \qquad (3.30)$$

while for very short bearings the second term tends to a value of 1.5, so

$$W_L \left(\frac{L}{D} \to 0\right) \simeq -\frac{5}{4} \pi e_1^2 e_2 . \qquad (3.31)$$

Thus the very short bearing has 2.5 times the load capacity per unit length of the very long bearing. It is worth noting that this improvement is reminiscent of that brought about by the edge effect in the thrust bearings as discussed in section 3.1.3, and leads one to conjecture that the edge effect might also be responsible for the improvement in the journal bearing case. That this is indeed the case will be shown later. In general, normalising with respect to the very long bearing behaviour,

$$\frac{W_L}{W_L(\frac{L}{D} \to \infty)} = \frac{-W_L}{\frac{\pi}{2} e_1^2 e_2} = 1 + \frac{3D}{2L} \tanh\frac{L}{D} \qquad (3.32)$$

and this is shown in Fig.6 .

By investigating the flow and pressure distributions in the journal bearing, the reason for this L/D dependence will be explained, and this will lead to the concept of grooved squeeze-film bearings.

3.2.1 Mass flow considerations

Applying the asymptotic theory of Pan[17], Beck and Strodtman[26] derived an analytic solution for $Q = (PH)^2$ which can be rearranged in the form

$$Q(\theta,\bar{z}) = 1 + \frac{3}{2} e_1^2 - 2 e_2 \cos\theta \left\{ 1 + \frac{3}{2} e_1^2 \left(1 - \cosh\bar{z} + \sinh\bar{z} \tanh\frac{L}{D} \right) \right\} \tag{3.33}$$

where $\bar{z} = z/R$ is the axial co-ordinate. The time averaged non-dimensional mass flow rate per unit width in the axial direction is

$$M_z = -\frac{\bar{H}}{2} \frac{\partial Q}{\partial \bar{z}} \tag{3.34}$$

where the time averaged film thickness is

$$\bar{H} = \frac{1}{2\pi} \int_0^{2\pi} H \, d\tau = 1 - e_2 \cos\theta \tag{3.35}$$

so that

$$M_z(\theta,\bar{z}) = K(\theta)\left(\sinh\bar{z} - \cosh\bar{z} \, \tanh\frac{L}{D} \right) \tag{3.36}$$

where

$$K(\theta) = \frac{3}{2} e_1^2 e_2 \cos\theta \tag{3.37}$$

for small values of e_1^2 and e_2. The mass flow rate per unit width crossing the ambient boundary at $\bar{z} = 0$ at some particular orientation θ is then

$$M_{\bar{z}}(\theta,0) = -K(\theta)\tanh\frac{L}{D} \qquad (3.38)$$

from which it can be seen that the axial flow is small and proportional to L/D for short bearings, and tends asymptotically to a maximum value $-K(\theta)$ as the bearing length becomes large. Also, because of the $\cos\theta$ dependence of $K(\theta)$ the axial mass flow rate is a maximum at $\theta = 0$ and $\theta = \pi$, and vanishes at $\theta = \frac{\pi}{2}$ and $\theta = \frac{3\pi}{2}$, while there are sign changes in the flow rate at $\theta = \frac{\pi}{2}$ and $\theta = \frac{3\pi}{2}$. The total mass flow rate crossing the ambient boundary at $\bar{z} = 0$ in the region $\pi/2 \leqslant \theta \leqslant 3\pi/2$ is

$$M_{\bar{z}_1} = -\tanh\frac{L}{D}\int_{\pi/2}^{3\pi/2} K(\theta)\,d\theta = -3e_1^2 e_2 \tanh\frac{L}{D} \qquad (3.39)$$

while that crossing the remainder of the same ambient boundary is

$$M_{\bar{z}_2} = -\tanh\frac{L}{D}\int_{-\pi/2}^{\pi/2} K(\theta)\,d\theta = 3e_1^2 e_2 \tanh\frac{L}{D}. \qquad (3.40)$$

Remembering that e_2 is negative for a radial displacement in the direction $\theta = \pi$, then $M_{\bar{z}_1} > 0$ and $M_{\bar{z}_2} < 0$, implying that there is a net flow of gas into the film in the small clearance region and out of the film in the large clearance region. Also, since $|M_{\bar{z}_1}| = |M_{\bar{z}_2}|$, the same mass of gas enters the film as leaves it, which is hardly surprising under steady conditions with no sources or sinks.

The axial penetration of this flow into the film can be studied by considering the structure of equation (3.36), from which it is clear that the axial flow plotted as a function of $\bar{z}/\bar{z}_L$, where $\bar{z}_L = L/R$ is the non-dimensional length of the bearing, will be a curve whose shape depends on the function ($\sinh \bar{z} - \cosh \bar{z} \tanh L/D$), modified only by the multiplicative factor $K(\Theta)$ for different orientations around the bearing. So, removing the effect of the Θ - dependence, the axial distribution of the axial mass flow rate per unit width is conveniently expressed in terms of the ambient edge value by the function

$$\frac{M_{\bar{z}}(\Theta, \bar{z})}{M_{\bar{z}}(\Theta, 0)} = \frac{\left(\sinh \bar{z} - \cosh \bar{z} \tanh \frac{L}{D}\right)}{\tanh \frac{L}{D}} \tag{3.41}$$

which is plotted against $\bar{z}/\bar{z}_L$ in Fig.7 . Because of axial symmetry, only half the bearing length need be shown.

The circumferential mass flow rate per unit width is

$$M_{\Theta}(\Theta, \bar{z}) = -\left(\frac{\bar{H}}{2}\frac{\partial Q}{\partial \Theta} - Q\frac{\partial \bar{H}}{\partial \Theta}\right)$$

$$= \frac{3}{2} e_1^2 e_2 \sin \Theta \left(\cosh \bar{z} - \sinh \bar{z} \tanh \frac{L}{D}\right) \tag{3.42}$$

for small e_1^2 and e_2, and is evidently a maximum at $\Theta = \frac{\pi}{2}$ and $\Theta = \frac{3\pi}{2}$, vanishing at $\Theta = 0$ and π. The maximum values are

$$M_{\Theta}\left(\frac{\pi}{2}, \bar{z}\right) = \frac{3}{2} e_1^2 e_2 \left(\cosh \bar{z} - \sinh \bar{z} \tanh \frac{L}{D}\right) \tag{3.43}$$

and

$$M_{\Theta}\left(\frac{3\pi}{2}, \bar{z}\right) = -\frac{3}{2} e_1^2 e_2 \left(\cosh \bar{z} - \sinh \bar{z} \tanh \frac{L}{D}\right) \tag{3.44}$$

where the difference in signs merely indicates that the flows in the sectors $0 \leqslant \theta \leqslant \pi$ and $\pi \leqslant \theta \leqslant 2\pi$ are in opposite directions, the flow in either case being directed from the small clearance (high pressure) to large clearance (low pressure) region of the bearing. Again, it is convenient to remove the θ - dependence by normalising the axial distribution of the circumferential flow in terms of its ambient edge value,

$$\frac{M_\theta(\theta,\bar{z})}{M_\theta(\theta,o)} = \left(\cosh \bar{z} - \sinh \bar{z} \tanh \frac{L}{D}\right)$$

(3.45)

which is plotted in Fig.8 as a function of axial position $\bar{z}/\bar{z}_L$ for various values of L/D. Note that the total circumferential mass flow rate through the film at $\theta = \pi/2$ is

$$\int_{0}^{\bar{z}_L} M_\theta\left(\frac{\pi}{2},\bar{z}\right) d\bar{z} = 3 e_1^2 e_2 \tanh \frac{L}{D}$$

(3.46)

which is the same as that which enters the film in the regions $\pi/2 \leqslant \theta < \pi$, $\bar{z} = 0$ and $\bar{z} = \bar{z}_L$, and leaves the film in the regions $0 \leqslant \theta < \pi/2$, $\bar{z} = 0$ and $\bar{z} = \bar{z}_L$.

The result of all this is that it would appear that the overall flow pattern in the bearing region $0 \leqslant \theta \leqslant \pi$, $0 \leqslant \bar{z} \leqslant \bar{z}_L$ is as shown schematically in Fig.9 . The flow enters the film predominantly at $\theta = \pi$ across the ambient boundaries at $\bar{z} = 0$ and $\bar{z} = \bar{z}_L$, turning circumferentially to flow from the small clearance to the large clearance region, and finally diverging to leave the film predominantly at $\theta = 0$, $\bar{z} = 0$ and $\bar{z} = \bar{z}_L$. In other

words, there is a net flow of gas through the film in a circumferential sense and the bearing acts like a pump.

In a very short bearing ($\frac{L}{D} \ll 1$) the axial mass flow rate is very small ($\propto L/D$) but has a linear axial distribution (see Fig. 7) implying that the axial pressure distribution is constant at any orientation θ. The circumferential flow (Fig. 8) is also small and has the same value throughout the bearing length at any particular orientation θ.

As the bearing length increases to give a moderate value for L/D, the axial flow rate distribution tends to lose its linearity implying an axial pressure gradient which is greatest near an ambient edge and decreases with penetration into the film. The circumferential flow also exhibits a deviation away from the constant distribution implying a greater circumferential flow near the boundaries than in the centre of the bearing. The absolute magnitude of the flow is increased over that of the very short bearing, as given by equations (3.38) and (3.42).

In very long bearings (L/D $\gg$ 1) the magnitude of the flow is a maximum, and both the axial and circumferential flows tend to be concentrated near the ambient ends of the bearing with negligible flow in the interior. This again implies a constant axial pressure distribution in the interior, but it can be expected to have a markedly different value from that of the short bearing.

Turning now to the time averaged pressure distribution,

$$\bar{P} = \frac{\sqrt{Q}}{2\pi} \int_0^{2\pi} \frac{d\tau}{H} \tag{3.47}$$

where Q and H are given by equations (3.33) and (3.29)
respectively, for small $e_1{}^2$ and e_2,

$$\bar{P} = 1 + \frac{5}{4}e_1^2 + e_1^2 e_2 \cos\theta \left\{ 1 + \frac{3}{2}\left(\cosh\bar{z} - \sinh\bar{z} \tanh\frac{L}{D}\right)\right\}. \tag{3.48}$$

Remembering once again that $e_2 < 0$ for a positive force in
the $\theta = 0$ direction, it can be seen that, as is to be
expected, the pressure is a maximum at $\theta = \pi$ and minimum
at $\theta = 0$. The axial pressure distribution at these two
orientations is given in Fig.10 . The very short bearing
has a constant axial pressure distribution

$$\bar{P}\left(L/D \to 0\right) = 1 + \frac{5}{4}e_1^2 + \frac{5}{2}e_1^2 e_2 \cos\theta \tag{3.49}$$

while the very long bearing has this same value at the edge,
but in the interior the pressure is

$$\bar{P}\left(L/D \to \infty\right) = 1 + \frac{5}{4}e_1^2 + e_1^2 e_2 \cos\theta . \tag{3.50}$$

The axial pressure gradient at the ambient edge is

$$\left.\frac{\partial\bar{P}}{\partial\bar{z}}\right|_{\bar{z}=0} = -\frac{3}{2}e_1^2 e_2 \cos\theta \tanh\frac{L}{D} \tag{3.51}$$

which is seen to be proportional to $\tanh\frac{L}{D}$ at any orien-
tation θ . This is consistent with the increases in total
axial and circumferential flows observed earlier, since
the mass flow rate is proportional to the pressure gradient.

This constant axial pressure distribution in short
bearings is reminiscent of the thrust plate discussed in

section 3.1.2, and leads one to observe that for $L/D \ll 1$ the journal bearing behaves locally (at a particular orientation θ) like a flat thrust bearing, so that a pressure distribution given by equation (3.10) can be expected, where in this case

$$P_1 = \sqrt{(1 - e_2 \cos \theta)^2 + \tfrac{3}{2} e_1^2} \qquad (3.52)$$

to take account of the local film thickness. That is

$$\bar{P} = \sqrt{\frac{(1 - e_2 \cos \theta)^2 + \tfrac{3}{2} e_1^2}{(1 - e_2 \cos \theta)^2 - e_1^2}} \simeq 1 + \tfrac{5}{4} e_1^2 + \tfrac{5}{2} e_1^2 e_2 \cos \theta \qquad (3.53)$$

for small e_1^2 and e_2, agreeing with equation (3.49) which was derived from the full asymptotic theory for the journal bearing.

In the long bearing ($L/D \gg 1$) the edge pressure will again be given by equation (3.53), but because of circumferential flow the differential pressurising effect of the ambient boundaries following a non-zero eccentricity will be lost and the interior will behave as though the ambient pressure were

$$P_1 = \sqrt{1 + \tfrac{3}{2} e_1^2} \qquad (3.54)$$

as would be the case with $e_2 = 0$. This results in a local "flat plate" behaviour in the interior of the form

$$\bar{P} = \sqrt{\frac{1 + \tfrac{3}{2} e_1^2}{(1 - e_2 \cos \theta)^2 - e_1^2}} \simeq 1 + \tfrac{5}{4} e_1^2 + e_1^2 e_2 \cos \theta \qquad (3.55)$$

which agrees with equation (3.50).

All this implies that the idea of "local flat plate" behaviour might be useful in performing simple estimates for journal bearings. In long bearings, circumferential leakage reduces the bearing pressure differential below that of the ideal local flat plate constant value, so reducing the load capacity, as indicated in Fig.11 .

3.2.2   Externally-pressurised bearing analogy

This loss of pressure differential because of circumferential leakage is similar to that which occurs in externally pressurised journal bearings, if one considers the region between the feeding planes in a double feeding plane bearing (see p.116 of Grassam and Powell[38]). Fig.12 shows the similarity in the pressure profiles occurring at $\theta = 0$ and $\theta = \pi$. The dependence on L/D of the amount of circumferential leakage in the two cases is qualitatively similar in that reducing the magnitude of L/D improves the situation and restores the pressure profiles nearer to the flat plate distributions.

This analogy may prove useful in predicting the dynamic behaviour of the squeeze-film journal bearing.

3.2.3   Circumferential grooving

The result that a short bearing has negligible circumferential leakage flow compared with a long bearing, and that consequently the load capacity per unit length is nearer the ideal "flat plate" value, suggests that it should be possible to almost totally remove the circumferential leakage in a long bearing by introducing circumferential ambient boundaries. In this way any desired

bearing length could be operated with optimum load capacity by making it in the form of a number of short segmental journal bearings, mutually separated by deep narrow grooves maintained at ambient pressure.

If one looks at Fig.6 in conjunction with equation (3.28), it can be shown that a journal bearing segment of $L/D \simeq 0.2$ will provide a lift per unit length within 1% of the maximum that would be attained with an infinitesimally short segment, indicating that only 5 segments per unit overall value of L/D is required for a practical bearing. This has the advantage of keeping the segment length as large as possible so that the local squeeze number for the segment does not become small enough to cause appreciable loss in load capacity and violate the asymptotic theory assumption of large σ. By doing this a typical improvement of lift to be expected is 66% for $L/D = 3$. Alternatively, the overall bearing size can be reduced if a certain load is being designed for, and typically a circumferentially grooved bearing of $L/D = 1.8$ would give the same lift as a smooth bearing of $L/D = 3$.

3.2.4 Axial grooving

The developed film cross-section of a squeeze-film journal bearing is shown in Fig.13 where the circumferential leakage flow within the film is indicated by arrows, while the axial pressure profiles are given in Fig.10 . One is inclined to observe that if the ideal load capacity is given when the film behaves locally like a parallel flat plate bearing, then this ideal could be approximated by

making one of the surfaces out of a large number of flat strips, each separated by an ambient line boundary which runs from end to end of the bearing, as indicated in the developed view of Fig.14 . The strips nearest $\theta = 0$ and $\theta = \pi$ are totally isolated from eachother by the intervening ambient boundaries, so there is no circumferential leakage flow to produce an undesirable drop in pressure differential leading to reduced load capacity. Where there is circumferential flow locally because of mean gap taper, it has little effect on lift because it is a maximum in the strips centred at $\theta = \frac{\pi}{2}$ and $\theta = \frac{3\pi}{2}$ where the pressure forces act at right angles to the load line.

Consider such a squeeze-film journal, with deep narrow axial grooves running axially from end to end centred at circumferential positions given by

$$\theta = \theta_k = \frac{2\pi}{w}k \qquad\qquad (3.56)$$

as shown in Fig.15, where w is the number of grooves, and $k = 1,2,\ldots,w$. If each strip bearing is approximated by a parallel flat plate, the shaft will take the form of a w-sided polygonal prism. Suppose each groove has a non-dimensional width $\theta_{2\alpha}$ (where $\alpha \ll 1$), so that the width of each bearing strip is $\theta_{1-2\alpha}$. Suppose further that the k'th bearing strip has an instantaneous film thickness

$$H_k = H(\theta_{k-\frac{1}{2}}) = 1 - e_2 \cos\theta_{k-\frac{1}{2}} + e_1 \cos\tau \qquad (3.57)$$

where e_2 is the eccentricity and e_1 the excursion ratio as

before. The time averaged film thickness in the k'th strip will therefore be

$$\bar{H}_k = \frac{1}{2\pi}\int_0^{2\pi} H_k \, d\tau = 1 - e_2 \cos\theta_{k-\frac{1}{2}} \quad . \tag{3.58}$$

Using equation (3.53) for the local flat thrust plate behaviour, the time averaged pressure in the k'th segment is

$$\bar{P}_k = \sqrt{\frac{\bar{H}_k^2 + \frac{3}{2}e_1^2}{\bar{H}_k^2 - e_1^2}} \tag{3.59}$$

so the lift per unit length contributed by the k'th segment is

$$W_k = \frac{W_k'}{p_a R\theta_{1-2\alpha}} = (\bar{P}_k - 1)\cos\theta_{k-\frac{1}{2}} \tag{3.60}$$

or

$$W_k = \left\{ \sqrt{\frac{(1 - e_2\cos\theta_{k-\frac{1}{2}})^2 + \frac{3}{2}e_1^2}{(1 - e_2\cos\theta_{k-\frac{1}{2}})^2 - e_1^2}} - 1 \right\}\cos\theta_{k-\frac{1}{2}} \tag{3.61}$$

which can be expanded as a power series in eccentricity e_2. For small eccentricities, ignoring terms $O\{e_2^2\}$,

$$W_k \approx \left\{ \sqrt{\frac{1 + \frac{3}{2}e_1^2}{1 - e_1^2}} - 1 \right\}\cos\theta_{k-\frac{1}{2}} - \frac{\frac{5}{2}e_1^2 e_2\cos^2\theta_{k-\frac{1}{2}}}{(1 - e_1^2)^{\frac{3}{2}}\sqrt{1 + \frac{3}{2}e_1^2}} . \tag{3.62}$$

The first term is the contribution arising from a centred bearing ($e_2 = 0$), while the second term is the first order

contribution arising from the non-zero eccentricity. The total lift per unit length of the bearing is

$$W = \frac{W'}{p_a R \theta_{1-2\alpha}}$$

$$= \left\{ \sqrt{\frac{1 + \frac{3}{2}e_1^2}{1 - e_1^2}} - 1 \right\} \sum_{k=1}^{w} \cos \theta_{k-\frac{1}{2}} - \frac{\frac{5}{2}e_1^2 e_2 \sum_{k=1}^{w} \cos^2 \theta_{k-\frac{1}{2}}}{(1-e_1^2)^{3/2} \sqrt{1 + \frac{3}{2}e_1^2}} \qquad (3.63)$$

Using the relationship [58]

$$\sum_{k=1}^{w} \cos\left\{\alpha + (k-1)\beta\right\} = \cos\left\{\alpha + \frac{(w-1)}{2}\beta\right\} \cdot \frac{\sin \frac{w\beta}{2}}{\sin \frac{\beta}{2}} \qquad (3.64)$$

it can be shown that

$$\sum_{k=1}^{w} \cos \theta_{k-\frac{1}{2}} = 0 \qquad (w > 1) \qquad (3.65)$$

and

$$\sum_{k=1}^{w} \cos^2 \theta_{k-\frac{1}{2}} = \frac{1}{2} \sum_{k=1}^{w} (1 + \cos \theta_{2k-1}) = \frac{w}{2} \qquad (3.66)$$
$$(w > 2).$$

Thus, for $w > 2$ the total lift per unit length is

$$W = -\frac{\frac{5}{4} w e_1^2 e_2}{(1-e_1^2)^{3/2} \sqrt{1 + \frac{3}{2}e_1^2}} \qquad (3.67)$$

At present W is normalised with respect to $p_a R \theta_{1-2\alpha}$. A more suitable normalisation for the total lift would be with respect to $p_a D$, so that

$$\frac{W'}{p_a D} = \frac{W'}{p_a R \theta_{1-2\alpha}} \cdot \frac{\theta_{1-2\alpha}}{2} = -\frac{\frac{5}{4}\pi e_1^2 e_2 (1-2\alpha)}{(1-e_1^2)^{3/2} \sqrt{1 + \frac{3}{2}e_1^2}} \qquad (3.68)$$

Assuming that the grooves are really ambient line
boundaries ($\alpha = 0$), and that the excursion ratio is small
($e_1^2 \ll 1$) so that terms $O\{e_1^4\}$ can be ignored, the lift
per unit length finally reduces to

$$\frac{W'}{p_a D} \simeq -\frac{5}{4}\pi e_1^2 e_2 \qquad\qquad (3.69)$$

which is precisely the same as that obtained by Beck and
Strodtman[26] for the very short smooth journal (see equation
(3.28)), dealt with earlier. This simple approach seems
to justify the assumption that a journal bearing with a
number of narrow deep axial grooves tends to approximate
the optimum local "flat plate" behaviour. Note that
equation (3.69) is independent of the number of grooves,
so the same result would be obtained if as few as three
grooves were used.

Referring back to the analogy drawn between squeeze-
film and externally-pressurised bearings, one would as a
result of the above argument expect the externally press-
urised bearing to also benefit from axial grooving. It is
found that this is indeed the case[39] in that the load
capacity is increased if a few axial grooves are incorp-
orated. However other factors, such as increased power
consumption, extra machining costs, and possible lack of
symmetry due to manufacturing tolerances, all tend to
preclude the use of axial grooves in this context. It is
more usual for the bearing to have a few circumferential
grooves.

A possible practical attraction of axial compared

with circumferential grooves for squeeze-film journals is
that the former are automatically connected to ambient
pressure at the ends of the bearing, whereas the latter
might require vent-holes which would considerably complicate
their manufacture. One way of effectively introducing
circumferential grooves would be to have a single helical
groove starting at one ambient boundary and spiralling
towards the other end of the bearing, such that the pitch
of the helix divided by the diameter of the bearing is
about 0.2 to be within 1% of the optimum load capacity
condition. The lack of rotational symmetry of such a
bearing might well tend to limit its use, however, in
applications where self-induced bearing reactions are a
problem.

3.2.5 Non-uniform excursion

It has been shown that for a squeeze-film journal
bearing with an axially uniform excursion amplitude, it is
desirable to include extra ambient boundaries in the form
of circumferential or axial grooves maintained at ambient
pressure in order to remove the undesirable effects of
circumferential leakage flow. There is also a more
practical reason for using grooves, which we shall lead
up to by considering once again the flat thrust plate
with pressure distribution given by equation (3.10),

$$\bar{P} = \frac{P_1}{\sqrt{1 - e_1^2}} \qquad\qquad (3.70)$$

where P_1 is effectively an amplification factor modifying
the interior pressure given by equation (3.4) which would

have been obtained with Boyle's Law based on the true

ambient pressure $P_1 = 1$. In other words $P_1 = 1$ gives the

pressure distribution which would occur in an infinite

radius parallel flat disc bearing in which the film

pressure was initially at ambient. Remembering the result

of the mass content rule for a finite radius bearing

(equation 3.24) $P_1 = \sqrt{1 + \frac{3}{2}e_1^2}$, equation (3.70) becomes

$$\bar{P} = \sqrt{\frac{1 + \frac{3}{2}e_1^2}{1 - e_1^2}} \tag{3.71}$$

which can be expanded for small e_1^2 to give

$$\bar{P} = 1 + \frac{1}{2}e_1^2 + \frac{3}{4}e_1^2 \tag{3.72}$$

so that the effective pressure producing the bearing

force is

$$\bar{P} - 1 = \frac{1}{2}e_1^2 + \frac{3}{4}e_1^2 . \tag{3.73}$$

These two terms have been deliberately separated in order

to show the contribution $\frac{1}{2}e_1^2$ arising from the interior

Boyle's Law behaviour, and the contribution $\frac{3}{4}e_1^2$ represent-

ing the inward pumping or pressurising edge effect. It

can further be seen that the edge effect is the dominant

term, contributing 50% more to the load capacity than the

interior region. It follows that it is desirable to place

ambient boundaries in regions of large excursion amplitude.

In practice the vibratory component of a cylindrical

squeeze-film bearing usually takes the form of a thin-

walled piezoelectric ceramic tube operating in a radial

thickness, or hoop mode. Because of two dimensional stress effects in the piezoelectric material, the excursion amplitude is by no means uniform along the length of the tube, but tends to be a maximum at the mid-plane and tails off to a lower value at the two ends. Typically, the excursion at the ends might be 60% less than that at the centre[16], so there is a significant reduction in lift (typically [27] by a factor of 2.6) when the ambient boundaries are sited near the ends of the transducer, as they normally are, compared with that which could be achieved with a uniform excursion equal to that of the mid-plane. The situation is aggravated by the fact that the lift depends on the square of the excursion ratio (equation (3.28)). In one particular commercial design of accelerometer employing a squeeze-film bearing the mounting constraints were such that the piezoelectric tube used did not vibrate at all at its ends, while the region covered by the bearing was such that the ambient boundary excursion was only a third of that at the mid-plane.

It follows, though it has not as far as is known been discussed in the literature, that considerable improvements in lift should be possible in bearings using this kind of transducer if extra ambient boundaries are placed in positions of favourable excursion amplitude. Further work will be required in order to ascertain which of axial or circumferential grooving provides the greatest benefit, but it is felt that an immediate improvement would be seen if even a single circumferential groove were placed at the mid-plane where the excursion is a maximum.

Another example of where extra boundary length should
be beneficial is in a hemispherical bearing with its
excursion in the axial direction as shown in Fig.16 . It
is very difficult to construct a transducer which will
produce an excursion which is spherically symmetrical, so
all practical designs of hemispherical bearings so far
have relied on vibrating one of the surfaces in the axial
direction only. This results in a large local excursion
ratio in the polar region, and a very small local excurs-
ion ratio near the equator. In the case of a full hemi-
spherical bearing therefore, it will have to rely for its
lift totally on the interior Boyle's Law contribution,
unless the bearing is vented by a hole at the pole to
provide some edge effect amplification from the favourable
excursion occurring there. Again, it would appear that
grooving should improve the situation by increasing the
amplifying effect as a result of extra boundary length in
relatively high excursion ratio regions near the pole.
This is to some extent verified by Beck and Strodtman[24],
who found that they could optimise the lift by varying the
size of the polar vent-hole until a balance was achieved
between loss of bearing area and increased edge effect.

3.3 Dynamic performance

Where the dynamic behaviour of squeeze-film gas bearings
is concerned, there are two main areas of interest. The
first is the response of the supported mass to the forcing
effect of the time dependent squeeze force itself, referred
to as the "self-induced response", and the second is the
response of the system to some external disturbance, called

the "forced response". This latter case is usually typified by frequencies which are considerable lower than that of the squeeze motion itself, a property which is used to advantage in analyses[21].

3.3.1 Self-induced response

Beck and Strodtman[20] investigated the self-induced response in the infinitely long journal bearing, assuming that both the response frequency and the squeeze frequency were large so that PH was effectively constant over a squeeze cycle and the asymptotic theory could be used. They used both a variational analysis, employing the Mathieu equation, and a numerical technique which enabled them to predict stability boundaries. Their general conclusions were that the system would remain stable for a given excursion ratio provided the load was kept below, and the dimensionless mass above, certain critical values. When instability does occur, the response is at half the frequency of the squeeze motion.

Pan[41] pointed out that this is analogous to the magnetic excitation of an AC motor or generator, and contrasts with half-speed whirl in self-acting bearings where the stability threshold is governed by a lower limit on load and an upper limit on rotor mass. He also pointed out that this type of instability is likely to be of concern in the design of accelerometers using squeeze-films, where the specific weight of the proof mass might be quite low.

Chiang, Pan and Elrod[31] performed a similar analysis

on a mass supported between two opposed squeeze-film
thrust plates, finding that the response is essentially
synchronous with the squeeze motion, and that the behaviour
is that of a forced undamped spring-mass system. For a
given supported mass there is a critical drive frequency
at which resonance will occur in the mass response. Above
this critical frequency the response is 180° out of phase
with the motion of the nearer squeeze surface, enhancing
the squeeze action and leading to greater load capacity
and stiffness. When the frequency is below the critical
value the response is in phase with the nearer surface,
degrading the squeeze action and impairing the performance.
In terms of dimensionless mass M, where

$$M = \frac{mC\omega^2}{p_a A} , \tag{3.74}$$

m is the supported mass, and A is the bearing area, the
critical mass is

$$M_o = \frac{2}{\left(1 - e_2^2\right)} \tag{3.75}$$

where e_2 is the steady state displacement of the supported
mass. If $M > M_o$ the performance is improved and if
$M < M_o$ the performance is impaired.

This paper is of immediate interest as it gives an
indication of what to expect in the case of the axially
grooved journal bearing. Dynamically, this should behave
in a similar fashion to the rather peculiar double thrust

bearing of Fig.17, which consists of a number of long bearing strips, each corresponding with the projection in the direction of the load line of one of the bearing strips in the axially grooved journal. The width of the strips and the local excursion ratio decrease in a $\cos\theta$ fashion, while the mean film thickness varies in a ($\sec\theta - e_2$) fashion away from the centre. All the bearing strips are considered to be driven together in phase at the same angular frequency ω. If the number of strips is large, it has already been shown that the steady state lift produced by such a bearing is, on modifying equation (3.69),

$$F_J = \frac{F_J'}{p_a L D} \simeq -\frac{5}{4}\pi e_1^2 e_2 \qquad (3.76)$$

for small e_1^2 and e_2 where $e_2 < 0$ represents a positive upward force. The steady state lift produced by an equivalent double flat plate bearing, using equation (3.53), is

$$F_{FP} = \frac{F_{FP}'}{p_a L D} = \sqrt{\frac{(1-e_2)^2 + \frac{3}{2}e_1^2}{(1-e_2)^2 - e_1^2}} - \sqrt{\frac{(1+e_2)^2 + \frac{3}{2}e_1^2}{(1+e_2)^2 - e_1^2}} \qquad (3.77)$$

which for small e_1^2 and e_2 becomes

$$F_{FP} \simeq -5 e_1^2 e_2 . \qquad (3.78)$$

It follows that

$$F_{FP}' = \frac{4A}{\pi L D} F_J' \qquad (3.79)$$

so the double flat plate bearing will be equivalent in
steady state lift to the strange bearing of Fig.17, and
hence to that of the axially grooved journal if it has an
effective area

$$A = \frac{\pi}{4} LD \; . \tag{3.80}$$

The dimensionless mass, equation (3.74), will be

$$M = \frac{4 m C \omega^2}{\pi p_a L D} \tag{3.81}$$

and the response becomes unbounded when

$$M = M_o = \frac{4 m C \omega_o^2}{\pi p_a L D} = \frac{2}{(1 - e_z^2)} \; . \tag{3.82}$$

The lift will be improved if $M > M_o$ and degraded if $M < M_o$.

The same result should be true for the circumferentially
grooved bearing, or a very short journal bearing, as it
has been shown that they have the same pressure distribution
as the axially grooved journal under steady state conditions.
Circumferential flow in the journal segments should be
negligible under dynamic as well as static conditions
because the axial path lengths are relatively short, so the
same equivalent double flat thrust bearing should be
applicable as in the axially grooved case.

The paper by Chiang, Pan and Elrod[31] also produces
the following condition for marginal stability, using a
Mathieu equation approach like Beck and Strodtman[20] which
should also be applicable to the grooved journal bearing,

$$a_1 = \frac{1}{4} - \frac{1}{2}a_2 \qquad\qquad (3.83)$$

where

$$a_1 = \frac{1}{M}(a_3 + a_4) \qquad\qquad (3.84)$$

$$a_2 = \frac{2e_1}{M}\left\{\frac{a_3}{(1+e_2)} + \frac{a_4}{(1-e_2)}\right\} \qquad (3.85)$$

and

$$a_3 = 1 + \frac{3}{2}\left(\frac{e_1}{1+e_2}\right)^2 \qquad\qquad (3.86)$$

$$a_4 = 1 + \frac{3}{2}\left(\frac{e_1}{1-e_2}\right)^2 . \qquad\qquad (3.87)$$

For given values of e_1 and e_2, equation (3.83) can be solved for M, and the bearing will be stable for values of M greater than this. Damping of the squeeze motion, which takes place in the incompressible edge regions, has been ignored because the asymptotic theory ($\sigma \to \infty$) was used to derive the pressure distribution, so the stability result will be conservative.

3.3.2 Forced response

It is of considerable interest to the designer to know how the bearing will respond to external disturbances.

For instance, in the field of inertial navigation instruments one is interested in the response to small amplitude simple harmonic motions in the frequency range 20Hz to 2kHz, which is well below the driver frequency normally associated with a squeeze-film bearing.

For such a case, where the squeeze frequency is considerably larger than that of the external disturbance, Elrod[21] formulated governing equations in terms of the asymptotic theory so that the effect of the high frequency squeeze motion could be "smoothed out". Pan and Chiang[22] then applied this theory to the spherical squeeze-film hybrid bearing using a perturbation technique for small eccentricity and small vibration amplitude, to obtain the dynamic stiffness, damping, frequency response, and stability of the system. The conclusions reached in this paper are especially important as they may be relevent to other bearing geometries:

(i) the dynamic axial stiffness increased steadily with the frequency of the external disturbance, asymptotically levelling off at a value about one decade larger than the static stiffness;

(ii) the dynamic axial damping coefficient (proportional to the damping force divided by the frequency) decreases steadily with frequency, although it is always positive;

(iii) the spherical bearing is inherently stable with respect to both axial and radial modes for frequencies which are low compared with the squeeze frequency;

(iv) for most supported masses, the dynamic axial

compliance at resonance is less than the static compliance,
but for very large or very small masses the reverse is true;

(v)   the value of axial resonance frequency estimated
using the static axial stiffness can be as much as three
times too small.

All of these points should be applicable to flat thrust
and conical bearings, while the radial aspect of (iii) is
probably true for cylindrical bearings in addition.
However, because of our conclusion that grooved journal
bearings behave essentially like combinations of flat thrust
bearings, it can also be inferred that Pan and Chiang's
results are broadly valid for them as well.

3.4   Local squeeze-number in a bearing segment

A point that requires investigation is the magnitude
of the local squeeze number in a bearing segment. It can
be seen that this would become quite small if the number of
grooves is very large, leading to reduced load capacity
and violation of the asymptotic theory. It has already
been shown that only five segments per unit L/D are required
in a circumferentially grooved bearing. The squeeze number
for a smooth journal bearing is the same as that given in
equation (3.11), where in this case R is the radius of the
shaft. If the segment length is ℓ, in a circumferentially
grooved bearing of diameter D = 2R, the local squeeze
number for the segment will be

$$\sigma_\ell = \frac{12\mu\omega}{p_a}\left(\frac{\ell}{C}\right)^2 . \tag{3.88}$$

If ℓ/D $\leq$ 0.2,

$$\frac{\sigma_l}{\sigma} \leq 0.16 \ . \tag{3.89}$$

Typically $\sigma \sim 10^4$, so it can be seen σ_l will be $\sigma_l \sim 10^3$, which is well within the bounds of validity for the asymptotic theory. The same sort of comparison is required for the axially grooved case, and a more rigorous analysis is required than that given in section 3.3.4, so that an idea can be obtained of how many axial grooves are actually required to be within, say, 1% of the maximum attainable load capacity.

3.5 Comments regarding grooves

In this rather lengthy discussion simplified analyses have been used to show that, at least for small values of e_1^2 and e_2, quite considerable improvements in load capacity should be obtained in squeeze-film journal bearings by incorporating narrow, deep grooves maintained at ambient pressure. The finite width of the grooves represents a loss of bearing area, so care must be taken to ensure that, not more than (say) 1% of the bearing area is taken up by grooves so that the load capacity reduction from this source will be no more than 1%. Setting a criterion for the groove depth is not so easy and study is required to see how deep the grooves should be in order to behave like proper ambient boundaries. For instance, the local squeeze number in the grooves should be low enough for compressibility effects to be negligible, and the groove cross-sectional area should be sufficiently large so as to present a

negligible restriction to flow under all conditions of
operation of the bearing. In particular, for circum-
ferential grooves it is not easy to say for certain that
they need be specially connected to ambient via vent holes,
as a simple argument can be put forward which indicates
that over many cycles of the squeeze motion there will be
a transient flow of gas through the film to equalise the
groove and ambient edge pressures, but whether or not this
is so requires further analysis, and possibly experiment.
Some of these points are amplified in the next two sub-
sections.

3.5.1 Groove depth limitations

It is necessary to ascertain how deep the grooves
in squeeze-film bearings should be made in order to avoid
compressibility effects. A groove is there to behave as
an ambient boundary, and the gas in the groove must be
able to move about freely in an incompressible fashion so
that adjustments to changes in eccentricity can take place
quickly. If the groove is too shallow, the local squeeze-
film action in the groove could produce compressibility
effects to detract from the edge pressurising effect,
which has been shown to be all important.

Suppose that the local squeeze number in a groove is

$$\sigma_{\ell_g} = \frac{12 \mu \omega}{p_a} \left(\frac{R}{h_o} \right)^2 \tag{3.90}$$

where h_o is the mean film thickness in the groove. The
effective squeeze number in a bearing segment is as given
in equation (3.88), where ℓ is the length of the segment

in the circumferentially grooved bearing, or is the width of a segment in the axially grooved bearing. Supposing that there will be negligible compressibility in the groove if $\sigma_{\ell_g} <$ 1, equations (3.88) and (3.90) can be combined to give

$$\sigma_{\ell_g} = \left(\frac{RC}{\ell h_o}\right)^2 \sigma_\ell < 1 \ . \tag{3.91}$$

In the circumferentially grooved bearing it is desirable to set $\ell/R \sim 0.4$, while at present there is no estimate for ℓ/R in the axially grooved case, so using $\ell/R = 0.4$ in equation (3.91) to provide an estimate for h_o, its use for the axially grooved case will be justified later. Thus

$$\sigma_{\ell_g} \simeq \left(\frac{5C}{2h_o}\right)^2 \sigma_\ell < 1 \ . \tag{3.92}$$

Since σ_ℓ is typically of the order 10^3,

$$\frac{C}{h_o} < 0.013 \tag{3.93}$$

so, as a rough guide,

$$h_o > 100 \ C \tag{3.94}$$

which means that for $C \sim 2$ microns, we should have $h_o > 0.2$mm.

3.5.2 Effect of trapped volume in circumferential grooves

In circumferentially grooved bearings it may or may
not be necessary to physically vent each groove to the
ambient by means of small holes in the groove bottoms.
It would be desirable to avoid this for manufacturing
reasons, and one can give a qualitative argument to show
that vent holes are not necessary to produce an ambient
pressure in the grooves. There should be a net leakage
flow of gas through the bearing from the outer ambient
boundaries which will gradually adjust the groove pressure
to the same value.

If there are no vent-holes, then under dynamic cond-
itions each groove will tend to behave as a trapped
volume which could feasibly resonate in an analogous
manner to pneumatic hammer in externally-pressurised
bearings. If the cross-sectional area of a groove is too
small, then the gas might meet a considerable restriction
when it tries to flow circumferentially from one side of
the bearing to the other following rapid changes in eccen-
tricity under dynamic conditions. This would cause a
sudden build-up of pressure in the groove on the small
clearance side of the bearing, and a corresponding drop
in pressure in the large clearance region. This now alters
the boundary conditions locally round the groove edge of
a segment, leading to changes in the pressurising edge
effect locally in the segment. One can then envisage a
situation where the natural resonance condition of the
bearing might be augmented because the differential dynamic

film forces are increased, and under certain circumstances this might cause the bearing surfaces to touch.

3.6 Possibility of entrance losses

In the edge region, gas flows in and out of the bearing film in response to the squeeze-motion. If the ambient boundary, approached from the interior of the film, is marked by a sharp discontinuity in the film thickness, there is the possibility that during the suction stroke gas entering the film round the sharp corner will over-shoot due to its inertia and form a transient eddy inside the film immediately adjacent to the sharp edge. This would alter the boundary conditions and tend to restrict the flow into the film during the suction stroke, so reducing the load capacity of the bearing.

A vaguely similar situation occurs in externally-pressurised gas bearings, where the flow entering the film from an orifice may experience the effects of inertia, separation, and shock, depending on the circumstances prevailing. McCabe et al[64] indicate that a loss coefficient can be defined embracing all three of these effects in terms of the Reynolds' number of the entrance flow, the loss coefficient increasing monotonically with the Reynolds' number. For squeeze-film gas bearings, a measure of the transient Reynolds' number for the edge regions is $\rho \omega c^2/\mu$, and for typical values

$$\rho = 1 \text{ kg/m}^3 \qquad \text{(density)}$$

$$\mu = 2 \times 10^{-5} \text{ N s/m}^2 \qquad \text{(viscosity)}$$

$$\omega = 4\pi \times 10^4 \text{ rad/s} \qquad \text{(squeeze angular frequency)}$$

$$C = 2 \text{ } \mu m \qquad \text{(nominal clearance)}$$

we have

$$\frac{\rho \omega C^2}{\mu} \simeq 0.024 .$$

This very small value is several orders of magnitude below the threshold value associated with transition to turbulent flow, and implies that the film is substantially free from effects producing entrance losses.

Even if the transient Reynolds' number were appreciable it is highly unlikely that entrance losses would occur due to flow separation, as recent unpublished work at Queen Mary College (London) indicates that there is a minimum size of eddy that can exist, and that this minimum size is larger than the nominal film thickness C normally encountered in squeeze-film bearings. In any case, sharp edges to the boundaries are unlikely to occur in practice as manufacturing processes will tend to round off corners, enabling the entrance flow to be gradually introduced into the film without abrupt changes of direction.

That the edge flow velocity u is typically small compared with the sonic velocity 'a' can be shown quite easily. A measure of velocity in the edge region is

$$u = O\left\{\frac{\omega R}{\sqrt{\sigma}}\right\} \tag{3.95}$$

where R is a typical bearing dimension and σ is the squeeze number. The velocity of sound is related to the density ρ and pressure p of the gas thus

$$a = \sqrt{\frac{\gamma p}{\rho}} \tag{3.96}$$

where γ ($\simeq 1.4$ for air) is the ratio of the specific heats at constant pressure and constant volume. The effective Mach number of the edge flow is then

$$M_{edge} = \frac{u}{a} = O\left\{\sqrt{\frac{\rho \omega C^2}{12\mu}}\right\} \qquad (3.97)$$

which is seen to be proportional to the square root of the transient Reynolds' number of the edge region. Typically, $M_{edge} \sim 0.04$, so there should be no threat of transient shock waves and choking to interfere with flow through the edge region since $M_{edge} \ll 1$.

4. GOVERNING EQUATIONS

On the basis of the previous discussion it was decided to investigate theoretically the effect of both axial and circumferential grooving in the common configurations applied to a squeeze-film gas bearing, namely cylindrical, conical, and hemispherical, taking into account both static and dynamic behaviour. We are concerned here primarily with the forced dynamic response rather than self-induced motion, because it has not yet received much attention in the literature and the pointers of reference 22 require verification for geometries other than hemispherical. To obtain fair comparison, the analysis must also include smooth bearings of the same geometries. The most convenient way to do all this is to derive governing equations in terms of generalised curvilinear co-ordinates, covering both the static and forced dynamic behaviour, so that any particular problem within the framework outlined above can be studied by inserting the appropriate co-ordinates.

As it has not been tackled by any other author in this context, the effect of slip-flow will be included in these generalised equations, rather than as a separate study, so that the equations are set up if use is required at a later stage. Estimates of the effect of a non-negligible molecular mean free path can then be obtained for simple geometries where analytic solutions can be found.

There follows a discussion of some of the assumptions to be made in setting up the generalised equations, followed by a derivation of the equations and a study of available solution methods.

4.1 Assumptions

In deriving Reynolds' equation it would be more satisfactory to use the kind of perturbation approach employed by Elrod[6] and Langlois[1], but since only minor alterations are being made to include slip flow, and the derivation of Reynolds' equation appears in many textbooks (see for example Chapters 3 and 4 of Cameron[42]), we will restrict our attention to an outline of the main assumptions used in deriving the governing equations for the generalised asymptotic theory; these governing equations for an ideal compressible lubricant being really an amalgamation of the Navier-Stokes equations, the continuity equation, the energy equation, and the equation of state.

Our particular interest is in high frequency operation of squeeze-films $(\sigma \to \infty)$, and normally we would expect high frequency changes in volume of a gas to take place adiabatically. However, the film thickness is so small compared with the other dimensions of the bearing that heat transfer between the gas and the surfaces maintains the film in a virtually isothermal state[53]. This makes the energy equation redundant, and the equation of state for a perfect gas simply results in

$$p \propto \rho \qquad (4.1)$$

where p and ρ are respectively the film pressure and density.

In the Navier-Stokes equations[42] the film is taken to lie in the x,y plane with the film thickness extending in the z-direction. The pressure is assumed constant

through the film thickness, and a criterion for this is[32,34]

$$\frac{\rho \omega^2 C^2}{p} \ll 1 \qquad (4.2)$$

where ω is the angular frequency of the squeeze motion and C the nominal film clearance. It is assumed that the inertia terms can be ignored compared with the viscous shear forces, and a criterion for this is [32]

$$\frac{\rho \omega C^2}{\mu} \ll 1 \qquad (4.3)$$

where μ is the viscosity. Pan[32] interprets the inequalities (4.2) and (4.3) as limiting respectively the square of the Mach number and the transient Reynolds number of the squeeze motion.

Velocities in the x and y directions are assumed large compared with that in the z direction. A measure of the velocity in the z direction is $\frac{\sigma p_a C^3}{12 \mu R^2}$, where R is a typical measure of the bearing dimensions. A measure of the velocity in the edge region, where the lateral flow takes place, is $\frac{\sqrt{\sigma} p_a C^2}{12 \mu R}$, so a criterion for neglecting the velocity component in the z direction compared with the other components is

$$\sqrt{\sigma} \frac{C}{R} \ll 1 \quad . \qquad (4.4)$$

A further assumption is that velocity gradients in the x and y directions are small compared with that in the z

direction. Respective measures for the former and latter

are $\dfrac{\sigma p_a C^2}{12 \mu R^2}$ and $\dfrac{\sqrt{\sigma} p_a C}{12 \mu R}$, so the required criterion is
again

$$\sqrt{\sigma}\, \frac{C}{R} \ll 1 \ . \tag{4.5}$$

Gas at the relatively low pressures encountered in gas bearings has a viscosity virtually independent of pressure and dependent mainly on temperature, so under isothermal conditions the viscosity can be assumed constant. Keeping these criteria in mind, the full asymptotic governing equations will now be derived, including the dynamic behaviour and slip-flow, in terms of generalised curvilinear co-ordinates. The derivation is based on papers by Pan[17,22], Elrod[21], and Burgdorfer[43], and is given in full to show particularly how the introduction of slip flow terms changes the governing equation and its boundary conditions.

4.2 Generalised asymptotic governing equations including time-dependence and slip flow

4.2.1 Navier-Stokes equation

Assuming that the effects of fluid inertia and external forces (e.g. gravitational) are negligible compared with viscous shearing forces, the Navier-Stokes equations reduce to the vector form

$$\frac{1}{\mu}\nabla p = \frac{1}{3}\nabla\cdot(\nabla \underline{v}) + \nabla^2 \underline{v} \tag{4.6}$$

where ∇ is the gradient vector, μ is the viscosity

(assumed constant), p the film pressure, and $\underline{v} = (v_1, v_2, v_3)$ is the velocity vector of the flow referred to a set of generalised orthogonal curvilinear co-ordinates x_1, x_2, x_3 in directions given by the unit vectors $\hat{x}_1$, $\hat{x}_2$, $\hat{x}_3$. The fundamental magnitudes are s_1, s_2, s_3 such that a typical elemental volume element is $s_1\delta x_1$. $s_2\delta x_2$. $s_3\delta x_3$. The x_3 direction is through the film thickness $h = h(x_1, x_2, t)$ which is contained between the two surfaces $x_3 = a$ and $x_3 = b$ such that $h =(b-a)$. If it is assumed that velocity gradients in the $\hat{x}_1$ and $\hat{x}_2$ directions are small compared with that in the $\hat{x}_3$, and that $v_1 \gg v_3$ and $v_2 \gg v_3$, the Navier-Stokes equations become in terms of these generalised co-ordinates,

$$\frac{\partial p}{\partial x_1} = \frac{\mu}{s_2 s_3}\cdot\frac{\partial}{\partial x_3}\left(\frac{s_1 s_2}{s_3}\cdot\frac{\partial v_1}{\partial x_3}\right) \tag{4.7}$$

$$\frac{\partial p}{\partial x_2} = \frac{\mu}{s_3 s_1}\cdot\frac{\partial}{\partial x_3}\left(\frac{s_1 s_2}{s_3}\cdot\frac{\partial v_2}{\partial x_3}\right) \tag{4.8}$$

$$\frac{\partial p}{\partial x_3} = 0 \tag{4.9}$$

equation (4.9) representing the further assumption that the pressure remains constant throughout the film thickness in the $\hat{x}_3$ direction. If it is finally assumed that s_1, s_2, s_3 are independent of x_3, the Navier-Stokes equations become simply

$$\frac{\partial p}{\partial x_1} = \frac{\mu s_1}{s_3^2}\cdot\frac{\partial^2 v_1}{\partial x_3^2} \tag{4.10}$$

$$\frac{\partial p}{\partial x_2} = \frac{\mu s_2}{s_3^2} \cdot \frac{\partial^2 v_2}{\partial x_3^2} \qquad (4.11)$$

$$\frac{\partial p}{\partial x_3} = 0 \qquad . \qquad (4.12)$$

4.2.2 Introduction of slip flow

Double integration of equations (4.10) and (4.11) with respect to x_3 gives the velocity components

$$v_1 = \frac{s_3^2}{2\mu s_1} \cdot \frac{\partial p}{\partial x_1} x_3^2 + C_1 x_3 + C_2 \qquad (4.13)$$

$$v_2 = \frac{s_3^2}{2\mu s_2} \cdot \frac{\partial p}{\partial x_2} x_3^2 + C_3 x_3 + C_4 \qquad (4.14)$$

where C_1 to C_4 are constants to be evaluated from boundary conditions yet to be specified. Burgdorfer[43] showed that the following boundary conditions become appropriate when the molecular mean free path of the gas is appreciable compared with the nominal film thickness:

$$v_1(x_3 = a) = \frac{\lambda}{s_3} \cdot \frac{\partial v_1}{\partial x_3} \bigg|_{x_3 = a} \qquad (4.15)$$

$$v_1(x_3 = b) = -\frac{\lambda}{s_3} \cdot \frac{\partial v_1}{\partial x_3} \bigg|_{x_3 = b} \qquad (4.16)$$

$$v_2(x_3 = a) = \frac{\lambda}{s_3} \cdot \frac{\partial v_2}{\partial x_3} \bigg|_{x_3 = a} \qquad (4.17)$$

$$V_2(x_3 = b) = -\frac{\lambda}{s_3} \cdot \frac{\partial v_2}{\partial x_3}\bigg|_{x_3 = b} \qquad (4.18)$$

where λ is the molecular mean free path of the gas. Using these, the velocity components become

$$V_1 = \frac{s_3^2}{2\mu s_1} \cdot \frac{\partial p}{\partial x_1}\left\{ x_3^2 - (b+a)x_3 - \frac{\lambda}{s_3}(b-a) + ab \right\} \qquad (4.19)$$

$$V_2 = \frac{s_3^2}{2\mu s_1} \cdot \frac{\partial p}{\partial x_2}\left\{ x_3^2 - (b+a)x_3 - \frac{\lambda}{s_3}(b-a) + ab \right\}. \qquad (4.20)$$

The volumetric rates of flow of gas in the $\hat{x}_1$ and $\hat{x}_2$ directions are respectively

$$q_1 = \int_a^b v_1 dx_3 = -\frac{s_3^2 h^3}{12\mu s_1} \cdot \frac{\partial p}{\partial x_1}\left(1 + \frac{6\lambda}{s_3 h}\right) \qquad (4.21)$$

$$q_2 = \int_a^b v_2 dx_3 = -\frac{s_3^2 h^3}{12\mu s_2} \cdot \frac{\partial p}{\partial x_2}\left(1 + \frac{6\lambda}{s_3 h}\right). \qquad (4.22)$$

4.2.3 Continuity equation

In terms of the generalised co-ordinates, the continuity equation takes the form

$$\frac{1}{s_1 s_2}\left\{ \frac{\partial}{\partial x_1}(\rho s_2 q_1) + \frac{\partial}{\partial x_2}(\rho s_1 q_2) \right\} + \frac{\partial}{\partial t}(\rho h) = 0 \qquad (4.23)$$

where ρ is the density. Equation (4.23) can easily be derived by considering the mass flow rates entering and leaving opposite faces of a column of gas of height h and

base area $s_1 s_2 \delta x_1 \delta x_2$, and it expresses the fact that in the absence of sources and sinks the mass of gas contained in the column must remain constant. The two terms within the curly bracket take account of the gas flow in the directions $\hat{x}_1$ and $\hat{x}_2$, while the time derivative term allows for the squeezing action arising from the time dependence of the film thickness h.

Substituting for q_1 and q_2 from equations (4.21) and (4.22), the continuity equation (4.23) becomes

$$\frac{1}{s_1 s_2}\left\{\frac{\partial}{\partial x_1}\left[\frac{s_2}{s_1}s_3^2 \rho h^3\left(1+\frac{6\lambda}{s_3 h}\right)\frac{\partial p}{\partial x_1}\right] + \frac{\partial}{\partial x_2}\left[\frac{s_1}{s_2}s_3^2 \rho h^3\left(1+\frac{6\lambda}{s_3 h}\right)\frac{\partial p}{\partial x_2}\right]\right\} = 12\mu\frac{\partial}{\partial t}(\rho h).$$

$$(4.24)$$

Assuming that the film behaviour is isothermal, the density and pressure are related through the equation of state for an ideal gas

$$\frac{p}{\rho} = \text{constant.} \tag{4.25}$$

For all the bearing geometries usually considered, $s_3 = 1$, and this fact together with equation (4.25) can be used to simplify equation (4.24) so that it finally becomes the modified Reynolds' equation,

$$\frac{1}{s_1 s_2}\left\{\frac{\partial}{\partial x_1}\left[\frac{s_2}{s_1}p h^3\left(1+\frac{6\lambda}{h}\right)\frac{\partial p}{\partial x_1}\right] + \frac{\partial}{\partial x_2}\left[\frac{s_1}{s_2}p h^3\left(1+\frac{6\lambda}{h}\right)\frac{\partial p}{\partial x_2}\right]\right\} = 12\mu\frac{\partial}{\partial t}(p h).$$

$$(4.26)$$

4.2.4 Non-dimensionalisation of the governing equation

It is convenient to non-dimensionalise this equation so as to make it applicable to all sizes and shapes of bearing likely to be encountered. To this end the spatial inde-

pendent variables are non-dimensionalised with respect to some typical bearing dimension, R say, so that in terms of the new non-dimensionalised generalised co-ordinates u_1 and u_2 a typical element of area is $\ell_1 \delta u_1 . \ell_2 \delta u_2$ where ℓ_1 and ℓ_2 are now the fundamental magnitudes in the u_1 and u_2 directions. The other non-dimensionalised variables are

$$P = p/p_a \qquad \text{(pressure)}$$

$$\bar{\rho} = \rho/\rho_a \qquad \text{(density)}$$

$$\bar{\mu} = \mu/\mu_a \qquad \text{(viscosity)} \qquad (4.27)$$

$$H = h/C \qquad \text{(film thickness)}$$

$$\bar{\lambda} = \lambda/\lambda_a \qquad \text{(mean free path)}$$

where ambient conditions are expressed by the subscript 'a'. C is the nominal film thickness, ω is the angular frequency of the squeeze motion, and $\bar{\mu} = 1$ under isothermal conditions. Now $\lambda \propto \frac{1}{\rho}$, so $\bar{\lambda} = \frac{1}{P}$, and the non-dimensionalised form of Reynolds' equation becomes

$$\frac{1}{\ell_1 \ell_2} \left\{ \frac{\partial}{\partial u_1} \left[\frac{\ell_2}{\ell_1} \left(1 + \frac{6m}{PH} \right) PH^3 \frac{\partial P}{\partial u_1} \right] + \frac{\partial}{\partial u_2} \left[\frac{\ell_1}{\ell_2} \left(1 + \frac{6m}{PH} \right) PH^3 \frac{\partial P}{\partial u_2} \right] \right\} = \frac{\sigma}{\omega} \cdot \frac{\partial}{\partial t} (PH)$$

$$(4.28)$$

where use has been made of the Knudsen number,

$$m = \frac{\lambda_a}{C} \qquad (4.29)$$

and squeeze number

$$\sigma = \frac{12 \mu_a \omega}{p_a} \left(\frac{R}{C} \right)^2 . \qquad (4.30)$$

Again, it is convenient to define the dependent variable $\psi = PH$, in terms of which the governing equation (4.28)

becomes

$$\frac{1}{2\ell_1\ell_2}\left\{\frac{\partial}{\partial u_1}\left[\frac{\ell_2}{\ell_1}\left(1+\frac{6m}{\psi}\right)\left(\frac{\partial}{\partial u_1}(H\psi^2)-3\psi^2\frac{\partial H}{\partial u_1}\right)\right]\right.$$

$$\left.+\frac{\partial}{\partial u_2}\left[\frac{\ell_1}{\ell_2}\left(1+\frac{6m}{\psi}\right)\left(\frac{\partial}{\partial u_2}(H\psi^2)-3\psi^2\frac{\partial H}{\partial u_2}\right)\right]\right\}=\frac{\sigma}{\omega}\frac{\partial\psi}{\partial t}. \quad (4.31)$$

Supposing that ambient boundaries occur at $u_1 = \bar{a}$ and
$u_1 = \bar{b}$, equation (4.31) can be solved for ψ subject to
the following boundary conditions

$$\psi(u_1=\bar{a},u_2) = H(u_1=\bar{a},u_2)$$
$$\psi(u_1=\bar{b},u_2) = H(u_1=\bar{b},u_2). \quad (4.32)$$

4.2.5 Separation of scales of time-dependence

In addition to the angular frequency ω of the squeeze
motion, the bearing might experience some relatively long
term transient behaviour following some external disturbance
such that characteristic times for the transient and
squeeze motions are respectively

$$T = \nu t$$
$$\tau = \omega t \quad (4.33)$$

where ν is some angular frequency characteristic of the
transient behaviour. Elrod[21] showed that if the motion
due to the external disturbances were quasistatic compared
with the squeeze motion, $\nu\ll\omega$, then the two time scales
T and τ can be separated and the behaviour of the film
can be found in a time averaged sense with respect to the
squeeze motion. Pan and Chiang[22] applied this treatment
to the case of small amplitude harmonic motions in spherical

hybrid squeeze-film bearings, and the intention of the
present work is to generalise Pan and Chiang's approach
so as to be applicable to all squeeze film bearing geom-
etries, and to include the effect of slip flow.

The time scales are separated by writing the film
thickness in the form

$$H(u_1,u_2,T,\tau) = H_\infty(u_1,u_2,T) + H_s(u_1,u_2,\tau) \qquad (4.34)$$

where H_∞ is quasi-static with reference to the squeeze
motion (associated with H_s) such that

$$H_s(u_1,u_2,\tau+2\pi) = H_s(u_1,u_2,\tau) \qquad (4.35)$$

and

$$\frac{1}{2\pi}\int_\tau^{\tau+2\pi} H_s\,d\tau' = 0 \qquad (4.36)$$

where τ' is a dummy variable for τ. Assuming that it is
possible to write

$$\psi(u_1,u_2,t) = \psi(u_1,u_2,T,\tau) \qquad (4.37)$$

the right hand side of the governing equation (4.31) can
be written

$$\frac{\sigma}{\omega}\frac{\partial\psi}{\partial t} = \gamma\frac{\partial\psi}{\partial T} + \sigma\frac{\partial\psi}{\partial\tau} \qquad (4.38)$$

where

$$\gamma = \frac{12\mu\nu}{p_a}\left(\frac{R}{C}\right)^2 = \frac{\nu}{\omega}\sigma \qquad (4.39)$$

is called the "vibration number" by Pan and Chiang[22], so that

$$\frac{1}{2\ell_1\ell_2}\left\{\frac{\partial}{\partial u_1}\left[\frac{\ell_2}{\ell_1}\left(1+\frac{6m}{\psi}\right)\left(\frac{\partial}{\partial u_1}(H\psi^2)-3\psi^2\frac{\partial H}{\partial u_1}\right)\right]\right.$$
$$\left.+\frac{\partial}{\partial u_2}\left[\frac{\ell_1}{\ell_2}\left(1+\frac{6m}{\psi^2}\right)\left(\frac{\partial}{\partial u_2}(H\psi^2)-3\psi^2\frac{\partial H}{\partial u_2}\right)\right]\right\} = \gamma\frac{\partial\psi}{\partial T}+\sigma\frac{\partial\psi}{\partial\tau} \qquad (4.40)$$

4.2.6 Asymptotic governing equation

Equation (4.40) implies that

$$\frac{\partial\psi}{\partial\tau} = 0\left\{\frac{1}{\sigma},\frac{\gamma}{\sigma}\right\} \qquad (4.41)$$

so for large σ, $\frac{\gamma}{\sigma}\rightarrow 0$ since $\frac{\nu}{\omega}\ll 1$, and

$$\int_t \psi = \psi_\infty(u_1,u_2,T). \qquad (2.42)$$
$$\sigma\rightarrow\infty$$

The governing equation for the asymptotic solution ψ_∞ is obtained by integrating equation (4.40) over one cycle of the squeeze motion, and following the same sort of argument as Pan and Chiang[22], it becomes

$$\frac{1}{2\ell_1\ell_2}\left\{\frac{\partial}{\partial u_1}\left[\frac{\ell_2}{\ell_1}\left(1+\frac{6m}{\psi_\infty}\right)\left(\frac{\partial}{\partial u_1}(H_\infty\psi_\infty^2)-3\psi_\infty^2\frac{\partial H_\infty}{\partial u_1}\right)\right]\right.$$
$$\left.+\frac{\partial}{\partial u_2}\left[\frac{\ell_1}{\ell_2}\left(1+\frac{6m}{\psi_\infty}\right)\left(\frac{\partial}{\partial u_2}(H_\infty\psi_\infty^2)-3\psi_\infty^2\frac{\partial H_\infty}{\partial u_2}\right)\right]\right\} = \gamma\frac{\partial\psi_\infty}{\partial T}. \qquad (4.43)$$

4.2.7 Asymptotic boundary conditions

Equation (4.43) is now in terms only of quantities which vary slowly relative to the squeeze motion. The solution ψ_∞ (independent of τ) cannot satisfy the present boundary conditions (4.32) since H is specifically τ-dependent, so more appropriate boundary conditions must be derived. Near an ambient boundary the vanishing of the right hand side of equation (4.41) must be prevented in the asymptotic limit $\sigma \to \infty$, in which case there is a requirement for

$$\frac{\partial \psi}{\partial u_1} = O\{\sqrt{\sigma}\} \tag{4.44}$$

near $u_1 = \bar{a}$ and $u_1 = \bar{b}$. Thus the boundary regions are appropriately characterised by the stretched co-ordinates

$$\xi_1 = \sqrt{\sigma}\,\left|\,(u_1 - \bar{a})\,\right|$$
$$\xi_2 = \sqrt{\sigma}\,\left|\,(u_1 - \bar{b})\,\right|. \tag{4.45}$$

Only quantities involving ψ will vary appreciably in the boundary region, so that in terms of the edge co-ordinates ξ_i equation (4.40) can be approximated by

$$\frac{H_i}{2\ell_1^2}\left(\frac{\partial^2 \psi_i^2}{\partial \xi_i^2} + 12m\,\frac{\partial^2 \psi_i}{\partial \xi_i^2}\right) = \frac{\partial \psi_i}{\partial \tau} + O\left\{\frac{1}{\sigma},\frac{1}{\sqrt{\sigma}},\frac{1}{\sigma}\right\} \quad (i=1,2) \tag{4.46}$$

where

$$H_1 = H(u_1 = \bar{a},\, u_2,\, T,\, \tau)$$
$$H_2 = H(u_1 = \bar{b},\, u_2,\, T,\, \tau) \tag{4.47}$$

and

$$\psi_1 = \psi(u_1 = \bar{a}, u_2, T, \tau)$$

$$\psi_2 = \psi(u_1 = \bar{b}, u_2, T, \tau) \tag{4.48}$$

are boundary values. Time averaging equation (4.46) over one squeeze cycle,

$$\frac{1}{2\pi} \int_{\tau}^{\tau+2\pi} \frac{H_i}{2\ell_i^2} \left(\frac{\partial^2 \psi_i^2}{\partial \xi_i^2} + 12m \frac{\partial^2 \psi_i}{\partial \xi_i^2} \right) d\tau' = \frac{1}{2\pi} \left\{ \psi_i(\tau+2\pi) - \psi_i(\tau) \right\} + O\left\{ \frac{\gamma}{\sigma}, \frac{1}{\sqrt{\sigma}}, \frac{1}{\sigma} \right\}. \tag{4.49}$$

ψ_i is periodic in τ within $O\left\{\frac{\gamma}{\sigma}\right\}$, so for large σ the right hand side of equation (4.49) can be neglected, and

$$\frac{1}{2\pi} \int_{\tau}^{\tau+2\pi} \frac{H_i}{2\ell_i^2} \left(\frac{\partial^2 \psi_i^2}{\partial \xi_i^2} + 12m \frac{\partial^2 \psi_i}{\partial \xi_i^2} \right) d\tau' = 0. \tag{4.50}$$

Boundary conditions in terms of the stretched co-ordinates are

$$\psi_i(\xi_i = 0) = H_i \qquad i = 1, 2$$

$$\psi_1(\xi_1 \to \infty) = \psi_\infty(u_1 = \bar{a})$$

$$\psi_2(\xi_2 \to \infty) = \psi_\infty(u_1 = \bar{b}). \tag{4.51}$$

Equation (4.50) can be double integrated with respect to ξ_i to give

$$\frac{1}{2\pi} \int_{\tau}^{\tau+2\pi} \frac{H_i}{2\ell_i^2} \left(\psi_i^2 + 12m\psi_i \right) d\tau' = C_1 \xi_i + C_2 \tag{4.52}$$

and when $\xi_i = 0$, equations (4.51) give

$$\frac{1}{2\pi} \int_{\tau}^{\tau+2\pi} \frac{H_i}{2\ell_i^2} \left(H_i^2 + 12m H_i \right) d\tau' = C_2. \tag{4.53}$$

As $\xi_i \to \infty$, C_1 must vanish to ensure that the left hand

side of equation (4.52) remains finite, and

$$\frac{1}{2\pi}\int_{\tau}^{\tau+2\pi} \frac{H_i}{2\ell_1^2}\left(\psi_\infty^2 + 12m\,\psi_\infty\right) d\tau' = \frac{1}{2\pi}\int_{\tau}^{\tau+2\pi} \frac{H_i}{2\ell_1^2}\left(H_i^2 + 12m\,H_i\right) d\tau'. \qquad (4.54)$$

The left hand side represents conditions just outside the boundary region at $\xi_i \rightarrow \infty$, and so becomes

$$H_\infty\left(\psi_\infty^2 + 12m\,\psi_\infty\right) = \frac{1}{2\pi}\int_{\tau}^{\tau+2\pi}\left(H_i^3 + 12m\,H_i^2\right) d\tau' \qquad (4.55)$$

or

$$\left(\psi_\infty^2 + 12m\,\psi_\infty\right)_i = \frac{A_i}{H_\infty} \qquad (4.56)$$

where

$$A_i = \frac{1}{2\pi}\int_{\tau}^{\tau+2\pi}\left(H_i^3 + 12m\,H_i^2\right) d\tau' \qquad i = 1,2 \ . \qquad (4.57)$$

Solving the quadratic equation for ψ_∞ at the two boundaries,

$$\psi_\infty(u_1 = \bar{a}) = -6m + \sqrt{36m^2 + \frac{A_1}{H_\infty}} \qquad (4.58)$$

$$\psi_\infty(u_1 = \bar{b}) = -6m + \sqrt{36m^2 + \frac{A_2}{H_\infty}} \qquad (4.59)$$

where the positive root has been taken, since the negative one has no physical significance. Equations (4.58) and (4.59) now provide the required boundary conditions on the governing equation (4.43) for the asymptotic solution ψ_∞.

In the absence of the externally imposed disturbing

frequency ($\gamma = 0$), the right hand side of equation (4.43) vanishes and it reduces to the normal steady state equation formulated by Pan[17], modified by the slip flow factor $(1+\frac{6m}{\psi_\infty})$. In the additional absence of slip flow (m = 0) the governing equation and its boundary conditions (4.58) and (4.59) reduce precisely to the expressions derived by Pan[17].

4.2.8 Governing equations for the edge region

Damping in the film due to the squeeze motion is confined to the boundary region where incompressible flow in and out of the film takes place, and it is interesting to see if the presence of slip flow modifies the situation in this respect. To do this, it is assumed that

$$\psi_i(u_1,u_2,T,\tau) = \psi_\infty(u_1,u_2,T) + \psi_e(u_1,u_2,\tau) \qquad (4.60)$$
$$i = 1,2$$

where the edge correction ψ_e only assumes an appreciable magnitude near a boundary. In other words, ψ_e varies with the stretched edge co-ordinate ξ_i near boundaries i = 1,2 while ψ_∞ does not vary with ξ_i. Thus

$$\frac{\partial\psi_i}{\partial u_1} = \frac{\partial\psi_\infty}{\partial u_1} + \sqrt{\sigma}\,\frac{\partial\psi_e}{\partial\xi_i} \qquad (4.61)$$

and

$$\frac{\partial^2\psi_i}{\partial u_1^2} = \frac{\partial^2\psi_\infty}{\partial u_1^2} + \sigma\,\frac{\partial^2\psi_e}{\partial\xi_i^2}. \qquad (4.62)$$

Equation (4.46) becomes

$$\frac{H_i}{2\ell_i^2}\left\{\frac{\partial^2 \psi_e^2}{\partial \xi_i^2} + 2(\psi_\infty + 12m)\frac{\partial^2 \psi_e}{\partial \xi_i^2}\right\} = \frac{\partial \psi_e}{\partial \tau} + O\left\{\frac{1}{\sigma}, \frac{1}{\sqrt{\sigma}}, \frac{1}{\sigma}\right\}. \qquad (4.63)$$

From equation (4.62)

$$\frac{\partial^2 \psi_e}{\partial \xi_i^2} = O\left\{\frac{1}{\sigma}\right\} \qquad (4.64)$$

so equation (4.63) in the limit of $\sigma \to \infty$ becomes

$$\frac{H_i}{2\ell_i^2}\cdot\frac{\partial^2 \psi_e^2}{\partial \xi_i^2} = \frac{\partial \psi_e}{\partial \tau} \qquad (4.65)$$

subject to boundary conditions

$$\left.\begin{array}{l} \psi_e(\xi_i = 0) = H_i - \psi_\infty(\xi_i = 0) \\ \psi_e(\xi_i \to \infty) = 0 \end{array}\right\} \quad i = 1, 2. \qquad (4.66)$$

The diffusion type equation (4.65) is exactly the same as
that derived by Pan[17], but the value of ψ_∞ at $\xi_i = 0$ will
be modified in the boundary conditions (4.66) through the
relationships (4.58) and (4.59) which involve the Knudsen
number m. So the damping will be affected by slip flow,
although its magnitude will remain $O\left\{\frac{1}{\sqrt{\sigma}}\right\}$.
Equation (4.43) together with the boundary conditions
(4.58) and (4.59) now formulates any forced dynamic or
static squeeze-film problem satisfying the criteria for
validity discussed in section 4.1, and allows for the effect
of slip flow. Any particular problem can be treated by
substituting the appropriate non-dimensional co-ordinates
in place of the generalised co-ordinates u_1 and u_2, and
specifying the film thickness H_∞.

4.3 Discussion on solution methods

Equation (4.43) is not in general easy to solve, even with no slip flow (m = 0), but the presence of the slip flow terms complicates the issue considerably. Formally, under slip flow conditions the gas behaves as if the viscosity has an effective non-dimensional value

$$\bar{\mu} = \frac{1}{\left(1 + \frac{6m}{\psi_\infty}\right)} \tag{4.67}$$

so that equation (4.43) can be more conveniently written in the form

$$\frac{1}{2\ell_1\ell_2}\left\{\frac{\partial}{\partial u_1}\left[\frac{\ell_2}{\bar{\mu}\ell_1}\left(\frac{\partial}{\partial u_1}(H_\infty\psi_\infty^2) - 3\psi_\infty^2\frac{\partial H_\infty}{\partial u_1}\right)\right]\right.$$
$$\left. + \frac{\partial}{\partial u_2}\left[\frac{\ell_1}{\bar{\mu}\ell_2}\left(\frac{\partial}{\partial u_2}(H_\infty\psi_\infty^2) - 3\psi_\infty^2\frac{\partial H_\infty}{\partial u_2}\right)\right]\right\} = \gamma\frac{\partial\psi_\infty}{\partial T} \tag{4.68}$$

where for no slip flow $\bar{\mu}$ = 1. This equation is similar to that for the dynamic operation of the self-acting bearing, and Hsing and Chiang[44] discussed a special finite difference scheme for solving the equation numerically for the case of a high speed tilting pad bearing. However, apart from mentioning that numerical solution methods do exist, it is not proposed to pursue slip flow effects in depth in this work and most of the time we will be concerned with the case $\bar{\mu}$ = 1. An analytic solution will be obtained for the flat disc squeeze-film bearing to show the magnitude of the effect of slip flow, and this will be used to estimate the effect in grooved journal bearings, but otherwise we will neglect it and design experiments to avoid it.

Equation (4.68) with $\bar{\mu} = 1$ (no slip flow) and $\zeta = 0$ (static conditions), subject to the boundary conditions (4.58) and (4.59) has been used to obtain static solutions for all the commonly used smooth bearing geometries, namely the cylindrical journal[16, 26, 28, 29, 36], conical[17], hemispherical[19, 24], and flat thrust plate[28]. Most of these solutions use small perturbation analyses on displacements away from the nominal centred position, and finite difference numerical methods for larger displacements.

The dynamic equation (4.68) with $\bar{\mu} = 1$ and $\zeta \neq 0$ has only been treated in two papers to date[21, 22], but the perturbation solution method of reference[22] would seem to be appropriate to the present work. Before Elrod's extension of the asymptotic theory to cover dynamic operation[21], the dynamic behaviour investigated was mainly of the self-induced variety (references 20 and 25 and, more recently, 31). These, again, employed small perturbation techniques, and use was made of the Mathieu equation in references 20 and 30 to obtain stability boundaries.

Castelli and Pirvics[45], in a review of modern numerical methods, presented a variety of solution techniques, each having particular advantages depending on the application. For the time-independent problem ($\zeta = 0$), the column-wise influence coefficients method of Castelli[63] appears to be most suitable, involving considerable savings in computation time over relaxation methods, and considerable savings in computer storage compared with direct inversion methods. One of the main advantages of the method is in the exactness of the solution, and although numerical

instabilities can occur because of a mismatch between the finite difference equations and the differential equations they are meant to approximate, the situation can normally be improved by increasing the number of finite difference grid points, at the cost of increased computer storage and time requirements. The method is also widely applicable to problems outside the field of gas lubrication. Although differing in detail, the column method is to all intents and purposes the same as a matrix product method which has been in use at RAE (Farnborough) for some years[48], and which was used by Faddy[49] in his investigation of spiral grooved conical self-acting gyroscope spin bearings. The present writer had already gained a certain amount of confidence and familiarity with this version of the method, and had developed computer subroutines, so it was decided to retain the matrix product method in dealing with the static behaviour of squeeze-film bearings.

For the forced dynamic performance it was decided to use the semi-analytic perturbation treatment of Pan and Chiang[22] for small eccentricities and small vibration amplitudes which are of interest in inertial navigation instruments. This method reduces the amount of computer time needed by treating the static performance analytically and leaving the complex dynamic equation to be dealt with numerically. The static solution provides a valuable check for the numerical solution obtained by the matrix product method discussed above. Attempts to solve the dynamic equation analytically are usually foiled by the complexity of the coefficients required to satisfy the boundary

conditions, so one is forced to resort to the computer to obtain the effective dynamic stiffness and damping in the bearing. It has been found that the complex dynamic equation can be reduced to a system of two simultaneous ordinary differential equations which can be solved by a matrix method to be described later. This semi-analytic treatment is especially suitable for grooved bearings, where each segment has to be dealt with separately and the results summed to obtain the total dynamic bearing force. By confining the computation to the time-dependent aspect of the solution, considerable savings in computer storage and time are achieved.

To deal with dynamic behaviour at large eccentricities the step-jump method has considerable attractions in the context of the present work. Although it has not previously been applied to squeeze-film gas bearings, it was used to treat the self-acting journal bearing by means of an orbit program[46], and flexibly mounted externally-pressurised bearings[47] by means of a growth factor, to study stability. The great benefit in treating grooved squeeze-film bearings lies in the fact that the gas film details are solved only once for a particular eccentricity, and thereafter the dynamic parameters (mass and forcing frequency) can be varied over and over again without having to re-solve Reynolds' equation on each occasion, thus saving a large amount of computer time. The drawback of the step-jump method is that the assumption of linearity of the response with respect to the applied stimulus means that the solution must still be restricted to small amplitude motions, although the eccentricity is not restricted. It

is also difficult to separate out directly the stiffness and damping components of the dynamic force if these are explicitly required.

Both the semi-analytic perturbation and step-jump methods are amenable to stability and vibration response investigations, while the step-jump method is quite flexible in that extra perturbation effects, such as angular degrees of freedom, can be introduced without excessive programming complications.

5. ESTIMATES OF SLIP-FLOW EFFECT

When the molecular mean free path of the gas becomes comparable with the film thickness C, the Poiseuille flow between two surfaces (as in the edge region of the squeeze-film) takes on the structure indicated in Fig.18 . The laminar flow region, away from the surfaces, is characterised by a Maxwellian mass distribution, while in the boundary layer slip flow regions near the surfaces the mass distribution is no longer Maxwellian because collisions between gas molecules and the surfaces involve a different reflection coefficient from that which occurs when two gas molecules collide. Normally, in total laminar flow when $\lambda \ll C$ the slip flow regions are so narrow that their presence can be disregarded and the flow takes on its parabolic velocity distribution with zero velocity at the two surfaces (Fig.19). When the molecular mean free path becomes significant, $\lambda \sim C$, the velocity distribution is still parabolic, but slip occurs at the surfaces and the velocity distribution behaves as if the velocity drops to zero some small distance outside the film (Fig.19). Velocity gradients through the thickness of the film are reduced, so the shear forces opposing flow are reduced and the bearing cannot sustain as great a film pressure as in the case without slip flow. Consequently the load capacity is impaired.

As far as is known, slip-flow in squeeze-film gas bearings has not been treated in the literature. The intention here is not to explore the effect in any great detail, but to obtain an indication of its importance by

considering relatively simple cases where analytic solutions are possible.

5.1 Circular flat thrust bearing

To obtain an estimate for the amount of degradation in load capacity to be expected in squeeze-film bearings, the flat disc thrust bearing will be investigated, as the simple geometry results in an analytic solution being found.

Consider, then, a flat disc of radius R supported on a film of mean thickness h_o driven by a surface vibrating with an angular frequency ω under static loading conditions ($\zeta = 0$). The instantaneous film thickness is given by

$$h = (h_o + e_1 C \cos \omega t)$$ (5.1)

where C is some reference dimension, and e_1 the excursion ratio. In non-dimensionalised terms

$$H = \frac{h}{C} = (H_\infty + e_1 \cos \tau)$$ (5.2)

where $\tau = \omega t$, and the time averaged film thickness is

$$H_\infty = \frac{1}{2\pi} \int_0^{2\pi} H \, d\tau = \frac{h_o}{C} .$$ (5.3)

It is appropriate to use polar co-ordinates (r, θ), such that an element of area is $r \delta\theta . \delta r$. Normalising distances in the radial and circumferential directions with respect to R, the normalised elemental area becomes

$\bar{r} \delta\theta.\delta\bar{r}$, where $\bar{r} = r/R$, so in the generalised governing equation (4.43) we use $u_1 = \bar{r}$, $u_2 = \theta$, $h_1 = 1$, $h_2 = \bar{r}$. Since the discs are parallel and the excursion is uniform, all film effects will be independent of θ, so the governing equation reduces to

$$\frac{d}{d\bar{r}} \left\{ \bar{r} \left(1 + \frac{6m}{\psi_\infty} \right) \frac{d\psi_\infty^2}{d\bar{r}} \right\} = 0 \qquad (5.4)$$

which is subject to the boundary condition given by equation (4.58),

$$\psi_\infty(\bar{r} = 1) = -6m + \sqrt{36m^2 + \frac{A(\bar{r} = 1)}{H_\infty}} \qquad (5.5)$$

together with the symmetry condition

$$\left. \frac{d\psi_\infty}{d\bar{r}} \right|_{\bar{r} = 0} = 0 \qquad (5.6)$$

where

$$A(\bar{r}) = \frac{1}{2\pi} \int_0^{2\pi} (H^3 + 12mH^2) d\tau = (H_\infty^3 + 12mH_\infty^2) + \frac{3}{2} e_1^2 (H_\infty + 4m) \qquad (5.7)$$

so that equation (5.5) becomes

$$\psi_\infty(\bar{r} = 1) = -6m + \sqrt{(H_\infty + 6m)^2 + \frac{3}{2} e_1^2 \left(1 + \frac{4m}{H_\infty} \right)} \quad . \qquad (5.8)$$

To solve equation (5.4), integrate with respect to $\bar{r}$, and rearrange to give

$$\left(\psi_\infty + 6m \right) \frac{d\psi_\infty}{d\bar{r}} = \frac{\text{constant}}{\bar{r}} \quad . \qquad (5.9)$$

The only way in which condition (5.6) can be satisfied
is if the constant vanishes, so

$$\left(\psi_\infty + 6m\right)\frac{d\psi_\infty}{d\bar{r}} = 0 \ . \tag{5.10}$$

In general ($\psi_\infty + 6m) \neq 0$, so

$$\frac{d\psi_\infty}{d\bar{r}} = 0 \tag{5.11}$$

and consequently

$$\psi_\infty = \text{constant.} \tag{5.12}$$

Hence, in order to satisfy boundary condition (5.8),

$$\psi_\infty = -6m + \sqrt{\left(H_\infty + 6m\right)^2 + \frac{3}{2}e_1^2\left(1 + \frac{4m}{H_\infty}\right)} \ . \tag{5.13}$$

To show that slip flow ($m > 0$) always results in a
loss of bearing pressure, expand ψ_∞ for small excursion
ratios ($e_1 \ll 1$) so that

$$\psi_\infty = 1 + \frac{3}{4}\left(\frac{1 + 4m}{1 + 6m}\right)e_1^2 + O\{e_1^4\} \tag{5.14}$$

where $H_\infty = 1$ for simplicity. The time averaged film
pressure is

$$\bar{P} = \frac{1}{2\pi}\int_0^{2\pi} P\,d\tau = \frac{1}{2\pi}\int_0^{2\pi}\frac{\psi_\infty}{H}\,d\tau = \frac{\psi_\infty}{\sqrt{1 - e^2}} \tag{5.15}$$

which can in turn be expanded in terms of e_1^2 to give

$$\bar{P} = 1 + \frac{1}{2}e_1^2 + \frac{3}{4}\left(\frac{1+4m}{1+6m}\right)e_1^2 + O\{e_1^4\} . \qquad (5.16)$$

When m = 0 we immediately recognise the expression derived in equation (3.72) when non-uniform excursion was being discussed, so it can be seen that when $m \neq 0$ slip flow alters the dominant edge effect term. This is not surprising as the slip flow will be confined to the edge region where incompressible Poiseuille type flow occurs in and out of the film. The interior Boyle's Law behaviour will not be changed. Since

$$\left(\frac{1+4m}{1+6m}\right) \leqslant 1 \qquad (5.17)$$

it follows that, if $O\{e_1^4\}$ terms are ignored, the pressurising effect of the boundary will be reduced for $m > 0$ and the overall load capacity will suffer.

Typically, a squeeze-film thrust bearing might have a nominal clearance of $C \sim 2$ microns, operating with helium gas at a pressure of one atmosphere, in which case the mean free path will be $\lambda_a \sim 0.18$ micron, so an estimate for the Knudsen number is m = 0.1. The effective mean pressure generated in the film is

$$\bar{P} - 1 = \frac{\psi_\infty}{\sqrt{1-e_1^2}} - 1 \qquad (5.18)$$

where ψ_∞ is given by equation (5.13) with $H_\infty = 1$. For m = 0.1 and e_1 = 0.5 the effective pressure is $(\bar{P} - 1)$ = 0.336, compared with $(\bar{P} - 1)$ = 0.354 when m = 0, so it can be seen that in this case there will be about 5% loss in

load capacity because of slip flow.

5.2 Grooved journal bearing

The influence of slip flow in squeeze-film journal bearings can be investigated with the help of the previously derived solution for the thrust bearing, provided the journal is sufficiently grooved for the pressure to behave locally like the ideal "flat plate" distribution.

Assume a film thickness as given by equation (5.2), but this time let

$$H_\infty = 1 - e_2 \cos \theta \qquad (5.19)$$

where e_2 is the eccentricity. Using this, the time averaged pressure distribution will be

$$\bar{P} = \frac{\psi_\infty}{\sqrt{H_\infty^2 - e_1^2}} \qquad (5.20)$$

where ψ_∞ is given by equation (5.13). The time averaged non-dimensional lift per unit length of the bearing will be

$$W_L = \frac{W_L'}{p_a D} = \frac{1}{2} \int_0^{2\pi} (\bar{P} - 1) \cos \theta \, d\theta . \qquad (5.21)$$

For small values e_1^2 and e_2, the pressure can be expanded in the form

$$\bar{P} \simeq \left\{ 1 + \frac{1}{2} e_1^2 + \frac{3}{4} \frac{(1 + 10m + 24m^2)}{(1 + 6m)^2} \right\} + e_1^2 e_2 \cos \theta \left\{ 1 + \frac{3}{2} \frac{(1 + 9m + 24m^2)}{(1 + 6m)^2} \right\}.$$

$$(5.22)$$

Using this expression, the lift per unit length becomes

$$W_L \simeq -\frac{\pi}{2} e_1^2 e_2 \left\{ 1 + \frac{3}{2} \left(\frac{1 + 9m + 24m^2}{1 + 12m + 36m^2} \right) \right\} . \qquad (5.23)$$

If this is compared with the Beck and Strodtman result[26], equation (3.28), where the term involving L/D represents the edge pressurising effect, it can be seen that the presence of slip flow again affects the pressurising effect of the edge and does not change the interior behaviour of the film. Since

$$\left(\frac{1 + 9m + 24m^2}{1 + 12m + 36m^2} \right) \leqslant 1 \qquad (5.24)$$

it follows that the edge pressurising effect will be degraded, as in the case of the thrust bearing.

Taking a typical example of nominal clearance $C \sim 2$ microns, employing helium gas at pressure of one atmosphere ($\lambda_a \sim 0.18$ micron), so that $m \simeq 0.1$, we obtain

$$W_L \simeq -2.254 \left(\frac{\pi}{2} e_1^2 e_2 \right)$$

compared with

$$W_L \simeq -2.5 \left(\frac{\pi}{2} e_1^2 e_2 \right)$$

when m = 0, from which it can be seen that there is a 9.4% loss in load capacity when the excursion ratio and eccentricity are small. This estimate will probably also be representative for the journal aspect of conical and hemispherical squeeze-film bearings.

5.3 Comments on slip-flow

These two cases show that the load capacity of squeeze-
film gas bearings can be substantially reduced if they are
operated under conditions where the molecular mean free
path of the gas is appreciable compared with the nominal
film thickness. The presence of slip-flow is seen to
diminish the edge pressurising effect, while the interior
Boyle's Law behaviour remains unaffected, so we can expect
degraded performance particularly in journal bearings where
the edge effect is the dominant source of the load capacity.
This occurs when the circumferential leakage flow is a
minimum and the full value of the edge pressure is
experienced along the entire axial length of the bearing,
as when L/D is small or there are a sufficient number of
grooves. It appears that a round figure of 10% might be
typical of the loss in load capacity to be expected in
grooved journal bearings unless care is taken, and this
would probably apply to the journal aspect of grooved
hemispherical and conical bearings as well. The thrust
aspect of the load capacity in the latter two types of
bearing will be degraded by about 5%.

Having shown that slip flow constitutes an appreciable
problem which should be taken account of in design work,
it is not intended to pursue the effect further and in the
rest of this work it will be assumed that $m \ll 1$, or more
specifically, that $m \leqslant 0.01$.

6. THEORETICAL ANALYSES

Using the asymptotic theory set up in section 4, we will now perform more rigorous analyses on segmented squeeze-film bearings so that the simplified treatment of section 3 can be more confidently accepted.

The flat disc bearing will be considered first. Although the static performance will not be affected to any great extent by the introduction of ambient line boundaries, the forced response should change considerably as the number of segments is increased.

This is followed by the infinite length axially grooved journal bearing, which is shown to be a good approximation to the finite length axially grooved journal for $L/D \gtrsim 1$, and the finite length ungrooved journal, which also embraces the circumferentially grooved journal bearing.

Most of the analysis will depend on perturbation theory for small eccentricity and small vibration amplitude, depending on the context, as this covers the bulk of applications of interest to the present writer, but methods are outlined for treating large values of eccentricity and vibration amplitude.

6.1 Flat annular thrust segment

While the static behaviour of flat squeeze-film thrust bearings is well known[1,2,10], and the self-induced response has been investigated[2,31], the forced response has not been treated explicitly, although certain broad statements have been made in other contexts[22,52]. The forced response of an annular squeeze-film bearing segment is of interest

in the present work as one can envisage a thrust bearing
composed of a number of concentric annular segments
separated by circular ambient line boundaries. Such a
bearing would be relatively easy to manufacture compared
with a journal bearing, and would lend itself to empirical
investigations of the effect of grooving on dynamic
behaviour.

Consider, then, an annular region $0 \leqslant \theta \leqslant 2\pi$,
$r_1 \leqslant r \leqslant r_2$, expressed in terms of polar co-ordinates (r, θ),
with ambient pressure boundaries at $r = r_1$ and $r = r_2$. If
the spatial variables are normalised with respect to the
radial width of the annulus, the normalised polar co-
ordinates are $\bar{r} = r/(r_2 - r_1)$ and θ . The normalised film
thickness is

$$H = \frac{h}{C} = H_\infty + e_1 \cos \tau \qquad (6.1)$$

where H_∞ is quasi-static relative to the squeeze motion,

$$H_\infty = \frac{1}{2\pi} \int_0^{2\pi} H \, d\tau = \text{Real}\left\{ 1 + \delta e^{iT} \right\} \qquad (6.2)$$

and where $\tau = \omega t$ and $T = \nu t$. ω and ν are the angular
frequencies respectively of the squeeze motion and of the
forced response, e_1 is the excursion ratio, and δ is the
forced response amplitude.

Setting $\ell_1 = \bar{r}$, $u_1 = \theta$, $\ell_2 = 1$, $u_2 = \bar{r}$, $\bar{\mu} = 1$ in
equation (4.68), and noting that both H_∞ and ψ_∞^2 are
independent of θ (for a parallel film), the governing
equation becomes

$$\frac{1}{\bar{r}}\left\{\frac{\partial}{\partial\bar{r}}\left[\bar{r}\frac{\partial}{\partial\bar{r}}(H_\infty\psi_\infty^2)\right]\right\} = 2\gamma_\ell\frac{\partial\psi_\infty}{\partial T} \qquad (6.3)$$

where γ_ℓ is the local vibration number for the annular segment, based on the radial width $(r_2 - r_1)$,

$$\gamma_\ell = \frac{12\mu\nu}{P_a}\left(\frac{r_2-r_1}{C}\right)^2 = \left(\frac{r_2-r_1}{R}\right)^2\gamma. \qquad (6.4)$$

Here, γ is a global vibration number based on some arbitrary radius R such that $r_1 < r_2 \leqslant R$.

Applying perturbation theory for small response amplitudes ($\delta \ll 1$), we expand ψ_∞^2 in terms of δ,

$$\psi_\infty^2(\bar{r}) = Q_o + \delta e^{iT}Q_2 + O\{\delta^2\}. \qquad (6.5)$$

The boundary conditions (equations (4.58) and (4.59)) at $\bar{r} = \bar{r}_1 = r_1/(r_2 - r_1)$ and $\bar{r} = \bar{r}_2 = r_2/(r_2 - r_1)$ are

$$\psi_\infty^2 = H_\infty^2 + \tfrac{3}{2}e_1^2 \simeq 1 + \tfrac{3}{2}e_1^2 + 2\delta e^{iT} \qquad (6.6)$$

so that

$$\left.\begin{array}{l} Q_o = 1 + \tfrac{3}{2}e_1^2 \\ Q_2 = 2 \end{array}\right\} \text{ at } \bar{r} = \bar{r}_1 \text{ and } \bar{r} = \bar{r}_2. \qquad (6.7)$$

Using the expressions (6.2) and (6.5) for H_∞ and ψ_∞^2 in equation (6.3) and ignoring terms $O\{\delta^2\}$, the following perturbation equations result:

$$\frac{d}{d\bar{r}}\left(\bar{r}\,\frac{dQ_0}{d\bar{r}}\right) = 0 \tag{6.8}$$

$$\frac{d^2 Q_2}{d\bar{r}^2} + \frac{1}{\bar{r}}\frac{dQ_2}{d\bar{r}} - i\left(\frac{r_2 - r_1}{R}\right)^2 \frac{\gamma}{\sqrt{Q_0}}\,Q_2 = 0 \tag{6.9}$$

subject to boundary conditions (6.7).

The zero-order equation (6.8) has the well known solution

$$Q_0 = 1 + \frac{3}{2}\,e_1^2 \tag{6.10}$$

which can be used to obtain the static pressure distribution in the absence of the forced vibration ($\delta = 0$).

By writing

$$K_1^2 = -i\left(\frac{r_2 - r_1}{R}\right)^2 \frac{\gamma}{\sqrt{Q_0}} \tag{6.11}$$

$$z = K_1 \bar{r} \tag{6.12}$$

the first order equation (6.9) can be reduced to

$$\frac{d^2 Q_2}{dz^2} + \frac{1}{z}\cdot\frac{dQ_2}{dz} + Q_2 = 0 \tag{6.13}$$

which is a Bessel equation whose general solution is the cylinder function

$$Q_2(z) = A J_0(z) + B Y_0(z) \tag{6.14}$$

where $J_o(z)$ and $Y_o(z)$ are respectively Bessel functions of the first and second kinds. However, evaluation of the constants A and B so as to satisfy the boundary conditions (6.7) results in exceedingly complicated expressions when one attempts to separate out the real and imaginary components of Q_2, rendering this solution virtually useless.

A more helpful approach is to resort to a numerical method. By writing $K_2 = iK_1{}^2$ and

$$Q_2 = u + iv \qquad (6.15)$$

equation (6.9) can be reduced to a system of two simultaneous second-order ordinary differential equations

$$\frac{d^2u}{d\bar{r}^2} + \frac{1}{\bar{r}}\frac{du}{d\bar{r}} + K_2 v = 0 \qquad (6.16)$$

$$\frac{d^2v}{d\bar{r}^2} + \frac{1}{\bar{r}}\frac{dv}{d\bar{r}} - K_2 u = 0 \qquad (6.17)$$

subject to the boundary conditions u = 2 and v = 0 at $\bar{r} = \bar{r}_1$ and $\bar{r} = \bar{r}_2$. This system of equations can then be approximated by finite difference equations and solved by the matrix method given in Appendix A.

The film pressure is

$$P = \frac{\psi_{\phi}}{H} \qquad (6.18)$$

which, time averaged over a cycle of the squeeze motion, becomes

$$\bar{P} = \frac{1}{2\pi} \int_0^{2\pi} P \, d\tau = \frac{\psi_\infty}{\sqrt{1 - e_1^2}} .$$

(6.19)

Substituting for H_∞ and ψ_∞ from equations (6.2) and (6.5), to first order in δ we have

$$\bar{P} = \sqrt{\frac{Q_0}{1 - e_1^2}} \left\{ 1 + \delta \cos T \left[\frac{u}{2Q_0} - \frac{1}{(1 - e_1^2)} \right] - \delta \sin T . \frac{v}{2Q_0} \right\} .$$

(6.20)

6.1.1 Force in segment

The force generated by the film pressure is

$$F' = \int_{r_1}^{r_2} (\bar{P} - 1) p_a . 2\pi r \, dr$$

(6.21)

which, for convenience, will be normalised with respect to $p_a \pi R^2$,

$$F = \frac{F'}{p_a \pi R^2} = \left(\frac{r_2 - r_1}{R} \right)^2 \int_{\bar{r}_1}^{\bar{r}_2} 2(\bar{P} - 1) \bar{r} \, d\bar{r} .$$

(6.22)

On inserting the expression (6.20) for $\bar{P}$ the force can be separated into three components,

$$F = F_0 + F_1 \cos T + F_2 \sin T$$

(6.23)

where

$$F_0 = \frac{F_0'}{p_a \pi R^2} = \left(\frac{r_2 - r_1}{R} \right)^2 (\bar{r}_2^2 - \bar{r}_1^2) \left\{ \sqrt{\frac{Q_0}{1 - e_1^2}} - 1 \right\}$$

(6.24)

$$F_1 = \frac{F_1{'}}{p_a \pi R^2} = \delta \left(\frac{r_2 - r_1}{R}\right)^2 \sqrt{\frac{Q_0}{1 - e_1^2}} \left\{ \frac{1}{Q_0} \int_{\bar{r}_1}^{\bar{r}_2} u\bar{r}\, d\bar{r} - \left(\frac{\bar{r}_2^2 - \bar{r}_1^2}{1 - e_1^2}\right) \right\} \qquad (6.25)$$

$$F_2 = \frac{F_2{'}}{p_a \pi R^2} = -\frac{\delta}{Q_0} \left(\frac{r_2 - r_1}{R}\right)^2 \sqrt{\frac{Q_0}{1 - e_1^2}} \int_{\bar{r}_1}^{\bar{r}_2} v\bar{r}\, d\bar{r} \,. \qquad (6.26)$$

F_0 is the familiar static force which would be observed in the absence of any externally applied disturbance ($\delta = 0$), the bearing force per unit area being a constant for a given value of e_1. F_1 and F_2 are respectively the in-phase and quadrature components of the dynamic force arising from a non-zero value for δ.

6.1.2 Dynamic stiffness of segment

By dividing the dynamic force components by $(-\delta)$, the in-phase (S_1) and quadrature (S_2) components of the dynamic stiffness may be obtained, namely

$$S_1 = \frac{C}{p_a \pi R^2} S{'} = \left(\frac{r_2 - r_1}{R}\right)^2 \sqrt{\frac{Q_0}{1 - e_1^2}} \left\{ \left(\frac{\bar{r}_2^2 - \bar{r}_1^2}{1 - e_1^2}\right) - \frac{1}{Q_0} \int_{\bar{r}_1}^{\bar{r}_2} u\bar{r}\, d\bar{r} \right\} \qquad (6.27)$$

$$S_2 = \frac{C}{p_a \pi R^2} S_2{'} = \frac{1}{Q_0} \left(\frac{r_2 - r_1}{R}\right)^2 \sqrt{\frac{Q_0}{1 - e_1^2}} \int_{\bar{r}_1}^{\bar{r}_2} v\bar{r}\, d\bar{r} \,. \qquad (6.28)$$

6.1.3 Dynamic behaviour of segmented thrust bearing

By adding together a number w of such segments we are able to construct a complete thrust bearing composed of concentric annular segments separated by ambient line boundaries.

Consider such a bearing with, for discussional purposes, an inner to outer radius ratio of $R_o = 0.2$. Let the outer radius be R_1 and define the basic smooth bearing as consisting of a single segment ($w = 1$). This will be compared with a bearing of the same overall geometry but having different numbers of segments, as shown in Fig.20.

If S_1 and S_2 now refer to the stiffness components of the combined bearing, rather than to the contributions of a particular segment, their variation with the vibration number γ is shown in Fig.21 for $w = 1,2,4,8$ and $e_1 = 0.5$. For brevity, S_2 will be refered to as the 'damping', although it is really the 'damping force per unit displacement'. The stiffness is seen to increase monotonically from the static value, levelling off asymptotically for large γ to a value approximately twice that of the static stiffness, while the 'damping' increases linearly with γ for small γ, reaches a peak, and then decreases gradually as γ becomes large. The effect of segmenting the bearing is to delay the increase in dynamic stiffness, and to shift the peak in damping to higher values of γ. In fact, for $w = 8$, the peak damping occurs at the extreme top end of the scale of interest for γ, and the dynamic stiffness has only reached half its asymptotic rise. The peak value of damping is independent of the number of segments since the assumption of line boundaries separating segments implies that the total bearing area is the same in all cases. The shift in the peak damping towards higher values of γ for increasing w is understandable in that a reduction in the segment radial width allows higher radial velocities to be

accommodated in the film before limiting compressibility effects begin to dominate. In the region to the left of a damping peak, the radial flow in the film as a result of a non-zero value of δ is predominantly incompressible, with damping increasing linearly with γ . The damping peak represents the region where compressibility has increased to a significant level and the film is stiffening rapidly. To the right of the damping peak compressibility dominates and a second squeeze-film bearing effect becomes super-imposed on the basic squeeze-film associated with σ . The "incompressible" edge regions of this second squeeze-film, where the damping takes place, have a radial extent $0\left\{\frac{1}{\sqrt{\gamma}}\right\}$, so as γ becomes large the damping shrinks to zero and the dynamic stiffness levels off to add to the σ - dependent basic static stiffness of the film.

6.1.4 Vibration response

To observe the response of a supported mass m to an externally imposed vibrational force

$$F'_{ext.} = p_a \pi R^2. \, Real\left\{f e^{i\nu t}\right\} \tag{6.29}$$

it is convenient to use the method employed by Pan and Chiang[22] in their work on the spherical squeeze-film hybrid bearing. If the dynamic force in the film is

$$F'_{dyn} = p_a \pi R^2. \, Real\left\{\delta e^{i\nu t}(S_1 - i S_2)\right\} \tag{6.30}$$

and the response displacement amplitude of the supported

mass is

$$x = C \cdot \text{Real} \{\delta e^{ivt}\} .$$

(6.31)

The equation of motion of the system is

$$m \ddot{x} + F'_{dyn.} = F'_{ext.} .$$

(6.32)

Substituting for x, $F'_{dyn.}$ and $F'_{ext.}$ from equations (6.29), (6.30), and (6.31) in equation (6.32), and defining the dimensionless mass M_1 by

$$M_1 = \frac{m P_a}{144 \pi \mu^2 R} \left(\frac{C}{R}\right)^5$$

(6.33)

the following expression for the dimensionless dynamic compliance can be obtained:

$$\frac{\delta}{f} = \frac{1}{(S_1 - M_1 \gamma^2) - i S_2} = \delta_1 e^{i\alpha}$$

(6.34)

where the amplitude and phase are

$$\delta_1 = \frac{P_a \pi R^2}{C} \cdot \delta_1' = \frac{1}{\sqrt{(S_1 - M_1 \gamma^2)^2 + S_2^2}}$$

(6.35)

and

$$\alpha = \tan^{-1} \frac{S_2}{(S_1 - M_1 \gamma^2)} .$$

(6.36)

The vibration number γ is as defined in equation (4.39).

Because the clearance ratio C/R appears raised to the

fifth power in equation (6.33) the dimensionless mass is usually a very small number. Typically, a bearing might have the following characteristics:

$$R \simeq 0.05 m.$$

$$m \simeq 1 \ kg$$

$$c \simeq 5 \times 10^{-6} m$$

$$p_a \simeq 10^5 \ N/m^2$$

$$\mu \simeq 2 \times 10^{-5} \ Ns/m^2 \ .$$

These values result in a dimensionless mass $M_1 \sim 10^{-6}$.

Resonance occurs when $\gamma = \sqrt{(S_1/M_1)}$, in which case

$$\delta_1 \bigg|_{resonance} = \frac{1}{S_2} \qquad\qquad (6.37)$$

and

$$\alpha \bigg|_{resonance} = \frac{\pi}{2} \qquad\qquad (6.38)$$

Curves of $M_1 \gamma^2$ (M_1 fixed) are superimposed on those of S_1 in Fig.21, and the intersection of these two families of curves gives the values of γ where resonance occurs. Since M_1 is typically of the order of 10^{-6} it can be seen that resonances will appear at the top end of the spectrum near $\gamma = 1000$.

Fig.22 shows how the dynamic compliance δ_1 varies with γ in a bearing with two segments (w = 2). For a given dimensionless mass the compliance remains independent of γ for small γ , increases to a peak as the resonance condition is approached, and then drops sharply away for higher values of γ . It can be seen that the value of δ_1

at resonance varies with M_1, being a minimum for the particular dimensionless mass which results in a resonance coinciding with a condition of maximum 'damping'. In the case of a bearing with $w = 2$ this occurs for $M_1 \simeq 230 \times 10^{-6}$, when the peak value of δ_1 is about 2.05 times the static compliance. Away from this minimum condition, for values of M_1 both smaller and larger than 230×10^{-6}, the peak compliance increases rapidly, its locus being indicated by the broken line in Fig.22 .

The situation with $w = 8$ is shown in Fig.23, where in this case the minimum peak compliance appears at the top end of the ζ-spectrum for a non-dimensional mass of about 1×10^{-6}.

The value of ζ at resonance, $\zeta_{res.}$, normalised with respect to the 'static' resonance value $\zeta_o = \sqrt{S_1(\zeta = o)/M_1}$, is plotted against M_1 in Fig.24 . It can be seen that a resonance frequency calculated on the basis of the static stiffness $S_1(\zeta = 0)$ can be as much as 50% too low, the discrepancy becoming smaller as the number of segments is increased.

Fig.25 shows the resonance compliance normalised with respect to the static compliance, as a function of M_1 . For each value of w the dynamic compliance at resonance goes through a minimum value coinciding with a condition of maximum damping. Away from the minimum, the compliance increases rapidly and care would be needed in design to avoid unacceptably large response amplitudes of the supported mass.

Fortunately, given a particular value for M_1, one can

carefully choose the number of segments, so as to position the resonance peak at a value of ζ close to maximum damping, in which case the peak compliance exceeds the static compliance by not much more than a factor of two. For instance, if $M_1 \simeq 10^{-6}$ one would choose $w = 8$, in which case the peak compliance would occur at $\zeta \approx 1000$ and over most of the range of interest, $0 \leqslant \zeta \leqslant 1000$, the dynamic compliance would not differ substantially from the static value.

6.1.5 Stability

Following Pan and Chiang[22], a state of neutral stability of the system exists if $S_2(\nu) = 0$. If the angular frequency at which this occurs is ν_o, then a critical mass may be defined as

$$m_o = \frac{p_a \pi R^2}{C \nu_o^2} \cdot S_1(\nu_o) \ . \tag{6.39}$$

The condition for instability to set in following a small change from the state of neutral stability is[65]

$$\left. \frac{\partial S_2}{\partial \nu} \right|_{\nu = \nu_o} \delta m > 0 \tag{6.40}$$

where δm is an incremental mass change from m_o. From Fig.21 it can be seen that $S_2 = 0$ only when $\nu = 0$ (that is, when $\zeta = 0$), so

$$\nu_o = 0 \ . \tag{6.41}$$

Since S_1 does not vanish at ν_o, equation (6.39) implies that

$$m_0 = \infty .$$
(6.42)

Thus, any real mass must be less that the critical mass, and

$$\delta m < 0 .$$
(6.43)

Also

$$\frac{\partial S_2}{\partial \nu}\bigg|_{\nu = \nu_0} = \left(\frac{\partial S_2}{\partial \zeta} \cdot \frac{\partial \zeta}{\partial \nu}\right)\bigg|_{\nu = \nu_0} > 0 .$$
(6.44)

Inequalities (6.43) and (6.44) together result in

$$\frac{\partial S_2}{\partial \nu}\bigg|_{\nu = \nu_0} \delta m < 0$$
(6.45)

so (6.40) does not hold, and the system is always stable.

6.1.6 Comments on the flat thrust bearing

The above analysis has shown that the flat thrust bearing benefits from segmentation by ambient line boundaries in that the vibration response can be limited by careful choice of the number of segments. Provided the total bearing area remains the same, the static load capacity will not be affected by the presence of the extra boundaries, to within $0\left\{\frac{1}{\sqrt{\sigma}}\right\}$. The thrust bearing, whether segmented or unsegmented, is inherently stable with respect to forced vibration.

In general, large resonance compliance peaks occur unless the combination of w , M_1 and S_1 results in a resonance vibration number near that associated with

maximum damping. In the example given, the best that could be achieved was a minimum compliance resonance value of about twice the static compliance. This appears to disagree with the general findings of Pan and Chiang[22], who state that for a wide range of mass the dynamic compliance at resonance is less than the static one, implying this to be true for flat thrust bearings as well as for hemispherical bearings. However, their particular case never exceeded a value $S_2 = 0.1$. Equation (6.37) of section 6.1.4 above then implies that the dynamic compliance at resonance must always exceed a value of $\delta_1\big|_{resonance} = 10$. This is contradicted by Fig.7 of reference 22, which thus appears to be in error.

6.2 Infinite length axially grooved journal bearing

At first sight the study of an infinite length bearing appears to be somewhat academic, as real bearings are manifestly not infinitely long. However, it will be shown that the axially grooved journal bearing is a remarkably good approximation to a finite length bearing having the same cross-sectional geometry for $L/D \gtrsim 1$, and this considerably simplifies the analysis.

6.2.1 Perturbation solution for pressure distribution

Consider a long journal bearing of radius R with deep narrow grooves running axially from end to end in one of the surfaces, so that the cross sectional geometry is as shown in Fig.26 . The grooves are sited circumferentially in positions given by

$$\theta = \theta_k = \frac{2\pi}{w} k \qquad k = 1, 2, \cdots, w \qquad (6.46)$$

where w is the number of grooves. The width of a groove is $R\theta_{2\alpha}$ ($\alpha \ll 1$), so that the width of a bearing strip is $R\theta_{1-2\alpha}$. In particular the k'th bearing strip extends circumferentially from $\theta_{k-1+\alpha}$ to $\theta_{k-\alpha}$, and the film thickness in the bearing segment is given by

$$H = \frac{h}{C} = 1 + e_2 \cos\theta + \delta \cos\theta \cos T + e_1 \cos\tau \qquad (6.47)$$

where the following non-dimensionalised quantities have been used; $T = \nu t$ for the time scale of the forced response, and $\tau = \omega t$ for the time scale of the squeeze motion, where ν and ω are angular frequencies associated with the external disturbance and the squeeze motion respectively, such that $\nu \ll \omega$.

Non-dimensionalising spatial variables with respect to R, the governing equation (4.43) reduces to the rearranged form

$$\frac{\partial}{\partial\theta}\left(H_\infty \frac{\partial\psi_\infty^2}{\partial\theta} - 2\psi_\infty^2 \frac{\partial H_\infty}{\partial\theta}\right) = 2\gamma \frac{\partial\psi_\infty}{\partial T} \qquad (6.48)$$

where

$$H_\infty = \frac{1}{2\pi}\int_0^{2\pi} H\, d\tau = 1 + e_2 \cos\theta + \delta \cos\theta \cos T \qquad (6.49)$$

is the film thickness time averaged with respect to the squeeze motion.

With m = 0, the boundary conditions (4.58) and (4.59) reduce to

$$\psi_\infty^2 = \frac{\overline{H^3}}{H_\infty} = H_\infty^2 + \frac{3}{2}e_1^2 \qquad (6.50)$$

at an ambient boundary, where $\overline{H^3}$ is a time averaged quantity

$$\overline{H^3} = \frac{1}{2\pi} \int_0^{2\pi} H^3 d\tau .$$ (6.51)

Expressing the film thickness in the form

$$H_\infty = 1 + e_2 \cos\theta + \delta \cos\theta \; e^{iT}$$ (6.52)

and expanding ψ_∞^2 in terms of small eccentricity e_2 and vibration amplitude δ,

$$\psi_\infty^2 \simeq Q_0 + e_2 Q_1 + \delta e^{iT} Q_2$$ (6.53)

so that

$$\psi_\infty \simeq \sqrt{Q_0} \left\{ 1 + \frac{1}{2} e_2 \frac{Q_1}{Q_0} + \frac{1}{2} \delta e^{iT} \frac{Q_2}{Q_0} \right\}$$ (6.54)

the governing equation (6.48) can be separated into three ordinary second order differential equations representing the steady state static, first order perturbation in eccentricity, and first order perturbation in vibration amplitude, effects,

$$\frac{d^2 Q_0}{d\theta^2} = 0$$ (6.55)

$$\frac{d^2 Q_1}{d\theta^2} + \sin\theta \, \frac{dQ_0}{d\theta} + 2Q_0 \cos\theta = 0$$ (6.56)

$$\frac{d^2 Q_2}{d\theta^2} + \sin\theta \frac{dQ_0}{d\theta} + 2Q_0 \cos\theta = i \frac{\gamma}{\sqrt{Q_0}} Q_2 \qquad (6.57)$$

while for small e_2 and δ the boundary condition (5.29) separates into the following for Q_0, Q_1, and Q_2,

$$\left.\begin{array}{l} Q_0 = 1 + \frac{3}{2} e_1^2 \\[2mm] Q_1 = Q_2 = 2 \cos\theta \end{array}\right\} \text{ at } \theta = \theta_{k-1+\alpha} \text{ and } \theta_{k-\alpha} \qquad (6.58)$$

where we are seeking solutions for Q_0, Q_1, and Q_2 in the k'th bearing segment.

Equation (6.55) subject to the boundary condition (6.58) simply leads to the static zero eccentricity ('flat plate') solution

$$Q_0 = \text{constant} = 1 + \frac{3}{2} e_1^2 . \qquad (6.59)$$

Equation (6.56) then simplifies to the form

$$\frac{d^2 Q_1}{d\theta^2} + 2Q_0 \cos\theta = 0 \qquad (6.60)$$

having the solution

$$Q_1 = 2Q_0 \cos\theta + C_1 \theta + C_2 \qquad (6.61)$$

which satisfies the boundary conditions at $\theta = \theta_{k-1+\alpha}$ and $\theta = \theta_{k-\alpha}$ if

$$C_1 = \frac{2(1-Q_0)}{\theta_{1-2\alpha}} (\cos\theta_{k-\alpha} - \cos\theta_{k-1+\alpha}) \qquad (6.62)$$

$$C_2 = \frac{2(1-Q_0)}{\theta_{1-2\alpha}} (\theta_{k-\alpha} \cos\theta_{k-1+\alpha} - \theta_{k-1+\alpha} \cos\theta_{k-\alpha}). \qquad (6.63)$$

Equation (6.57) simplifies to the form

$$\frac{d^2 Q_2}{d\theta^2} + 2Q_0 \cos\theta = i\frac{\gamma}{\sqrt{Q_0}} Q_2 \qquad (6.64)$$

An analytic solution has been obtained in the form

$$Q_2 = A e^{\bar{K}\theta} + B e^{-\bar{K}\theta} + \frac{2Q_0}{(1+\bar{K}^2)}\cos\theta \qquad (6.65)$$

where $\bar{K}^2 = i\dfrac{\gamma}{\sqrt{Q_0}}$, and A and B are rather cumbersome

constants involving trigonometric expressions, but it does

not prove easy to use in the long run because the complex

constant $\bar{K}$ results in a very complicated expression for

dynamic stiffness and damping. A less involved way of

solving equation (6.64) is to let

$$Q_2 = u + iv \qquad (6.66)$$

so that equation (6.64) can be separated by equating real

and imaginary parts,

$$\frac{d^2 u}{d\theta^2} + \frac{\gamma}{\sqrt{Q_0}} v + 2Q_0 \cos\theta = 0$$
$$\frac{d^2 v}{d\theta^2} - \frac{\gamma}{\sqrt{Q_0}} u = 0 \qquad (6.67)$$

subject to boundary conditions

$$\left. \begin{array}{l} u = 2\cos\theta \\ v = 0 \end{array} \right\} \text{ at } \theta = \theta_{k-1+\alpha} \text{ and } \theta_{k-\alpha} . \qquad (6.68)$$

This system of second-order ordinary differential equations

can then be solved numerically for u and v using standard

techniques. For instance, equations (6.67) can be reduced to a system of four first-order differential equations which can be solved using a Runge-Kutta technique[59]. Alternatively, a matrix method similar to that employed in section 6.1 for the thrust bearing seems to work well, and this is described in Appendix B.

Having obtained solutions for Q_0, and Q_1, and Q_2 we are in a position to find the τ-wise time averaged pressure distribution in the k'th bearing segment, given by

$$\bar{P} = \frac{1}{2\pi}\int_0^{2\pi} \frac{\psi_\infty}{(H_\infty + e_1 \cos\tau)} d\tau = \frac{\psi_\infty}{\sqrt{H_\infty^2 - e_1^2}}. \tag{6.69}$$

This in turn can be expanded for small e_2 and δ in the form

$$\bar{P} = \bar{P}_0 + e_2 \bar{P}_1 + \delta e^{i\tau} \bar{P}_2 \tag{6.70}$$

where

$$\bar{P}_0 = \sqrt{\frac{Q_0}{1-e_1^2}} \tag{6.71}$$

$$\bar{P}_1 = \bar{P}_0 \left\{ \frac{Q_1}{2Q_0} - \frac{\cos\theta}{(1-e_1^2)} \right\} \tag{6.72}$$

$$\bar{P}_2 = \bar{P}_0 \left\{ \frac{Q_2}{2Q_0} - \frac{\cos\theta}{(1-e_1^2)} \right\}. \tag{6.73}$$

6.2.2 Static force at small eccentricities

The steady state static ($\gamma = 0$) non-dimensional force per unit length contributed by the k'th segment is then

$$W_{s_k} = \frac{W'_{s_k}}{p_a D} = -\frac{1}{2} \int_{\theta_{k-1+\alpha}}^{\theta_{k-\alpha}} \left(\bar{P}_0 - 1 + e_2 \bar{P}_1 \right) \cos \theta \, d\theta \ . \tag{6.74}$$

On performing the integrations, one finds after a considerable amount of tedious trigonometric manipulation,

$$
\begin{aligned}
W_{s_k} = \ & -(\bar{P}_0 - 1) \sin \theta_{\frac{1}{2}-\alpha} \cos \theta_{k-\frac{1}{2}} + \frac{1}{4} e_1^2 e_2 \frac{\bar{P}_0}{(1-e_1^2)} \theta_{1-2\alpha} \\
& - \frac{e_2 \bar{P}_0}{4 Q_0} (2 - \bar{P}_0 - Q_0) \sin \theta_{1-2\alpha} \cos \theta_{2k-1} \\
& + 3 e_1^2 e_2 \frac{\bar{P}_0}{Q_0 \theta_{1-2\alpha}} \sin^2 \theta_{\frac{1}{2}-\alpha} \sin^2 \theta_{k-\frac{1}{2}} \ .
\end{aligned}
\tag{6.75}
$$

The total static lift per unit length of the bearing will then be the sum of all the segment contributions

$$W_s = \sum_{k=1}^{w} W_{s_k} \ . \tag{6.76}$$

At first sight this looks a formidable proposition, but if use is made of the relationships [58]

$$\sum_{k=1}^{w} \sin\{\alpha + (k-1)\beta\} = \sin\left\{\alpha + (w-1)\frac{\beta}{2}\right\} \frac{\sin \frac{1}{2} w \beta}{\sin \frac{1}{2} \beta}$$

$$\sum_{k=1}^{w} \cos\{\alpha + (k-1)\beta\} = \cos\left\{\alpha + (w-1)\frac{\beta}{2}\right\} \frac{\sin \frac{1}{2} w \beta}{\sin \frac{1}{2} \beta} \tag{6.77}$$

it is quite straightforward to show that

$$\sum_{k=1}^{w} \cos \theta_{k-\frac{1}{2}} = 0 \qquad (w > 1) \qquad (6.78)$$

$$\sum_{k=1}^{w} \cos \theta_{2k-1} = 0 \qquad (w > 2) \qquad (6.79)$$

$$\sum_{k=1}^{w} \sin^2 \theta_{k-\frac{1}{2}} = \frac{1}{2} w \qquad (w > 2) \qquad (6.80)$$

while

$$\sum_{k=1}^{w} \theta_{1-2\alpha} = 2\pi (1 - 2\alpha) . \qquad (6.81)$$

Thus, for $w > 2$,

$$W = \frac{\pi}{2} e_1^2 e_2 (1 - 2\alpha) \frac{\overline{P}_0}{(1 - e_1^2)} + \frac{3}{4} e_1^2 e_2 \frac{\overline{P}_0 w^2}{Q_0 \pi (1-2\alpha)} \sin^2 \frac{\pi}{w} (1-2\alpha) \qquad (6.82)$$

for small e_2, where at present there is no restriction on the excursion ratio e_1, and for small e_1^2 the expression can be simplified to

$$W \simeq \frac{\pi}{2} e_1^2 e_2 (1-2\alpha) + \frac{3}{4} e_1^2 e_2 \frac{w^2}{\pi(1-2\alpha)} \sin^2 \frac{\pi}{w} (1-2\alpha) . \qquad (6.83)$$

If the number of grooves is such that $w \gg \pi (1 - 2\alpha)$,

$$W \simeq \frac{5}{4} \pi e_1^2 e_2 (1-2\alpha) \qquad (6.84)$$

which, rather gratifyingly, agrees with the result given by the simplified analysis in section 3.2.4. We see that for small e_1^2 the lift per unit length of the infinitely long axially grooved squeeze-film bearing is directly

proportional to the eccentricity and the bearing area, and proportional to the square of the excursion ratio, so that the groove width α should be kept as small as possible.

Comparing equations (6.83) and (3.73), the first term can be identified as being the interior Boyle's Law contribution, and the second term as the edge pressurising effect. Thus as the number of grooves increases, the edge effect augments the basic Boyle's Law behaviour more and more, tending asymptotically to the limit given by equation (6.84) for large w. Physically, this is because the circumferential leakage flow, which is appreciable when only a few grooves are present, is reduced to negligible proportions as the number of grooves is increased. This can be shown quite easily by going back to the governing equation (6.48) and extracting the normalised circumferential mass flow rate per unit length,

$$M_\theta = -\left(\frac{H_\infty}{2}\frac{\partial \psi_\infty^2}{\partial \theta} - \psi_\infty^2 \frac{\partial H_\infty}{\partial \theta}\right) \qquad (6.85)$$

which, for small e_1^2 and e_2, becomes in the k'th segment

$$M_{\theta_k} \simeq -\frac{3}{2}e_1^2 e_2 \frac{w}{\pi(1-2\alpha)} \sin\frac{\pi}{w}(1-2\alpha)\sin\frac{\pi}{w}(2k-1). \qquad (6.86)$$

When $w \gg \pi(1 - 2\alpha)$ this reduces to

$$M_{\theta_k} \simeq -\frac{3}{2}e_1^2 e_2 \sin\frac{\pi}{w}(2k-1) \qquad (6.87)$$

which vanishes as w becomes large. For a given number of grooves, the sinusoidal structure of equation (6.87) indicates that the circumferential flow is greatest in

the segments near $\theta = \frac{\pi}{2}$ and $\theta = \frac{3\pi}{2}$, and least near $\theta = 0$ and $\theta = \pi$. This is to be expected, as the mean gap taper is a maximum at $\theta = \frac{\pi}{2}$ and $\theta = \frac{3\pi}{2}$, while the gap is uniform at $\theta = 0$ and $\theta = \pi$.

This infinite length bearing solution is not merely of academic interest, because numerical solutions for the finite length bearing indicate that for small values of e_1^2 and e_2 the lift per unit length is very closely approximated to by equation (6.82) for $L/D \geqslant 1$.

6.2.3 Static force at large eccentricities

While the perturbation solution obtained in section 6.2.1 was valid only for small values of e_2, the numerical procedure described here is used to accommodate large eccentricities.

Concerning ourselves only with static behaviour ($\gamma = 0$), for the k'th bearing strip equation (6.48) must be solved, namely

$$\frac{\partial}{\partial \theta}\left(H_\infty \frac{\partial Q}{\partial \theta} - 2Q \frac{\partial H_\infty}{\partial \theta}\right) = 0 \qquad (6.88)$$

where $Q = \psi_\infty^2$, subject to boundary conditions (6.50),

$$Q = H_\infty^2 + \frac{3}{2} e_1^2 \qquad (6.89)$$

at $\theta = \theta_{k-\alpha}$ and $\theta = \theta_{k-1+\alpha}$, where the film thickness is now

$$H_\infty = 1 + e_2 \cos \theta . \qquad (6.90)$$

Expanding equation (6.88),

$$H_\infty \frac{\partial^2 Q}{\partial \theta^2} + e_2 \sin \theta \frac{\partial Q}{\partial \theta} - 2(H_\infty - 1)Q = 0 . \tag{6.91}$$

The non-dimensional width of the k'th bearing strip is $\theta_{1-2\alpha}$, so if

$$\Delta\theta = \frac{\theta_{1-2\alpha}}{(m-1)} \tag{6.92}$$

where m is an integer, finite difference grid points can be defined by

$$\bar{\theta}_i = \theta_{k-1+\alpha} + (i-1)\Delta\theta \qquad i = 1, 2, \ldots, m . \tag{6.93}$$

The following finite difference approximations can then be used for i = 2,3,..., m-1:

$$Q(\bar{\theta}_i) = q_i$$

$$H_\infty(\bar{\theta}_i) = H_i$$

$$\left. \frac{dQ}{d\theta} \right|_{\theta = \bar{\theta}_i} = \frac{1}{2\Delta\theta}(q_{i+1} - q_{i-1}) \tag{6.94}$$

$$\left. \frac{d^2Q}{d\theta^2} \right|_{\theta = \bar{\theta}_i} = \frac{1}{\Delta\theta^2}(q_{i+1} - 2q_i + q_{i-1})$$

while the boundary conditions (6.89) are given by

$$q_1 = H_1^2 + \frac{3}{2}e_1^2$$

$$q_m = H_m^2 + \frac{3}{2}e_1^2 . \tag{6.95}$$

Equation (6.91) can now be written in the finite difference

form

$$\alpha_i q_{i+1} + \beta_i q_i + \bar{\alpha}_i q_{i-1} = \mu_i \tag{6.96}$$

where, for a regular field point ($i \neq 1$ and $i \neq m$), $\mu_i = 0$,

$$\alpha_i = \frac{H_i}{\Delta\theta^2} + \frac{e_2 \sin \bar{\theta}_i}{2\Delta\theta}$$

$$\beta_i = 2\left\{ H_i\left(1 - \frac{1}{\Delta\theta^2}\right) - 1 \right\} \tag{6.97}$$

$$\bar{\alpha}_i = \frac{H_i}{\Delta\theta^2} - \frac{e_2 \sin \bar{\theta}_i}{2\Delta\theta}$$

and, at the ambient boundaries $i = 1$ and $i = m$,

$$\alpha_i = \bar{\alpha}_i = 0$$
$$\beta_i = 1 \tag{6.98}$$
$$\mu_i = H_i^2 + \frac{3}{2}\theta_1^2 \; .$$

The system of equations (6.96) is written in the matrix form

$$A \underline{q} = \underline{f} \tag{6.99}$$

where A is the (m x m) matrix

$$A = \begin{Vmatrix} \beta_1 & \alpha_1 & & & & \\ \bar{\alpha}_2 & \beta_2 & \alpha_2 & & & \\ & \bar{\alpha}_3 & \beta_3 & \alpha_3 & & \\ & & \diagdown & \diagdown & \diagdown & \\ & & & & \alpha_{m-1} & \\ & & & & \bar{\alpha}_m & \beta_m \end{Vmatrix}$$

while $\underline{q}$ and $\underline{f}$ are the (m x 1) column vectors

$$\underline{q} = \begin{Vmatrix} q_1 \\ q_2 \\ \cdot \\ \cdot \\ \cdot \\ q_m \end{Vmatrix} \qquad \underline{f} = \begin{Vmatrix} \mu_1 \\ \mu_2 \\ \cdot \\ \cdot \\ \cdot \\ \mu_m \end{Vmatrix} .$$

The required solution is then simply

$$\underline{q} = A^{-1} \underline{f} . \qquad (6.100)$$

Having achieved a numerical solution for Q in the form of equation (6.100), the time-averaged pressure distribution is given by equation (6.69),

$$\overline{P} = \sqrt{\frac{Q}{H_\infty^2 - e_1^2}} \qquad (6.101)$$

from which the force per unit length contributed by the k'th bearing strip can be calculated, namely

$$W_{s_k} = \frac{W_{s_k}'}{p_a D} = -\frac{1}{2} \int_{\theta_{k-1+\alpha}}^{\theta_{k-\alpha}} (\overline{P} - 1) \cos \theta \, d\theta . \qquad (6.102)$$

The integral is readily evaluated numerically by means of a Simpson's rule routine, and the total lift per unit length of the bearing is given by equation (6.76).

6.2.4 Comparisons of the static forces in ungrooved and axially grooved infinite length journal bearings

The above numerical method has been used to obtain the static force per unit length of the axially grooved squeeze-film bearing of infinite length and the results were compared with those for the corresponding ungrooved bearing.

Fig.27 shows in full lines the lift per unit length as a function of eccentricity for various values of excursion ratio in a bearing with 20 infinitesimally narrow grooves ($\alpha = 0$). For comparison is shown the corresponding set of curves (broken lines) for the smooth bearing as derived from reference 16. It can be seen that both sets are characterised by an approximately constant stiffness (gradient of the curves) at low eccentricities, but which increases rapidly at high eccentricities. The grooved bearing, however, exhibits much greater lift, especially at low values of eccentricity and excursion ratio. For example, the improvement in load capacity is 87% when $e_1 = 0.4$ and $e_2 = 0.5$.

The percentage improvement in lift of the grooved bearing over the smooth one is shown in more detail in Fig 28 as a function of eccentricity for various excursion ratios, and it can be seen immediately that the best improvement occurs for low values of e_1 and, to a lesser extent, of e_2. In the limit of $w \to \infty$ and e_1^2, $e_2 \ll 1$ the improvement is 150%, as predicted by the analytic treatment of section 6.2.2 .

Fig.29 compares the analytically and numerically

derived solutions obtained in sections 6.2.2 and 6.2.3 for various values of e_1 and e_2 when $w = 20$ and $\alpha = 0$. Agreement is very good at low eccentricities, but the curvature seen in the numerical results is lost in the analytic case because the perturbation theory extended only to first order in e_2. However, the discrepancy is only 3.4% at $e_2 = 0.1$, so the analytic solution does give a good, if pessimistic, idea of what is happening at low eccentricities, and provides a reliable check on the numerical results.

Fig.30 shows the dependence of lift per unit length on the number of grooves for various excursion ratios and groove widths when the eccentricity is 0.1, using the analytic approach. The lift increases monotonically with w, levelling asymptotically at quite moderate numbers. No appreciable increase in lift is apparent if the number of grooves is taken beyond 18 or 20, and as few as 3 or 4 grooves gives quite a signficant improvement in lift compared with that of the smooth bearing shown in broken lines to the left of the figure. This latter result is analagous to the sort of improvement observed in the externally pressurised journal bearing reported in reference 39. Increasing the groove width, represented by the parameter α, results in a proportionate loss in lift.

Note that if $\mathscr{l} = \dfrac{2\pi R}{w}(1 - 2\alpha)$ is the circumferential width of a bearing segment, so that $\mathscr{l}/R = \dfrac{2\pi}{w}(1 - 2\alpha)$, it is found that $\mathscr{l}/R \lesssim 0.3$ for $w \gtrsim 20$, justifying our premature acceptance of the criterion governing groove

depth, inequality (3.94), in section 3.5.1 .

6.2.5 Dynamic force at small eccentricities

Assuming that a solution has been obtained for Q_2, as expressed by equation (6.66), the steady state dynamic force contribution per unit length from the k'th bearing segment is

$$W_{D_k} = \frac{W'_{D_k}}{p_a D} = -\frac{1}{2} \delta e^{iT} \int_{\theta_{k-1+\alpha}}^{\theta_{k-\alpha}} \bar{P}_2 \cos\theta \, d\theta \qquad (6.103)$$

where $\bar{P}_2$ is given by equation (6.73). Retaining the real part, equation (6.103) becomes

$$W_{D_k} = \frac{\delta}{2} \cos T \left\{ \frac{\bar{P}_0}{(1-e_1^2)} \int_{\theta_{k-1+\alpha}}^{\theta_{k-\alpha}} \cos^2\theta \, d\theta - \frac{\bar{P}_0}{2Q_0} \int_{\theta_{k-1+\alpha}}^{\theta_{k-\alpha}} u \cos\theta \, d\theta \right\}$$
$$+ \frac{\delta}{4} \sin T \cdot \frac{\bar{P}_0}{Q_0} \int_{\theta_{k-1+\alpha}}^{\theta_{k-\alpha}} v \cos\theta \, d\theta . \qquad (6.104)$$

Performing the integration of the first term, and manipulating,

$$W_{D_k} = \frac{\delta}{2} \cos T \left\{ \frac{\bar{P}_0}{2(1-e_1^2)} (\theta_{1-2\alpha} + \cos\theta_{2k-1} \sin\theta_{1-2\alpha}) - \frac{\bar{P}_0}{2Q_0} \int_{\theta_{k-1+\alpha}}^{\theta_{k-\alpha}} u \cos\theta \, d\theta \right\}$$
$$+ \frac{\delta}{4} \sin T \cdot \frac{\bar{P}_0}{Q_0} \int_{\theta_{k-1+\alpha}}^{\theta_{k-\alpha}} v \cos\theta \, d\theta . \qquad (6.105)$$

The total dynamic force per unit length is then

$$W_D = \sum_{k=1}^{w} W_{D_k} \qquad (6.106)$$

so that, on using equations (6.79) and (6.81), for $w > 2$

$$W_D = \frac{\delta}{2} \cos T \left\{ \frac{\bar{P}_0 \pi (1-2\alpha)}{(1-e_i^2)} - \frac{\bar{P}_0}{2Q_0} \sum_{k=1}^{w} \int_{\theta_{k-1+\alpha}}^{\theta_{k-\alpha}} u \cos \theta \, d\theta \right\}$$

$$+ \frac{\delta}{4} \sin T \frac{\bar{P}_0}{Q_0} \sum_{k=1}^{w} \int_{\theta_{k-1+\alpha}}^{\theta_{k-\alpha}} v \cos \theta \, d\theta .$$

(6.107)

The coefficients of cos T and sin T respectively constitute the stiffness and damping components of the dynamic force.

Before going on to consider the vibration response, we will discuss the finite length axially grooved journal bearing, showing that the infinite length bearing is a very good approximation to the finite length bearing for $L/D \gtrsim 1$ with respect to the static behaviour.

6.3 Finite length axially grooved journal bearing

The infinite length axially grooved bearing succumbed relatively easily to analytic solution by perturbation theory because it involved a single spatial variable. In the finite length bearing, however, the axial flow cannot immediately be ignored so the problem contains two dimensions in the spatial variables. This makes an analytic solution much more difficult, and it is easier to turn again to numerical methods.

6.3.1 Numerical solution for $\gamma = 0$

To obtain the static force, we expand the governing equation (4.43), with $\gamma = 0$, bearing in mind the structure of equation (6.49) when $\delta = 0$, so that

$$H_\infty \left(\frac{\partial^2 Q}{\partial \theta^2} + \frac{\partial^2 Q}{\partial \bar{z}^2} \right) + e_2 \sin \theta \frac{\partial Q}{\partial \theta} + 2(H_\infty - 1)Q = 0$$

(6.108)

where $Q = (PH)^2$, and $\bar{z} = z/R$ is the normalised axial co-ordinate, such that $z_L = L/R$ is the non-dimensional length of the bearing. Because of symmetry, only the domain $0 \leq \theta \leq \pi$, $0 \leq \bar{z} \leq \frac{z_L}{2}$ need be considered, so that for an even number of grooves the k'th segment covers the region $\theta_{k-1+\alpha} \leq \theta \leq \theta_{k-\alpha}$, $0 \leq \bar{z} \leq \frac{z_L}{2}$. If there is an odd number of grooves, the segments of interest occupy the regions $\theta_{k-1+\alpha} \leq \theta \leq \theta_{k-\alpha}$, $0 \leq \bar{z} \leq \frac{z_L}{2}$, $k \neq (w+1)/2$ and $\theta_{\frac{(w-1)}{2}+\alpha} \leq \theta \leq \pi$, $0 \leq \bar{z} \leq \frac{z_L}{2}$. On an ambient boundary, equation (4.58) holds in the form

$$Q = H_\infty^2 + \frac{3}{2} e_1^2 \tag{6.109}$$

while at the mid-plane, $\bar{z} = z_L/2$,

$$\left. \frac{\partial Q}{\partial \bar{z}} \right|_{\bar{z} = \frac{z_L}{2}} = 0 . \tag{6.110}$$

To solve equation (6.108) in the k'th segment, a uniform grid is used with m and n points respectively in the circumferential and axial directions, so that the grid spacing is

$$\Delta\theta = \frac{\theta_{1-2\alpha}}{(m-1)} \tag{6.111}$$

$$\Delta z = \frac{z_L}{2(n-1)}$$

such that the i,j'th grid point has co-ordinates $\bar{\theta}_i = (\theta_{k-1+\alpha} + (i-1)\Delta\theta)$, $\bar{z}_j = (j-1)\Delta z$, where $i = 1,2,\ldots,$ m and $j = 1,2,\ldots,$ n. Using the following finite difference approximations,

$$Q(\bar{\theta}_i, \bar{z}_j) = q_{ij}$$

$$\left.\frac{\partial Q}{\partial \theta}\right|_{(\bar{\theta}_i, \bar{z}_j)} = \frac{1}{2\Delta\theta}(q_{i+1,j} - q_{i-1,j})$$

$$\left.\frac{\partial^2 Q}{\partial \theta^2}\right|_{(\bar{\theta}_i, \bar{z}_j)} = \frac{1}{\Delta\theta^2}(q_{i+1,j} - 2q_{ij} + q_{i-1,j})$$

$$\left.\frac{\partial^2 Q}{\partial \bar{z}^2}\right|_{(\bar{\theta}_i, \bar{z}_j)} = \frac{1}{\Delta z^2}(q_{i,j+1} - 2q_{ij} + q_{i,j-1})$$

$$H_\infty(\bar{\theta}_i) = H_i$$

(6.112)

equation (6.108) can be represented in finite difference terms at the i,j'th grid point in the generalised form

$$\alpha_{ij}\, q_{i+1,j} + \bar{\alpha}_{ij}\, q_{i-1,j} + \beta_{ij}\, q_{ij} + \delta_{ij}\, q_{i,j+1} + \bar{\delta}_{ij}\, q_{i,j-1} = \mu_{ij} \qquad (6.113)$$

where, for a regular field point,

$$\alpha_{ij} = \frac{H_i}{\Delta\theta^2} + \frac{e_2 \sin\bar{\theta}_i}{2\Delta\theta}$$

$$\bar{\alpha}_{ij} = \frac{H_i}{\Delta\theta^2} - \frac{e_2 \sin\bar{\theta}_i}{2\Delta\theta}$$

$$\beta_{ij} = 2(H_i - 1) - 2H_i\left(\frac{1}{\Delta\theta^2} + \frac{1}{\Delta z^2}\right)$$

(6.114)

$$\delta_{ij} = \bar{\delta}_{ij} = \frac{H_i}{\Delta z^2}$$

$$\mu_{ij} = 0 .$$

For all bearing segments, other than $k = \frac{(w+1)}{2}$ where w is odd, the boundary condition (6.109) reduces to the following finite difference form at $i = 1$, $i = m$, $j = 1$

$$\alpha_{ij} = \bar{\alpha}_{ij} = \delta_{ij} = \bar{\delta}_{ij} = 0 .$$

$$\beta_{ij} = 1$$

$$\mu_{ij} = H_i^2 + \frac{3}{2}e_1^2$$

(6.115)

and equation (6.110) is represented by (6.114) at $j = n$, with the exception that

$$\delta_{in} = 0$$
$$\bar{\delta}_{in} = \frac{2H_i}{\Delta z^2}$$

(6.116)

If w is odd, the segment $k = \frac{(w+1)}{2}$ is a special case where equation (6.109) holds on the boundaries $\bar{z} = 0$ and $\theta = \theta_{(\frac{w-1}{2})+\alpha}$, equation (6.110) holds on the boundary $\bar{z} = z_L/2$, and we have the extra condition at $\theta = \pi$,

$$\frac{\partial Q}{\partial \theta}\Bigg|_{\theta = \pi} = 0 \ .$$

(6.117)

These conditions are all represented by equations (6.115) at $i = 1$ and $j = 1$, equations (6.116) at $j = n$, together with the following: equations (6.114) at $i = m$, except that $\alpha_{mj} = 0$, $\bar{\alpha}_{mj} = \frac{2H_m}{\Delta \theta^2}$; equations (6.114) at the corner ($i = m$, $j = n$) except that $\alpha_{mn} = \delta_{mn} = 0$, $\bar{\alpha}_{mn} = \frac{2H_m}{\Delta \theta^2}$, $\bar{\delta}_{mn} = \frac{2H_m}{\Delta z^2}$.

In this awkward segment the grid spacing in the θ-direction is halved in order to retain the same number of grid points, in which case $\Delta \theta = \frac{\theta_{1-2\alpha}}{2(m-1)}$ in this segment.

A matrix solution of the general two-dimensional finite difference equation (6.113) is given in Appendix C. By using the symmetry properties of the bearing, the computation can be confined to a quarter of the total bearing region, permitting quite a considerable saving in time. n need be only half as large as would be required for the total bearing region, and summation for the total force need only be taken over half the segments.

Having solved for Q, the time averaged pressure distribution is once more given by equation (6.101), and this integrated over the area of the segment leads to its contribution to the total lift of the bearing, obtained by summing over all such contributions. The necessary integrations can be performed numerically by means of a two-dimensional Simpson's Rule routine.

6.3.2 Discussion on static force

Results of the numerical analysis given in section 6.3.1 indicate that for most L/D ratios the lift per unit length of finite length axially grooved squeeze-film bearings is virtually indistinguishable in behaviour from the full curves of Fig.27 . This is true to all intents and purposes for $L/D \gtrsim 1$, so the infinite length case is of especial interest because it can be used to predict the load carrying capacity of most axially grooved bearings of finite length. This is because each bearing segment is in the form of a relatively long strip, where the dominant boundaries are the axial ones even in quite short bearings. The short circumferential boundaries at the ends contribute only a small proportion of the total edge pressurising effect, unless the bearing is very short and the lengths of the circumferential and axial boundaries become comparable in magnitude. In other words, the infinite length case is a good approximation for the finite length bearing if

$$\frac{L}{D} \gg \frac{\pi}{w}(1-2\alpha) .$$

(6.118)

Investigation of the improvement in lift to be obtained

by axially grooving finite length bearings is complicated
by the basic L/D dependence of the ungrooved bearing.
However, a typical example is furnished by considering the
case where L/D = 3. The ungrooved bearing has a lift per
unit length given by equation (3.28) for small e_1^2 and e_2,
resulting in

$$W_{\text{ungrooved}} = \frac{3}{4} \pi e_1^2 e_2 .$$
(6.119)

If the bearing is sufficiently axially grooved, the
infinite length solution for small e_1^2 and e_2, given by
equation (6.84), will be a good approximation, and

$$W_{\text{axially grooved}} = \frac{5}{4} \pi e_1^2 e_2 (1-2\alpha).$$
(6.120)

The percentage improvement in lift arising from the
grooving is thus 67% for $\alpha = 0$.

Remembering that in the limit of large numbers of
grooves we have shown that the circumferentially and
axially grooved bearings are performing basically the same
task of eliminating circumferential leakage flow, we can
obtain a limiting curve for the effect of axial grooving
on lift for various L/D by studying the limiting circum-
ferentially grooved behaviour, as given by equations (3.28)
and (3.31). On this basis it is found that

$$\frac{W_{\text{grooved}}}{W_{\text{ungrooved}}} = \frac{2 \cdot 5}{\left(1 + \frac{3D}{2L} \tanh \frac{L}{D}\right)}$$
(6.121)

where $W_{\text{ungrooved}}$ is the lift of the smooth bearing with a

given L/D ratio, and $W_{grooved}$ is the lift of the same bearing with a large number of circumferential or axial grooves. This function is plotted in Fig.31 as a function of L/D, showing that the improvement due to grooving increases rapidly for moderate values of L/D, and would level off asymptotically at a figure of 2.5 for large L/D if the curve had been carried far enough. The improvement is just under 50% for L/D = 2, 67% for L/D = 3, 100% for L/D = 6. The improvement for short bearings, L/D < 1 is largely nullified by the fact that the circumferential leakage flow is inherently low anyway, so grooving will not significantly change the lift, although even for L/D = 1 there is about 18% improvement to be gained from grooving. Of course, although the improvement curve of Fig.31 increases with L/D, the actual lift per unit length of the grooved bearing remains independent of L/D because we have removed the circumferential leakage flow.

6.4 Dynamic response of axially grooved journal bearings

As the static behaviour of most finite length axially grooved journal bearings is indistinguishable from that of the infinite length bearing of the same cross-section, we will also restrict our attention to the latter when considering the dynamic response of the system. The case of small eccentricity ($e_2 \ll 1$) and small forced vibration amplitude ($\delta \ll 1$) is of especial interest to manufacturers of inertial navigation instruments, so this will be investigated in detail, but a method for treating large eccentricities will be suggested for use elsewhere if the need arises.

6.4.1 Dynamic stiffness at small eccentricities

The steady state dynamic force per unit length in an infinitely long axially grooved journal bearing was given by equation (6.107) in section 6.2.5, and this can be expressed in the form

$$W_D = \frac{W_D'}{p_a D} = \text{Real}\left\{\delta e^{iT}(U - iV)\right\} \tag{6.122}$$

where

$$U = \frac{C}{p_a D} U' = \frac{\bar{P_0}}{2}\left\{\pi\left(\frac{1-2\alpha}{1-e_i^2}\right) - \frac{1}{Q_0}\sum_{k=1}^{w}\int_{\theta_{k-1+\alpha}}^{k-\alpha} u \cos\theta \, d\theta\right\} \tag{6.123}$$

and

$$V = \frac{C}{p_a D} V' = \frac{\bar{P_0}}{4Q_0}\sum_{k=1}^{w}\int_{\theta_{k-1+\alpha}}^{\theta_{k-\alpha}} v \cos\theta \, d\theta \tag{6.124}$$

respectively constitute the in-phase and quadrature components of the dynamic stiffness per unit length of the bearing.

The γ-dependence of U and V is shown in Fig.32 for various numbers of grooves, w. The dynamic stiffness increases monotonically with γ from the static value U(γ = 0), reaching a higher constant value for large γ. The dynamic 'damping' increases linearly with γ for small γ, levels off, and then decreases gradually to zero for large γ. As in the case of the thrust bearing (section 6.1.4), increasing the number of bearing segments pushes the damping peak to higher values of γ, and delays the onset of the asymptotic rise in the dynamic stiffness.

However, there are slight differences to be seen in comparing Figs.21 and 32 which can be explained qualitatively with the help of our 'flat plate' model. The static stiffness of the thrust bearing is independent of the number of segments, while that of the axially grooved journal bearing increases to an asymptotic value for large numbers of segments. We have already accounted for this by showing that circumferential leakage flow reduces the load capacity (and stiffness) as the number of grooves is decreased, and that as the number of grooves increases the behaviour tends more closely to that of the ideal local flat plate. For large w (no circumferential leakage flow) the bearing behaviour fits the ideal flat plate model locally, and so the dynamic damping curves appear very similar to those for the thrust bearing in Fig.21 with the peak damping having a constant value as w varies. The vibration number at which the peak damping occurs increases with w, as the decreasing width of the bearing strips allows higher circumferential velocities to exist in the film before limiting compressibility effects begin to dominate. In the relatively wide strips associated with a small value of w, there is a certain amount of circumferential leakage superimposed on the flow arising from the forced response, so the damping peak is boosted slightly.

6.4.2 Vibration response

A treatment similar to that of section 6.1.4 for the thrust bearing can be used to investigate the forced response of the system when a mass m per unit length is

supported by the bearing. An external force per unit length

$$W'_{ext} = p_a D. \, \text{Real} \left\{ f e^{i\nu t} \right\}$$

(6.125)

is supposed to act, generating a dynamic film force per unit length

$$W'_D = p_a D. \, \text{Real} \left\{ \delta e^{i\nu t} (U - iV) \right\}$$

(6.126)

which causes a supported mass response displacement of magnitude

$$x = C. \, \text{Real} \left\{ \delta e^{i\nu t} \right\}.$$

(6.127)

The equation of motion for the system is thus

$$m\ddot{x} + W'_D = W'_{ext}$$

(6.128)

resulting in a dynamic compliance

$$\frac{\delta}{f} = \frac{1}{(U - M_1 \gamma^2) - iV} = \delta_1 e^{i\gamma}$$

(6.129)

where M_1 is the dimensionless mass per unit length,

$$M = \frac{m p_a}{288 \mu^2} \left(\frac{C}{R} \right)^5$$

(6.130)

and γ is the vibration number defined in equation (4.39).
The amplitude and phase of the unit dynamic compliance are

$$\delta_1 = \frac{p_a D}{C} \cdot \delta_1' = \frac{1}{\sqrt{(U - M_1 \gamma^2)^2 + V^2}}$$

$$\gamma = \tan^{-1} \frac{V}{(U - M_1 \gamma^2)} \ . \qquad (6.131)$$

A resonance condition occurs when $\gamma = \sqrt{U/M_1}$, in which case

$$\delta_1 \Big|_{\text{resonance}} = \frac{1}{V}$$

$$\gamma \Big|_{\text{resonance}} = \frac{\pi}{2} \ . \qquad (6.132)$$

Curves of $M_1 \gamma^2$ (M_1 fixed) are superimposed on those of U in Fig.32, and the intersections of the two families give the values of γ at which resonance occurs.

In Fig.33, the dynamic compliance δ_1 is plotted as a function of γ for various values of dimensionless mass per unit length M_1 when w = 10. For a given mass, the compliance at low γ differs little from the static value. As the resonance condition (6.132) is approached, the compliance increases rapidly up to a peak, and then drops sharply away to zero for large γ . The peak value of δ_1 varies with M_1, being a minimum for that value of M_1 which results in a resonance which coincides with maximum damping. For w = 10, this occurs for a mass per unit length $M_1 \simeq 0.0025$, in which case the dynamic compliance at resonance is just under twice the static compliance. For masses both greater and smaller than this, the peak compliance increases rapidly. For very small masses, the resonance occurs above our scale of interest (at $\gamma > 1000$) and over most of the range $0 \leqslant \gamma \leqslant 1000$ the dynamic

compliance is less than the static value.

Fig.34 is a similar graph for w = 40. The maximum damping in this case occurs at $\gamma \simeq 500$, so the minimum peak compliance is pushed to a higher value of γ than in the last example where w = 10. The mass which results in the minimum peak compliance is reduced by a factor of about 250 compared with that when w = 10.

As for the thrust bearing (Fig.24), it is useful to observe the ratio γ_{res}/γ_o (value of γ at resonance, divided by $\gamma_o = \sqrt{U(\gamma = 0)/M_1}$), and this is plotted in Fig.35 . Again, it can be seen that a resonance frequency calculated from the combination of $U(\gamma = 0)$ and M_1 can be as much as 50% too low . It is not surprising that this value is similar to that obtained for the thrust bearing, because the grooved journal bearing behaves locally like a flat thrust bearing.

Fig.36 shows the peak compliance normalised with respect to the static compliance as a function of M_1 . The behaviour is qualitatively similar to that of the thrust bearing (Fig.25), except that the increased damping in the journal bearing for small w results in a slightly reduced peak compliance at the point of maximum damping compared with that at large values of w.

In inertial navigation instruments, the following might be typical:

$$R = 20 \text{ mm}$$
$$m = 2.5 \text{ kg/m}$$
$$C = 2.5 \times 10^{-6} \text{m}$$
$$P_a = 10^5 \text{ N/m}^2$$

$$\mu = 2 \times 10^{-5} \text{ N s/m}^2 .$$

leading to a typical dimensionless mass per unit length

$$M_1 \sim 10^{-7} .$$

Such a value for M_1 would produce a resonance well above the upper limit of ζ for which we are interested, so the dynamic compliance can be expected to be less than the static value over most of the ζ-spectrum, regardless of the number of grooves. However, if it is wished to suppress this resonance, one should choose a large number of grooves, $w \sim 60$ say, so as to make the resonance coincide with the condition of maximum damping. Making such a large number of grooves, without at the same time losing a significant amount of bearing area, would prove difficult in practice.

In a situation where the bearing axis is intended to operate vertically, much larger values of M_1 could be met, and in such a case it would be perfectly feasible to choose the number of grooves carefully so as to ensure maximum available damping at resonance, and so limit the response amplitude.

6.4.3 Stability

An argument similar to that for the thrust bearing in section 6.1.5 can be used to show that, at least for small eccentricities and small forced response amplitudes, the axially grooved journal bearing is always stable with respect to external vibration when $\zeta \ll \sigma$.

The external exciting force per unit length W'_{ext} is suddenly removed, so that the equation of motion (6.128) becomes

$$m\ddot{x} + W_D' = 0 . \tag{6.133}$$

A state of neutral stability is supposed to exist if
$V = 0$, in which case equations (6.126), (6.127) and (6.133)
define a critical mass per unit length

$$m_o = \frac{p_a D}{C \nu_o^2} \cdot U(\nu_o) \tag{6.134}$$

where ν_o is the angular frequency at which $V = 0$. As in
section 6.1.5, the condition for instability to ensue from
a slight change away from the state of neutral stability is

$$\left. \frac{\partial V}{\partial \nu} \right|_{\nu = \nu_o} \cdot \delta m > 0 \tag{6.135}$$

where δm is an incremental change in mass from m_o.

Once again we have $V = 0$ only when $\nu = 0$ (or $\zeta = 0$),
in which case

$$\nu_o = 0 \tag{6.136}$$

and, since U does not vanish at $\nu = \nu_o$, equation (6.134)
results in

$$m_o = \infty . \tag{6.137}$$

The same argument as in section 6.1.5 then shows that
condition (6.135) cannot be satisfied, and hence the
bearing is always stable with respect to forced vibration
when the eccentricity and response amplitude are small.

6.5 Finite length ungrooved journal bearing

So that proper comparisons can be made with grooved bearings, the finite length ungrooved journal bearing must be analysed. The static behaviour is well documented [16,26,27,28], and the stability of the self-induced response has been treated for the infinite length case [20], but the forced response has not been dealt with in the literature. As in section 6.4 , we will mainly concern ourselves with small eccentricities and small vibration amplitudes ($e_1 \ll 1$ and $\delta \ll 1$), as these are specifically of interest to the writer.

6.5.1 Pressure distribution at small eccentricities

Consider an ungrooved journal bearing of radius R, length L, nominal clearance C such that the normalised film thickness is

$$H = \frac{h}{C} = 1 + e_2 \cos \theta + \delta \cos \theta \cos T + e_1 \cos \tau \qquad (6.138)$$

where $T = \nu t$ and $\tau = \omega t$ are time scales associated with respectively the forced response and the squeeze motion; e_2 is the eccentricity, e_1 the excursion ratio, and δ the amplitude of the forced response. The film thickness, time-averaged with respect to the squeeze motion, is

$$H_\infty = \frac{1}{2\pi} \int_0^{2\pi} H \, d\tau = 1 + \text{Real}\left\{ e_2 e^{i\theta} + \frac{\delta}{2} \left[e^{i(\theta-T)} + e^{i(\theta+T)} \right] \right\}. \qquad (6.139)$$

Normalising the spatial variables with respect to R,

so that the circumferential and axial non-dimensional co-ordinates are θ and $\bar{z}$, on setting $\ell_1 = \ell_2 = 1$, $u_1 = \theta$, $u_2 = \bar{z}$, $m = 1$ (no slip flow), the governing equation (4.43) becomes

$$\left(\frac{\partial^2}{\partial\theta^2} + \frac{\partial^2}{\partial\bar{z}^2}\right) H_\infty \psi_\infty^2 - 3\frac{\partial H_\infty}{\partial\theta}\frac{\partial \psi_\infty^2}{\partial\theta} - 3\psi_\infty^2 \frac{\partial^2 H_\infty}{\partial\theta^2} = 2\gamma \frac{\partial \psi_\infty}{\partial T} \tag{6.140}$$

subject to the boundary conditions (4.58) at $\bar{z} = 0$ and $\bar{z} = \bar{z}_L = L/R$ in the form

$$H_\infty \psi_\infty^2 = H_\infty^3 + \frac{3}{2}e_1^2 H_\infty \tag{6.141}$$

and the symmetry conditions at $\theta = 0$ and $\theta = \pi$,

$$\frac{\partial}{\partial\theta}(H_\infty \psi_\infty^2) = 0. \tag{6.142}$$

If both e_2 and δ are small, perturbation theory can be used to obtain a solution for ψ_∞. To first order in e_2 and δ, let

$$H_\infty \psi_\infty^2 = g_0(\bar{z}) + \text{Real}\left\{ g_1(\bar{z}) e_2 e^{i\theta} + \frac{\delta}{2}\left[g_2(\bar{z}) e^{i(\theta-T)} + g_2^*(\bar{z}) e^{i(\theta+T)} \right] \right\} \tag{6.143}$$

where $g_2(\bar{z})$ and $g_2^*(\bar{z})$ are a complex conjugate pair,

$$g_2(\bar{z}) = u(\bar{z}) + iv(\bar{z})$$
$$g_2^*(\bar{z}) = u(\bar{z}) - iv(\bar{z}). \tag{6.144}$$

Using expansions (6.139) and (6.143) in the governing equation (6.140), the following set of perturbation equations arise:

$$\frac{d^2 g_0}{d\bar{z}^2} = 0 \qquad\qquad (6.145)$$

$$\frac{d^2 g_1}{d\bar{z}^2} - g_1 + 3g_0 = 0 \qquad\qquad (6.146)$$

$$\left.\begin{array}{l} \dfrac{d^2 u}{d\bar{z}^2} - u - K_3 v + 3g_0 = 0 \\[2mm] \dfrac{d^2 v}{d\bar{z}^2} - v + K_3 u - J\sqrt{g_0} = 0 \end{array}\right\} \qquad (6.147)$$

where $K_3 = \dfrac{J}{\sqrt{g_0}}$. The ambient boundary conditions (6.141) become

$$\left.\begin{array}{l} g_0 = 1 + \dfrac{3}{2} e_1^2 \\[2mm] u = g_1 = 3\left(1 + \dfrac{1}{2} e_1^2\right) \\[2mm] v = 0 \end{array}\right\} \ at \ \bar{z} = 0 \ and \ \bar{z} = z_L . \quad (6.148)$$

The symmetry boundary conditions (6.142) are automatically satisfied by assuming an expansion having the structure of equation (6.143), which involves only a cosine dependence on θ .

The solution of the zero order equation (6.145), subject to the boundary conditions (6.148), is simply

$$g_0 = 1 + \frac{3}{2} e_1^2 . \qquad\qquad (6.149)$$

The first order equation in eccentricity, (6.146), has a solution of the form

$$g_1(\bar{z}) = \bar{A} \cosh \bar{z} + \bar{B} \sinh \bar{z} + 3g_0 \qquad (6.150)$$

which satisfies the boundary conditions (6.148) if

$$\bar{A} = - 3e_1^2$$

$$\bar{B} = 3e_1^2 \tanh \frac{L}{D} \qquad (6.151)$$

(where $L/D = \bar{z}_L /2$). Thus

$$g_1(\bar{z}) = 3\left\{g_0 - e_1^2\left(\cosh \bar{z} - \tanh\frac{L}{D}\cdot\sinh \bar{z}\right)\right\}. \qquad (6.152)$$

The simultaneous equations (6.147) must be solved to obtain the first order solution in vibration amplitude, g_2, subject to boundary conditions (6.148). The numerical method discussed in Appendices A and B once again proves useful, and is described fully in Appendix D.

Having achieved solutions for g_0, g_1, u, v we can determine the τ-wise time averaged pressure distribution $\bar{P}$, given by equation (6.69). This, for small values of e_2 and δ can be expressed in the form

$$\bar{P} = \bar{P}_0 + e_2\bar{P}_1 + Real\left\{\delta e^{iT}\left(\bar{P}_2 - i\bar{P}_3\right)\right\} \qquad (6.153)$$

where

$$\bar{P}_0 = \sqrt{\frac{g_0}{1-e_1^2}} \qquad (6.154)$$

$$\bar{P}_1 = \frac{1}{2}\bar{P}_0 \cos\theta \left\{\frac{g_1}{g_0} - 1 - \frac{2}{(1-e_1^2)}\right\}. \qquad (6.155)$$

$$\bar{P}_2 = \tfrac{1}{2}\bar{P}_0 \cos\theta \left\{ \frac{u}{g_o} - 1 - \frac{2}{(1-e_1^2)} \right\} \qquad (6.156)$$

$$\bar{P}_3 = \frac{\bar{P}_0 v \cos\theta}{2 g_o} \quad . \qquad\qquad (6.157)$$

6.5.2 Static force

The steady state static force at small eccentricities is

$$F_0 = \frac{F_0'}{p_a \pi R^2} = -\frac{4}{\pi} \int_0^{\frac{z_L}{2}} \int_0^{\pi} \left(\bar{P}_0 - 1 + e_2 \bar{P}_1 \right) \cos\theta \, . \, d\theta \, . \, d\bar{z} \quad . \qquad (6.158)$$

Substituting for $\bar{P}_1$ from equation (6.155), this becomes

$$F_0 = -e_2 \bar{P}_0 \int_0^{z_L/2} \left\{ \frac{g_1}{g_o} - 1 - \frac{2}{(1-e_1^2)} \right\} d\bar{z} \qquad (6.159)$$

where g_1 is given by equation (6.152), so that

$$F_0 = e_1^2 e_2 z_L \bar{P}_0 \left\{ \frac{1}{(1-e_1^2)} + \frac{3}{g_o z_L} \tanh\frac{z_L}{2} \right\} \quad . \qquad (6.160)$$

This expression has no restriction on the excursion ratio e_1. If e_1^2 is assumed small ($e_1^2 \ll 1$), equation (6.160) reduces to Beck and Strodtman's result [26], given in equation (3.28), and discussed in section 3.2 .

6.5.3 Static stiffness

The static stiffness, expressed in terms of $L/D = z_L/2$, is

$$S_o = \frac{C}{P_a \pi R^2} \cdot S_o' = \frac{F_o}{e_2} \qquad (6.161)$$

so

$$S_o = 2 e_1^2 \bar{P}_o \frac{L}{D} \left\{ \frac{1}{(1-e_1^2)} + \frac{3D}{2 g_o L} \tanh \frac{L}{D} \right\} \qquad (6.162)$$

where $\bar{P}_o$ and g_o are given by equations (6.154) and (6.149).

For purposes of comparison, it is convenient to discuss the static stiffness per unit length,

$$\frac{S_o}{(L/D)} = 2 e_1^2 \bar{P}_o \left\{ \frac{1}{(1-e_1^2)} + \frac{3}{2 g_o} \cdot \frac{\tanh (L/D)}{(L/D)} \right\} . \qquad (6.163)$$

Since $\tanh (L/D) \sim L/D$ for small L/D, the infinitesimally short journal bearing has a stiffness per unit length

$$\left. \frac{S_o}{(L/D)} \right|_{L/D \ll 1} \simeq 2 e_1^2 \bar{P}_o \left\{ \frac{1}{(1-e_1^2)} + \frac{3}{2 g_o} \right\} . \qquad (6.164)$$

At the other extreme,

$$\left. \frac{\tanh (L/D)}{(L/D)} \right|_{L/D \gg 1} \simeq 0 \qquad (6.165)$$

so for large L/D,

$$\left. \frac{S_o}{(L/D)} \right|_{L/D \gg 1} \simeq \frac{2 e_1^2 \bar{P}_o}{(1-e_1^2)} . \qquad (6.166)$$

We see that the very short bearing has a stiffness per unit length which exceeds that of the very long bearing by an amount $\dfrac{3 e_1^2 \bar{P}_o}{g_o}$.

The function expressed in equation (6.163) is shown in Fig.37 for various values of e_1. Normalisation with respect to the behaviour of the very long bearing, equation (6.166), has been used so as to make all the curves of the same order of magnitude for simple comparison. On this basis it can be seen that, for small e_1, the very short bearing has almost 2.5 times the stiffness of the very long bearing, agreeing with the findings of Beck and Strodtman[26] (see section 3.2, and Fig.6). As L/D increases the stiffness drops until, for large L/D, the improvement arising from the edge-pressurising tanh (L/D) term is lost completely because of circumferential leakage flow. With increasing excursion ratio e_1 the improvement in stiffness at small values of L/D is not so marked[26, 28], because the interior 'Boyle's Law' term in $\frac{1}{(1-e_1^2)}$ begins to dominate over the edge-pressurising term in tanh (L/D), and circumferential leakage becomes large even in quite short bearings. The improved stiffness in short bearings is reduced from about 145% for $e_1 = 0.1$ to 13% for $e_1 = 0.9$. At the more representative condition $e_1 = 0.5$, the improvement is $\sim 80\%$.

This dependence on e_1 is shown perhaps more clearly in Fig.38, where a curve for L/D = 0 has been included as a limiting case, even though it is not strictly valid according to the theory given in section 4.

6.5.4 Dynamic stiffness

The dynamic spring and damping forces are respectively

$$F_1 = \frac{F_1'}{p_a \pi R^2} = -\frac{4\delta}{\pi} \int_0^{L/2} \int_0^{\pi} \bar{P}_2 \cos\theta \, d\theta \, d\bar{z} \qquad (6.167)$$

$$F_2 = \frac{F_2'}{P_a \pi R^2} = -\frac{4\delta}{\pi} \int_0^{z_L/2} \int_0^{\pi} \bar{P}_3 \cos\theta \, d\theta \, d\bar{z} \qquad (6.168)$$

where $\bar{P}_2$ and $\bar{P}_3$ were given in equations (6.156) and (6.157).

The in-phase and quadrature components of the dynamic stiffness are thus

$$S_1 = \frac{F_1}{\delta} = \frac{c}{P_a \pi R^2} \cdot S_1' = -\frac{4}{\pi} \int_0^{z_L/2} \int_0^{\pi} \bar{P}_2 \cos\theta \, d\theta \, d\bar{z} \qquad (6.169)$$

$$S_2 = \frac{F_2}{\delta} = \frac{c}{P_a \pi R^2} \cdot S_2' = -\frac{4}{\pi} \int_0^{z_L/2} \int_0^{\pi} \bar{P}_3 \cos\theta \, d\theta \, d\bar{z} \qquad (6.170)$$

so that

$$S_1 = \bar{P}_0 \left\{ \frac{1}{2} z_L \left(\frac{3 - e_1^2}{1 - e_1^2} \right) - \frac{1}{q_0} \int_0^{z_L/2} u \, d\bar{z} \right\} \qquad (6.171)$$

and

$$S_2 = -\frac{\bar{P}_0}{q_0} \int_0^{z_L/2} v \, d\bar{z} \qquad (6.172)$$

where u and v were solutions of the simultaneous equations (6.147).

S_1 is plotted as a function of the vibration number γ in Fig.39 , showing a general rise from the static value S_0 for a given L/D, and levelling off at a higher constant value for large γ . With increasing L/D, the onset of the rise in S_1 is displaced towards smaller values of γ , the overall increase in stiffness with L/D

being attributable to the general increase in bearing projected area which follows an increase in length of a bearing when the diameter is kept constant.

A similar set of curves for S_2 is given in Fig.40, where it can be seen that the peak 'damping' is displaced towards the lower end of the γ-scale with increasing L/D, reaching a constant value of γ for large L/D when the bearing is effectively 'infinitely' long (in that the edge-pressurising effect is, to all intents and purposes, lost).

Bearings with different values of L/D can more easily be compared with the help of Fig.41, where the functions

$$\frac{S_1}{(L/D)} = \frac{2c}{p_a \pi R} \cdot \frac{S_1'}{L}$$

$$\frac{S_2}{(L/D)} = \frac{2c}{p_a \pi R} \cdot \frac{S_2'}{L}$$

(6.173)

have been plotted, being the dynamic stiffness components per unit length of the bearing. For small γ the damping is negligible, and the stiffness tends to the static behaviour discussed in section 6.5.3 . For larger γ , it can be seen that the peak damping component of the stiffness per unit length increases to some limiting value for large L/D, about 50% larger than the peak damping for L/D = 0.2 . Physically, this is because in the large L/D bearing the flow in response to the forced vibration is mainly circumferential, being associated with much larger path lengths than in the case of the predominantly axial response flow in very short bearings. The constant value

of γ at peak damping for large L/D is understandable in that the almost exclusively circumferential flow in such cases results in a limiting flow velocity amplitude being set up because the same effective path length ($\sim \pi R$) occurs regardless of the size of L/D. The shift in peak damping to higher values of γ for small L/D is because higher film velocities can be associated with the shorter path lengths before viscous shear forces rise to a level where the compressibility of the gas limits the process.

6.5.5 Vibration response

Once again we use the approach of Pan and Chiang[22]. Suppose the bearing supports a mass m per unit length, so that an externally applied vibrational force per unit length

$$\frac{F'_{ext}}{L} = \frac{p_a \pi R^2}{L} \cdot \text{Real}\left\{ f e^{i\nu t} \right\} \tag{6.174}$$

causes a dynamic film force per unit length

$$\frac{F'_{dyn}}{L} = \frac{p_a \pi R^2}{L} \cdot \text{Real}\left\{ \delta e^{i\nu t}(S_1 - i S_2) \right\} \tag{6.175}$$

and a mass response displacement amplitude

$$x = C \cdot \text{Real}\left\{ \delta e^{i\nu t} \right\} \tag{6.176}$$

such that the equation of motion is

$$L m \ddot{x} + F'_{dyn} = F'_{ext} . \tag{6.177}$$

Using equations (6.174) to (6.177), and remembering that the vibration number is

$$\jmath = \frac{12\mu\gamma}{p_a} \left(\frac{R}{C}\right)^2 \qquad (6.178)$$

the dynamic compliance of the system can be written in the form

$$\frac{\delta}{f} = \delta_1 e^{i\gamma} = \frac{1}{(S_1 - M_1\jmath^2) - iS_2} \qquad (6.179)$$

where the amplitude and phase are

$$\delta_1 = \frac{p_a\pi R^2}{C}\delta_1' = \frac{1}{\sqrt{(S_1 - M_1\jmath^2)^2 + S_2^2}} \qquad (6.180)$$

$$\gamma = \tan^{-1}\frac{S_2}{(S_1 - M_1\jmath^2)} \quad.$$

These expressions are exactly the same as those for the axially grooved journal bearing, section 6.4.2, except that the normalisation for δ_1 is different, and this time the dimensionless mass per unit length is

$$M_1 = \frac{mLp_a}{144\pi\mu^2 R}\left(\frac{C}{R}\right)^5 \quad. \qquad (6.181)$$

Once more, resonance occurs when $\jmath = \sqrt{S_1/M_1}$, in which case

$$\delta_1\bigg|_{\text{resonance}} = \frac{1}{S_2}$$

$$\gamma\bigg|_{\text{resonance}} = \frac{\pi}{2} \quad. \qquad (6.182)$$

Curves of $M_1 \gamma^2$ (M_1 fixed), superimposed on those of S_1
in Fig.39, enable the resonance values of γ to be
determined.

The dynamic compliance δ_1 is shown as a function of
γ in Fig.42 for the case L/D = 0.2, and the behaviour is
seen to be qualitatively similar to that of Fig.33 for
the infinite length axially grooved journal bearing.
Again there is an optimum value for M_1 which results in a
resonance coinciding with the condition of maximum 'damping',
thus limiting the response. For very small normalised
masses, resonance occurs outside the range of interest
(at $\gamma > 1000$) so, assuming that excitations resulting in
vibration numbers in excess of 1000 are highly attenuated
in practice, the dynamic compliance will be smaller than
the static compliance over most of the range of γ. If it
is necessary to swamp an unwanted peak compliance in the
range $\gamma > 1000$, this can be accomplished by making a small
reduction in L/D so as to shift the peak damping to coincide
with the resonance condition. It can be seen that the peak
compliance at maximum damping is about twice the static
compliance when L/D = 0.2. The locus of the peak damping,
shown in Fig.42, indicates that the peak compliance
achieves large values when the normalised mass deviates far
from the optimum value of $M_1 \simeq 8 \times 10^{-5}$.

A family of such loci is shown in Fig.43 as a function
of M_1. The peak compliance $\delta_1 \big|_{resonance}$ has been normalised
with respect to the static compliance $\delta_1 (\gamma = 0)$ so that
curves for different values of L/D appear of the same order
of magnitude. This shows clearly how the large peak

damping for large L/D results in an optimum dynamic compliance differing little from the static value, while the decreased peak damping in shorter bearings leads to optimum dynamic compliances nearer twice the static value. The value of M_1 at which the optimum peak compliance occurs is very sensitive to small changes in L/D for short bearings, so the system can be 'tuned' for optimum conditions relatively easily by making slight adjustments to the size of L/D during design work. Of course this can only be done if the specified static loading conditions can also be met.

Fig.44 shows how the resonance value of γ differs from the value $\gamma_0 = \sqrt{S_1(\gamma = 0)/M_1}$ when M_1 is varied. It can be seen that the estimate γ_0 based on the static stiffness can be as much as 80% too low for large L/D, while the discrepancy at small values of L/D ($\simeq 0.2$) is about 30%.

6.5.6 Stability

Exactly the same argument as used in section 6.4.3 for the axially grooved journal bearing shows that the finite length ungrooved bearing is always stable with respect to forced vibration when the eccentricity e_2 and vibration amplitude δ are small.

6.6 Circumferentially grooved journal bearing

The static force in a circumferentially grooved journal bearing was discussed in section 3.2.3; for dynamic behaviour, we can draw on the results of section 6.5 if L/D is taken to refer to a bearing segment rather than to the overall bearing.

6.6.1 Static stiffness

A circumferentially grooved bearing, composed of bearing segments each of length-diameter ratio ℓ/D, will have a static stiffness per unit length given by equation (6.163), namely

$$\frac{S_0}{(\ell/D)} = 2e_1^2\bar{P}_0\left\{\frac{1}{(1-e_1^2)} + \frac{3}{2g_0}\cdot\frac{\tanh(\ell/D)}{(\ell/D)}\right\} \qquad (6.183)$$

where $\bar{P}_0$ and g_0 are defined in equations (6.154) and (6.149). If there are w such bearing segments, mutually separated by ambient line boundaries, the total length-diameter ratio will be

$$\frac{w\ell}{D} = \frac{L}{D} \qquad (6.184)$$

and the segmented bearing will have a projected area equal to that of the ungrooved bearing of length-diameter ratio L/D, which has a static stiffness per unit length given directly by equation (6.163). The maximum possible stiffness is obtained when there are a large number of segments in the circumferentially grooved bearing, in which case

$$\frac{S_0}{(\ell/D)}\bigg|_{\ell/D\to 0} \longrightarrow 2e_1^2\bar{P}_0\left\{\frac{1}{(1-e_1^2)} + \frac{3}{2g_0}\right\}. \qquad (6.185)$$

This quantity, normalised with respect to the behaviour of the ungrooved bearing, equation (6.163), is shown in Fig.45 . If $\ell/D \leqslant 0.2$ there will be at most a 1% discrepancy in using these curves. The benefits to be obtained from

grooving are seen to be most marked for small values of excursion ratio, with the improvement decreasing rapidly with increasing e_1. This is shown more obviously if the same information is presented in the form of Fig.46 . A realistic value for e_1 is 0.5, in which case the improvement due to grooving is about 30% for L/D = 2, 50% for L/D = 4, 60% for L/D = 6.

6.6.2 Dynamic stiffness components

The dynamic stiffness of a circumferentially grooved journal bearing of arbitrary length-diameter ratio L/D can be obtained from Fig.41 if the curve for L/D = 0.2 is scaled by the arbitrary value of L/D. For instance, a grooved bearing with L/D = 3 will have a dynamic stiffness as shown in Fig.47. Also shown is the dynamic stiffness of the ungrooved bearing having L/D = 3, obtained by scaling by a factor of 3 the L/D = 3 curve in Fig.41. Similar curves for the 'damping' S_2 are given in Fig.48. The segment length-diameter ratio of ℓ/D = 0.2 in the grooved bearing ensures that the static performance is within 1% of the best attainable.

The effect of grooving can be seen to increase the static stiffness and to delay the onset of the asymptotic increase in dynamic stiffness by about two decades of the vibration number γ . The peak damping is shifted from γ = 1.6 to γ = 75, and reduced in magnitude by approximately 25%.

6.6.3 Vibration response

The effect of circumferential grooving on the vibration response in the typical case of L/D = 3 is shown in

Fig.49 . The dynamic compliance, given by equation (6.180), has been normalised with respect to the static stiffness of the ungrooved 'bearing' so as to make comparison more easy. Because the peak damping occurs at a low vibration number (γ = 1.6), the ungrooved bearing has small peak compliances when the non-dimensional mass per unit length M_1 is relatively large, the minimum peak compliance being very close to the static value when $M_1 \simeq 2.6$. The grooved bearing, on the other hand, has small peak compliances higher up the γ-scale near γ = 75, the minimum value being about 1.4 times that of the ungrooved bearing static compliance and occurring when $M_1 \simeq 0.0013$. Grooving the bearing results in a reduction in static compliance of nearly 30%.

It can be seen that very large dynamic compliances can result if M_1 is such that a peak compliance is associated with a value of γ insufficiently close to the condition of maximum damping. The normalised mass per unit length, equation (6.181), can be written

$$M_1 = \frac{p_a m}{72 \pi \mu^2}\left(\frac{L}{D}\right)\left(\frac{C}{R}\right)^5 .$$

(6.186)

Typical values for a bearing required to support a mass under full gravitational loading might be

L/D = 3

C/R = 1.25 x 10^{-4}

m = 2.5 kg/m

p_a = 10^5 N/m^2

μ = 2 x 10^{-5} N s/m^2

resulting in $M_1 \sim 5 \times 10^{-7}$. This produces a peak compliance well outside the range of interest of γ, so both the grooved and ungrooved bearing will have a dynamic compliance smaller than or equal to the appropriate static value in the range $0 \leqslant \gamma \leqslant 1000$. However, if the bearing axis is vertical and the gravitational load is not directly taken by the bearing, M_1 can take on much larger values and resonance peaks in the compliance curves will occur for $\gamma < 1000$. In such cases care must be taken in design work to avoid unacceptably large response displacements. For $L/D = 3$, when M_1 differs from 2.6 by more than (say) an order of magnitude, circumferential grooving would be desirable with a value of ℓ/D for the bearing segments chosen so as to make the peak resonance coincide with maximum damping. For $M_1 \gtrsim 0.02$ one should choose ℓ/D in the range $\ell/D > 0.2$, which means that the static stiffness will no longer be optimised, although large dynamic responses would be avoided. For $M_1 < 0.02$, ℓ/D should lie in the range $\ell/D \leqslant 0.2$ in which case both the static and dynamic compliance can be optimised to an acceptable degree.

6.6.4 Stability

For the same argument as used in section 6.4.3 the circumferentially grooved journal bearing should always be stable with respect to forced vibration at small amplitudes near zero eccentricity.

6.7 Step-jump method for dynamical analysis

The foregoing dynamic results have only been valid
for small eccentricities and small vibration amplitudes,
which are of interest to the writer in their application
to inertial navigation instruments. For other applications,
where it might be necessary to investigate large
eccentricity performance, perturbation theory becomes of
little use and the step-jump method has certain advantages
which make it attractive in the context of the present
work. Detailed results have not been obtained, as interest
is particularly aimed at small eccentricity behaviour, but
the method will be outlined so as to be useful if required
in future study. Although it has not been used in the
treatment of squeeze-film bearings, the step-jump method
has been applied to stability investigations in self-
acting[46, 57] and externally-pressurised[47, 57] bearings,
and to the vibration response of externally pressurised
gas bearings[47] and oil and grease self-acting bearings[55].

The step-jump procedure computes the response of the
film to sudden jumps of the shaft in each of its degrees
of freedom, and stores the information in the form of
polynomial expansions. These time-dependent responses
can then be used repeatedly in the equations of motion of
the system as the dynamic parameters are varied, avoiding
the time-consuming necessity for re-solving the governing
equation for each case. This is the real advantage in the
present work where an axially grooved bearing might
require twenty solutions of the governing equation per
single value for the total bearing force, because the

contribution from each of the bearing segments must be summed. This then has to be repeated for many time steps to obtain the film response information, so if there are twenty-five time steps the governing equation must be solved 500 times. If in addition it is necessary to repeat this process again each time a parameter in the dynamic equations is varied, it is easy to see that the cost would be prohibitive. Using the step jump method the film response is stored once and for all, and there is no necessity to use the governing equation again while a family of dynamic results is obtained centred on the original equilibrium situation.

In outline, one assumes that the bearing system has two degrees of translational freedom (in a reference direction, and at right angles to it). One could also include two angular degrees of freedom to give conical motion but, for simplicity, we will restrict ourselves to simple translation. The bearing is allowed to take up an equilibrium position at some eccentricity e_2, and the steady state static force is computed from the initial distribution $Q = Q_{init} = (PH)^2$, using the governing equation (4.43) and its boundary conditions (4.58) and (4.59) with $\gamma = 0$ and $\delta = 0$. The bearing is then given an instantaneous step shaft displacement in one of its degrees of freedom so that under isothermal conditions $Q = (PH)^2$ remains constant during the jump. In other words, just after the jump the value of Q is the same as for the original equilibrium condition, but the film thickness distribution H is now different. Consequently the film

pressure changes abruptly to a new value, as does the static force. Writing the governing equation in the form

$$\phi(Q) = \gamma \frac{\partial}{\partial T} \sqrt{Q} = \frac{\gamma}{2\sqrt{Q}} \frac{\partial Q}{\partial T} \tag{6.187}$$

where $\phi(Q)$ represents the left hand side of equation (4.43), one can express the time derivative in backward difference form,

$$\phi(Q) = \frac{\gamma}{2\sqrt{Q_{init}}} \cdot \frac{(Q - Q_{init})}{\nu \Delta t} \tag{6.188}$$

where Q is evaluated at time t in terms of the value Q_{init} obtained at time $(t - \Delta t)$. Using this new value for $(PH)^2$, the static force is computed and stored, while $(PH)^2$ is stored in Q_{init} ready for the next time step. This is repeated over and again, so that a record is obtained of the transient behaviour of the static force until a new equilibrium situation is reached. We thus have a response curve like that shown in Fig.50 where $F_{ij}(t)$ is the force in the j direction arising from a displacement δx_i in the i direction, or alternatively i and j represent respectively the 'cause' and 'effect' directions. Dimensionless responses are expressed in the form

$$R_{ij}(t) = \frac{F_{ij}(t) - F_j(0)}{\delta x_i} = \frac{\delta F_{ij}(t)}{\delta x_i} \tag{6.189}$$

where $F_j(0)$ is the original equilibrium force in the j direction, then these responses are stored conveniently in the form of the Laguerre polynomial expansion

$$R_{ij}(t) - R_{ij}(\infty) = \sum_{n=0}^{\infty} A_n^{(ij)} L_n(\alpha t) e^{-\alpha t} \qquad (6.190)$$

where $R_{ij}(\infty)$ is the response after equilibrium has once more been restored, and α is an attenuation constant. The series is truncated at some value $n = m_L$, such that by trial and error adjustment of α and m_L one obtains as close a fit of the polynomial expansion to the response curve as is desired. This procedure is also carried out for a step jump in the other degree of freedom j so that we end up with a set of four responses, the ii, ij, ji, and jj responses, all stored in the same form as equation (6.190).

Information is now stored about dimensionless film forces which will always apply for small deviations from the original equilibrium conditions, regardless of what other forces are affecting the shaft.

6.7.1 Stability

To investigate stability, the approach is to subject the bearing, initially in some static state of equilibrium, to some sudden small disturbance, and to observe the response. If the response decays the system is stable, but if it grows then an unstable situation is indicated.

If M_1 is the normalised mass of the shaft, the equations of motion for the two degrees of freedom can be expressed as follows:

$$M_1 \, \delta \ddot{x}_i = \delta F_{ii} + \delta F_{ij}$$
$$M_1 \, \delta \ddot{x}_j = \delta F_{ji} + \delta F_{jj} \; . \qquad (6.191)$$

If the disturbance to each degree of freedom is assumed to take the form

$$\delta x = \delta \bar{x} \, e^{\beta t} \tag{6.192}$$

then the system will be stable if the real part of β is negative. Using equation (6.192), and taking the Laplace transform of equation (6.190), one can typically write

$$\delta F_{ij} = \left\{ R_{ij}(\infty) + \sum_{n=1}^{m_i} A_{n-1}^{(ij)} \, \xi^n \right\} \delta \bar{x}_i \, e^{\beta t} \tag{6.193}$$

where

$$\xi = \frac{\beta/\alpha}{(1 + \beta/\alpha)} \tag{6.194}$$

and

$$A_n^{(ij)} = \alpha \int_0^{\infty} \left\{ R_{ij}(t) - R(\infty) \right\} L_n(\alpha t) \, dt \, . \tag{6.195}$$

Substituting this in equations (6.191) a solution exists if the following polynomial equation is satisfied

$$\sum_{n=0}^{2(m_i+2)} \bar{C}_n \, \xi^n = 0 \tag{6.196}$$

where the $\bar{C}_n$ are coefficients arising from the dynamical equations. The roots of this equation can then be found numerically, and if the real part of any of the resulting β's is positive, the system will be unstable. The stability threshold is then determined by trying

different values of mass M_1 until the value M_o is found at the cross-over point between positive and negative values of the real part of β . From the results of the preceding sections, it is anticipated that it will be found that $M_o = \infty$.

6.7.2 Frequency response

To investigate the vibration response it is assumed that a sinusoidal displacement stimulus is applied to the bearing housing, having non-dimensional components

$$\delta x_i^{(B)} = \delta \bar{x}_i^{(B)} e^{iT}$$

$$\delta x_j^{(B)} = \delta \bar{x}_j^{(B)} e^{iT}$$

$$(6.197)$$

where $T = \nu t$ is the normalised time and ν is the angular frequency of the forcing stimulus. The amplitude and phase of this stimulus with respect to the reference direction are thus

$$\delta \bar{X}^{(B)} = \sqrt{\left(\delta \bar{x}_i^{(B)}\right)^2 + \left(\delta \bar{x}_j^{(B)}\right)^2}$$

$$(6.198)$$

$$\phi_B = \tan^{-1} \frac{\delta \bar{x}_j^{(B)}}{\delta \bar{x}_i^{(B)}} \quad .$$

In response to this stimulus, the bearing shaft is assumed to have non-dimensional displacement amplitudes

$$\delta x_i^{(S)} = \delta \bar{x}_i^{(S)} e^{iT}$$

$$\delta x_j^{(S)} = \delta \bar{x}_j^{(S)} e^{iT}$$

$$(6.199)$$

whose amplitude and phase relative to the reference direction are

$$\delta \bar{x}^{(S)} = \sqrt{\left(\delta \bar{x}_i^{(S)}\right)^2 + \left(\delta \bar{x}_j^{(S)}\right)^2}$$

(6.200)

$$\phi_s = \tan^{-1} \frac{\delta \bar{x}_j^{(S)}}{\delta \bar{x}_i^{(S)}}.$$

The film forces depend on

$$\delta x_i = \delta x_i^{(S)} - \delta x_i^{(B)} = \delta \bar{x}_i \, e^{iT}$$

$$\delta x_j = \delta x_j^{(S)} - \delta x_j^{(B)} = \delta \bar{x}_j \, e^{iT}$$

(6.201)

so the equations of motion for the shaft can be written in the normalised form

$$M_1 \gamma^2 \frac{d^2}{dT^2} \left(\delta x_i + \delta x_i^{(B)}\right) = \delta F_{ii} + \delta F_{ji}$$

$$M_1 \gamma^2 \frac{d^2}{dT^2} \left(\delta x_j + \delta x_j^{(B)}\right) = \delta F_{ij} + \delta F_{jj}$$

(6.202)

where M_1 is the non-dimensional mass and γ is the vibration number previously defined. For convenience, the forces on the right-hand side are written in the typical form

$$\delta F_{ij} = \delta x_i \sum{}'_{ij} = \delta x_i \sum_{n=1}^{m_L-1} D_n^{(ij)} \xi^{n-1}$$

(6.203)

where the $D_n^{(ij)}$ are coefficients involving the Laguerre coefficients $A_n^{(ij)}$ of equation (6.193), and ξ is defined in equation (6.194). Using these, equations (6.202) can be written in the matrix form

$$\bar{D} \, \underline{\delta \bar{x}} = - M_1 \gamma^2 \, \underline{\delta \bar{x}}^{(B)} \qquad\qquad (6.204)$$

where

$$\bar{D} = \left\| \begin{array}{cc} \left(M_1\gamma^2 + \Sigma_{ii}\right) & \Sigma_{ji} \\ \\ \\ \Sigma_{ij} & \left(M_1\gamma^2 + \Sigma_{jj}\right) \end{array} \right\|$$

$$\underline{\delta\bar{x}} = \left\| \begin{array}{c} \delta\bar{x}_i \\ \\ \delta\bar{x}_j \end{array} \right\| \qquad\qquad \underline{\delta\bar{x}}^{(B)} = \left\| \begin{array}{c} \delta\bar{x}_i^{(B)} \\ \\ \delta\bar{x}_j^{(B)} \end{array} \right\| .$$

The solution of equation (6.204) is then simply

$$\underline{\delta\bar{x}} = - M_1 \gamma \left[\bar{D}\right]^{-1} \underline{\delta\bar{x}}^{(B)} \qquad\qquad (6.205)$$

from which the component displacements of the shaft can
be found using equation (6.201), and then substituted into
equations (6.200). By varying the amplitude and phase of
the stimulus, equations (6.198), and sweeping over the
range $0 \leqslant \gamma \leqslant 1000$, the weaknesses in the bearing can be
discovered and minimised by appropriate use of grooving.

6.7.3 Experience of using the step-jump method

Detailed stability and frequency response results have not as yet been obtained for squeeze-film bearings using the step-jump method, but an outline of some of the work done and problems met may be of use to others interested in using the method at some future date.

It was noticed that other workers[47, 55, 57] used a fixed time increment ΔT in equation (6.188) in obtaining a response curve similar to that shown in Fig.50 . This was considered wasteful in computer time, as most of the rapid changes in response occur early in the transient and for most of the decay the response changes very slowly. A varying time-step was thought more economical, the requirement being a small value for ΔT immediately after the step-jump, and then a progressively lengthening time increment as the response decays asymptotically to the new state of equilibrium. It must be ensured that the short initial time step is sufficiently long so as to allow the response force to take on a time averaged value with respect to the basic squeeze motion. A typical squeeze frequency is 20kHz, having a period of 50 μs. With a nominal vibration number γ = 10 (which has no significance at this stage, merely serving to scale the time T), the initial time step chosen was ΔT = 0.01, being equivalent to a real period of 250 μs. There is thus sufficient time for five cycles of the squeeze motion before the first response force is calculated. A square law increase in ΔT was then chosen such that 25 time steps covered the whole of the response decay to the asymptotic equilibrium condition.

A typical example is shown in Fig.51 where a full set of four responses is given for a smooth cylindrical squeeze-film journal bearing with L/D = 1, e_1 = 0.5, initially in the centred position (e_2 = 0), subjected to step-jumps $\delta\bar{x}_i = \delta\bar{x}_j$ = 0.08 in the reference direction and at right-angles to it. The vibration number has a nominal value γ = 10. After 25 time increments ΔT the responses are within 0.4% of their final equilibrium values.

These responses were then approximated by a Laguerre polynomial expansion of the form given in equation (6.190) with the help of a FORTRAN subroutine used by Dewar[55] in his work on grease bearings. To make the responses compatible with Dewar's routine, a Lagrange interpolation routine was written to convert the irregularly spaced 25 point curves into a set of curves with 100 equally spaced points. Considerable savings in computer time were found using this method rather than establishing the original response curves by means of the equally spaced time grid.

To solve the polynomial equation (6.196) for the roots of β in the stability investigation, a subroutine by B.E. Taylor of RAE (Farnborough) was used based on a procedure due to Müller[56]. A considerable amount of difficulty was encountered in that the first couple of roots found by this routine tended to be spurious, and much time was wasted in attempting to find a reason for this annoying behaviour. A more sophisticated routine based on the Müller method appeared later in the form of a UNIVAC MATH-PACK, but this too produced spurious roots. Further investigation showed that Elrod and Glanfield had

also suffered from this problem when using the Taylor routine in their work on flexibly mounted externally-pressurised gas bearings[47]. The net conclusion seems to be that both the Müller procedures were working quite correctly, but that the spurious roots were caused by the initial conditions used in starting the programs. This has yet to be tested, but it is worth noting that Scowen[57], in his extension of Elrod and Glanfield's work[47], has achieved sensible results in spite of several spurious roots, but the basis he used for doing this is not at present known to this writer.

6.8   Conical and hemispherical bearings

The static and dynamic performance of conical and hemispherical bearings will not differ substantially from that of the flat circular thrust bearing in the axial direction, and from that of the cylindrical journal bearing in the radial direction, so it is not intended to dwell on them in detail, but merely to indicate how the governing equations can be modified to treat these geometries.

6.8.1   Conical bearings

If the cone semi-angle is Γ and the maximum radius is R, a convenient co-ordinate system is (r, θ) where r is measured from the apex along a generator and θ is the circumferential co-ordinate such that $\theta = \pi$ is the direction of the radial displacement of the shaft. Normalising these variables with respect to R, non-dimensionalised co-ordinates $(\xi = r/R, \theta)$ can be used such that an element of non-dimensional area is $\xi \sin \Gamma \, d\theta \, . \, d\xi$. The governing equation is then (4.43) with $u_1 = \theta$, $u_2 = \xi$,

$\ell_1 = \xi \sin \Gamma$, $\ell_2 = 1$, and the normalised film thickness can be expressed as

$$H = \frac{h}{C} = H_\infty + e_1 \sin \Gamma \cos \tau \qquad (6.206)$$

where, as usual, e_1 is the excursion ratio, $\tau = \omega t$ is the normalised time associated with the squeeze motion, and H_∞ is the film thickness time-averaged with respect to τ, namely

$$H_\infty = 1 + \sin \Gamma \left(e_z + \delta_z \cos T_z \right) + \cos \Gamma \cos \theta \left(e_R + \delta_R \cos T_R \right). \qquad (6.207)$$

Here, e_z and e_R are the normalised axial and radial steady displacements, while δ_z and δ_R are amplitudes of the forced responses in the axial and radial directions respectively associated with normalised times $T_z = \nu_z t$ and $T_R = \nu_R t$. One can treat axial and radial forced vibrations separately by setting either δ_z or δ_R equal to zero. Equation (4.43) is solved subject to ambient boundary conditions (4.58) and (4.59) with $\bar{a} = \xi_1$ and $\bar{b} = \xi_2$, where $\xi_1 = r_1/R$ and $\xi_2 = r_2/R$ for ambient boundaries at $r = r_1$ and $r = r_2$. If slip flow is not present, one sets $m = 0$ in equations (4.43), (4.58) and (4.59). Notice that if $\Gamma = \pi/2$, the problem reduces to the annular flat thrust plate considered in section 6.1, and if $\Gamma \to 0$ we tend towards a cylindrical journal bearing, so the results of a conical bearing analysis would not be expected to produce any surprises.

The film pressure, time averaged with respect to τ, is

$$\overline{P} = \frac{\psi_{\infty}}{\sqrt{H_{\infty}^2 - e_1^2 \sin^2 \Gamma}} \qquad (6.208)$$

from which the axial and radial bearing forces can be
obtained:

$$F_{\overline{z}} = \frac{F_{\overline{z}}'}{p_a \pi R^2} = -\frac{\sin^2 \Gamma}{\pi} \int_{\xi_1}^{\xi_2} \int_0^{2\pi} (\overline{P} - 1)\, \xi\, d\theta . d\xi$$

$$\qquad (6.209)$$

$$F_R = \frac{F_R'}{p_a \pi R^2} = -\frac{\sin 2\Gamma}{2\pi} \int_{\xi_1}^{\xi_2} \int_0^{2\pi} (\overline{P} - 1)\, \xi \cos\theta . d\theta . d\xi .$$

From these, the steady state static forces and steady
state dynamic forces can be separated out as desired.

Circumferentially grooved conical bearings can be
treated by summing together w conical segments defined
by ambient boundaries at $\xi = \xi_1$, $\xi = \xi_2$, $\xi = \xi_3$,
... , $\xi = \xi_{w+1}$. Axial grooving can be dealt with by
considering a bearing segment region $\xi_1 \leqslant \xi \leqslant \xi_2$,
$\theta_{k-1+\alpha} \leqslant \theta \leqslant \theta_{k-\alpha}$ (as in section 6.3) and changing the
limits of the integrals in equations (6.209) before
summing over all the w segments to obtain the total
bearing forces.

The static performance of the ungrooved conical
bearing was discussed by Pan[17] as an illustration of his
asymptotic theory, but the forced dynamic response has not
been treated in the literature.

6.8.2 Hemispherical bearings

An hemispherical bearing of radius R can be described by the co-ordinates (θ, ϕ), such that an element of area is $R \sin\phi \, d\theta . R d\phi$, and there are ambient boundaries near the pole at $\phi = \phi_1$ and near the equator at $\phi = \phi_2$. Normalising the spatial dimensions of the elemental area with respect to R, the normalised elemental area becomes $\sin\phi . d\theta . d\phi$ so that $u_1 = \theta$, $u_2 = \phi$, $\ell_1 = \sin\phi$, $\ell_2 = 1$ in the governing equation (4.43). The normalised film thickness is

$$H = \frac{h}{C} = H_\infty + e_1 \cos^n\phi \cos\tau \qquad (6.210)$$

where n = 1 for a purely axial excursion, and n = 0 for a spherically symmetric excursion. The time averaged film thickness is

$$H_\infty = 1 + \cos\phi \left(e_z + \delta_z \cos T_z \right) + \sin\phi \cos\theta \left(e_R + \delta_R \cos T_R \right)$$

$$(6.211)$$

where e_z, e_R, δ_z, δ_R have the same meaning as in section 6.8.1 . Equation (4.43) is solved subject to ambient boundary conditions (4.58) and (4.59) at $\bar{a} = \phi_1$ and $\bar{b} = \phi_2$.

The time-averaged pressure in this case is

$$\bar{P} = \frac{\psi_\infty}{\sqrt{H_\infty^2 - e_1^2 \cos^{2n}\phi}} \qquad (6.212)$$

leading to axial and radial bearing forces

$$F_z = \frac{F_z'}{p_a \pi R^2} = -\frac{1}{2\pi} \int_{\phi_1}^{\phi_2} \int_0^{2\pi} (\bar{P}-1) \sin 2\phi \, d\theta \, d\phi$$

$$(6.213)$$

$$F_R = \frac{F_R'}{p_a \pi R^2} = -\frac{1}{\pi} \int_{\phi_1}^{\phi_2} \int_0^{2\pi} (\bar{P}-1) \sin^2\phi \cos\theta \, d\theta \, d\phi .$$

The static and dynamic force components can be separated out as desired. As in the conical bearing, circumferential or axial grooving can be treated by redefining the ambient boundaries and solving equation (4.43) in each segment. The force contributions from each segment, obtained from equations (6.213) with new integration limits, can then be summed to obtain the total bearing forces.

The static and dynamic behaviour of the ungrooved hemispherical bearing were covered in references 19 and 22, while Beck and Strodtman[24] investigated the effect on static load capacity of varying the polar angle ϕ_1 .

6.8.3 Grooved bearings

The presence of ambient line boundaries in both conical and hemispherical bearings should make no difference to the axial static force but will improve the radial static force because circumferential leakage flow will be reduced. The amount of improvement cannot be expected to be great, as circumferential leakage in the smooth bearing is inherently small anyway because of the relatively short axial length of conical and hemispherical bearings. The journal aspect of most of these bearings would have

an effective slenderness ratio of $L/D \lesssim 1$ when approximated by a cylindrical journal bearing of the same radial projected area, and we have shown that the best improvement to be expected is about 18% for $L/D = 1$ when e_1^2 and e_R are small (see section 6.3.2). However, even this small amount of improvement would be valuable in difficult applications such as inertial navigation equipment where the bearings must be made as small, and consequently as efficient as possible. Enhanced static performance can be expected to be more pronounced in conical bearings where the cone semi-angle Γ is small and $\xi_1/\xi_2 \ll 1$, such as might be the case where the bearing is intended mainly to support radial loads.

The main benefits to accrue from grooving conical and hemispherical bearings should be found in the response to external vibration. As in flat thrust and cylindrical journal bearings, the placing of extra ambient boundaries should displace the peak dynamic 'damping' and the increase in dynamic stiffness to higher vibration numbers, so that the number of grooves can be chosen to 'tune' the bearing for minimum peak compliance depending on the mass being supported.

7 SUGGESTIONS FOR EXPERIMENTAL WORK

Experimental confirmation is desirable for the results of the effect of grooving obtained in section 6; in particular there are three main points to be tested:

(i)   forced dynamic stiffness

(ii) static stiffness of journal bearings

(iii) the effect of groove cross-sectional geometry.

The static stiffness is affected by grooving only in the journal aspect of squeeze-film bearings, provided there is no loss in total bearing area because of the finite width of the grooves, so a journal bearing would be needed to verify the results of sections 6.3 and 6.6 . For items (i) and (iii) above it would be sufficient to use flat thrust bearings. In this section an outline will be given of two proposed experimental rigs, one involving a flat annular thrust bearing, and the other a cylindrical journal bearing.

7.1 Thrust bearing rig

In section 6.1 we showed that the dynamic stiffness and damping in an annular segmented thrust bearing is strongly dependent on the number of segments w for a given value of the vibration number γ (see Fig.21), while the static stiffness remains independent of w provided the segments are separated by ambient line boundaries. A rig designed to confirm this is shown in Figs.52 - 56 .

Three pillars (1) , mounted on a heavy base (2) , support a piezoelectric sandwich transducer assembly (3)

by its centre electrode ④ via stiff flexures ⑤ and
the lugs ⑥ (see Fig.53). The centre electrode carries
high voltage to the transducer from a solder tag ⑦ ,
and is insulated from the rest of the apparatus by sheet
mica strips ⑧ and polythene tubing ⑨ . The transducer
itself consists of two steel cylindrical blocks ⑩
sandwiching two piezoelectric ceramic rings ⑪ between
them and the centre electrode. A high tensile bolt holds
the sandwich together, being insulated from the centre
electrode by polythene (or PTFE or polystyrene) tubing ⑬ .
Good electrical and mechanical continuity is obtained by
placing sheets of metal gauze between the piezoelectric
ceramic rings and the metal blocks. At the top and bottom
of the transducer stack, thin metal shim diaphragms ㉒
are used to ensure that movements of the transducer are
radially symmetric and that the dominant motion is in the
axial direction when the central flexure is displaced.
These shims are fixed to the upper transducer block by
bolts passing through the lower bearing plate ⑭ (see
Fig.54), and to the lower transducer block by bolts passing
through a ring ⑮ . The diaphragms are clamped at their
outer ends by similar rings ⑯ to triangular plates ⑰
carried on the main pillars ① . The main framework
constitutes the earthed electrode of the transducer, and
the necessary electrical connection is made via the solder
tag ⑱ . The piezoelectric rings ⑪ are poled in such
a way that an A.C. voltage applied across them through
solder tags ⑦ and ⑱ causes the transducer to vibrate
axially with a node occuring at the centre electrode.
Maximum axial movement occurs at the surface of the bearing

plate ⑭ and at the lower end of the bottom transducer
block ⑩. The system has a reasonably high Q (∼10),
so it is worth driving the transducer at its resonance
frequency (∼25 kHz), and this is easily accomplished by
means of a self-tuning oscillator which locks on to the
condition of minimum impedance. Such a transducer can
handle tens of watts of power, and should be quite capable
of providing an excursion amplitude of up to 10 μm.

Each pillar ① carries a block ⑲ at its top which
supports one of the feet of the probe tripod ⑳. For
clarity, in Fig.52 only the basic tripod framework is
shown, although it really carries the upper bearing
assembly and various probes as shown in Figs.55 and 56 .
The tripod feet ㉑ can be raised and lowered to adjust
the bearing gap by means of tapered wedges ㉒ driven by
fine pitched screws against the clamping bolts ㉔ .
A taper of 0.5° would allow a foot to be adjusted in height
by about 9 μm for each millimetre of horizontal travel of
its wedge, and this would result in a difference in bearing
gap of 4 μm across the diameter of the bearing. By this
means the bearing gap can be made both parallel and of any
desired magnitude. After adjustment the screws ㉓ can
be clamped by means of bolts ㉞ nipping the half-split
tops of the blocks ⑲ .

In Fig.56, the top plate of the probe tripod ⑳ is seen
to carry the upper bearing plate ㉕ mounted beneath a
piezoelectric force transducer ㉖ (ENDEVCO model 2103-100).
A special capacitance probe is used to monitor movements of
the upper bearing plate relative to the top plate ⑳, and

an optical probe ⑳ (MTI FOTONIC SENSOR) measures the displacement of the lower bearing surface relative to the top plate ⑳ . The holder ㉙ for the optical probe is a modified pin vice (ECLIPSE model 121) cemented into a steel cylinder ㉚ . Both probes ㉗ and ⑳ can be adjusted vertically in position by means of knurled nuts ㉛ , and can be clamped by means of set screws ㉜ in the bridging piece ㉝ . Electrical leads ㉞ to the probes are taken out through the top of the apparatus. The capacitance probe ㉗ is of special design in that the probe tip has to be eccentric to the main body so as to be situated sufficiently close to the side of the force transducer to 'see' the top (or back) face of the upper bearing plate. The probe, used with standard WAYNE KERR equipment, is designed to have a full scale range of about 15 μm, and the probe tip diameter is about 2mm.

To set the apparatus up, the probe tripod is slackened off so that the two bearing surfaces are resting against each other. The probe tripod is then raised until the desired nominal clearance is indicated by the optical probe (biassed so as to show static displacements rather than purely vibratory amplitudes). The tripod has then to be finely adjusted so as to give a parallel gap. To do this one can use the auto-collimation technique of Salbu[2] in which light from an auto-collimator is compared with a direct beam from the auto-collimator. If the gap is parallel, the two images will be superimposed, but if the gap is tapered then the two images will be separated by an amount proportional to the tilt error and the number of

repeated reflections. The tripod is adjusted until the two images coincide, and then the auto-collimator is moved through 90° and the adjustment repeated so as to achieve proper alignment of the bearing surfaces.

The basic squeeze motion is obtained by exciting the sandwich transducer at its resonance frequency using a self-tuning oscillator to lock on to the resonance. The amplitude of the squeeze motion can be kept constant by passing the signal from the optical probe through a filter, so that only the squeeze motion is sampled, and using it in a feedback circuit to control the output of the self-tuning oscillator. The static bearing force is then measured directly with the force transducer ㉖.

To obtain data on the dynamic behaviour of the bearing films, the whole apparatus is mounted on an electro-mechanical vibrator table (DERRITRON VP85 driven by amplifier 1500 WT) which is then excited at some frequency small compared with that of the squeeze motion. Because of its inertia the sandwich transducer vibrates, through its flexure ⑤ and diaphragms ㉒, relative to the probe tripod, so the squeeze motion of the bearing surface is modulated at the lower frequency. The amplitude of this modulating displacement relative to the top plate of the probe tripod is measured by the optical probe. Any motion of the upper bearing surface relative to the top plate is measured by the capacitance probe ㉗, so the true bearing gap can be monitored at all times.

Because the probe tripod is also being vibrated there

is the danger that the inertia of the upper bearing plate will result in a contribution to the force being registered by the force transducer. A small accelerometer (ENDEVCO 233E) can be mounted on the tripod top plate to measure the acceleration at the top plate, while the output from the capacitance probe can be used to obtain the correction to this acceleration for the upper bearing plate arising from its motion relative to the top plate. Knowing the bearing plate mass, its inertial force can be calculated and separated from the film force.

The combination of the force transducer ㉖ , the capacitance probe ㉗ and the optical probe ㉘ permits the excursion ratio e_1, vibration amplitude δ , nominal gap C, amplitude and phase of the dynamic film force to be obtained, from which the in-phase and quadrature components S_1 and S_2 of the dynamic stiffness can be separated and plotted as a function of the vibration number γ , similar to Fig.21 .

The bearing surfaces themselves should be flat to within one light fringe, so care has to be taken during assembly. The lower bearing plate should be bolted down to the top of the sandwich transducer and lapped afterwards to ensure that it remains flat, while the upper bearing plate should have the grooves machined in and be securely fixed to the force transducer before it is finally lapped. Probably the best method for manufacturing narrow deep grooves in patterns like those of Fig.20 would be to use a spark erosion technique.

To determine the effect of groove cross-section one

could use an upper bearing plate of the construction shown in Fig.57 . There are two segments (35) and (36) cemented to a base plate (37) which screws into the bottom of the force transducer. The bearing face is lapped flat after the attachment to the force transducer to avoid distortion of the bearing gap. A set of these bearing plates could be made with different combinations of groove width and depth, together with an ungrooved bearing, and the above experiment performed for a few random values of the vibration number γ to see how small the grooves can be made without affecting the dynamic force and to see whether or not grooves have to be physically vented to the ambient. Such a provision could be accommodated quite simply by machining a vent groove in the top surfaces of the bearing segments before they are cemented to the plate for attachment to the force transducer.

It might in practice be difficult to achieve high values of γ because the combination of the large sandwich transducer mass and its flexure will almost certainly result in a mechanical resonance well below the top end of the γ - spectrum of interest when the experiment is performed at atmospheric pressure. The effective vibration number can be increased most rapidly by decreasing the nominal clearance C, or by decreasing the ambient pressure P_a. The former approach can be used to a limited extent, until the gap and vibratory amplitudes become too small to place reliance on accuracy of measurement. Decreasing the ambient pressure requires the use of a sealed cover over the apparatus when mounted on the vibrator, while at the same time allowing access for electrical leads to the

transducer and probes. A further approach is to use a gas of high viscosity, which again requires the use of a sealed cover. However, a sealed cover is desirable in any case because squeeze-film bearings are very susceptable to condensation if the ambient humidity is appreciable, and the best way to avoid this problem is to run the bearing in a dry gas. So the answer seems to be to use a dry gas of high viscosity, such as neon, in a sealed container which can be connected to a vacuum pump so as to reduce the pressure to obtain data at high vibration numbers. Care should be taken to avoid introducing slip-flow effects when reducing the nominal gap C or the ambient pressure p_a (see section 5).

7.2 Cylindrical journal bearing rig

As a grooved journal bearing behaves locally like a flat thrust bearing, the thrust bearing rig results for dynamic stiffness should provide sufficient verification of the theory for journal bearings as well. A separate journal bearing study is required only for the static stiffness, to show that circumferential leakage flow in the film is removed by the presence of a sufficient number of grooves.

Such a rig should, as far as possible, cover the whole range of permissible eccentricities e_2 and excursion ratios e_1, a limitation being set by the criterion

$$e_1 + e_2 < 0.9$$

<div align="right">(7.1)</div>

to allow for manufacturing tolerances which might cause

touchdown. This criterion is indicated by the limiting
lines superimposed on the curves of Fig.27 . It is
desirable to compare directly ungrooved and grooved bearings
operating under similar conditions, rather than to simply
compare the grooved bearing performance with theory. As
the effect of grooving is most apparent for larger values
of L/D, an experiment should be designed taking this into
account so that, for instance, if a bearing with L/D = 3 is
chosen an improvement in bearing force and stiffness of
67% should be observed in the grooved bearing compared
with the same one without grooves. There should be at
least 20 grooves, each as narrow as possible, in the case
of axial grooving, while for circumferential grooving a
density of at least 5 segments per unit value of L/D should
be chosen, resulting in 14 grooves for L/D = 3 (bearing in
mind the comments of section 3.5 and the results of the
thrust bearing tests on groove cross-section of section 7.1).

The fact that we are interested in relatively large
L/D bearings poses quite a practical problem in that, as
we have indicated before, the piezoelectric ceramic tubes
commonly used to drive squeeze-film journal bearings
exhibit markedly non-uniform excursion amplitudes which,
apart from being inefficient from the edge pressurising
point of view, make experimental comparison with theory
difficult unless one builds a model of non-uniform
excursion into the equations. Because of this, and because
of the practical importance in connection with a squeeze-
film accelerometer design being considered at RAE (Farn-
borough) it is worth attempting to design a transducer
assembly which approximates a uniform excursion profile,

and which can be adapted relatively easily to provide any desired value of L/D.

The following idea arose from considering ways of constructing a circumferentially grooved bearing. Instead of using a single long piezoelectric tube to generate the squeeze motion and then place circumferential grooves on the non-vibrating surface one could make each segment a squeeze-film bearing in its own right by driving it with its own separate piezoelectric element. A schematic of the construction of such a transducer module is indicated in Fig.58, and consists of a short piezoelectric ceramic tube poled radially and held by shrink fits between inner and outer metal sleeves, which constitute the electrodes. When an alternating current is passed through the device, it vibrates in a radial mode, and because of the relatively small L/D ratio the two dimensional stress effects, which can cause considerable non-uniformity in the vibration amplitude profile for large values of L/D, are significantly reduced. So if a composite bearing transducer is built up by stacking several of these modules together on a shaft, the overall excursion profile will be approximately uniform except for a ripple having a period coinciding with the segment length. Such a bearing transducer is compared schematically with a single unsegmented transducer in Fig.59 . In fact such a transducer already has its circumferential grooves built in to it if a small axial space is left between adjacent segments.

However, this would present an ideal series of dirt traps which could cause problems in operation, so the following modification is proposed.

Some copper is plated on the ends of the metal sleeves so that when the segments are stacked together under a slight axial compression the copper is compressed between the adjacent segments, sealing the gap and providing the required electrical connections between adjacent sleeves. The whole assembly is then finished by grinding the bearing surface, and if necessary the copper strips are recessed slightly to provide a circumferential grooving or, to a lesser extent, to prevent excessive wear of the soft copper due to rubbing when the bearing is stopped and started. If sufficient copper is placed between adjacent segments, it should act as a relatively low compliance spring material to allow axial vibration of the segments resulting from a non-zero Poisson's ratio to take place without excessively damping the motion.

Such an assembly is highly speculative at present, but a single segment has been constructed at RAE (Farnborough) and supported a load, though the operating frequency in this case was very high ($\sim$170 kHz) owing to the small dimensions required in an accelerometer application.

As it stands, the transducer module shown in Fig.58 will require quite an appreciable voltage to generate an acceptably large electric field to produce the required vibratory amplitude. In instrument applications, it is desirable to work in terms of relatively low voltages,

and the following idea is an attempt to achieve large
electric fields with low voltages. In a visit to AERE
(Harwell), some piezoelectric ceramic material was seen
prepared in the form of a thin tape for use in the
manufacture of monolithic capacitors. Two such tapes
could be taken, and each have platinum ink screen-printed
on the upper surface in the offset manner indicated in
Fig.60 . If the two tapes were then placed together and
wound up in the form of a spiral, after firing we would
have a laminated ring of piezoelectric material which
could be machined on the inside and outside diameters
with only one platinum electrode being cut into in each
case because of the offset built in during the screen
printing process. The ring could then be plated on the
trued-up outside and inside diameters and shrunk into the
metal sleeves as before. The assembly would then be
poled so as to finally take on the form shown in Fig.61 .
Because of the small lamination thickness ($\sim$ 0.2 mm)
it should be possible to achieve high electric field
strengths using relatively low voltages and this makes
the idea quite attractive for accelerometer applications.

A rig for investigating the static stiffness of a
journal bearing based on a composite transducer system of
this sort is shown in Figs.62-64 . The transducer ③⑧ is
assembled on a shaft ③⑨ supported in the pillow blocks ④⓪
which form part of the massively built frame ④① . The
clamps ④⓪ which secure the shaft to the base are
integral with a beam ④② passing above the bearing sleeve
④③ and carrying a WAYNE KERR capacitance probe ④④
directed at the rim of a flange ④⑤ forming part of the

bearing sleeve. At the front of the rig an optical probe (46) (FOTONIC SENSOR), as used in the thrust bearing rig of section 7.1, is directed through a small hole in the bearing sleeve flange so as to monitor the squeeze motion of the bearing shaft. Provided no component of the Earth's gravitational field g acts in the direction of the optical probe, the capacitance probe gives all the necessary information about the eccentricity of the bearing sleeve relative to the shaft, while the optical probe enables the excursion ratio to be determined.

The rig is mounted on the face plate of an indexing head whose shaft is horizontal so that different static loads can be applied to the bearing by varying the component of g acting on the supported mass. By making the bearing sleeve sufficiently massive the eccentricity can be varied over the full range $0 \leqslant e_2 \leqslant 1$. The practical range of e_1 is limited by the amount of power available to the transducer, though by careful tuning a reasonably large excursion ratio should be possible.

The bearing sleeve can be prevented from sliding along the shaft by means of a system of three threads extending from the central flange to a metal spider (48) at each end of the shaft as shown in Fig.63 . Each of these spiders is pivoted on a ball (49) located in the hexagonal socket in the head of a cap screw (50) fixed to the end of the shaft. By adjusting this cap screw, the tension in the threads can be made just sufficient to hold the bearing sleeve in a central position to suit the probes.

Again, because of the danger of condensation in the bearing gap associated with the humidity of laboratory air, it might be desirable to enclose the rig in a sealed container so that the bearing could be run in a dry gas.

8. CONCLUDING DISCUSSION

We have shown by simplified analyses (section 3) that the static performance of the journal aspect of squeeze-film gas bearings can be improved by incorporating extra ambient boundaries to reduce the deleterious effect of circumferential leakage. This simple approach has been strengthened by the more rigorous treatment of section 6 which shows that quite moderate numbers of grooves are required to restore the static force to within 1% of the maximum which would be attained in the complete absence of circumferential leakage. In particular, for circumferential grooving a density of five bearing segments per unit value of L/D is sufficient, while for axial grooving there is no virtue in exceeding twenty grooves. The reduction in bearing force arising from the finite width of the grooves is directly proportional to the total bearing area lost because of the grooves.

The film pressure has been shown to consist of two components contributing to the static force: the Boyle's Law interior contribution, and the edge-pressurising effect; of which the latter exceeds the former by a factor of 1.5 for small values of e_1^2 and e_2. In grooved bearings full advantage is taken of the edge-pressurising term, but in ungrooved bearings circumferential leakage flow within the film tends to prevent the edge pressure from penetrating deep into the interior to augment the basic Boyle's Law behaviour. This is especially true for long cylindrical bearings where the edge pressure has virtually no effect at all on the interior behaviour.

The improvement in static force to be expected from grooving in cylindrical bearings is about 30% for L/D = 2, 50% for L/D = 4, 60% for L/D = 6 when e_1 = 0.5 for small eccentricities. The improvement is greatest for small values of e_1^2 and e_2. Conical and hemispherical bearings will not benefit quite so much from grooving as far as static performance is concerned because in general the effective L/D cannot be expected to exceed unity, in which case the best improvement will be of the order of 20% at small eccentricities and excursion ratios.

The forced dynamic behaviour was shown in section 6 to be considerably affected by the introduction of extra ambient boundaries. In the case of the flat thrust bearings increasing the number of segments displaced the peak damping towards the higher end of the γ-spectrum, while similarly displacing the onset of increased dynamic stiffness. Investigation of the vibration response indicated that very large resonance compliance peaks can occur if the supported mass is insufficiently close to a value which results in a resonance coinciding with maximum film damping. For a given supported mass, the number of grooves can be chosen so as to minimise the peak compliance to a value about twice that of the static compliance. The latter, incidentally, is unaffected by the number of grooves provided the total bearing area remains the same. Typical supported masses result in a resonance condition near the extreme top end of the γ-spectrum of interest, in which case 8 bearing segments would minimise the peak compliance while for most values of γ the dynamic compliance would not differ substantially

from the static value. The resonance frequency estimated
from the supported mass and static stiffness can be
too low by as much as 50% for the ungrooved thrust
bearing, with the discrepancy reducing as grooves are
added.

Forced dynamic performance in journal bearings follows
much the same pattern, with the changes in dynamic
stiffness and 'damping' being shifted towards higher values
of γ as the number of grooves increases in both
circumferentially and axially grooved bearings. On a
logarithmic γ - scale the effect of the number of grooves
w is most sensitive for moderate values of γ in axially
grooved bearings, while for circumferential grooves w
is most sensitive for large values of γ. It follows
that axial grooving would be the better choice for a
bearing operating with its axis vertical and supporting
a large mass, as it would be relatively easy to choose w
so as to arrange for maximum film damping to coincide with
the resonance condition. For horizontally mounted bearings
supporting small masses circumferential grooving might be
more appropriate as any resonance will tend to occur for
large values of γ where a small change in the segment
length could be used to minimise the peak compliance.
In between these two choices lies an area where either
circumferential or axial grooving could be used, and the
final decision probably has to be made on the basis of
relative ease of manufacture.

Conical and hemispherical bearings can be expected to
behave in substantially the same way as comparatively
short journal bearings.

In the absence of results from the thrust bearing experiment proposed in section 7, it is difficult to make definite statements about the size of the grooves to be. used other than that they should be deep and narrow. So as not to lose more than 1% of the bearing area, a circumferentially grooved journal bearing with $\ell/D = 0.2$ would require a groove width $\leqslant 0.002D$, which might be difficult in small bearings. In an axially grooved bearing with 20 grooves, the groove width should be $\leqslant 0.001\pi R$, which is roughly the same value as for circumferential grooves. However, using spark erosion techniques it is possible to machine very narrow slots provided they are not required to be very deep. In our case an estimate of about one hundred times the nominal film thickness was obtained for the groove depth in section 3.5.1, and this results in a typical groove-depth-to-width ratio of at least four, which is quite within the capabilities of spark erosion methods.

Segmentation of the bearing surface should lead to marked improvements in performance in situations involving non-uniform excursion, and this will apply to all existing designs of cylindrical squeeze-film bearings.

To ease future design work it would be desirable if the dynamic stiffness and 'damping' results of the numerical solutions for the various bearing types could be approximated by simple formulae using multiple regression techniques, such as were applied to self-acting thrust bearings by Brockwell, Ettles and Stokes[60]. More general treatments appear in many textbooks on statistics[61, 62],

and several algorithms have been written for use with computers. It appears that provided one avoids regions of curves where points of inflection occur it should be possible to fit a relatively simple formula to cover limited ranges of the various parameters of interest. Larger ranges might be covered by successively applying the technique to different regions of the curves.

Although many of the performance curves are for the realistic case $e_1 = 0.5$ it should be mentioned that considerable variations will occur if e_1 is markedly different from this value. Changes will be non-linear with e_1, but the overall behaviour given in the diagrams should be the same qualitatively, although the ordinate scale will need adjustment.

Unfortunately, for various reasons, it was not found possible to undertake the experimental work sketched in section 7, although a fair amount of preliminary design study was carried out. Patent action has been taken on the laminated piezoelectric transducer concept.

Appendix A

MATRIX SOLUTION OF FIRST ORDER PERTURBATION EQUATION IN SECTION 6.1

In section 6.1 we wish to solve the system of simultaneous equations

$$\frac{d^2u}{d\bar{r}^2} + \frac{1}{\bar{r}}\frac{du}{d\bar{r}} + K_2 v = 0$$

$$\frac{d^2v}{d\bar{r}^2} + \frac{1}{\bar{r}}\frac{dv}{d\bar{r}} - K_2 u = 0 \tag{A.1}$$

where $u = 2$ and $v = 0$ at $\bar{r} = \bar{r}_1$ and $\bar{r} = \bar{r}_2$. The interval of interest is $\bar{r}_1 \leqslant \bar{r} \leqslant \bar{r}_2$, so defining

$$\Delta R = \left(\frac{\bar{r}_2 - \bar{r}_1}{m-1}\right) = \frac{1}{(m-1)} \tag{A.2}$$

where m is an integer, the interval can be covered by the 'grid points' ξ_j, where

$$\xi_j = \bar{r}_1 + (j-1)\Delta R \qquad j = 1, 2, \cdots, m. \tag{A.3}$$

The following finite difference approximations can thus be made for grid points at $j = 2, 3, \ldots, m-1$:

$$u(\bar{r} = \xi_j) = u_j \tag{A.4}$$

$$v(\bar{r} = \xi_j) = v_j \tag{A.5}$$

$$\left.\frac{du}{d\bar{r}}\right|_{\bar{r}=\xi_j} = \frac{1}{2\Delta R}(u_{j+1} - u_{j-1}) \tag{A.6}$$

$$\left.\frac{dv}{d\bar{r}}\right|_{\bar{r}=\xi_j} = \frac{1}{2\Delta R}(v_{j+1} - v_{j-1}) \tag{A.7}$$

$$\left.\frac{d^2u}{d\bar{r}^2}\right|_{\bar{r}=\xi_j} = \frac{1}{\Delta R^2}(u_{j+1} - 2u_j + u_{j-1}) \tag{A.8}$$

$$\left.\frac{d^2v}{d\bar{r}^2}\right|_{\bar{r}=\xi_j} = \frac{1}{\Delta R^2}(v_{j+1} - 2v_j + v_{j-1}). \tag{A.9}$$

The boundary conditions are given by

$$u(\bar{r} = \xi_1) = u(\bar{r} = \xi_m) = 2$$

$$v(\bar{r} = \xi_1) = v(\bar{r} = \xi_m) = 0 \quad .$$

(A.10)

Using these approximations, at a regular field point
j = 2,3,..., m-1 equations (A.1) can be expressed in the
finite difference form

$$\frac{(u_{j+1} - 2u_j + u_{j-1})}{\Delta R^2} + \frac{(u_{j+1} - u_{j-1})}{2\xi_j \Delta R} + K_2 v_j = 0$$

$$\frac{(v_{j+1} - 2v_j + v_{j-1})}{\Delta R^2} + \frac{(v_{j+1} - v_{j-1})}{2\xi_j \Delta R} - K_2 u_j = 0 \quad .$$

(A.11)

Equations (A.11), together with boundary conditions (A.10),
are then embraced by the simultaneous matrix equations

$$M\underline{u} + K\underline{v} = \underline{a}$$

$$M\underline{v} - K\underline{u} = -\underline{a}$$

(A.12)

where M is the (m x m) tri-diagonal matrix

$$M = \begin{Vmatrix} 1 & 0 & & & & \\ \left(\frac{1}{\Delta R^2} - \frac{1}{2\xi_2 \Delta R}\right) & -\frac{2}{\Delta R^2} & \left(\frac{1}{\Delta R^2} + \frac{1}{2\xi_2 \Delta R}\right) & & & \\ & \left(\frac{1}{\Delta R^2} - \frac{1}{2\xi_3 \Delta R}\right) & -\frac{2}{\Delta R^2} & \left(\frac{1}{\Delta R^2} + \frac{1}{2\xi_3 \Delta R}\right) & & \\ & & \ddots & \ddots & \ddots & \\ & & & \left(\frac{1}{\Delta R^2} - \frac{1}{2\xi_{m-1} \Delta R}\right) & -\frac{2}{\Delta R^2} & \left(\frac{1}{\Delta R^2} + \frac{1}{2\xi_{m-1} \Delta R}\right) \\ & & & & 0 & 1 \end{Vmatrix}$$

K is the (m x m) diagonal matrix

$$
K = \begin{Vmatrix} 1 & & & & & \\ & K_2 & & & & \\ & & K_2 & & & \\ & & & \ddots & & \\ & & & & K_2 & \\ & & & & & 1 \end{Vmatrix}
$$

and $\underline{u}$, $\underline{v}$, $\underline{a}$, are the (m x 1) column vectors

$$
\underline{u} = \begin{Vmatrix} u_1 \\ u_2 \\ \cdot \\ \cdot \\ \cdot \\ \cdot \\ \cdot \\ \cdot \\ u_m \end{Vmatrix} \qquad \underline{v} = \begin{Vmatrix} v_1 \\ v_2 \\ \cdot \\ \cdot \\ \cdot \\ \cdot \\ \cdot \\ v_m \end{Vmatrix} \qquad \underline{a} = \begin{Vmatrix} 2 \\ 0 \\ \cdot \\ \cdot \\ \cdot \\ \cdot \\ 0 \\ 2 \end{Vmatrix} .
$$

The required solutions of equations (A.12) are then

$$
\underline{u} = [M + KM^{-1}K]^{-1}[KM^{-1} + I]\,\underline{a}
$$

$$
\underline{v} = M^{-1}[K\underline{u} - \underline{a}]
$$

(A.13)

Appendix B

MATRIX SOLUTION OF EQUATION (6.67)

In section 6.2 a solution is required for the simultaneous second-order ordinary differential equations (6.67),

$$\frac{d^2 u}{d\theta^2} + K_3 v + 2Q_0 \cos\theta = 0$$

$$\frac{d^2 v}{d\theta^2} - K_3 u = 0 \tag{B.1}$$

subject to the boundary conditions (6.68) at $\theta = \theta_{k-1+\alpha}$ and $\theta = \theta_{k-\alpha}$,

$$u = 2\cos\theta$$

$$v = 0 \tag{B.2}$$

where

$$K_3 = \frac{\zeta}{\sqrt{Q_0}} . \tag{B.3}$$

The following solution method is similar to that given in Appendix A for the flat annular thrust bearing.

The region of interest $\theta_{k-1+\alpha} \leqslant \theta \leqslant \theta_{k-\alpha}$ is partitioned into $(m-1)$ equal intervals of length

$$\Delta\theta = \frac{\theta_{1-2\alpha}}{(m-1)} \tag{B.4}$$

(m an integer), so that the value of θ at the j'th point is

$$\bar\theta_j = \theta_{k-1+\alpha} + (j-1)\Delta\theta \qquad j = 1, 2, \cdots, m. \tag{B.5}$$

Defining $X = \frac{1}{\Delta\theta^2}$, the following finite difference approximations can then be made:

$$u(\bar{\theta}_j) = u_j$$

$$v(\bar{\theta}_j) = v_j$$

$$\left.\frac{d^2u}{d\theta^2}\right|_{\theta=\bar{\theta}_j} = (u_{j+1} - 2u_j + u_{j-1}).X \tag{B.6}$$

$$\left.\frac{d^2v}{d\theta^2}\right|_{\theta=\bar{\theta}_j} = (v_{j+1} - 2v_j + v_{j-1}).X \quad .$$

Using these, at a regular field point $j = 2, 3, \ldots, m-1$, equations (B.1) can be expressed in the finite difference form

$$X.(u_{j+1} - 2u_j + u_{j-1}) + K_3 v_j + 2Q_0 \cos\bar{\theta}_j = 0$$
$$X.(v_{j+1} - 2v_j + v_{j-1}) - K_3 u_j = 0 \tag{B.7}$$

while boundary conditions (B.2) become

$$u_1 = 2\cos\bar{\theta}_1$$

$$u_m = 2\cos\bar{\theta}_m \tag{B.8}$$

$$v_1 = v_m = 0 \quad .$$

This system of m finite difference equations is more concisely expressed in the matrix form

$$M\underline{u} + K\underline{v} = \underline{a}$$
$$M\underline{v} - K\underline{u} = \underline{b} \tag{B.9}$$

where M and K are (m x m) matrices, and $\underline{u}$, $\underline{v}$, $\underline{a}$, $\underline{b}$ are (m x 1) column vectors,

$$M = \begin{Vmatrix} 1 & & & & & & \\ x & -2x & x & & & & \\ & x & -2x & x & & & \\ & & \ddots & \ddots & \ddots & & \\ & & & & x & -2x & x \\ & & & & & & 1 \end{Vmatrix}$$

$$K = \begin{Vmatrix} 1 & & & & \\ & K_3 & & & \\ & & K_3 & & \\ & & & \ddots & \\ & & & & K_3 \\ & & & & & 1 \end{Vmatrix} \qquad \underline{u} = \begin{Vmatrix} u_1 \\ u_2 \\ \cdot \\ \cdot \\ \cdot \\ u_m \end{Vmatrix}$$

$$\underline{v} = \begin{Vmatrix} v_1 \\ v_2 \\ \cdot \\ \cdot \\ \cdot \\ v_m \end{Vmatrix} \qquad \underline{a} = \begin{Vmatrix} 2\cos\bar{\theta}_1 \\ -2Q_o\cos\bar{\theta}_2 \\ -2Q_o\cos\bar{\theta}_3 \\ \cdot \\ \cdot \\ \cdot \\ -2Q_o\cos\bar{\theta}_{m-1} \\ 2\cos\bar{\theta}_m \end{Vmatrix} \qquad \underline{b} = \begin{Vmatrix} -2\cos\bar{\theta}_1 \\ 0 \\ 0 \\ \cdot \\ \cdot \\ \cdot \\ 0 \\ -2\cos\bar{\theta}_m \end{Vmatrix}$$

Straightforward manipulation of equations (B.9) provides
the required solutions

$$\underline{u} = [M + KM^{-1}K]^{-1}[\underline{a} - KM^{-1}\underline{b}]$$

$$\underline{v} = M^{-1}[K\underline{u} + \underline{b}]$$

<div align="right">(B.10)</div>

which can be evaluated numerically.

Appendix C

MATRIX SOLUTION OF EQUATION (6.113)

A second order two-dimensional partial differential equation with real coefficients can be expressed in the general finite difference system of equations (6.113), namely

$$\alpha_{ij} q_{i+1,j} + \bar{\alpha}_{ij} q_{i-1,j} + \beta_{ij} q_{ij} + \delta_{ij} q_{i,j+1} + \bar{\delta}_{ij} q_{i,j-1} = \mu_{ij} \qquad (c.1)$$

where i = 1,2,...,m and j = 1,2,...m.

The j'th column of these equations can be collected together in the matrix equation

$$A_j \underline{q}_j + B_j \underline{q}_{j+1} + C_j \underline{q}_{j-1} = \underline{f}_j \qquad (c.2)$$

where the A_j, B_j, C_j are (m x m) matrices,

$$
A_j =
\begin{Vmatrix}
\beta_{1j} & \alpha_{1j} & & & & & \bar{\alpha}_{1j} \\
\bar{\alpha}_{2j} & \beta_{2j} & \alpha_{2j} & & & & \\
& \bar{\alpha}_{3j} & \beta_{3j} & \alpha_{3j} & & & \\
& & \ddots & \ddots & \ddots & & \\
& & & & & \alpha_{m-1,j} \\
\alpha_{mj} & & & & & \bar{\alpha}_{mj} & \beta_{mj}
\end{Vmatrix}
$$

199

$$B_j = \begin{Vmatrix} \delta_{1j} & & & \\ & \delta_{2j} & & \\ & & \ddots & \\ & & & \delta_{mj} \end{Vmatrix}$$

$$C_j = \begin{Vmatrix} \bar{\delta}_{1j} & & & \\ & \bar{\delta}_{2j} & & \\ & & \ddots & \\ & & & \bar{\delta}_{mj} \end{Vmatrix}$$

and the q_j and $\underline{f}_j$ are (m x 1) column vectors

$$\underline{q}_j = \begin{Vmatrix} q_{1j} \\ q_{2j} \\ \vdots \\ q_{mj} \end{Vmatrix} \qquad \underline{f}_j = \begin{Vmatrix} \mu_{1j} \\ \mu_{2j} \\ \vdots \\ \mu_{mj} \end{Vmatrix} .$$

The elements $\bar{\alpha}_{ij}$ and α_{mj} in A_j take account of the possibility of a cyclic boundary condition in the i-direction, such as might occur in ungrooved cylindrical bearings if the computation were taken completely around the bearing in the θ -direction. In the context of the present work, $\bar{\alpha}_{ij} = \alpha_{mj} = 0$.

The system of equations (C.2) then reduce to

$$M \underline{q} = \underline{f} \qquad (C.3)$$

where M is an $(n \times n)$ matrix, and $\underline{q}$ and $\underline{f}$ are $(n \times 1)$ column vectors:

$$M = \begin{Vmatrix} A_1 & B_1 & & & & \\ C_2 & A_2 & B_2 & & & \\ & C_3 & A_3 & B_3 & & \\ & & & \ddots & & \\ & & & & & B_{n-1} \\ & & & & C_n & A_n \end{Vmatrix} \qquad \underline{q} = \begin{Vmatrix} q_1 \\ q_2 \\ \vdots \\ \\ q_n \end{Vmatrix} \qquad \underline{f} = \begin{Vmatrix} f_1 \\ f_2 \\ \vdots \\ \\ f_n \end{Vmatrix}.$$

Expressing M as the product of a lower triangular matrix L with an upper triangular matrix U, where

$$L = \begin{Vmatrix} I & & & & \\ L_2 & I & & & \\ & L_3 & I & & \\ & & & \ddots & \\ & & & & L_n & I \end{Vmatrix} \qquad U = \begin{Vmatrix} U_1 & D_1 & & & \\ & U_2 & D_2 & & \\ & & & \ddots & \\ & & & & D_{n-1} \\ & & & & U_n \end{Vmatrix}$$

and I is the unit (m x m) matrix, it is found that

$$U_1 = A_1$$

$$\left.\begin{aligned} L_j &= C_j U_{j-1}^{-1} \\ U_j &= A_j - L_j B_{j-1} \end{aligned}\right\} \quad j = 2, 3, \cdots, n \qquad \text{(C.4)}$$

$$D_j = B_j \qquad\qquad j = 1, 2, \cdots, n-1.$$

Equation (C.3) can now be expressed in the form

$$M\underline{q} = LU\underline{q} = L\underline{r} = \underline{f} \qquad\qquad \text{(C.5)}$$

where

$$U\underline{q} = \underline{r} \qquad\qquad \text{(C.6)}$$

and $\underline{r}$ is an (n x 1) column vector

$$\underline{r} = \left\| \begin{matrix} \underline{r}_1 \\ \underline{r}_2 \\ \cdot \\ \cdot \\ \cdot \\ \underline{r}_n \end{matrix} \right\|.$$

Equation (C.6) is first solved for $\underline{r}$, finding that

$$\underline{r}_1 = \underline{f}_1$$

$$\underline{r}_j = \underline{f}_j - L_j \underline{r}_{j-1} \qquad\qquad j = 2, 3, \cdots, n \qquad \text{(C.7)}$$

and this is used in equation (C.6) to obtain the required solution $\underline{q}$:

$$\underline{q}_n = U_n^{-1} \underline{r}_n$$

$$\underline{q}_{j-1} = U_{j-1}^{-1} (\underline{r}_{j-1} - B_{j-1} \underline{q}_j) \quad j = n, n-1, \cdots, 2.$$

(C.8)

This procedure is readily programmed as a FORTRAN subroutine and can be used for any problem expressible in the form of equation (C.1). Notice that matrix inversion occurs n times on each occasion the routine is traversed, so m should be made as small as possible in order to keep computing times down to a reasonable level, as the time involved is proportional to n x m^3.

Appendix D

MATRIX SOLUTION OF EQUATIONS (6.147)

In section 6.5.1 , a solution $g_2 = u + iv$ is required

satisfying the simultaneous equations (6.147)

$$\frac{d^2 u}{d\bar{z}^2} - u - K_3 v + 3g_0 = 0$$

$$\frac{d^2 v}{d\bar{z}^2} - v + K_3 u - \zeta \sqrt{g_0} = 0$$

(D.1)

subject to boundary conditions (6.148),

$$\left. \begin{array}{l} u = 3\left(1 + \frac{1}{2}e_1^2\right) \\ v = 0 \end{array} \right\} \text{ at } \bar{z} = 0 \text{ and } \bar{z} = z_L .$$

(D.2)

The solution procedure discussed here is similar to that

described in Appendix A for the thrust bearing, and to that

in Appendix B for the axially grooved journal bearing.

Since, because of symmetry, we only need consider the

interval $0 \leqslant \bar{z} \leqslant z_L/2$, the boundary conditions (D.2)

can be modified so as to become

$$\left. \begin{array}{l} u = 3\left(1 + \frac{1}{2}e_1^2\right) \\ v = 0 \end{array} \right\} \text{ at } \bar{z} = 0$$

(D.3)

$$\frac{du}{d\bar{z}} = \frac{dv}{d\bar{z}} = 0 \qquad \text{at} \quad \bar{z} = \frac{z_L}{2}$$

(D.4)

where the condition (D.4) represents the mid-plane

situation

$$\frac{d}{d\bar{z}}\left(H_\infty \psi_\infty^2\right) = 0 \qquad \text{at} \quad \bar{z} = \frac{z_L}{2}$$

(D.5)

in section 6.5.1 . Note that this latter condition is satisfied by the solutions g_0 and g_1 already obtained.

We proceed by partitioning the interval $0 \leq \bar{z} \leq z_L/2$ into $(m-1)$ equal intervals of length

$$\Delta \bar{z} = \frac{z_L}{2(m-1)} \tag{D.6}$$

(m an integer) such that the value of $\bar{z}$ at the j'th point is

$$\xi_j = (j-1)\Delta \bar{z} . \tag{D.7}$$

The following finite difference approximations are made:

$$u(\xi_j) = u_j$$

$$v(\xi_j) = v_j$$

$$\left.\frac{du}{d\bar{z}}\right|_{\xi_j} = \frac{1}{2\Delta \bar{z}}(u_{j+1} - u_{j-1})$$

$$\left.\frac{dv}{d\bar{z}}\right|_{\xi_j} = \frac{1}{2\Delta \bar{z}}(v_{j+1} - v_{j-1}) \tag{D.8}$$

$$\left.\frac{d^2 u}{d\bar{z}^2}\right|_{\xi_j} = \frac{1}{\Delta \bar{z}^2}(u_{j+1} - 2u_j + u_{j-1})$$

$$\left.\frac{d^2 v}{d\bar{z}^2}\right|_{\xi_j} = \frac{1}{\Delta \bar{z}^2}(v_{j+1} - 2v_j + v_{j-1}) .$$

Defining $X_1 = \frac{1}{\Delta \bar{z}^2}$, equations (D.1) can be written in the following finite difference form at a regular field point $j = 2, 3, \ldots, m$,

$$(u_{j+1} - 2u_j + u_{j-1})X_1 - u_j - K_3 v_j + 3g_0 = 0$$

$$(v_{j+1} - 2v_j + v_{j-1})X_1 - v_j + K_3 u_j - \sqrt{g_0} = 0 . \tag{D.9}$$

The ambient boundary conditions (D.3) become

$$u_1 = 3\left(1 + \tfrac{1}{2}e_1^2\right)$$

$$v_1 = 0$$

<div align="right">(D.10)</div>

and the mid-plane condition (D.4) is

$$\frac{1}{2\Delta z}\left(u_{m+1} - u_{m-1}\right) = 0$$

$$\frac{1}{2\Delta z}\left(v_{m+1} - v_{m-1}\right) = 0 .$$

<div align="right">(D.11)</div>

These latter equations are used to eliminate u_{m+1} and v_{m+1} (which lie outside the range of the grid) from equations (D.9) when at the mid-plane ($j = m$).

This system of m finite difference equations is collected together in the matrix form

$$M\underline{u} - K\underline{v} = \underline{a}$$

$$M\underline{v} + K\underline{u} = \underline{b}$$

<div align="right">(D.12)</div>

where,

$$X_2 = -\left(1 + 2X_1\right) .$$

<div align="right">(D.13)</div>

M and K are (m x m) matrices, $\underline{u}$ and $\underline{v}$ are (m x 1) column vectors,

$$M = \begin{Vmatrix} 1 & & & & & \\ X_1 & X_2 & X_1 & & & \\ & X_1 & X_2 & X_1 & & \\ & & \ddots & \ddots & \ddots & \\ & & & X_1 & X_2 & X_1 \\ & & & & 2X_1 & X_2 \end{Vmatrix}$$

$$K = \begin{Vmatrix} 1 & & & & & \\ K_3 & & & & & \\ & K_3 & & & & \\ & & \diagdown & & & \\ & & & \diagdown & & \\ & & & & K_3 & \\ & & & & & 1 \end{Vmatrix}$$

While $\underline{a}$ and $\underline{b}$ are ($m \times 1$) column vectors

$$\underline{a} = \begin{Vmatrix} 3\left(1+\tfrac{1}{2}e_1^2\right) \\ -3g_0 \\ -3g_0 \\ \vdots \\ \vdots \\ -3g_0 \\ 3\left(1+\tfrac{1}{2}e_1^2\right) \end{Vmatrix} \qquad \underline{b} = \begin{Vmatrix} 3\left(1+\tfrac{1}{2}e_1^2\right) \\ \gamma\sqrt{g_0} \\ \gamma\sqrt{g_0} \\ \vdots \\ \vdots \\ \gamma\sqrt{g_0} \\ 3\left(1+\tfrac{1}{2}e_1^2\right) \end{Vmatrix} .$$

The required solutions are then

$$\underline{u} = \left[M + KM^{-1}K \right]^{-1} \left[\underline{a} + KM^{-1}\underline{b} \right]$$

$$\underline{v} = M^{-1} \left[\underline{b} - K\underline{u} \right]$$

<div align="right">(D.14)</div>

which can be evaluated numerically. By considering half
the bearing length, instead of the whole length, computer
storage and central processor time are saved because
fewer grid points are needed to achieve the same accuracy.

LIST OF SYMBOLS

a	Boundary value of x_3; velocity of sound.
a_1, a_2, a_3, a_4	Defined in equations (3.84) to (3.87).
$\bar{a}$	Ambient boundary value of u_1.
$\underline{a}$	(m x 1) column vector.
A	Area; parameter used in the boundary condition (5.5); (m x m) matrix in equation (6.99).
A_j	(m x m) tri-diagonal matrix.
$A_n^{(ij)}$	Laguerre polynomial of degree n associated with F_{ij}.
A_1, A_2	Parameters in the boundary conditions (4.58) and (4.59).
b	Boundary value of x_3.
$\bar{b}$	Ambient boundary value of u_1.
$\underline{b}$	(m x 1) column vector.
B	Breadth of rectangular thrust bearing, section 2.1 .
B_j	(m x m) diagonal matrix.
C	Reference value of the film thickness.
C_j	(m x m) diagonal matrix.
C_1, C_2, C_3, C_4	Integration constants.
$\bar{C}_n$	Coefficients of the polynomial expansion (6.196).
D	Diameter, $D = 2R$.
D_j	Elements of the matrix U.
$D_n^{(ij)}$	Coefficients in equation (6.203).
$\bar{D}$	Matrix in equation (6.204).
e_R, e_Z	Normalised radial and axial displacements.
e_1	Excursion ratio.

e_2	Eccentricity ratio.
f	Amplitude of F_{ext}.
$\underline{f}$	($n \times 1$) column vector.
$\underline{f}_j$	($m \times 1$) column vector.
F, F'	Non-dimensional and actual bearing forces.
F_{dyn}, F'_{dyn}	Normalised and actual dynamic film forces.
F_{ext}, F'_{ext}	Normalised and actual externally imposed vibrational forces.
F_{FP}, F'_{FP}	Non-dimensional and actual bearing forces produced by a double opposed thrust bearing, section 3.3.1 .
F_{ij}	Dimensionless force in the j direction following a step jump displacement in the i direction.
F_j	Original equilibrium force in the j direction before the step-jump.
F_J, F'_J	Non-dimensional and actual bearing forces of the axially grooved journal bearing of section 3.3.1 .
F_R, F'_R	Normalised and actual radial forces.
F_Z, F'_Z	Normalised and actual axial forces.
F_0, F_1, F_2, F_3	Perturbation components of the normalised force F .
F'_0, F'_1, F'_2, F'_3	Perturbation components of the force F' .
g	Acceleration due to gravity.
g_0, g_1, g_2	Perturbation components of $H_\infty \psi_\infty^2$.
g_2^*	Complex conjugate of g_2 .
h	Instantaneous film thickness.
h_0	Mean film thickness.
H	Non-dimensional film thickness, $H = h/C$.
H_i	Value of H_∞ at the i'th finite difference grid point.

H_k	Non-dimensional film thickness in the k'th bearing strip, defined in equation (3.57).
H_s	Component of H associated with the squeeze motion.
H_1, H_2	Boundary values of H.
H_∞	Quasi-static non-dimensional film thickness.
$\bar{H}$	Time averaged non-dimensional film thickness.
$\bar{H}_k$	Time average of H_k .
$\overline{H^3}$	Time average of H^3 .
i	Integer, or $\sqrt{-1}$.
I	Unit matrix.
j	Integer.
J_0	Bessel function of the first kind.
k	Integer.
K	Factor defined in equation (3.37); (m x m) diagonal matrix.
K_1	Constant defined in equation (6.11) .
K_2	Constant, $K_2 = iK_1^2$.
K_3	Constant appearing in equations (6.147).
$\bar{K}$	Complex constant appearing in equation (6.65).
ℓ	Length of bearing segment in circumferentially grooved bearings, or width of bearing strip in axially grooved bearings.
ℓ_1, ℓ_2	Fundamental magnitudes of u_1 and u_2 .
L	(n x n) lower triangular matrix; length of bearing.
L_j	Elements of matrix L.
L_n	Laguerre polynomial of degree n.
m	Mass or mass per unit length; Knudsen number, equation (4.29); number of finite difference grid points in circumferential direction.

m_L	Highest degree of the truncated Laguerre polynomial expansion.
m_0	Critical mass, or critical mass per unit length.
M	(n x n) tri-diagonal matrix; dimensionless mass.
M_{edge}	Mach number of edge flow.
M_Z	Non-dimensional axial mass flow rate per unit width.
M_{Z_1}, M_{Z_2}	Non-dimensional total axial mass flow rates, defined in equations (3.39) and (3.40).
M_0	Non-dimensional critical mass, section 3.3.1.
M_1	Dimensionless mass, or dimensionless mass per unit length (depending on context).
M_Θ	Non-dimensional circumferential mass flow rate per unit width.
M_{Θ_k}	Value of M_Θ contributed by the k'th segment of the axially grooved journal bearing.
n	Integer; number of finite difference grid points in the axial direction.
p	Pressure.
p_a	Ambient pressure.
p_1	Initial pressure in Boyle's Law model.
P	Non-dimensional pressure, $P = p/p_a$.
P_1	Non-dimensional initial pressure, $P_1 = p_1/p_a$.
$\bar{P}$	Time averaged non-dimensional pressure.
$\bar{P}_k$	Time averaged non-dimensional pressure in k'th bearing strip, defined in equation (3.59).
$\bar{P}_0$, $\bar{P}_1$, $\bar{P}_2$, $\bar{P}_3$	Time averaged perturbation components of non-dimensionalised pressure.
q_i	Value of Q at the i'th finite difference grid point.

q_{ij}	Value of Q at i,j'th finite difference grid point.
q_1, q_2	Volumetric flow rates per unit width.
$\underline{q}$	(n x 1) column vector.
$\underline{q}_j$	(m x 1) column vector, section 5.3.1 .
Q	Dependent variable, $Q = (PH)^2$.
Q_{init}	Value of Q at previous time step.
Q_0, Q_1, Q_2	Zero'th, first order perturbation in eccentricity, and first order perturbation in vibration amplitude components of Q.
r	Radial co-ordinate.
r_j	Elements of column vector $\underline{r}$.
r_1, r_2	Ambient boundary values of r.
$\bar{r}$	Non-dimensional radial co-ordinate.
R	Reference dimension of the bearing (radius in disc and journal bearings).
R_{ij}	Dimensionless response in the j direction following a step jump displacement in the i direction.
R_0	Inner to outer radius ratio of annulus.
s_1, s_2, s_3	Fundamental magnitudes of the curvilinear co-ordinates x_1, x_2, x_3 .
S_0, S_0'	Dimensionless and actual static stiffness.
S_1, S_1'	Normalised and actual in-phase components of the dynamic stiffness.
S_2, S_2'	Normalised and actual quadrature components of the dynamic stiffness, often called 'damping'.
t	Time.
T	Non-dimensional time associated with the forced response, $T = \nu t$.
T_R, T_Z	Dimensionless times associated with ν_R and ν_z .

u	Real part of Q_2 or s_2 ; film velocity.
u_j	Value of u at the j'th finite difference grid point.
u_1, u_2	Non-dimensional generalised orthogonal curvilinear co-ordinates.
$\underline{u}$	$(m \times 1)$ column vector.
U	$(n \times n)$ upper triangular matrix; effective dimensionless dynamic stiffness per unit length.
U_j	Diagonal elements of matrix U.
U'	Dynamic stiffness per unit length.
v	Imaginary part of Q_2 or s_2 .
v_j	Value of v at the j'th finite difference grid point.
v_1, v_2, v_3	Components of the velocity vector $\underline{v}$.
$\underline{v}$	Velocity vector, section 4.2.1 ; $(m \times 1)$ column vector.
V, V'	Effective dimensionless and actual quadrat e component of the dynamic stiffness per unit length.
w	Number of grooves.
W, W'	Non-dimensional and actual bearing forces per unit length.
W_D, W'_D	Total non-dimensional and actual dynamic forces per unit length of axially grooved journal bearing.
W_{D_k}, W'_{D_k}	Non-dimensional and actual dynamic forces per unit length contributed by the k'th segment of the axially grooved journal.
W_{ext}, W'_{ext}	Dimensionless and actual external disturbing force per unit length.
$W_{grooved}$	Dimensionless force per unit length of grooved journal bearing.

W_k, W'_k	Dimensionless and actual bearing forces per unit length contributed by the k'th bearing strip, equation (3.60).
W_L, W'_L	Dimensionless and actual bearing forces per unit length.
W_S, W'_S	Total dimensionless and actual static forces per unit length of the axially grooved journal bearing.
W_{S_k}, W'_{S_k}	Dimensionless and actual static forces per unit length contributed by the k'th segment of the axially grooved journal.
$W_{ungrooved}$	Dimensionless force per unit length of the ungrooved journal bearing.
x	Shaft displacement response; cartesian co-ordinate.
x_1, x_2, x_3	Generalised orthogonal curvilinear co-ordinates.
$\hat{x}_1$, $\hat{x}_2$, $\hat{x}_3$	Unit vectors of the curvilinear co-ordinates x_1, x_2, x_3 .
y	Cartesian co-ordinate.
Y_0	Bessel function of the second kind.
z	Axial co-ordinate in journal bearings; cartesian co-ordinate; complex co-ordinate defined in equation (6.12).
z_L	Dimensionless length of the bearing, $z_L = z/R$.
$\bar{z}$	Dimensionless axial co-ordinate, $\bar{z} = z/R$.
$\bar{z}_j$	Value of $\bar{z}$ at the j'th finite difference grid point.
α	Half the fraction of the total circumferential length of an axially grooved journal bearing occupied by grooves; step jump attenuation constant; phase of normalised dynamic compliance.

α_i, $\bar{\alpha}_i$	Coefficients of q_{i+1} and q_{i-1} in equation (6.96).
α_{ij}, $\bar{\alpha}_{ij}$	Coefficients in the finite difference equations (6.113).
β	Growth factor.
β_i	Coefficient q_i in equation (6.96).
β_{ij}	Coefficient in the finite difference equations (6.113).
γ	Phase associated with the dynamic compliance; ratio of specific heats.
Γ	Cone semi-angle.
δ	Dimensionless response amplitude; small dimensionless distance into bearing interior from an ambient boundary, section 3.1.3 .
δ_r, δ_z	Normalised amplitudes of the forced response in the radial and axial directions.
δ_{ij}, $\bar{\delta}_{ij}$	Coefficients in the finite difference equations (6.113).
δF_{ij}	Defined in equation (6.193).
δm	Incremental mass change from m_0.
δu_1, δu_2	Elements of the normalised co-ordinates u_1, u_2 .
δx_i	Step jump displacement in the i direction.
δx_1, δx_2, δx_3	Elements of the generalised co-ordinates.
δ_1, δ'_1	Dimensionless and actual amplitudes of the dynamic compliance.
$\delta\bar{x}$	Amplitude of step-jump displacement stimulus.
$\underline{\delta\bar{x}}$, $\underline{\delta\bar{x}}^{(B)}$	Column vectors in equation (6.204).
$\Delta\theta$	Element of the angular co-ordinate θ .
ΔP	Effective non-dimensional pressure arising from Boyle's Law model.
ΔR	Defined in equation (A.2).

$\triangle t$	Time increment.
$\triangle z$	Finite difference grid spacing in the axial direction.
$\triangle \theta$	Finite difference grid spacing in the circumferential direction.
ζ	Vibration number, defined in equation (4.39).
ζ_ℓ	Local vibration number, equation (6.4).
ζ_{res}	Value of ζ at resonance.
ζ_0	Resonance value of ζ calculated on the basis of the combination of supported mass and static stiffness.
θ	Circumferential angular co-ordinate.
θ_k	Abbreviated way of expressing angles, defined in equation (3.56).
$\bar{\theta}_i$	Value of θ at the i'th finite difference grid point.
λ	Molecular mean free path of the gas.
λ_a	Value of λ under ambient conditions.
$\bar{\lambda}$	Dimensionless mean free path, $\bar{\lambda} = \lambda / \lambda_a$.
μ	Viscosity.
μ_a	Ambient viscosity.
μ_i	Right hand side of equation (6.96).
μ_{ij}	Coefficient in the finite difference equations (6.113).
$\bar{\mu}$	Dimensionless viscosity, $\bar{\mu} = \mu / \mu_a$.
ν	Angular frequency associated with the forced response.
ν_R, ν_z	Angular frequencies of forced vibrations in the radial and axial directions.
ν_0	Value of ν for which the quadrature component of dynamic stiffness vanishes.

ξ	Parameter defined in equation (6.194); normalised edge co-ordinate; radial co-ordinate in conical bearings.
ξ_j	Value of $\bar{r}$ at the j'th finite difference grid point.
ξ_1, ξ_2	Stretched co-ordinates for the boundary layers.
ρ	Density.
ρ_a	Ambient density.
$\bar{\rho}$	Dimensionless density, $\bar{\rho} = \rho / \rho_a$.
σ	Squeeze number, defined in equation (2.2).
σ, σ_{l_g}	Local squeeze numbers in a bearing segment, equation (3.88), and in a groove, equation (3.90).
$\angle_{ij}$	Defined in equation (6.203).
τ	Dimensionless time associated with the squeeze motion, $\tau = \omega t$.
τ'	Dummy variable for τ.
ϕ	Phase of step-jump displacement stimulus; spherical polar co-ordinate.
Φ	Operator representing the left-hand-side of equation (4.43).
ψ	Dependent variable, $\psi = PH$.
ψ_c	Edge correction component of ψ.
ψ_1, ψ_2	Ambient boundary values of ψ.
ψ_∞	Asymptotic value of ψ for large σ.
ω	Angular frequency associated with the squeeze motion.
ω_0	Critical value of ω, section 3.3.1 .
∇	Gradient vector operator.

REFERENCES

1   W.E. Langlois   "Isothermal Squeeze-films",
                         Quarterly of Applied Mathe-
                         matics, $\underline{XX}$, no.2, July 1962
                         pp.131-150.

2   E.O.J. Salbu   "Compressible squeeze-films and
                         squeeze-bearings", Journal of
                         Basic Engineering. Trans. ASME,
                         Series D, $\underline{86}$, June 1964,
                         pp.355-364.

3   N. Tipei   "Equatiile lubrificatiei cu gaze",
                         Communicarile, Acad. R.P.
                         Romine, $\underline{4}$, 1954, p.699.

4   G.I. Taylor   "Effects of compressibility at
    P.G. Saffman   low Reynold's numbers",
                         Journal Aero. Sci., $\underline{24}$, 1957,
                         p.553.

5   M. Reiner   "A centripetal pump effect in air",
                         Proc. 9'th, Congr. Appl. Mech.,
                         Brussels, $\underline{1}$, 1958, pp.424-438.

6   H.G. Elrod   "A derivation of the basic
                         equations for hydrodynamic
                         lubrication with a fluid having
                         constant properties". Q. Appli.
                         Math., $\underline{17}$, Jan. 1966. pp.349-359.

7   W.A. Gross   "Numerical analyses of gas lub-
                         ricating films", First Inter-
                         national Symposium on Gas Lubri-
                         cated Bearings, Oct. 1959, US
                         Government Printing Office, 1961.

8   W.A. Michael   "Approximate methods for time
                         dependent gas film lubrication
                         problems", IBM Research Report
                         RJ-205, May1, 1962.

9   W.A. Michael   "Small transient and periodic
                         squeeze motions in parallel gas
                         films", IBM Research Report
                         RJ-197, Sept.25, 1963.

10 S.B. Malanoski   "Discussion on ref.2 , J. Basic
    C.H.T. Pan   Eng.,Trans. ASME, Series D, $\underline{86}$,
                         1964, pp.364-366. Erratum, J.
                         Basic Eng., Trans. ASME, Series D,
                         $\underline{86}$, 1964, p.638.

11 H.G. Elrod
    A. Burgdorfer   "Refinements of the theory of the
                         infinitely-long self-acting
                         gas-lubricated journal bearing",
                         First International Symposium on
                         Gas-lubricated Journal Bearings,
                         Washington, D.C., Oct., 26-28
                         1959.

12   K.A. Liebler   "Squeeze-film bearings", paper
                            presented at an ultrasonics
                            symposium, 1965, Prepared by
                            Lear Siegler, Inc.(Instrument
                            Division), Grand Rapids,
                            Michigan, 1965.

13   T. Chiang   "Analysis and design data for
      C.H.T. Pan   the axial-excursion transducer
                            of squeeze-film Bearings", MTI
                            Technical Report No.MTI-65TR 25,
                            June 2, 1965.

14   C.H.T. Pan   "Analysis, design, and prototype
      (editor)   development of squeeze-film
                            bearings for AB-5 gyro", MTI
                            Report No.MTI-64TR66, Nov., 1964.

15   F.K. Orcutt   "Investigation of an axial-
      C. Kissinger   excursion transducer for squeeze-
      C.H.T. Pan   film bearings", MTI Technical
                            Report No. MTI-65-TR63,
                            Dec., 1965.

16   C.H.T. Pan   "Theory and experiments of squeeze-
      S.B. Malanoski   film gas bearings, Part 1
      P.H. Broussard   Cylindrical Journal bearing",
      J.L. Burch   J. Basic Eng., Trans. ASME,
                            Series D, 88, 1966, pp.191-198.

17   C.H.T. Pan   "On asymptotic analysis of
                            gaseous squeeze-film bearings",
                            J. Basic Eng., Trans. ASME,
                            Series D.

18   H.G. Elrod   "Theory and design data for con-
      S.B. Malanoski   tinuous-film self-acting journal
                            bearings of finite length",
                            Franklin Institute Laboratories
                            Interim Report I-A2049, Nov.,
                            1960.

19   T. Chiang   "Spherical squeeze-film hybrid
      S.B. Malanoski   bearing with small steady-
      C.H.T. Pan   state radial displacement", J.
                            Lub. Tech., Trans.ASME,
                            Series F, 89, July 1967,
                            pp.254-262.

20   J.V. Beck   "Stability of a squeeze-film
      C.L. Strodtman   journal bearing", J. Lub. Tech.,
                            Trans. ASME, Series F, 89,
                            July 1967, pp.369-373.

21   H.G. Elrod   "A differential equation for
                            dynamic operation of squeeze-
                            film bearings", Paper 1, 1967
                            Gas Bearing Symposium,
                            Southampton University.

22   C.H.T. Pan   "Dynamic behaviour of the
      T. Chiang   spherical squeeze-film hybrid
                         bearing", ASME, Paper 68-Lub
                         S-37.

23   R.C. Di Prima   "Asymptotic methods for an
                         infinitely long slider squeeze-
                         film bearing", J. Lub. Tech.,
                         Trans. ASME, Series F, $\underline{90}$,
                         Jan., 1968, pp.173-183.

24   J.V. Beck   "Load support of spherical
      C.L. Strodtman   squeeze-film gas bearings",
                         ASME, Paper 68-Lub S-3.

25   J.V. Beck   "Experimental and analysis of
      W.G. Holliday   a flat disc squeeze-film
      C.L. Strodtman   bearing including effects of
                         supported mass motions", ASME,
                         Paper 68-Lub S-35.

26   J.V. Beck   "Load support of the squeeze-
      C.L. Strodtman   film journal bearing of finite
                         length", J. Lub. Tech., Trans.
                         ASME, Series F, $\underline{90}$, Jan., 1968,
                         pp.157-161.

27   C.H.T. Pan   Discussion of reference 26,
      T. Chiang   appearing in J, Lub. Tech.,
                         Trans. ASME, Series F, $\underline{90}$,
                         July 1968, pp.655-658.

28   C.H.T. Pan   "Squeeze-film Bearings", RPI-MTI
      S.B. Malanoski   Gas Bearing Design Course,
                         Vol.2, Section 7, Aug. 1967.

29   C.H.T. Pan   "On error torques of squeeze-
      T. Chiang   film cylindrical journal
                         bearings", J, Lub. Tech., Trans.
                         ASME, Series F, $\underline{90}$, Jan. 1968,
                         pp.191-198.

30   C.L. Strodtman   Discussion of reference 29,
                         appearing in J. Lub. Tech. Trans.
                         ASME, Series F, $\underline{90}$, July 1968,
                         p.659.

31   T. Chiang   "Dynamic response of a double
      C.H.T. Pan   squeeze-film thrust plate", J.
      H.G. Elrod   Lub. Tech., Trans. ASME, Series
                         F, $\underline{92}$, April 1970, pp.363-369.

32   C.H.T. Pan   "The gaseous squeeze-film at
                         moderately large squeeze numbers",
                         MTI Technical Report No. MTI-
                         70TR26.

33   V.N. Constantinescu "Gas Lubrication", English
                         translation published by ASME,
                         New York, 1969.

34   V.N. Constantinescu   "On high frequency gas squeeze-films", Paper 26, Southampton Gas Bearing Symposium, April 22-25, 1969, Southampton University.

35   C.L. Strodtman   "An augmented, small-parameter equation for the squeeze-film journal bearing", J. Lub. Tech., Trans. ASME. Series F, 92, July 1970, pp.442-449.

36   C.L. Strodtman   "Optimisation of clearance in a squeeze-film journal bearing", J. Lub. Tech., Trans. ASME, Series F, 93, April 1971, pp.246-251.

37   J.S. Ausman   "Gas squeeze-film stiffness and damping torques on a circular disc oscillating about its diameter", J. Lub. Tech., Trans. ASME, Series F, 89, April, 1967.

38   N.S. Grassam
J.W. Powell
(editors)   "Gas lubricated bearings", London, Butterworths, 1964.

39   G.L. Fisher
J.L. Cher
O. Decker   "Some static and dynamic characteristics of high-speed shaft systems operating with gas lubricated bearings", First International Symposium on Gas-lubricated Bearings, Oct.26, 1959, Washington, D.C., pp.383-417.

40   Lear Siegler
Inc.   "Final Report on a Dynamic Film Suspension for Inertial Accelerometers", Lear Siegler Inc., Report No. GRR-67-1312.

41   C.H.T. Pan   Discussion on reference 21, loc. cit.

42   A. Cameron   "Principles of Lubrication", Longmans, London, 1966.

43   A. Burgdorfer   "The influence of the molecular mean free path in the performance of hydrodynamic gas lubricated bearings", J. Basic Eng. Trans., ASME, Series D, March 1959, pp.94-98.

44   F.C. Hsing
H.S. Chiang   "Dynamics of a pad supported on a highly compressible gas film", MTI Technical Report No.MTI-69TR28, April 2, 1969.

45	V. Castelli J. Pervics	"Review of numerical methods in gas bearing film analysis", J. Lub. Tech, Trans. ASME, Series F, 90, Oct. 1968, pp.777-790.
46	H.G. Elrod J.T. McCabe T.Y. Chu	"Determination of gas bearing stability by response to a step-jump", ASME Paper 67- Lub S-5
47	H.G. Elrod G.A. Glanfield	"Computer procedures for the design of flexibly mounted, externally pressurised gas lubricated journal bearings", Gas Bearing Symposium, March 1971, Southampton University, Paper 22.
48	M.R. Abbott	"Programme for solving an equation arising in lubrication theory", RAE Maths Computing Note Series, C331, 1964.
49	D. Faddy	"The theoretical performance of statically loaded pairs of conical gas bearings", RAE Technical Report, No.TR69174, 1969.
50	C.H.T. Pan P.H. Broussard	"Squeeze-film lubrication", 1967 Gas Bearing Symposium, University of Southampton, April, 1967, Paper 12.
51	E.A. Muijderman	Discussion of reference 50, loc. cit, p.B45.
52	E.A. Muijderman	"Spiral groove bearings", PhD. thesis published in book form by McMillan, London, 1964.
53	C.H.T. Pan	Discussion on reference 50, loc. cit., p.B50.
54	L.M. Milne-Thompson L.J. Comrie	"Standard four-figure mathematical tables", MacMillan, London, 1957, Edition B, p.221.
55	D.M. Dewar	"The development of a design procedure for grease and oil lubricated spiral grooved bearings", PhD. thesis, April, 1972, University of Southampton Internal Report No. ME/72/29.
56	D.E. Muller	"A method for solving algebraic equations using an automatic computer", Mathematical Tables and Other Aids, 10, 1956, pp.208-215.

57   G.D. Scowen   "Analysis and computer pro-
                           cedures for the design of
                           flexibly mounted self-acting
                           or externally-pressurised gas
                           lubricated two bearing systems",
                           Internal Report No. ME/72/43,
                           Nov. 1972.

58   F. Gerrish   "Pure Mathematics, vol. II",
                           Cambridge University Press,
                           1960, p.431.

59   B.W. Arden   "Numerical Algorithms - origins
      K.N. Astill   and applications", Addison-
                           Wesley, 1970, p.232.

60   K. Brockwell   "A design method for radially
      C. Ettles   grooved thrust washers",
      M. Stokes   Proc. Instn. Mech. Engrs.,
                           184, 1969-70, pp.82-92.

61   K. Hope   "Methods of multivariate
                           analysis", University of London
                           Press Ltd., 1968, chapter 6.

62   C.H. Goulden   "Methods of statistical analysis",
                           Second Edition, Wiley, New York,
                           1952, chapter 8.

63   V. Castelli   "Numerical methods", RPI-MTI
                           Gas Bearing Design Course Notes,
                           1966.

64   J.T. McCabe   "Summary of investigations of
      H.G. Elrod   entrance effects of circular
      S. Carfagno   thrust bearings", paper 17, 1969
      R. Colsher   Gas Bearing Symposium,
                           Southampton University, April.

65   J.H. Vohr   "Design data - gas lubricated
      C.H.T. Pan   spin axis bearings for gyro-
                           scopes", MTI Report 68TR29.
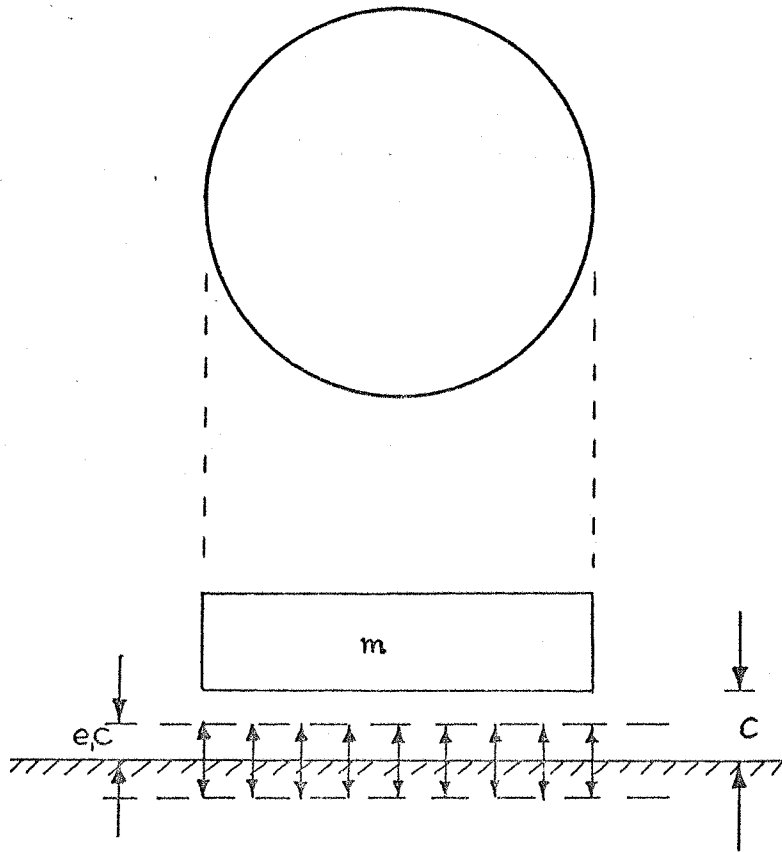
Fig.1

Fig.1 Parallel flat disc squeeze-film thrust bearing
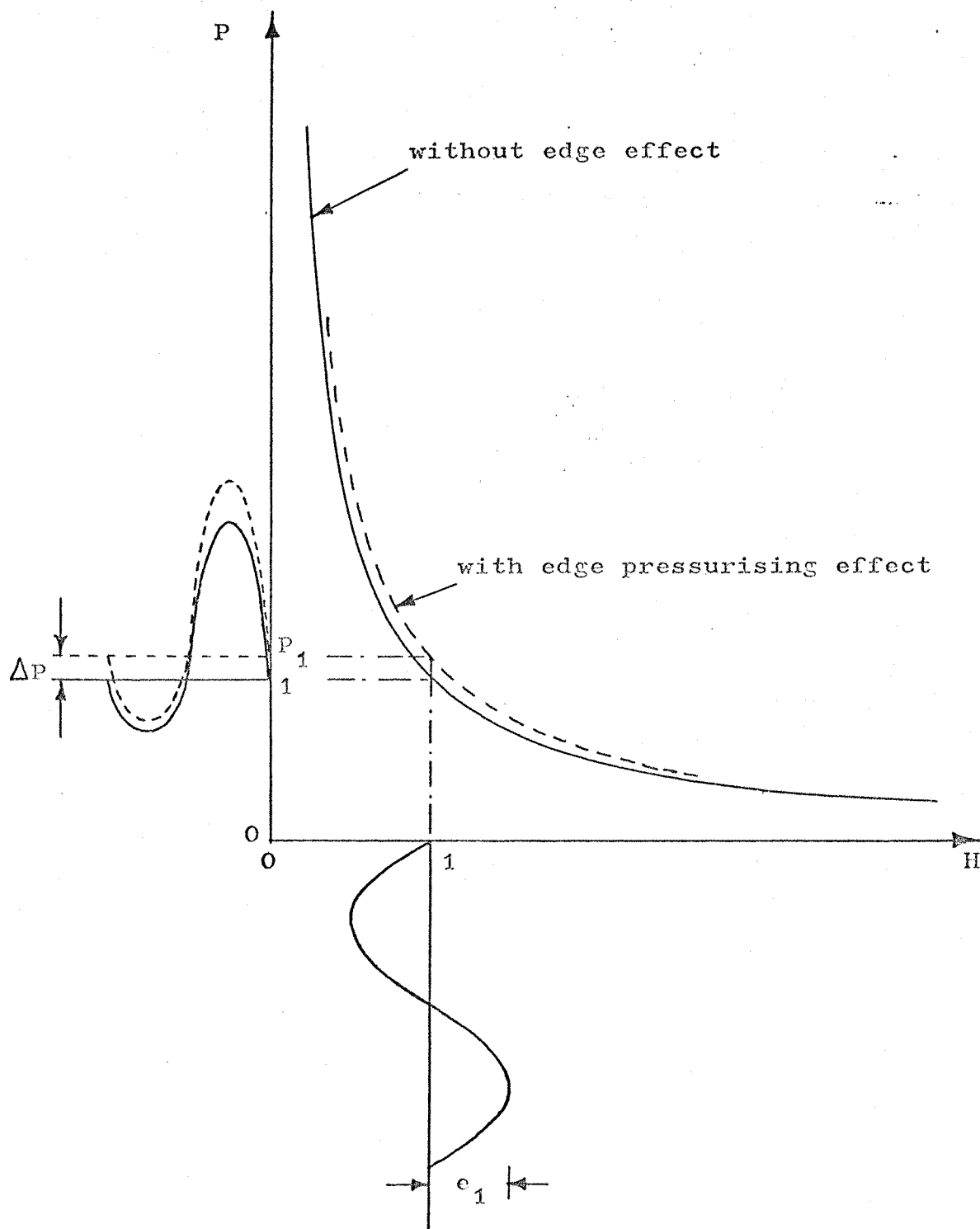
Fig. 2

Fig. 2   Boyle's Law model
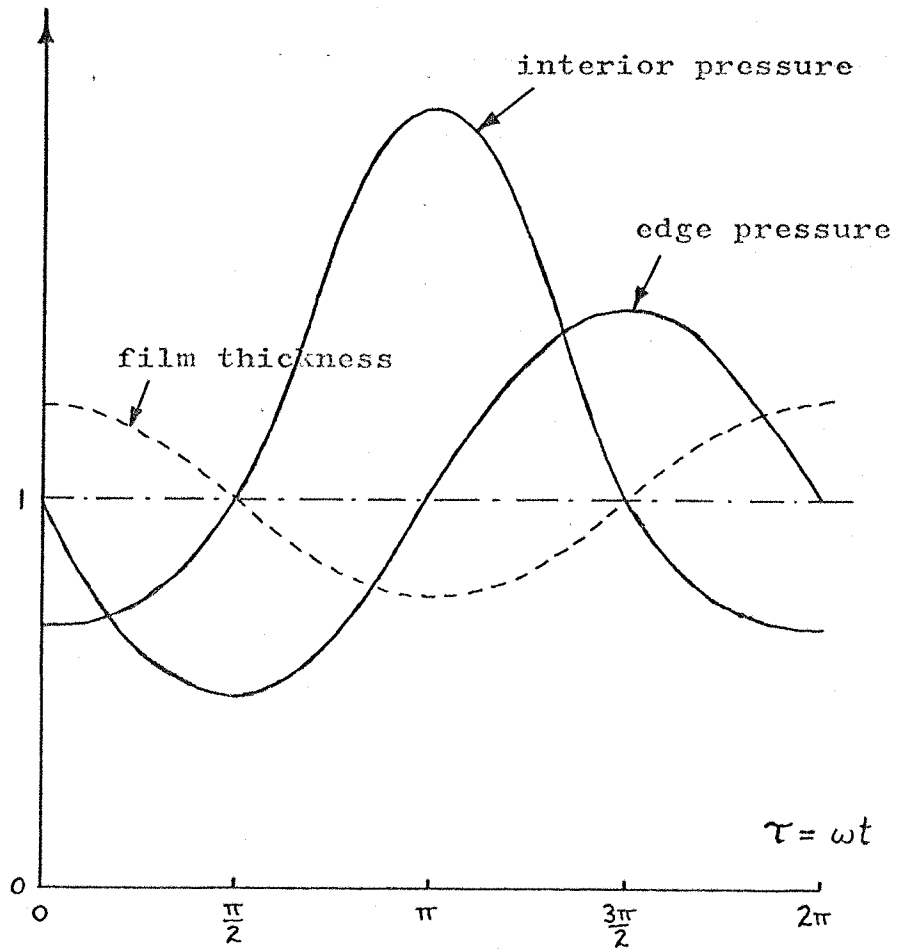
Fig.3

Fig.3   Interior and edge pressure variations with film
         thickness, showing phase relationships
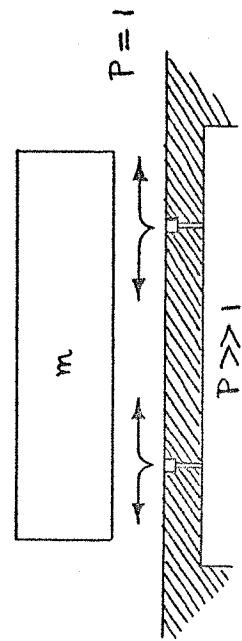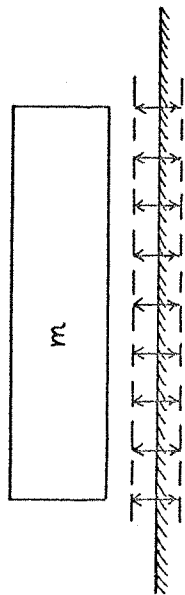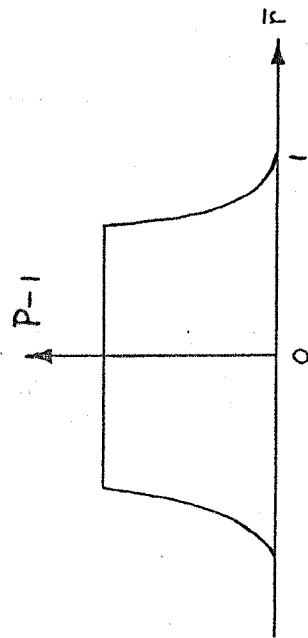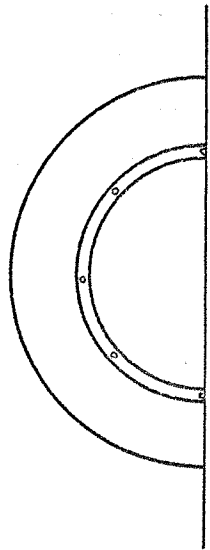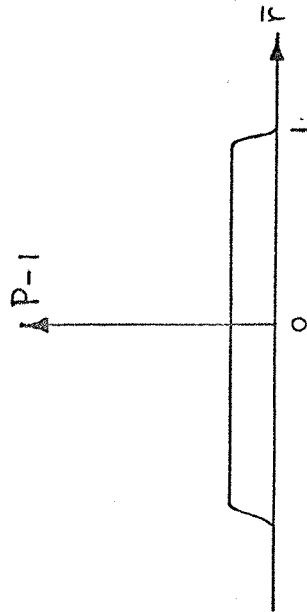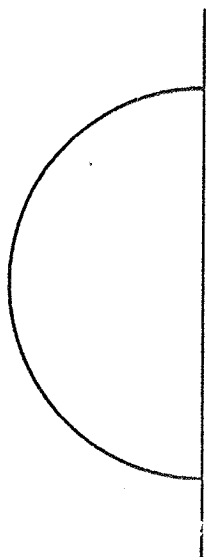
Fig. 4 Pressure distributions in squeeze-film and externally-pressurised thrust bearings
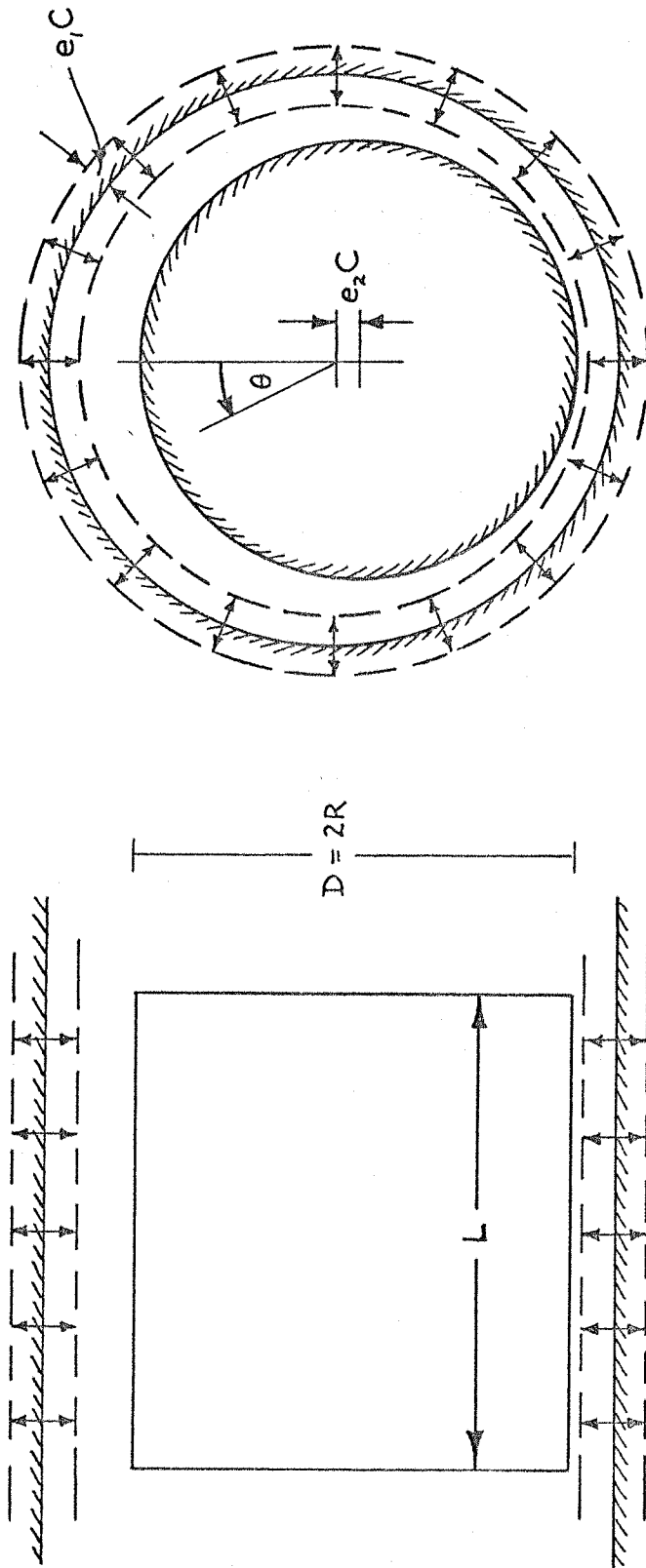
Fig.5

Fig.5   Squeeze-film journal bearing geometry
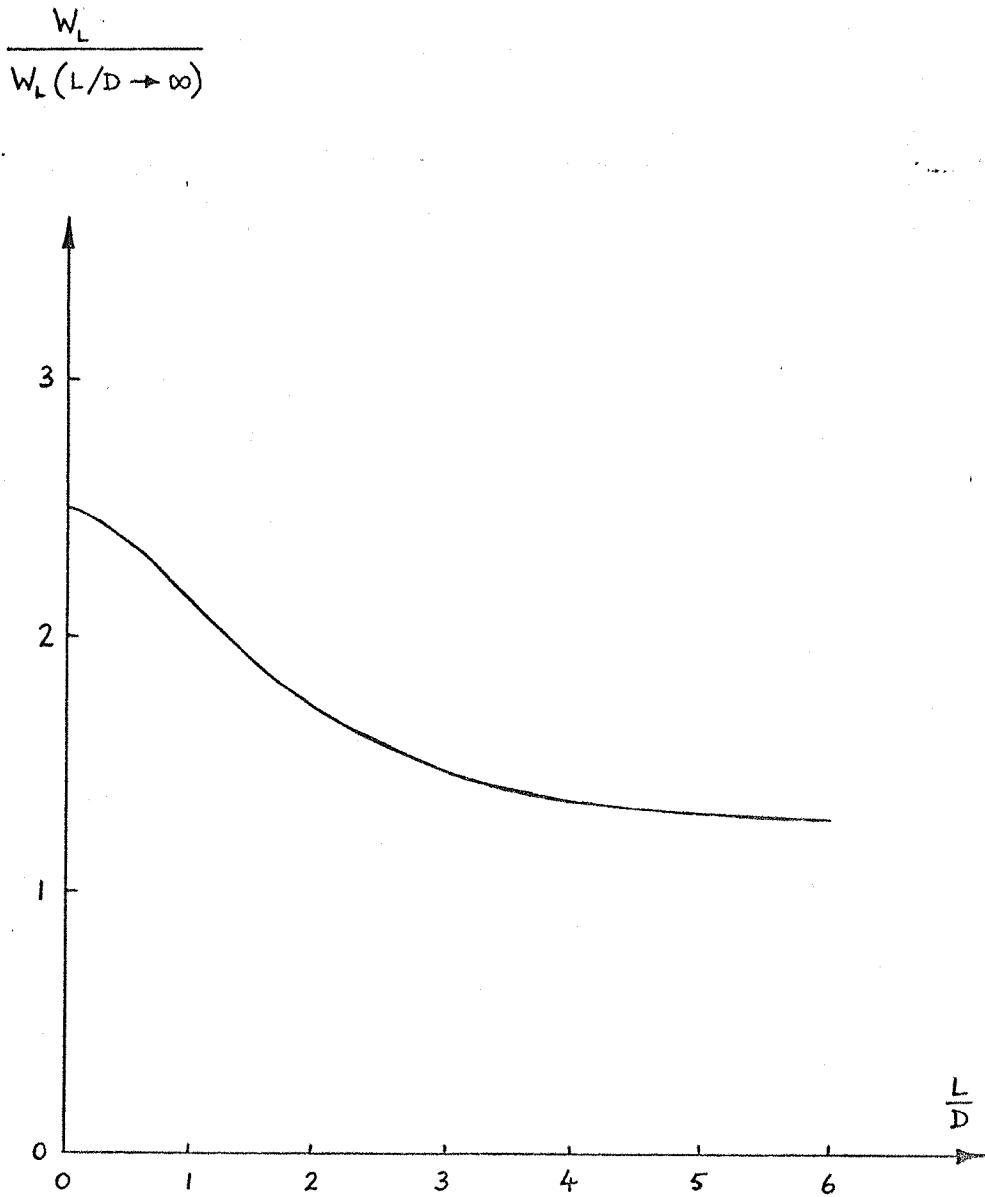
Fig.6

Fig.6   L/D dependence of bearing force per unit length
         in ungrooved cylindrical bearings

Fig.7

$$\frac{M_{\bar{z}}(\Theta, \bar{z})}{M_{\bar{z}}(\Theta, o)}$$
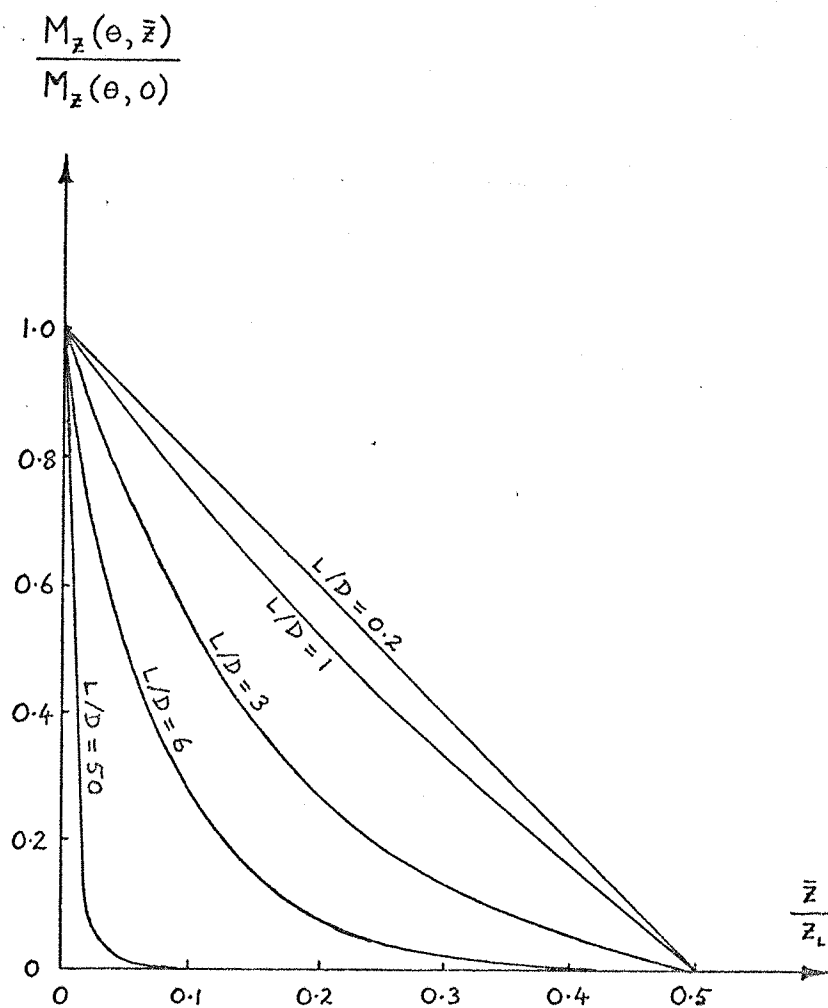
Fig.7   Axial penetration of the axial mass flow rate

for various values of L/D
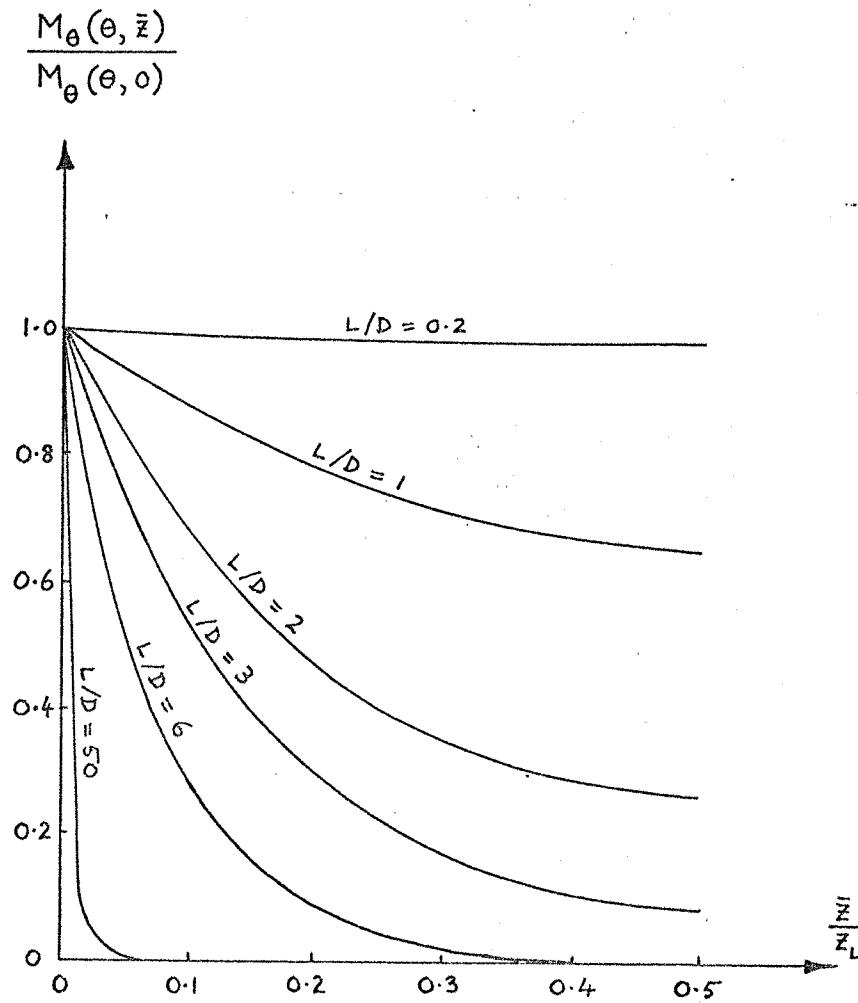
Fig.8

Fig.8   Axial distribution of the circumferential mass flow rate for various values of L/D
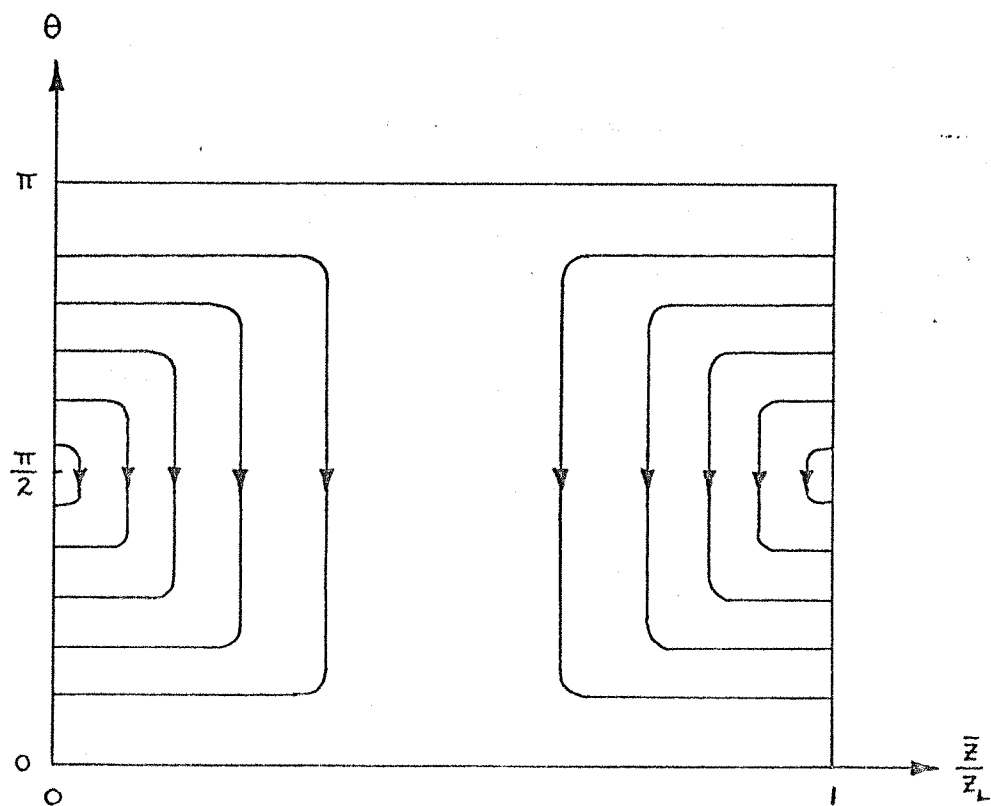
Fig.9

Fig.9   Schematic flow pattern in the bearing film
        region $0 \leqslant \theta \leqslant \pi$, $0 \leqslant \bar{z} \leqslant z_L$
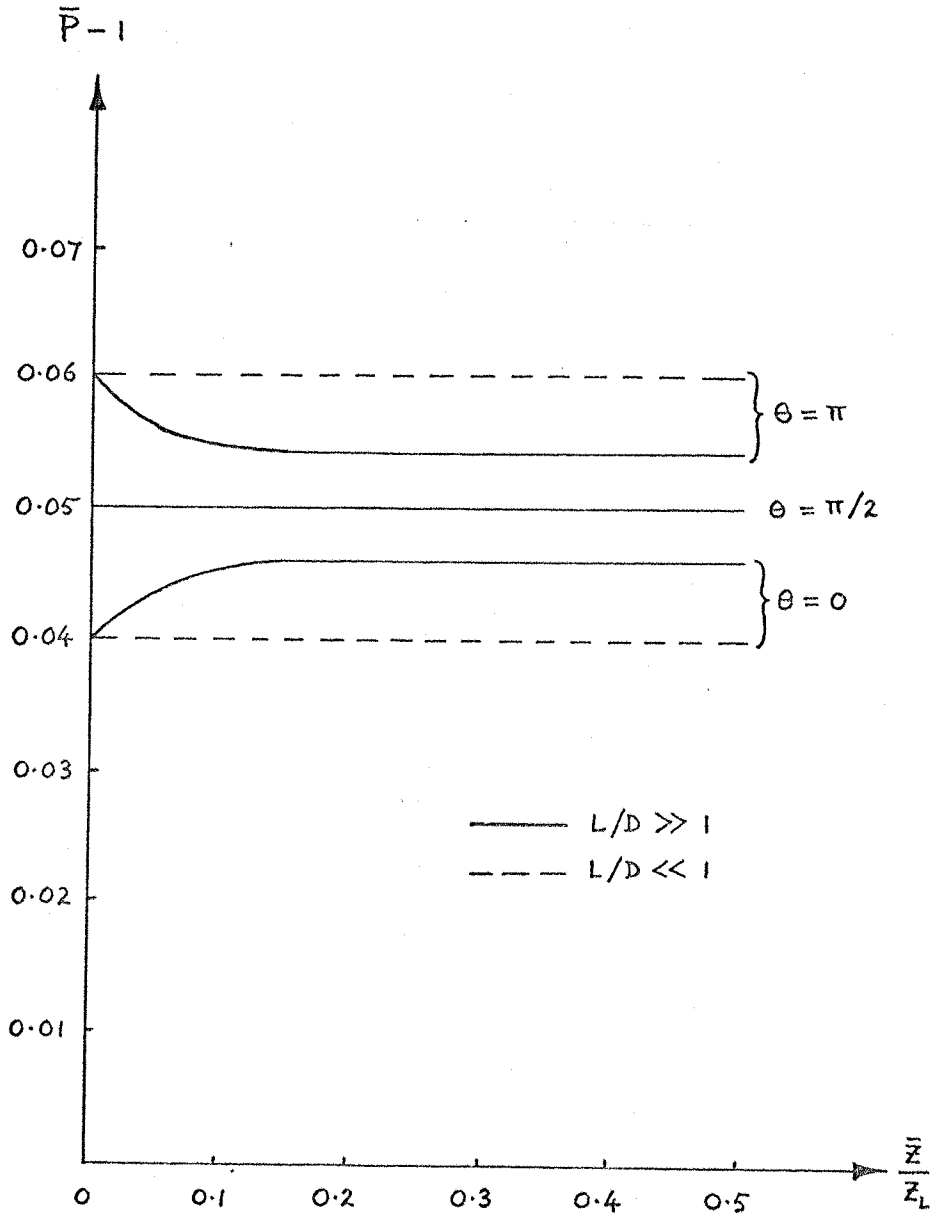
Fig. 10

Fig. 10   Axial pressure distributions in ungrooved journal bearings when $c_1 = 0.2$ and $c_2 = -0.1$

Fig.11

$$P(\theta, z_L/2) - 1$$
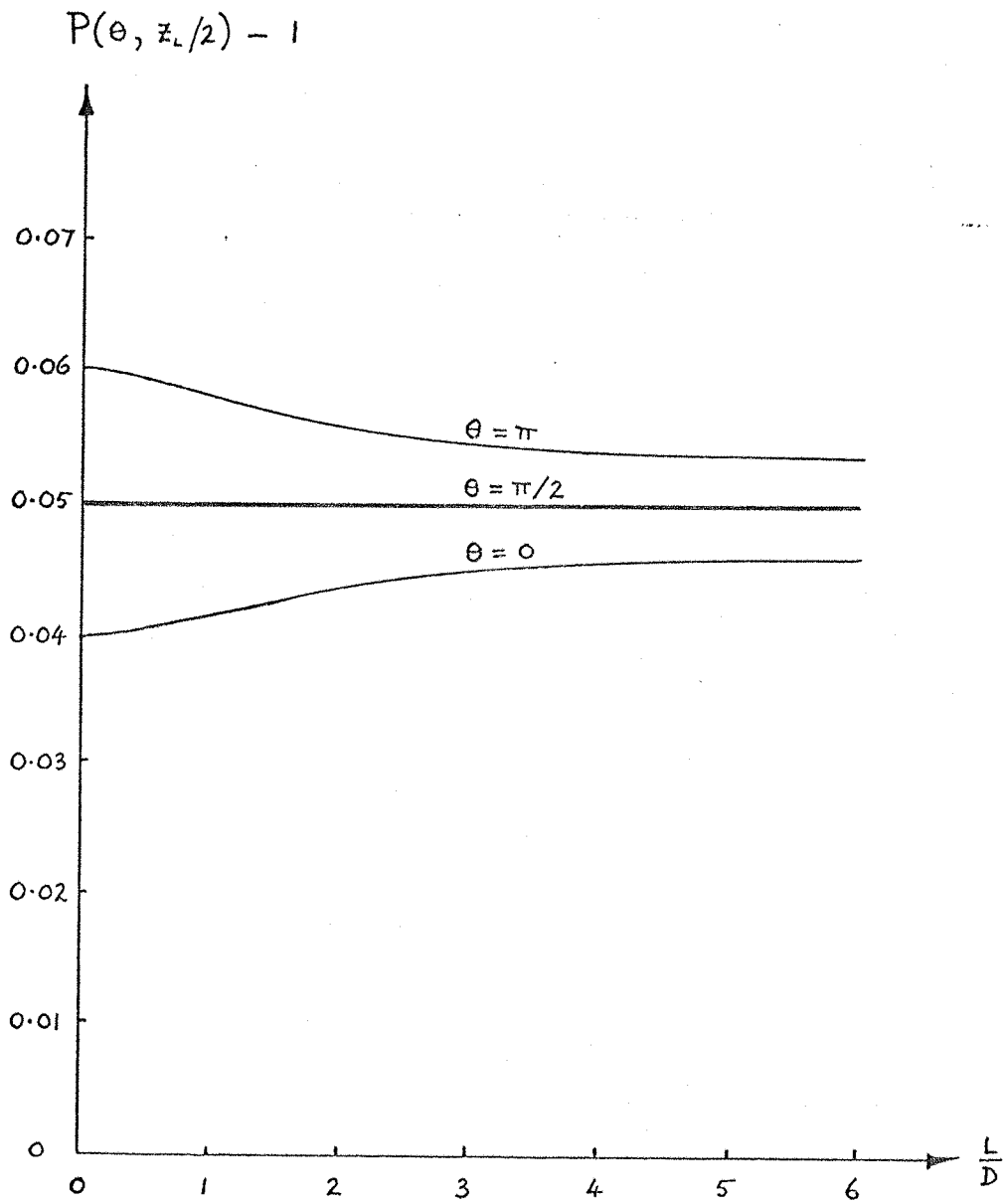
Fig.11   Mid-plane pressures at particular orientations

θ as functions of L/D
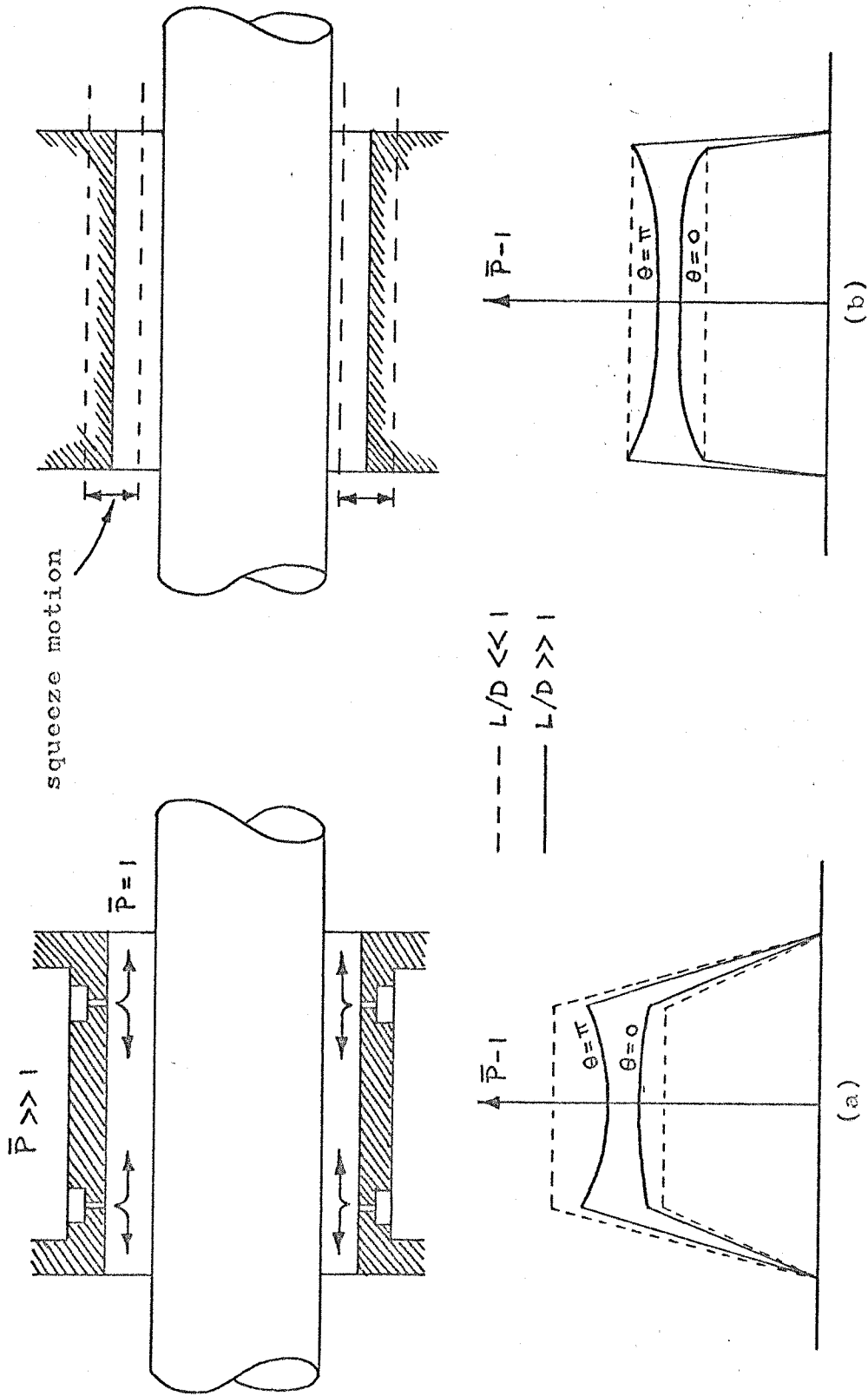
Fig.12

Fig.12   Comparative pressure profiles in (a) externally-pressurised and (b) squeeze-

film journal bearings
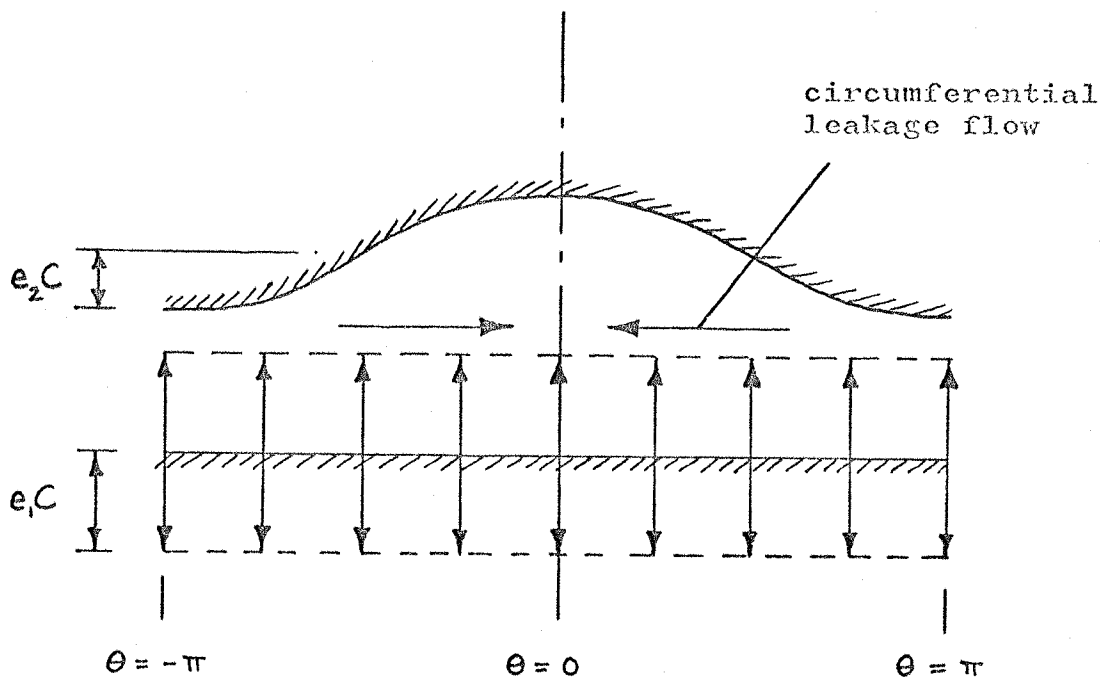
Fig.13

Fig.13   Developed film cross-section in an ungrooved
          squeeze-film journal bearing
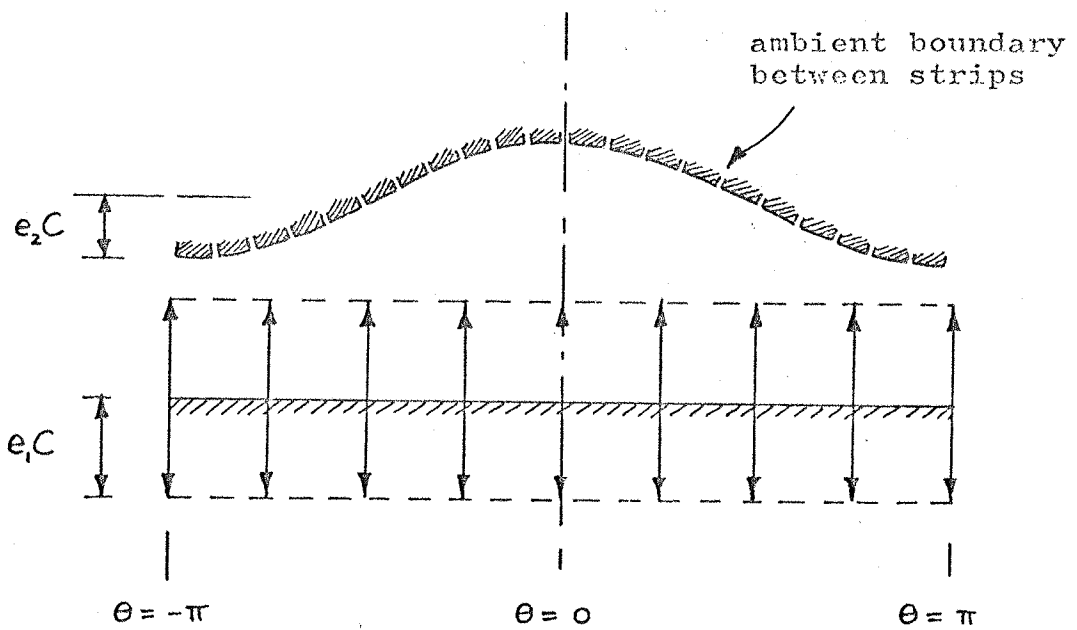
Fig. 14

Fig. 14   Developed film cross-section in an axially
grooved squeeze-film journal bearing
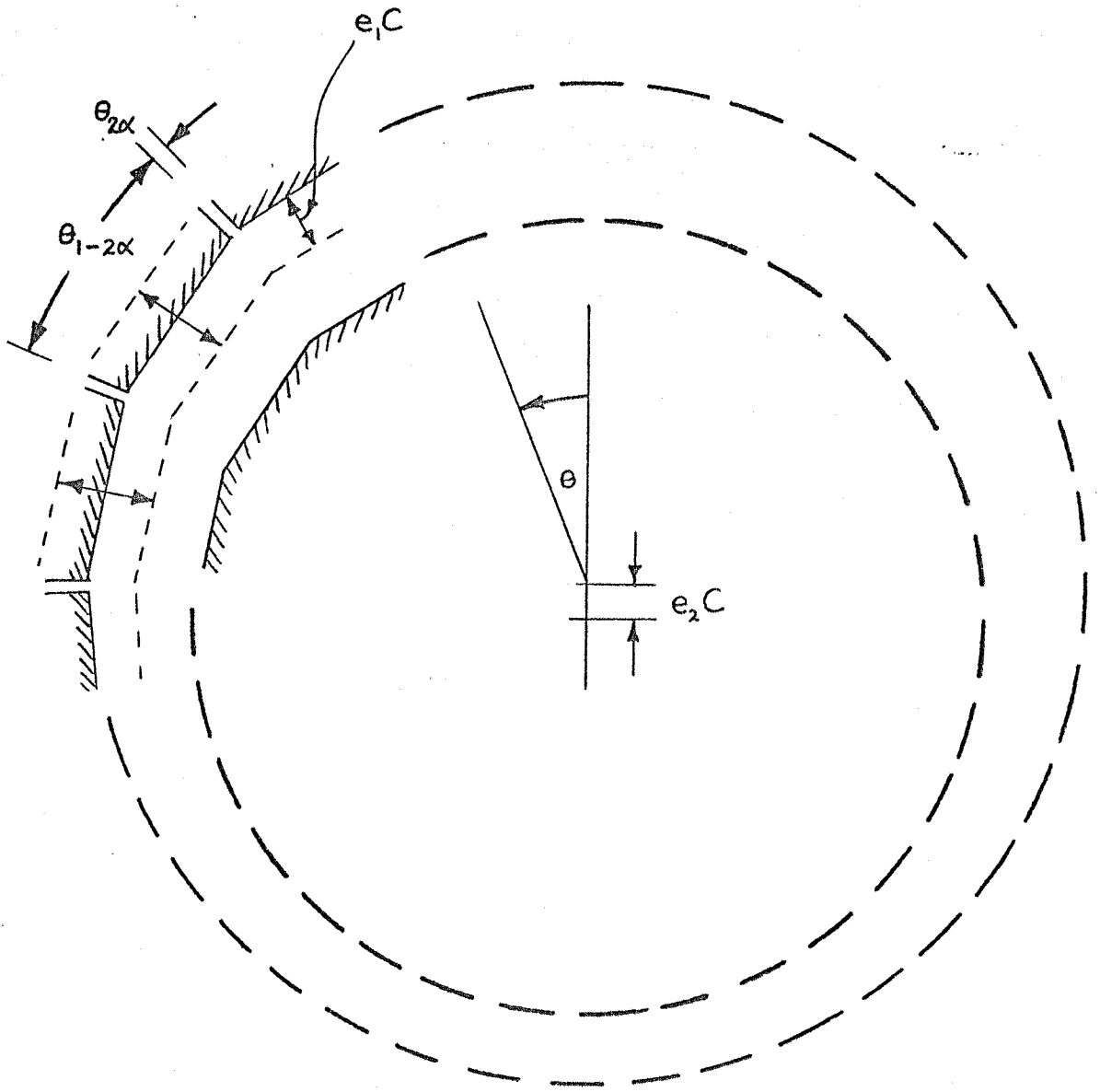
Fig. 15

Fig. 15 Squeeze-film journal bearing approximated by parallel flat strip bearing segments
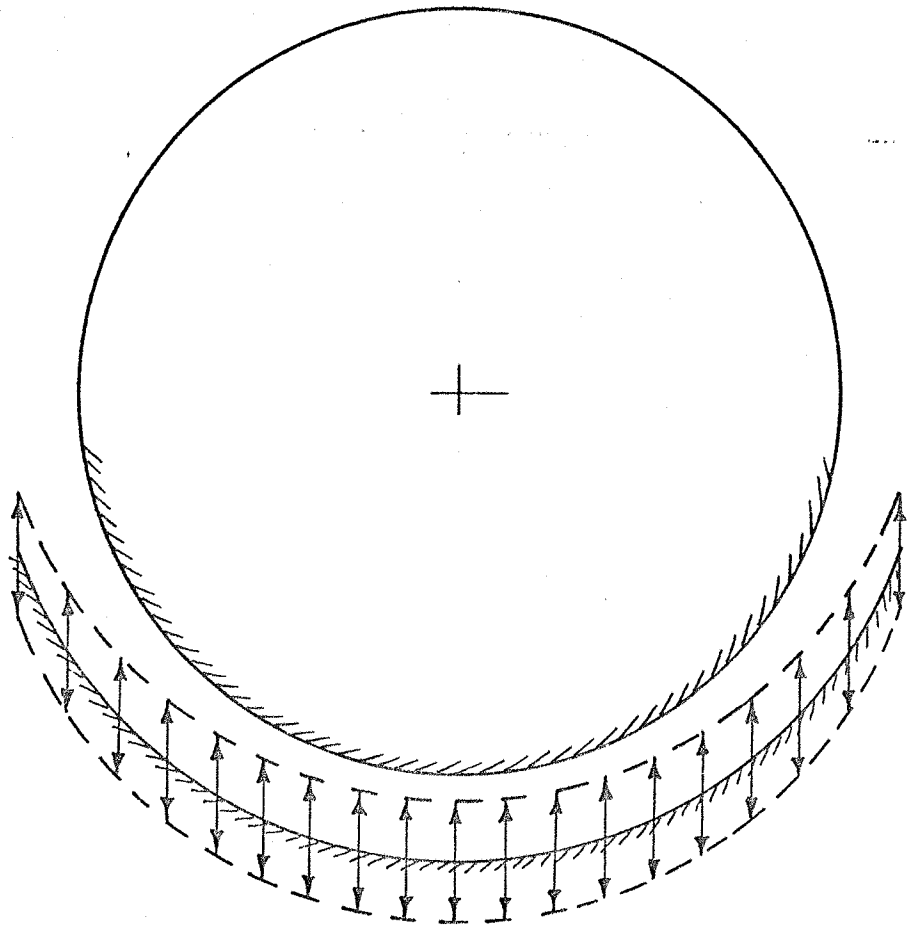
Fig. 16

Fig. 16   Axial excursion hemispherical bearing
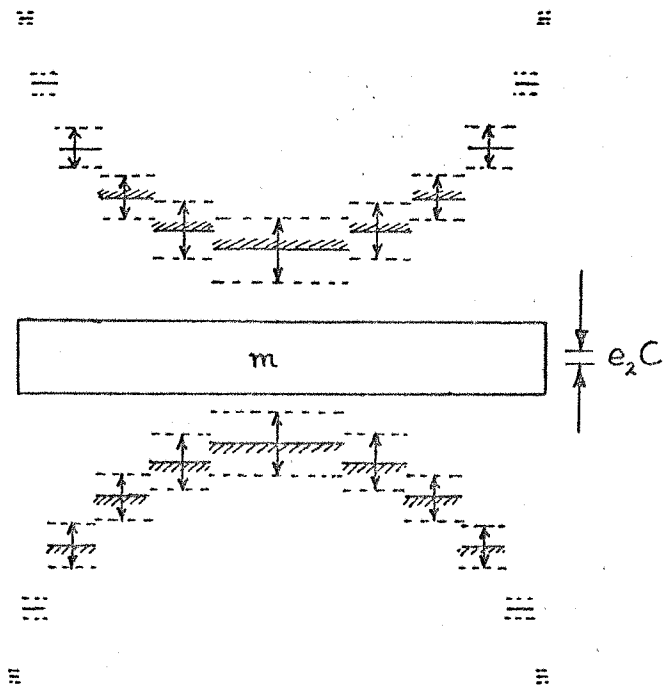
Fig.17

Fig.17   Opposed segmented thrust bearing equivalent in
          lift to an axially grooved journal bearing

Fig.18

slip flow region

flow

laminar flow region

slip flow region
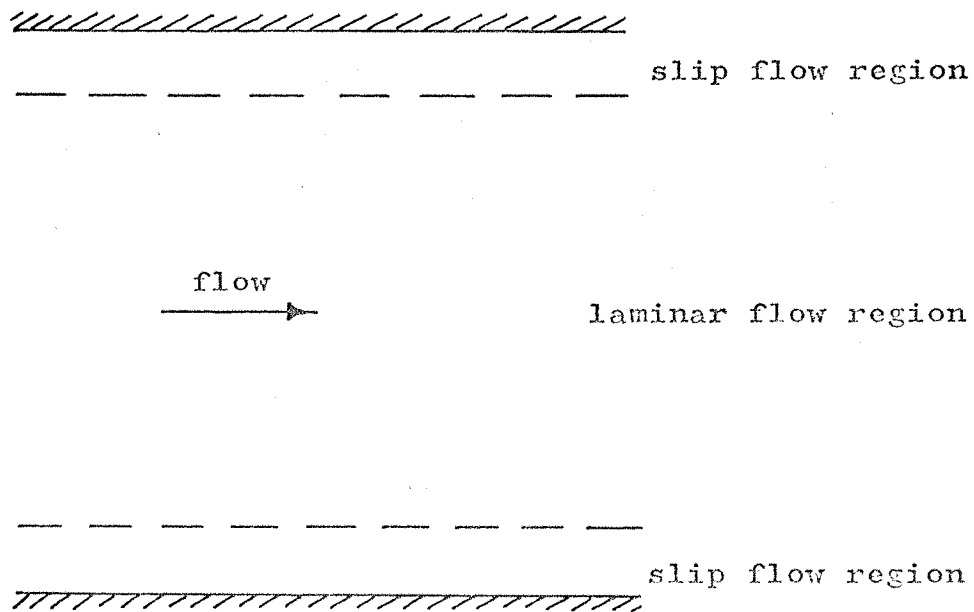
Fig.18   Poiseuille flow under slip flow conditions
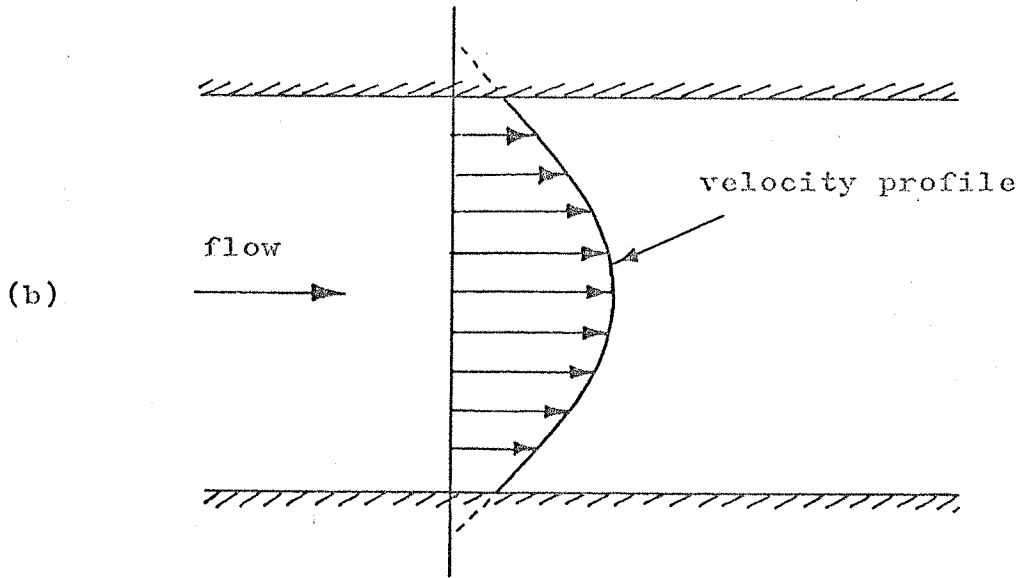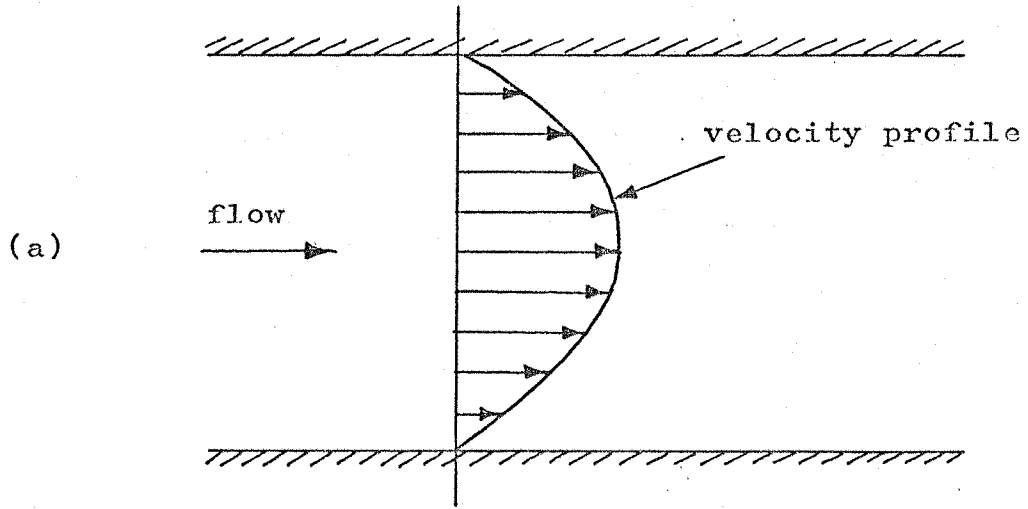
Fig.19

Fig.19   Poiseuille flow (a) without, and (b) with, slip flow
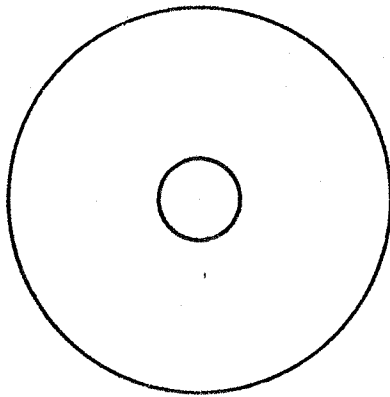
Fig.20

w = 1
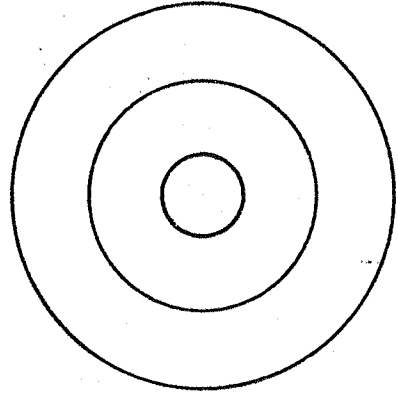
w = 2
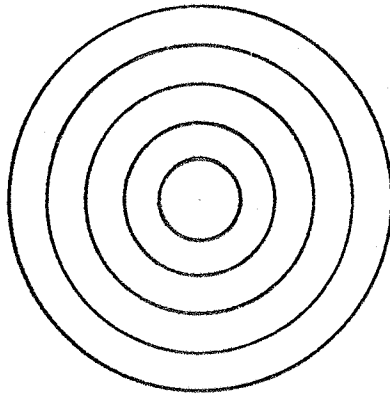
w = 4
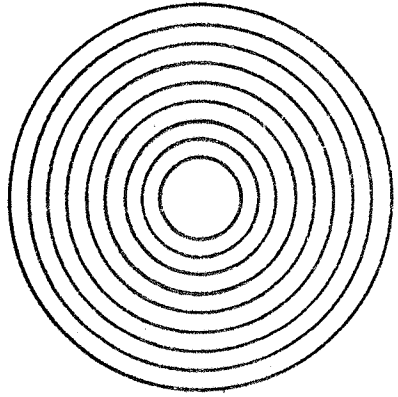
w = 8

Fig.20   Flat annular thrust bearing with various

numbers w of concentric segments
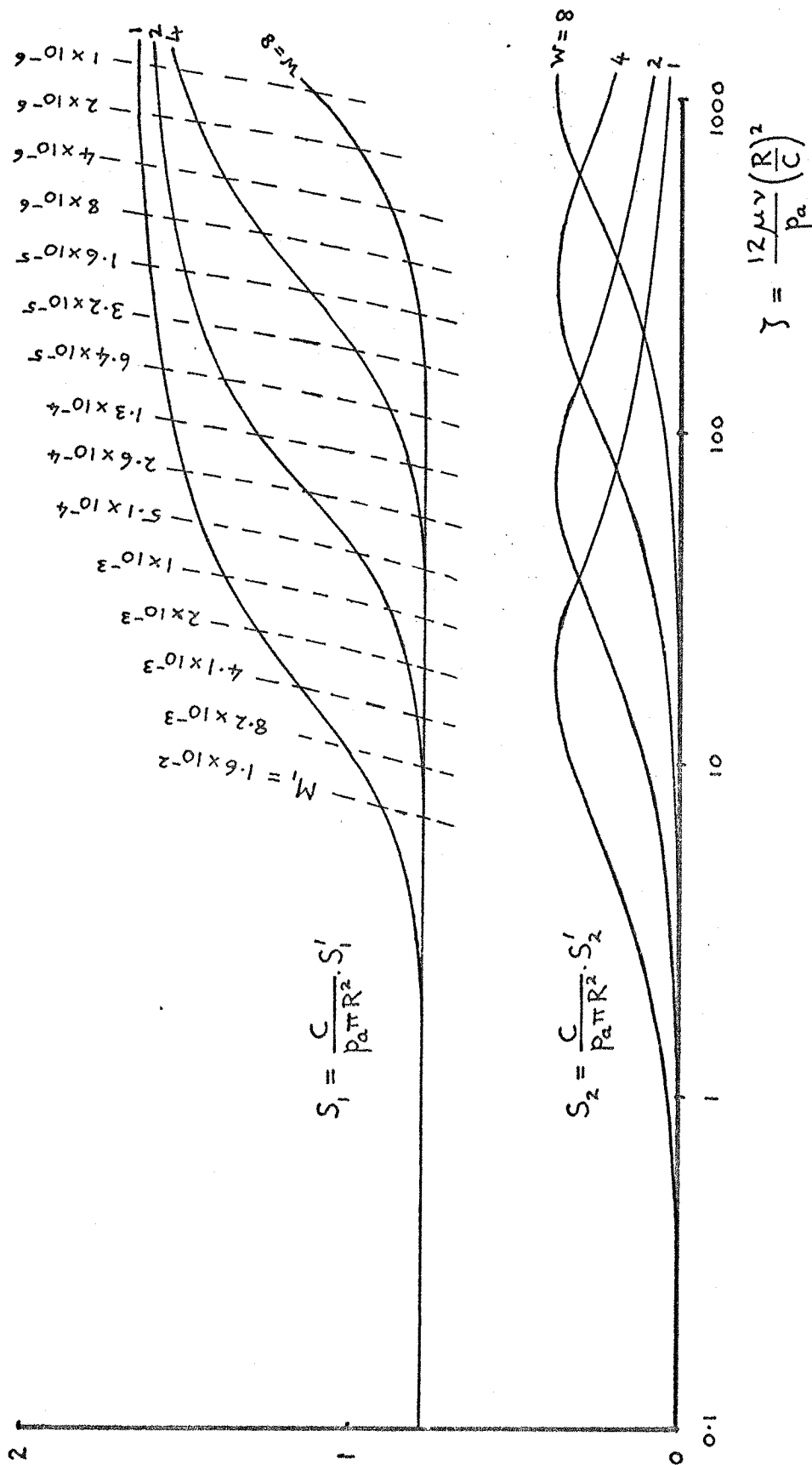
Fig.21

Fig.21 Dynamic stiffness components in a thrust bearing composed of different numbers

of concentric annular segments ($e_1 = 0.5$)

Fig.22

$$\delta_1 = \frac{P_a \pi R^2}{C} \delta_1'$$

$$\gamma = \frac{12 \mu \nu}{P_a} \left(\frac{R}{C}\right)^2$$
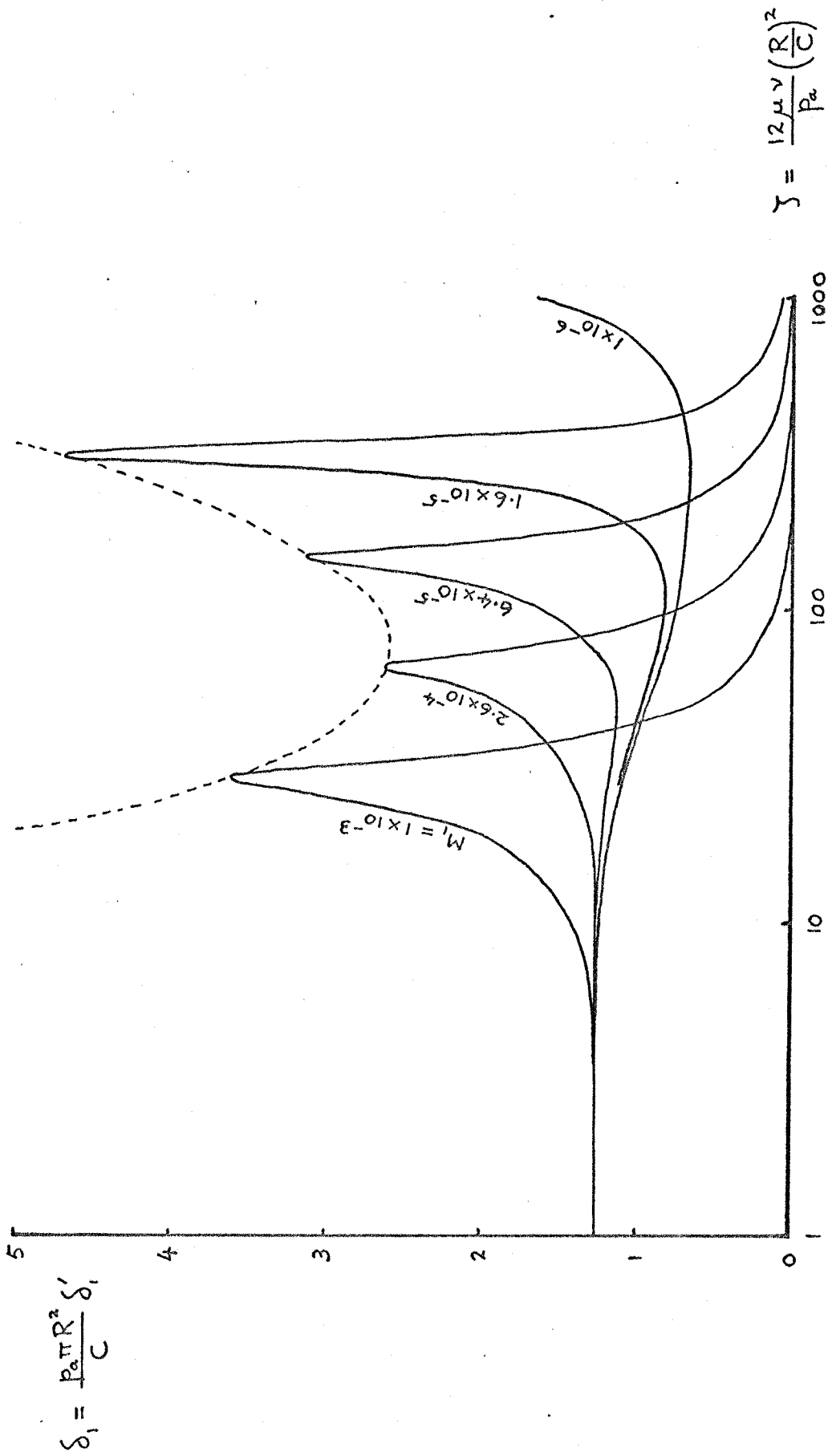
Fig.22   Dynamic compliance in an annular segmented thrust bearing with $w = 2$ and $e_1 = 0.5$

Fig.23

$$\zeta = \frac{12\mu\nu}{p_a}\left(\frac{R}{C}\right)^2$$

$$\delta_1 = \frac{p_a \pi R^2}{C} \cdot \delta_1'$$
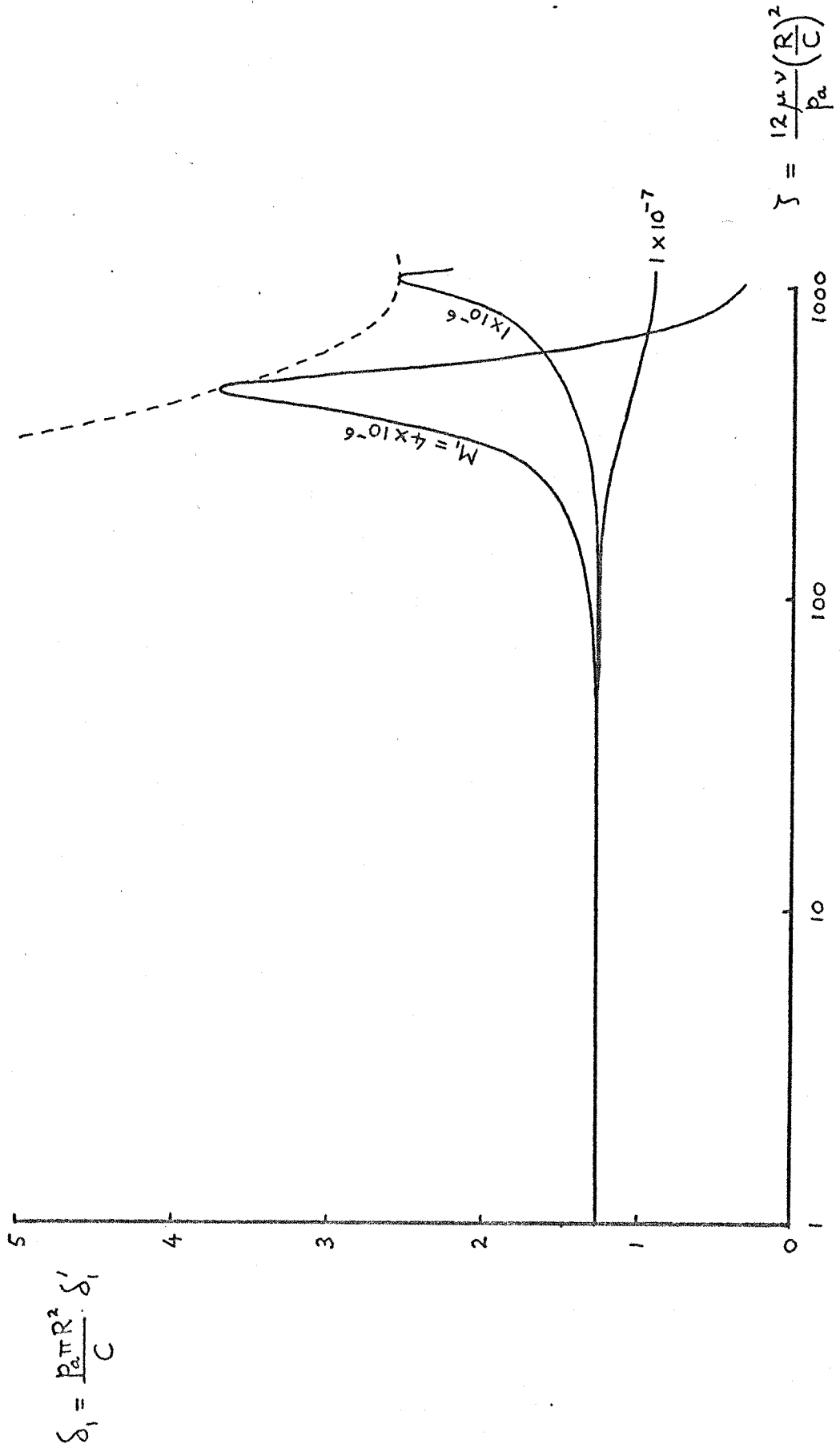
Fig.23 Dynamic compliance in an annular segmented thrust bearing with $w = 8$ and $e_1 = 0.5$
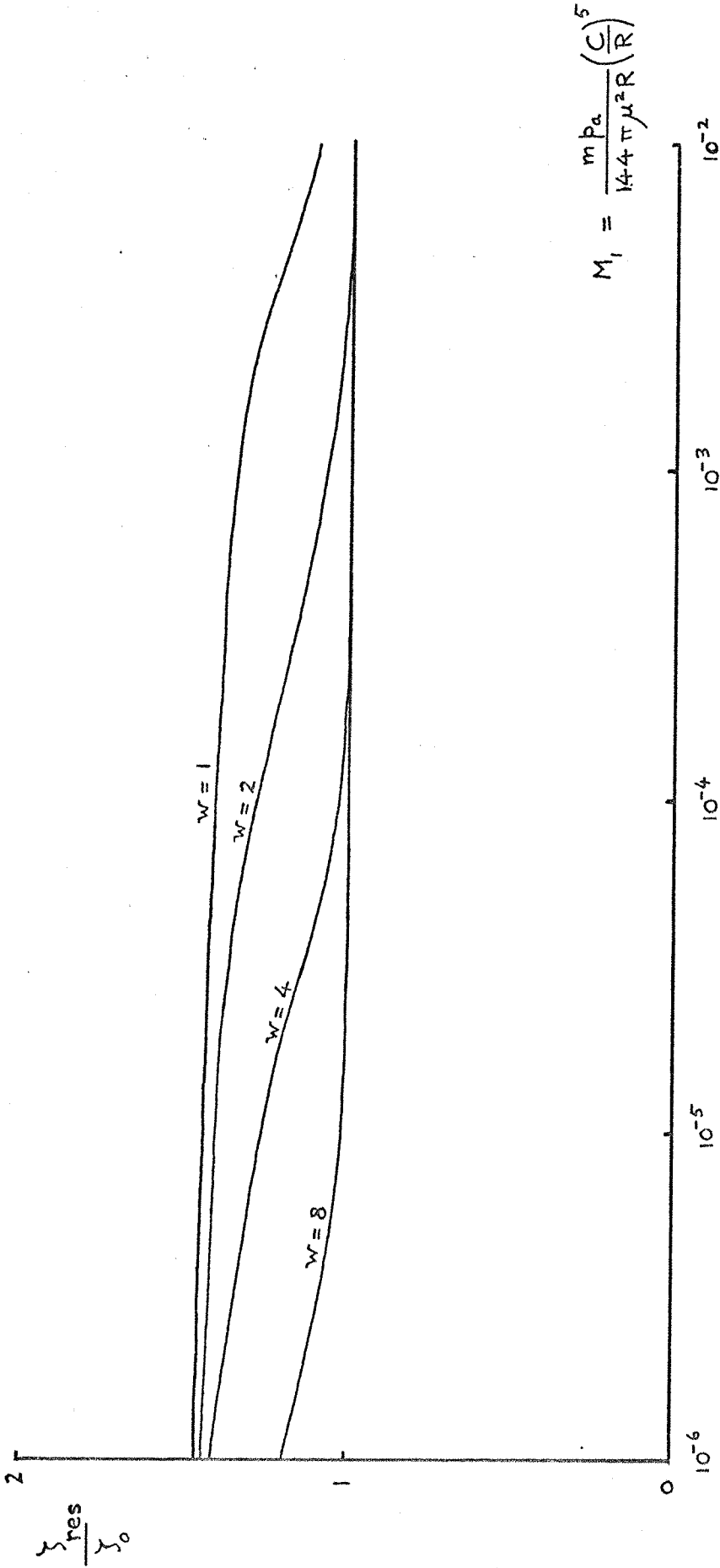
Fig.24

Fig.24   Variation of resonance frequency with dimensionless mass in an annular

segmented thrust bearing with different numbers of segments ($c_1 = 0.5$)

$$\frac{\delta_1 \big|_{\text{res.}}}{\delta_1(\zeta = 0)}$$

$$M_1 = \frac{m\,p_a}{144\pi\mu^2 R}\left(\frac{c}{R}\right)^5$$
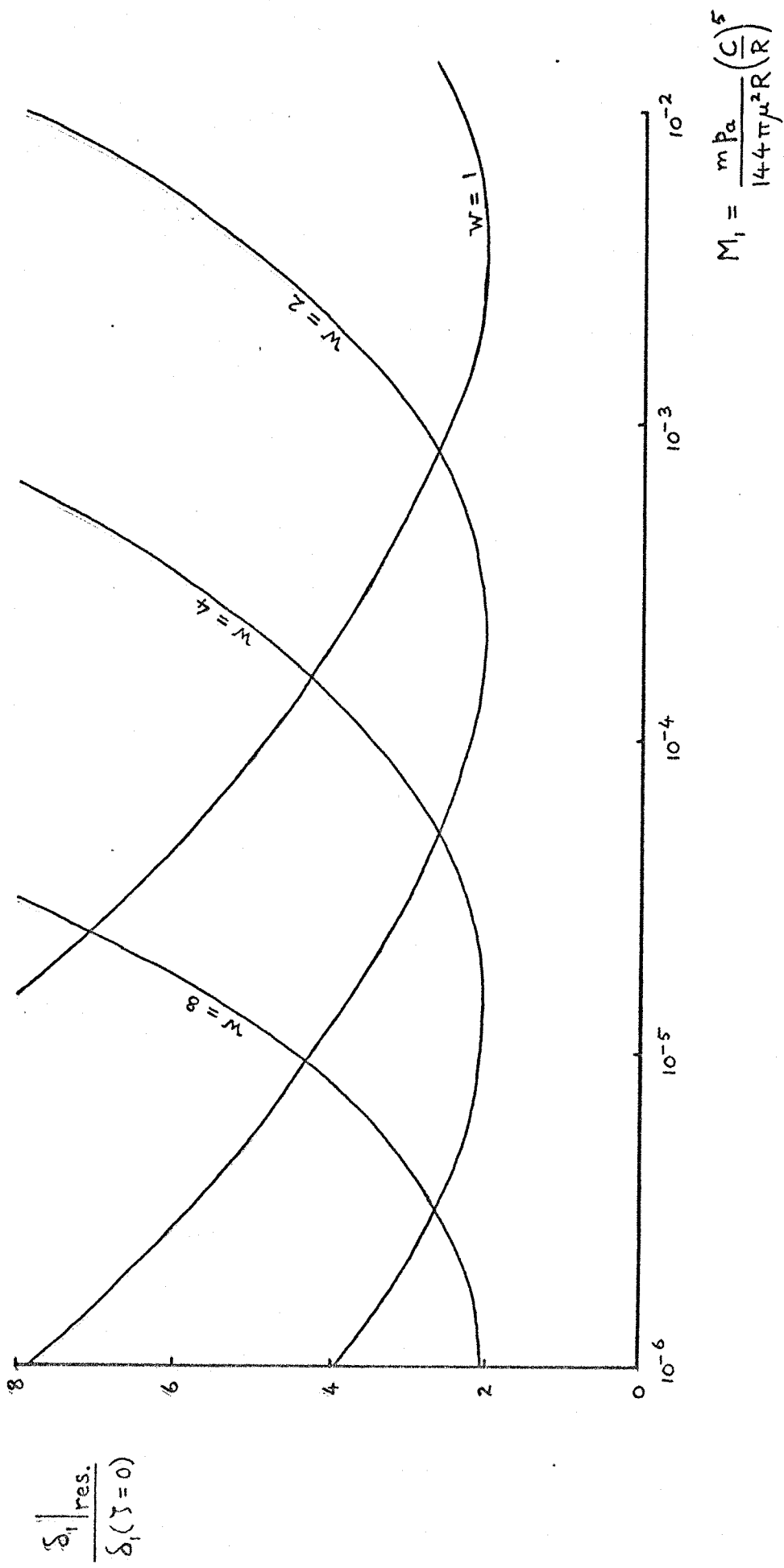
Fig.25   Variation with dimensionless mass of dynamic compliance at resonance in an

annular segmented thrust bearing with different numbers of segments $(e_1 = 0.5)$

Fig.25
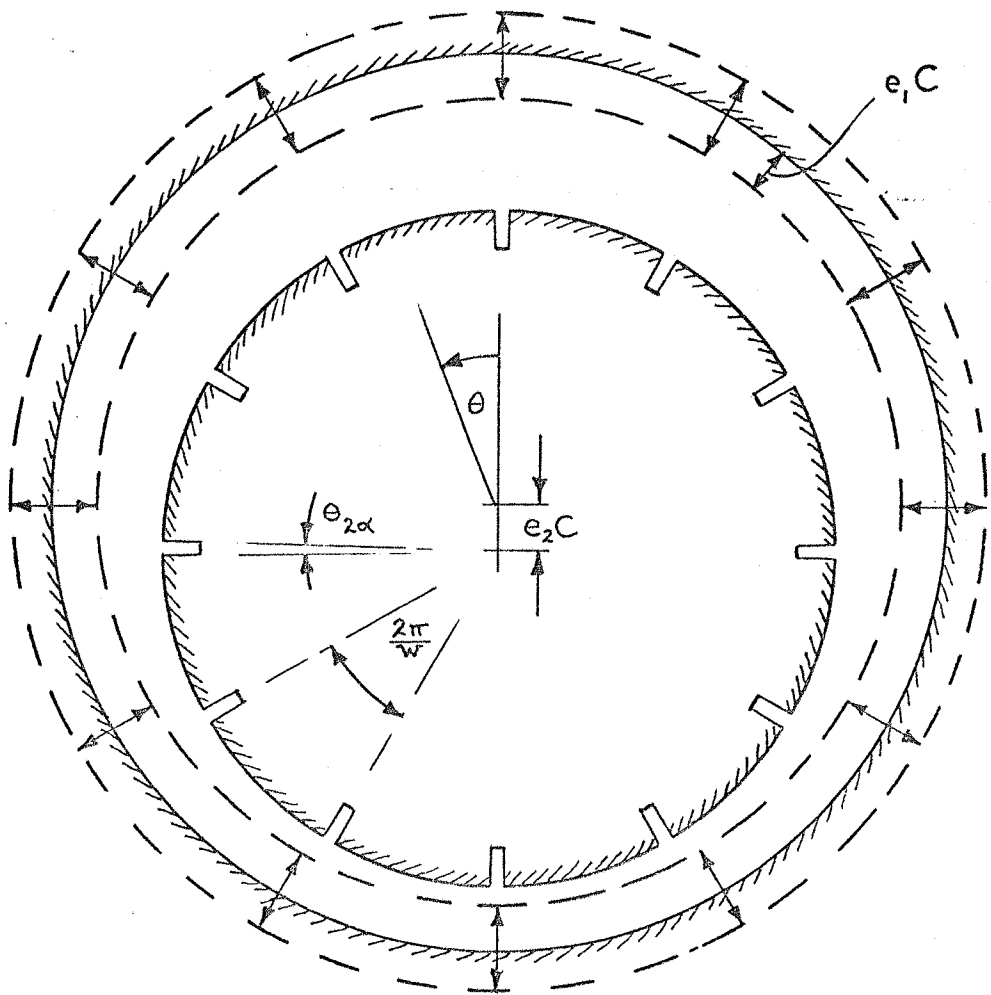
Fig. 26

Fig. 26   Cross-section of axially grooved journal bearing
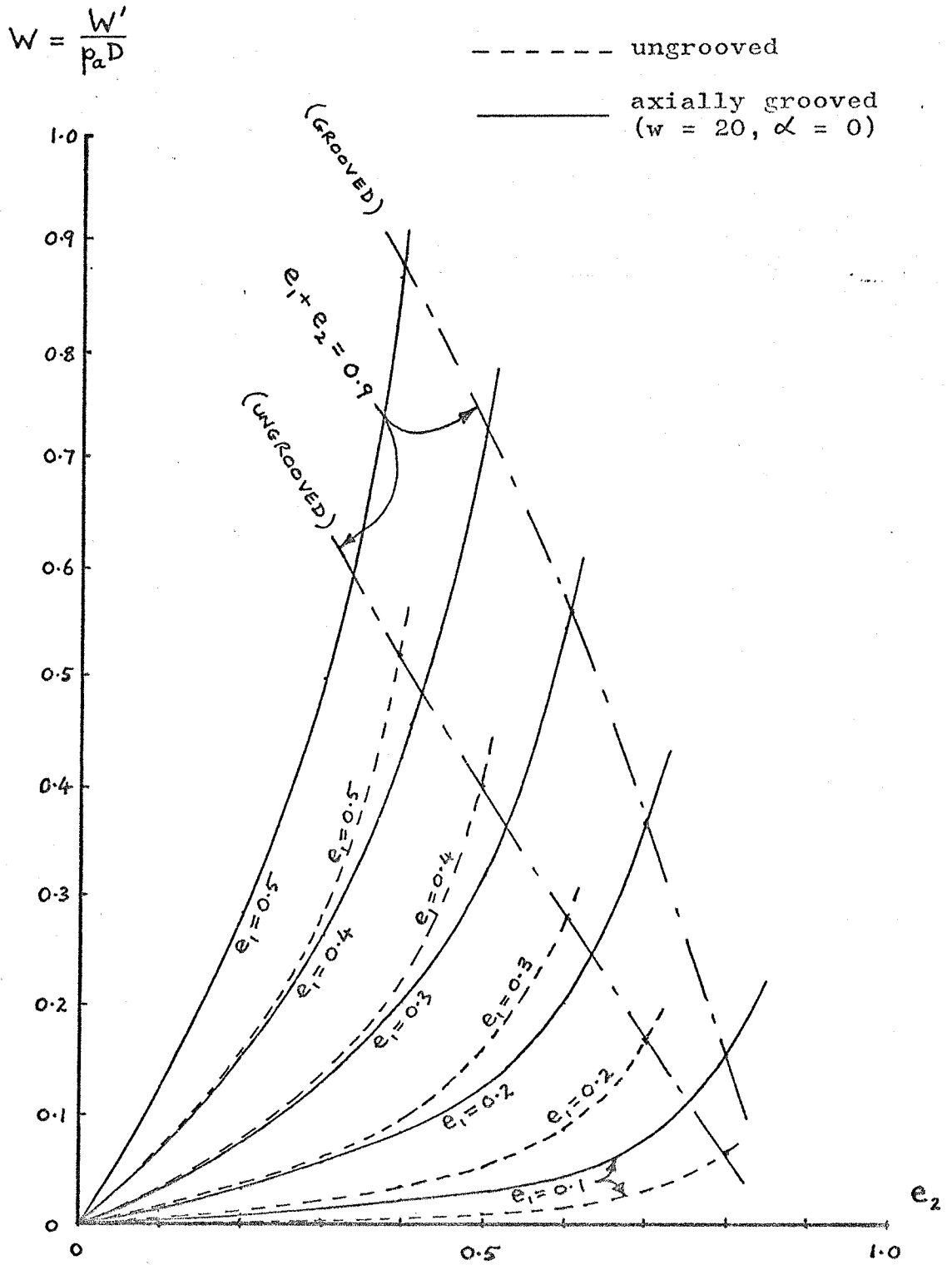
Fig.27

Fig.27   Variation with eccentricity of bearing force per
unit length in ungrooved and axially grooved
infinite length journal bearings
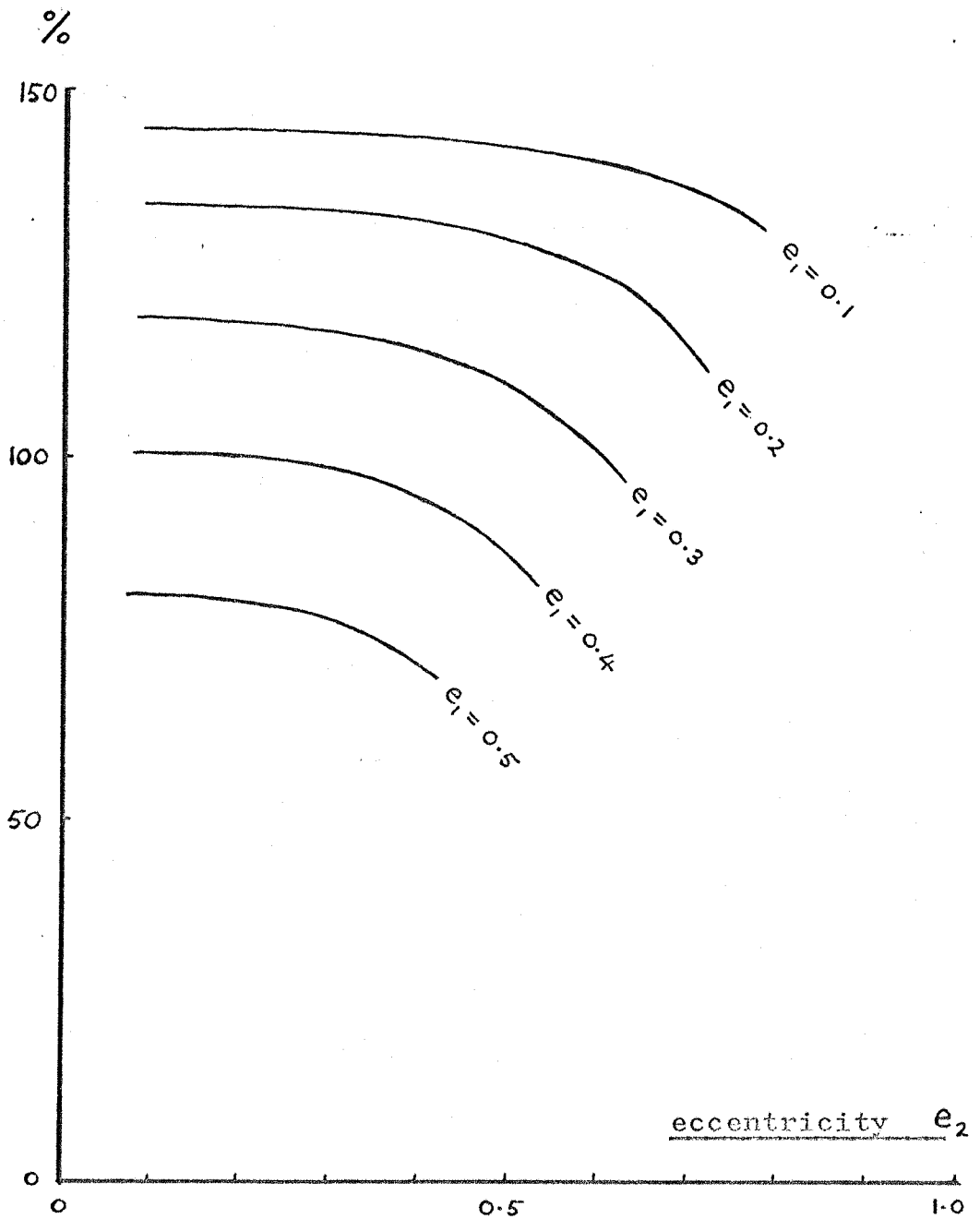
Fig.28

Fig.28   Percentage improvement in bearing force arising

from grooving an infinite length journal bearing

with $v = 20$ and $\alpha = 0$

Fig.29

$$W = \frac{W'}{P_a D}$$
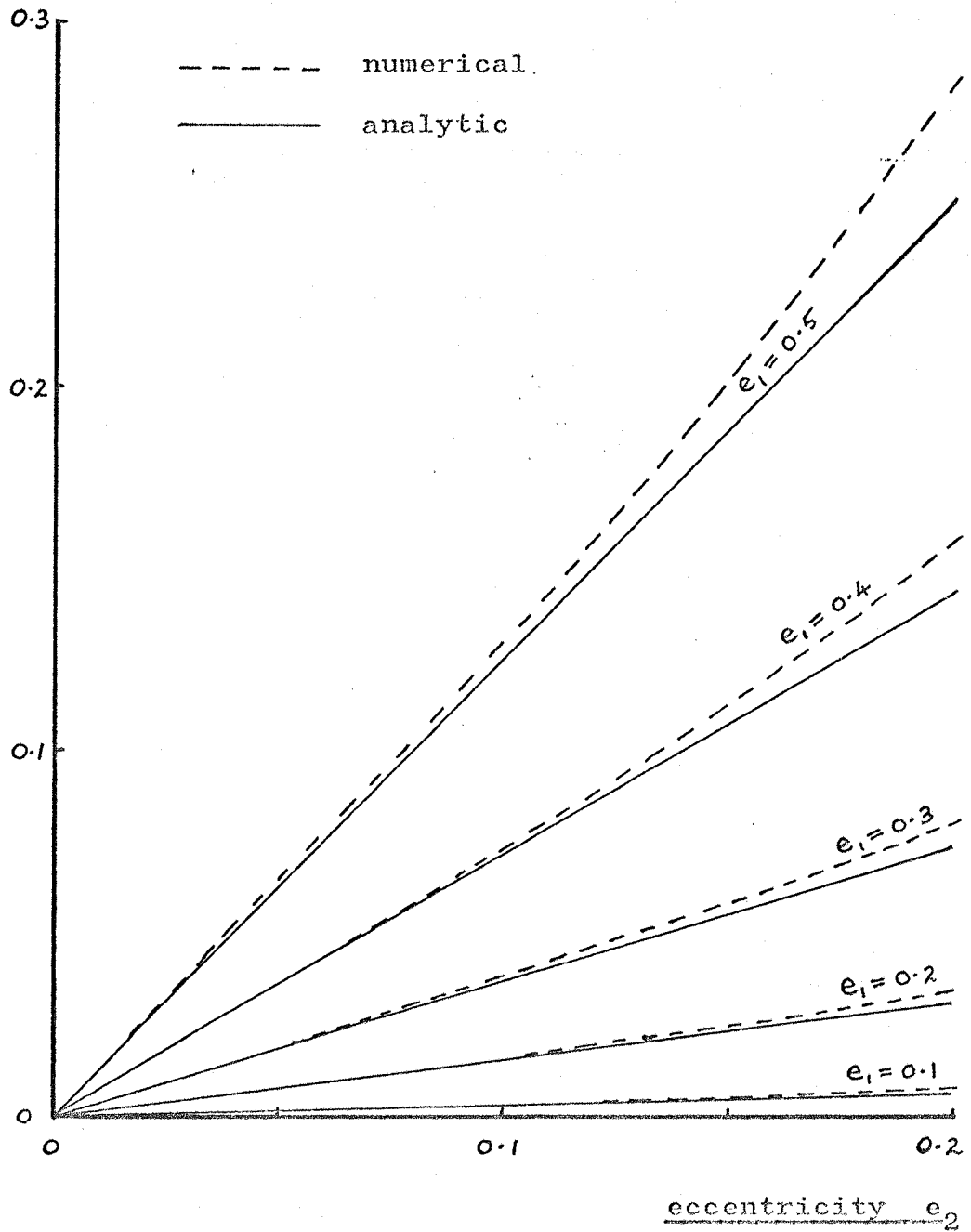
Fig.29   Comparison between analytic and numerical solutions

for the infinite length axially grooved journal

bearing with w = 20 and $\alpha = 0$
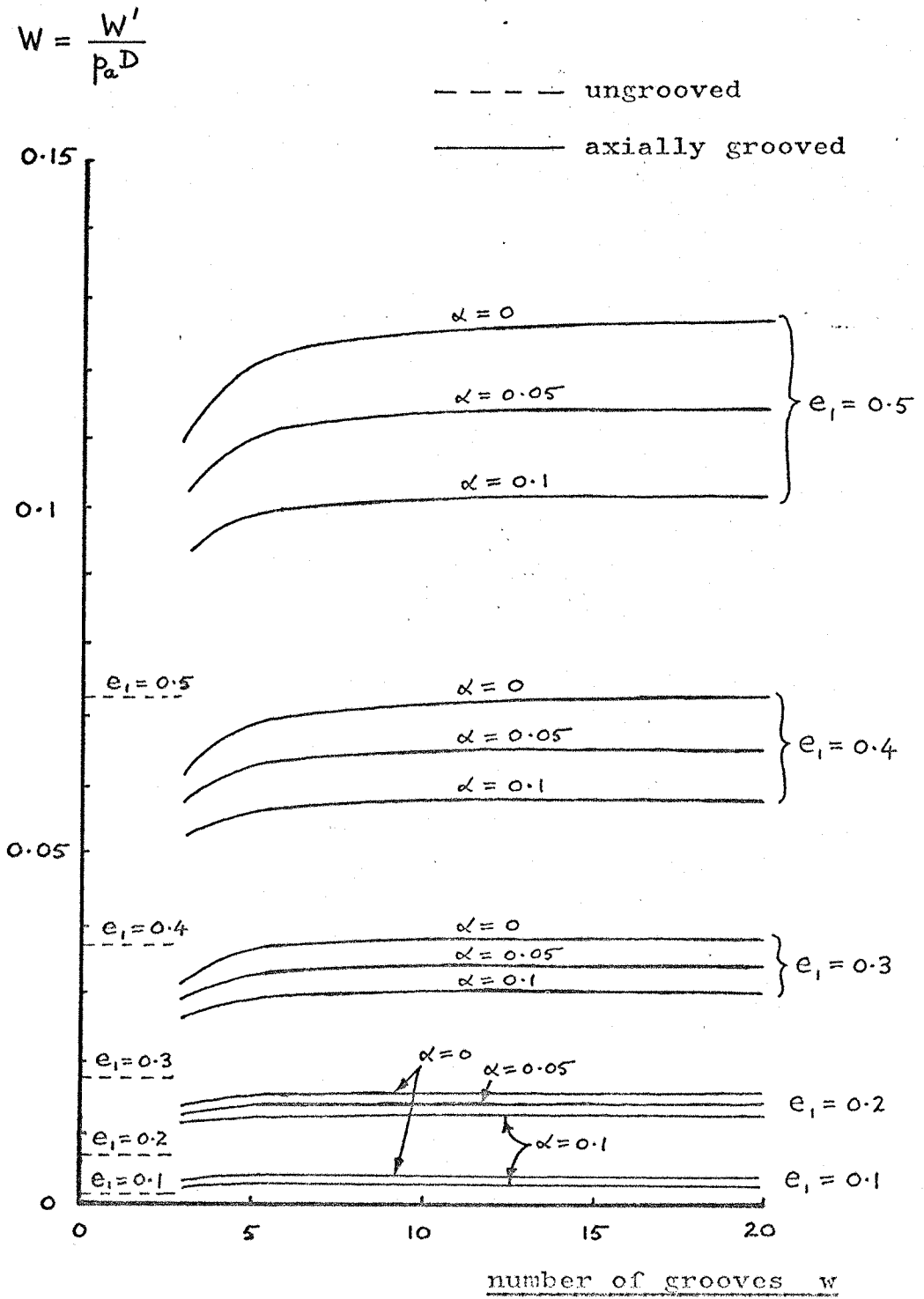
Fig. 30

Fig. 30   Journal bearing force per unit length as a function
of the number of grooves when $e_2 = 0.1$

Fig. 31

$\dfrac{W_{grooved}}{W_{ungrooved}}$

$e_1^2 \ll 1$

$e_2 \ll 1$

$\dfrac{L}{D}$
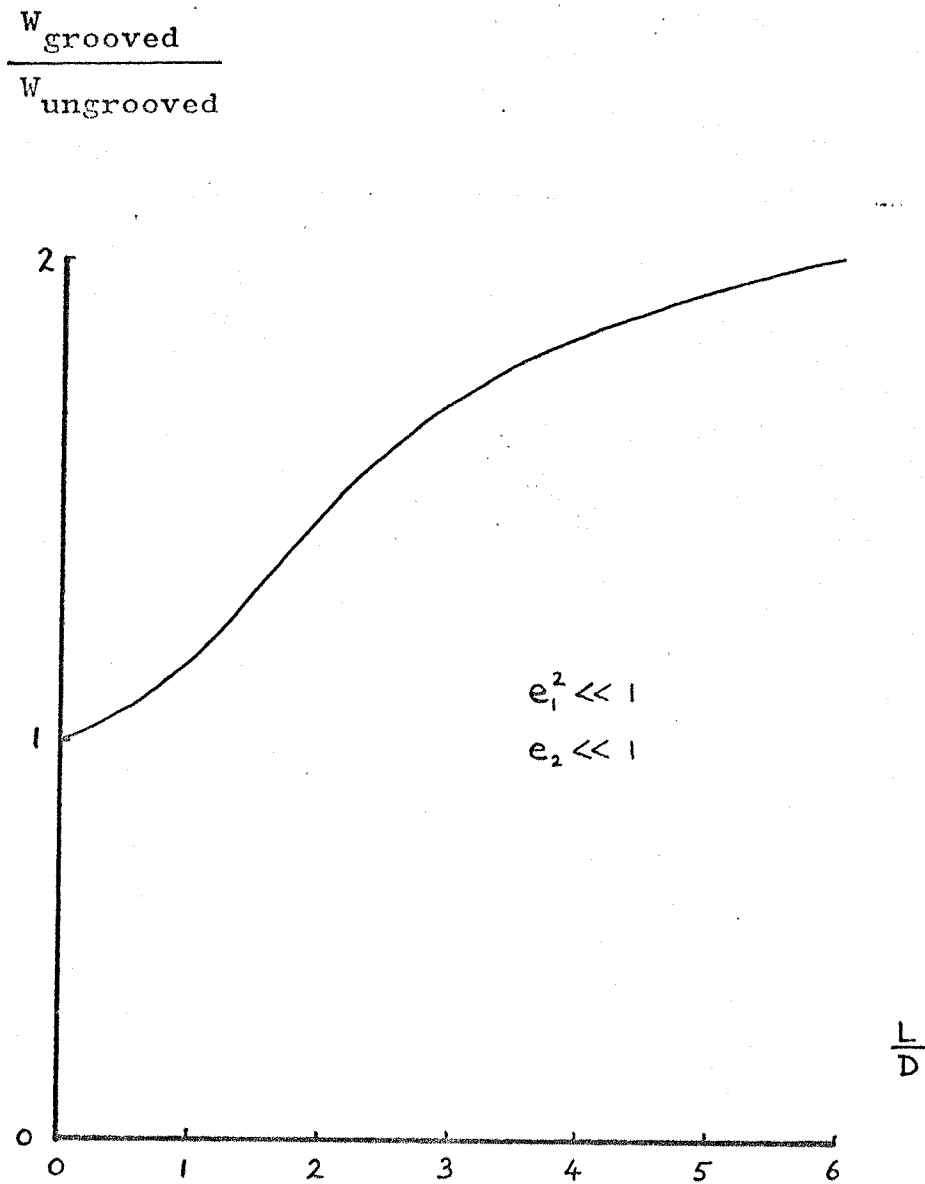
Fig. 31   Comparison between grooved and ungrooved journal

bearing forces as a function of L/D
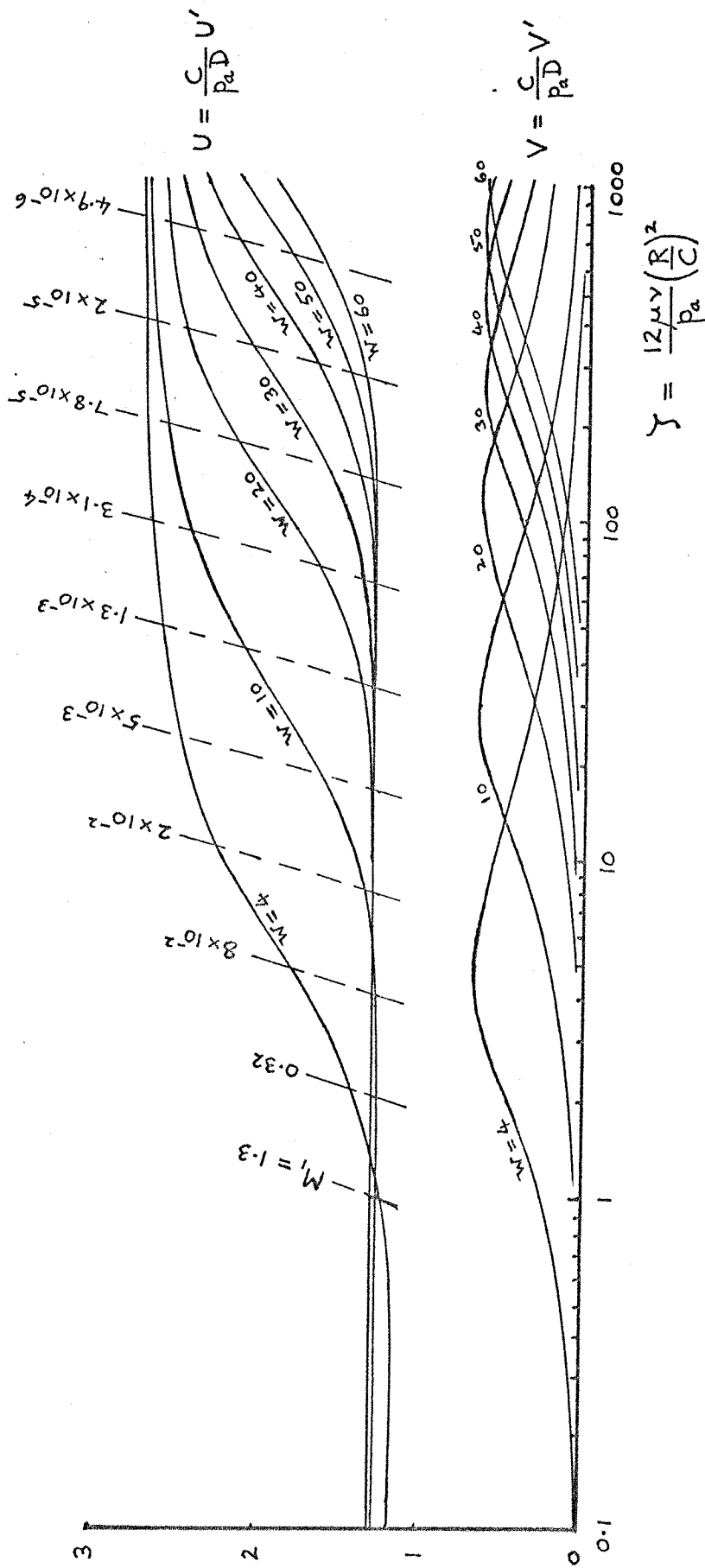
Fig.32

Fig.32   Dynamic stiffness components per unit length in an infinitely long axially

grooved journal bearing with different numbers of grooves ($c_1 = 0.5$)

Fig.33

$$\delta_1 = \frac{p_a D}{C} \delta_1'$$

$$\zeta = \frac{12 \mu \nu}{p_a} \left(\frac{R}{C}\right)^2$$
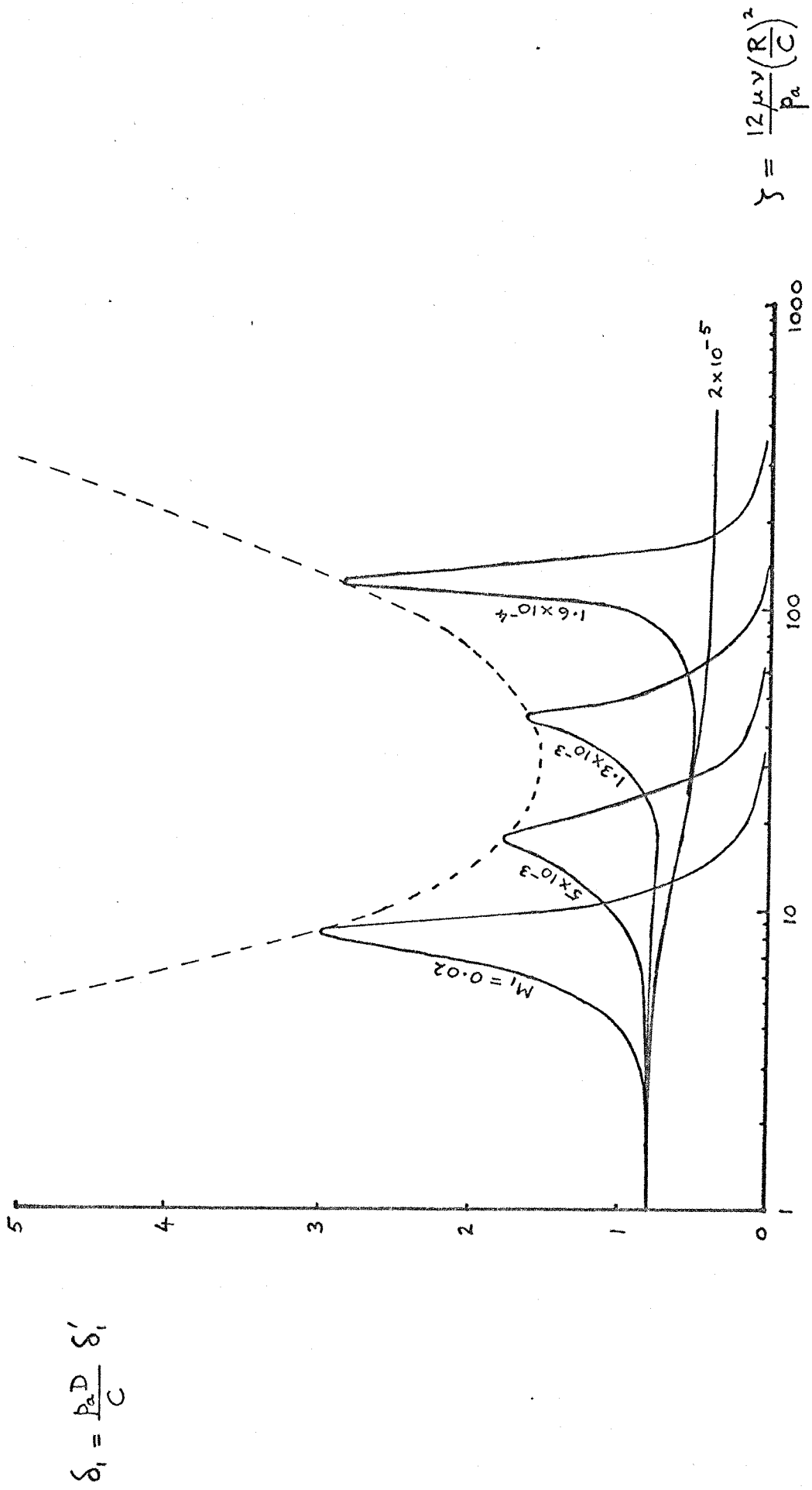
Fig.33   Dynamic compliance in an infinite length axially grooved journal bearing with 10 grooves when $\alpha = 0$ and $e_1 = 0.5$
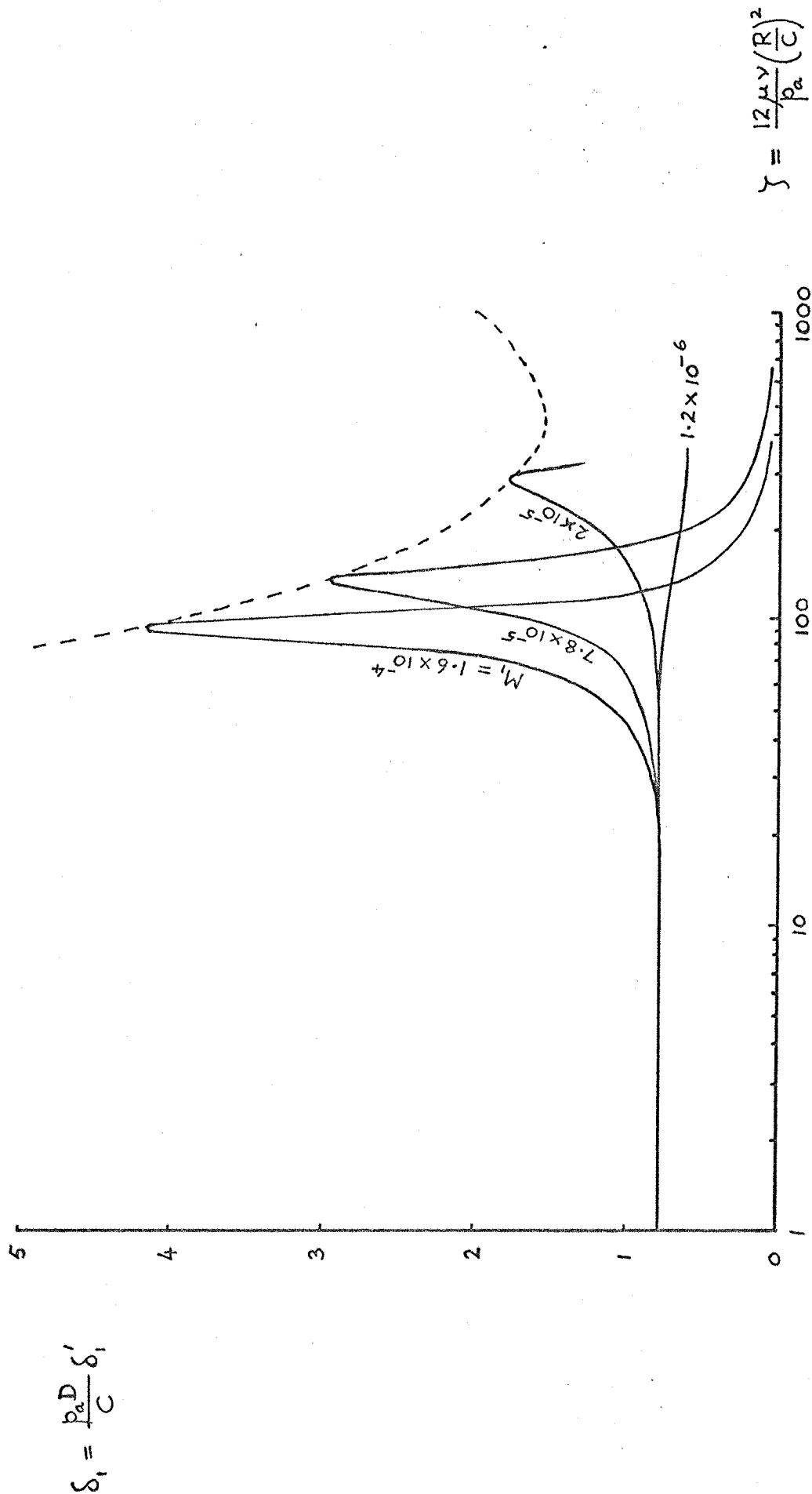
Fig.34   Dynamic compliance in an infinite length axially grooved journal bearing with

40 grooves when $\propto$ = 0 and e_1= 0.5

$$\gamma = \frac{12\mu\nu}{p_a}\left(\frac{R}{C}\right)^2$$

$$\delta_1 = \frac{p_a D}{C}\delta_1'$$
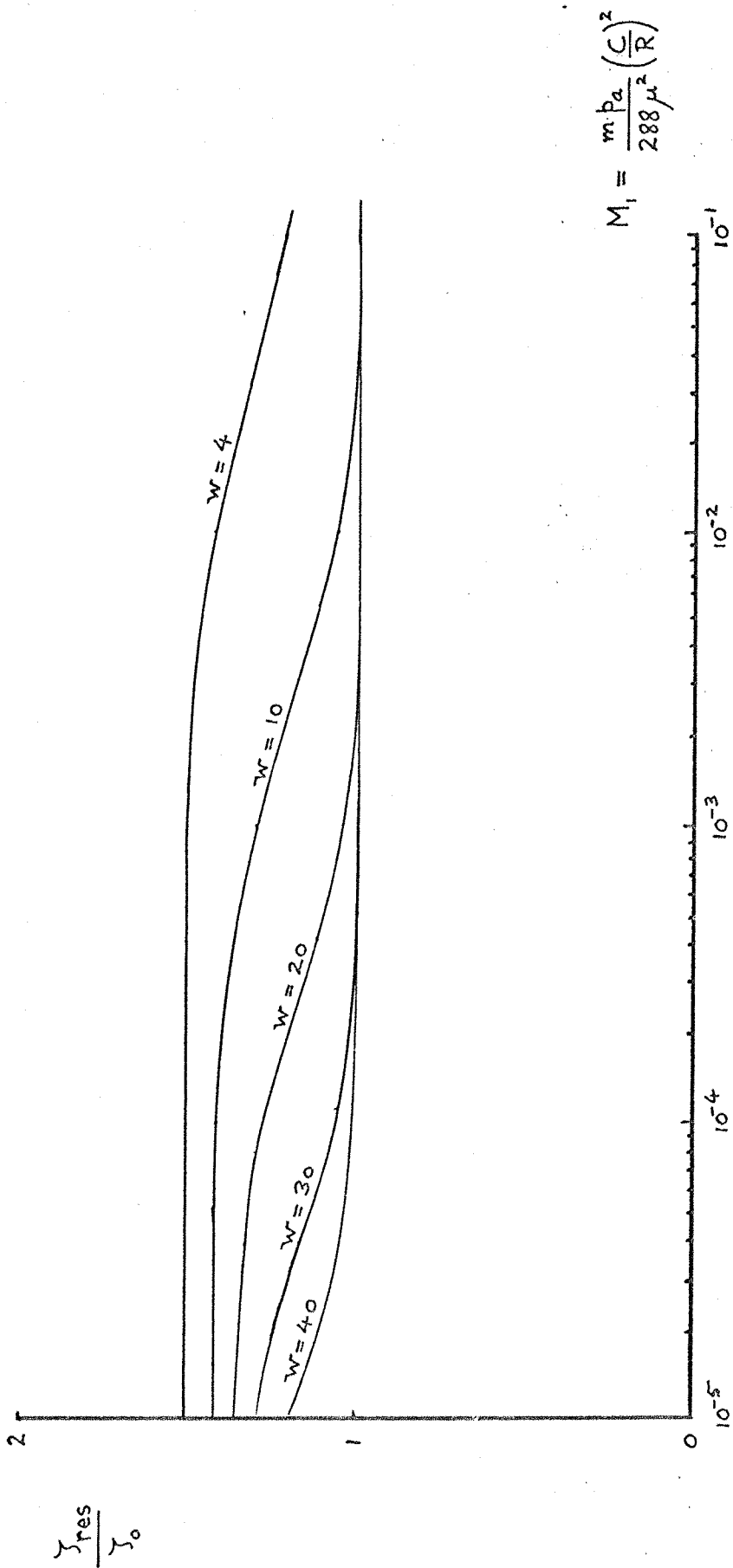
Fig.35

$$M_1 = \frac{m \, p_a}{288 \, \mu^2} \left(\frac{C}{R}\right)^2$$

$\dfrac{\gamma_{res}}{\gamma_o}$

Fig.35   Variation of resonance frequency with mass per unit length for different numbers

of grooves in an axially grooved infinite length journal bearing ($e_1 = 0.5$)
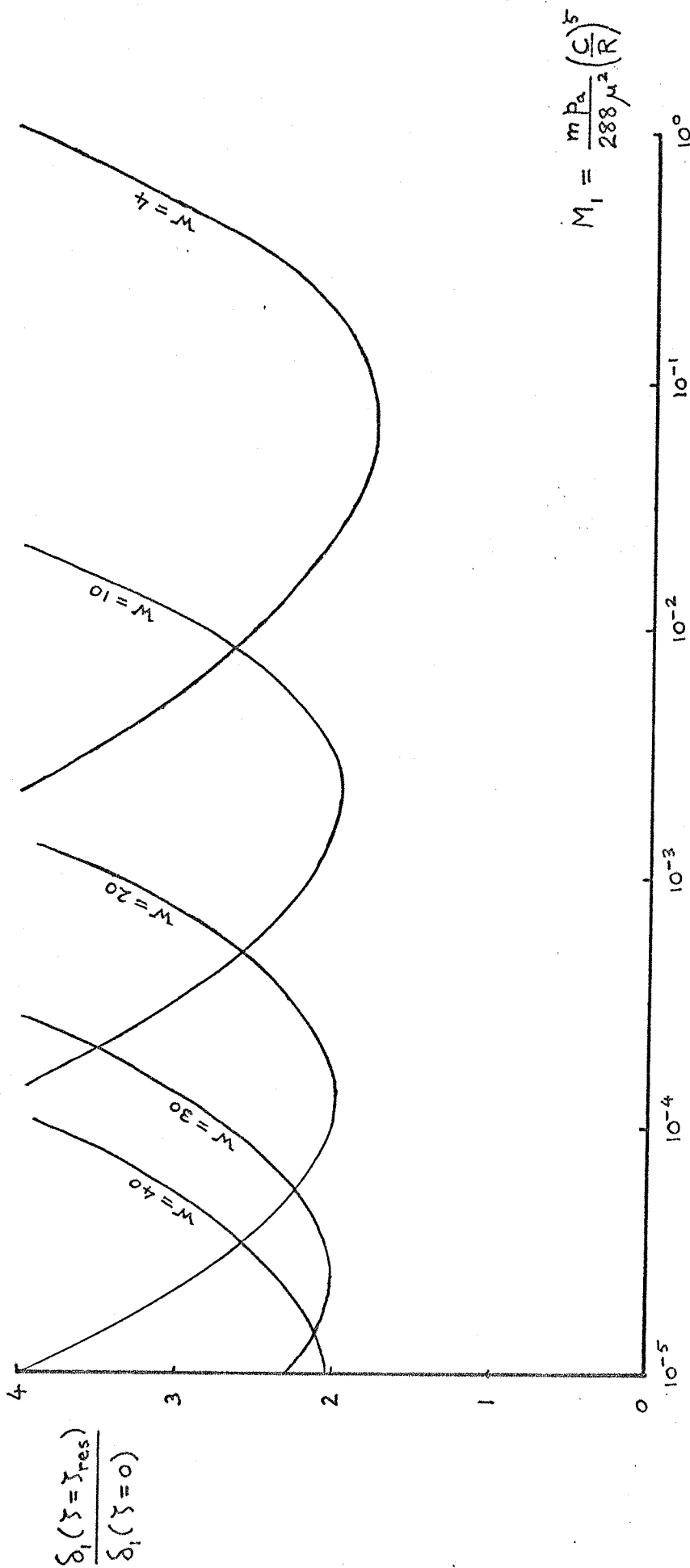
Fig.36

Fig.36   Variation of peak dynamic compliance with mass per unit length for different

numbers of grooves in an axially grooved infinite length journal bearing ($e_1 = 0.5$).

The vertical axis is labelled $\dfrac{\delta_1(\Upsilon = \Upsilon_{res})}{\delta_1(\Upsilon = 0)}$

The horizontal axis is labelled $M_1 = \dfrac{m\,p_a}{288\,\mu^2}\left(\dfrac{C}{R}\right)^5$

Curves are labelled $W = 4$, $W = 10$, $W = 20$, $W = 30$, $W = 40$.
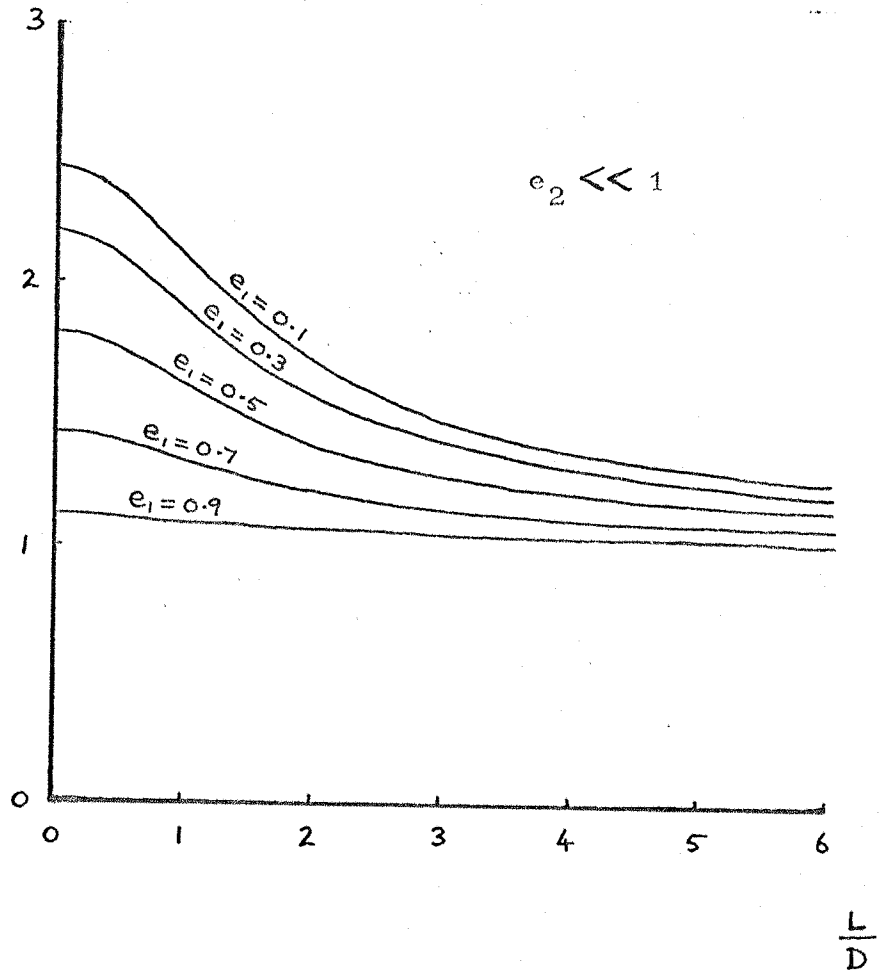
Fig. 37

Fig. 37 Static stiffness per unit length as a function of L/D for various excursion ratios in finite length journal bearings

Fig. 38

$$\frac{\left(\dfrac{S_o}{L/D}\right)}{\left(\dfrac{S_o}{L/D}\bigg|_{L/D\to\infty}\right)}$$

$e_2 \ll 1$
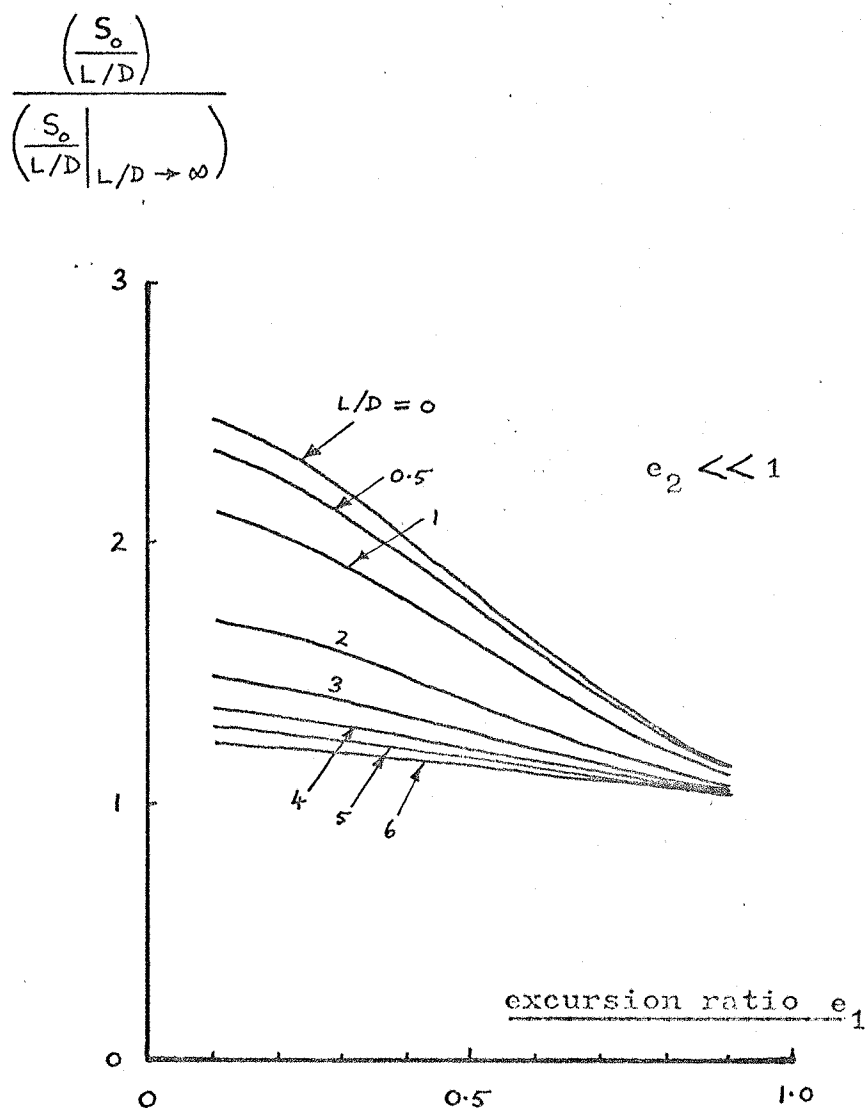
excursion ratio e_1

Fig. 38   Static stiffness per unit length as a function of excursion ratio for various values of L/D in finite length journal bearings
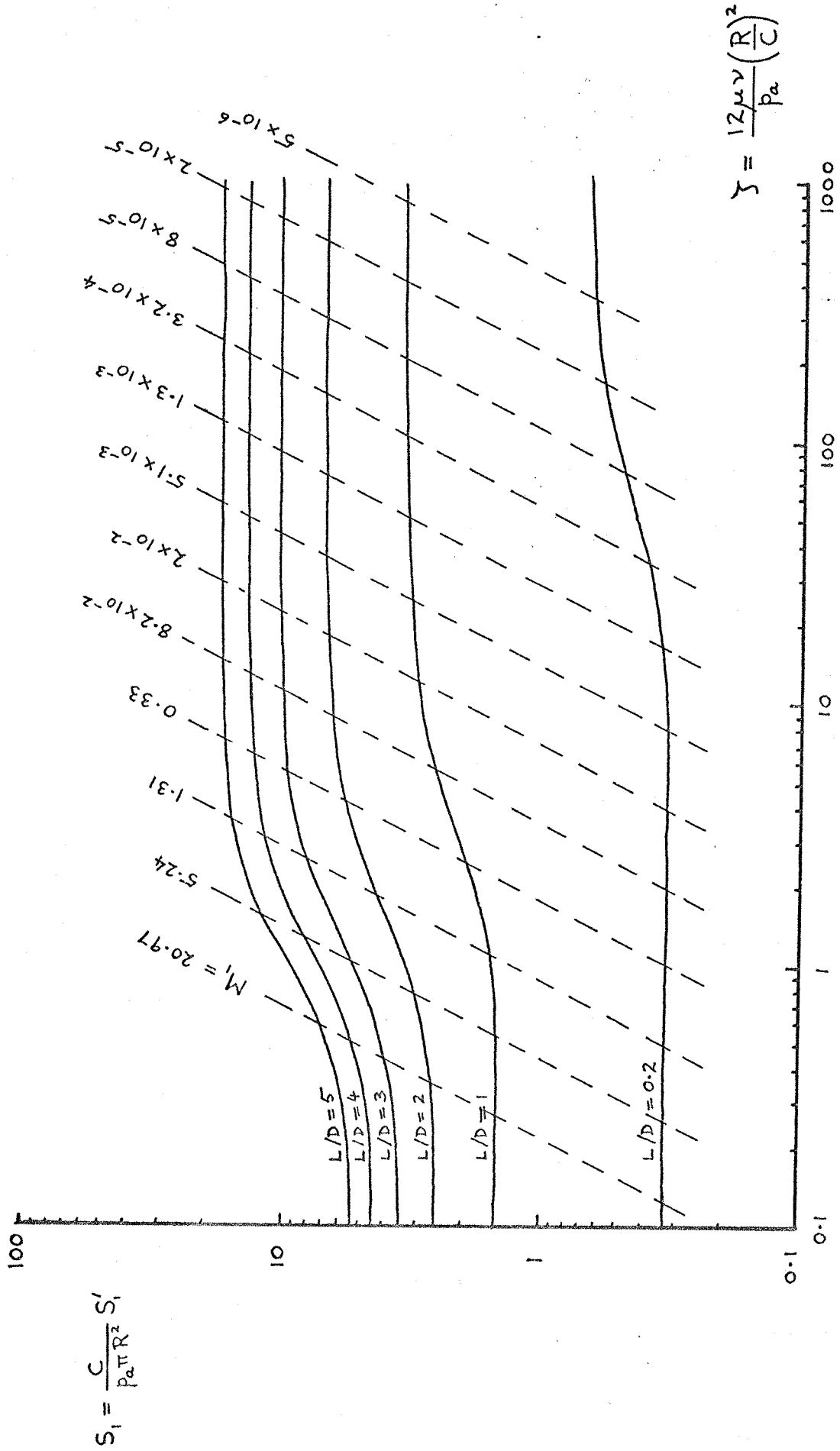
Fig.39   Dynamic stiffness in finite length journal bearings when $e_1 = 0.5$

$$\zeta = \frac{12\mu\nu}{p_a}\left(\frac{R}{C}\right)^2$$

$$S_1 = \frac{C}{p_a\pi R^2}\,S_1'$$

$M_1 = 20.97$

5.24

1.31

0.33

8.2×10^{-2}

2×10^{-2}

5.1×10^{-3}

1.3×10^{-3}

3.2×10^{-4}

8×10^{-5}

2×10^{-5}

5×10^{-6}

L/D = 5
L/D = 4
L/D = 3
L/D = 2
L/D = 1
L/D = 0.2

Fig.40

$S_2 = \dfrac{C}{P_a \pi R^2} S_2'$

$\gamma = \dfrac{12 \mu \nu}{P_a} \left(\dfrac{R}{C}\right)^2$

Fig. 40   Dynamic 'damping' in finite length journal bearings when $e_1 = 0.5$

Fig.41

$$\frac{S_1}{(L/D)} = \frac{2C}{p_a \pi R} \cdot \frac{S_1'}{L}$$

$$\frac{S_2}{(L/D)} = \frac{2C}{p_a \pi R} \cdot \frac{S_2'}{L}$$

$$\zeta = \frac{12\mu\nu}{p_a}\left(\frac{R}{C}\right)^2$$

L/D = 0.2

L/D = 1

2

3 x 4

5

L/D = 0.2

L/D = 1

2

5 x 3 4
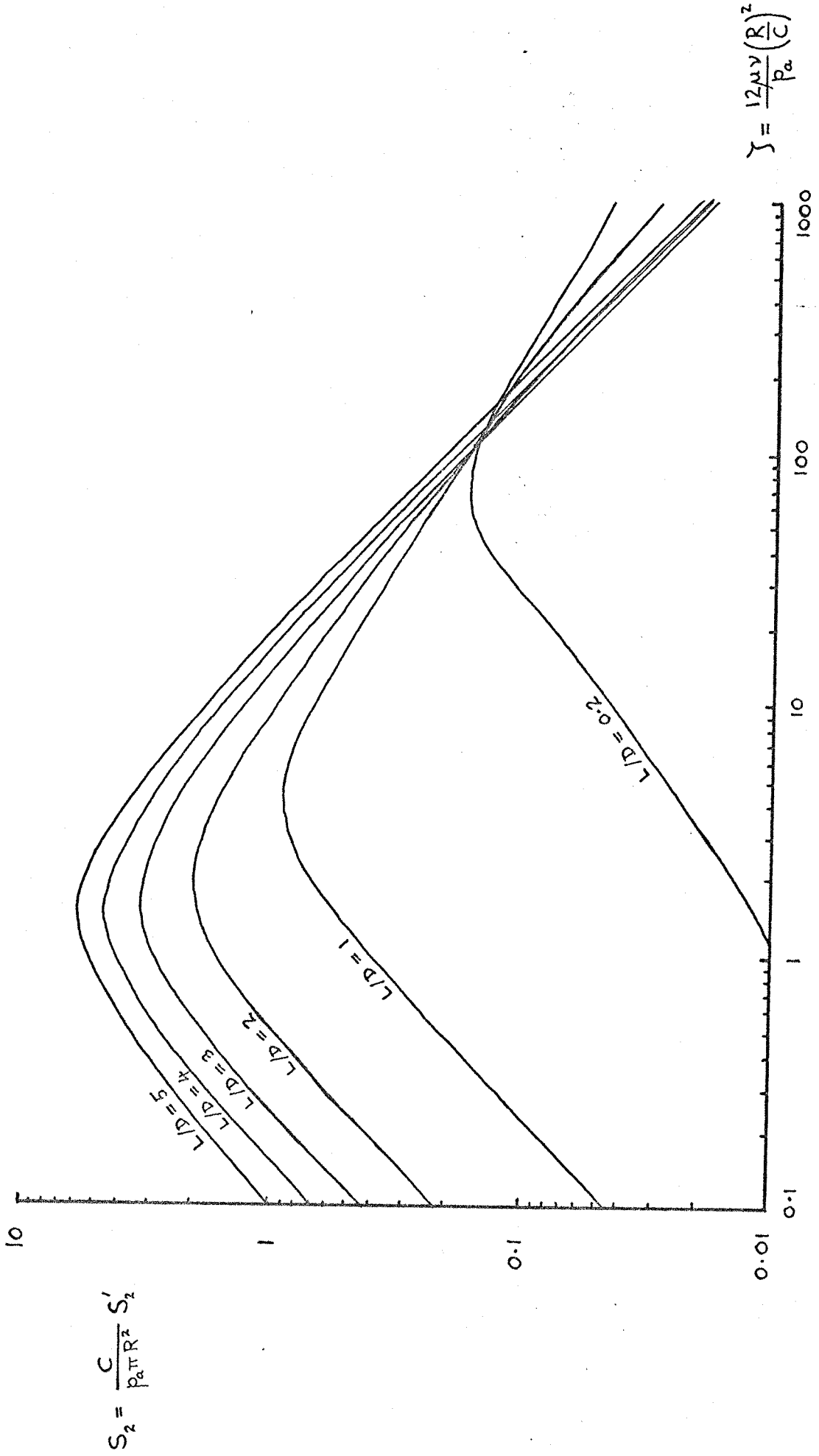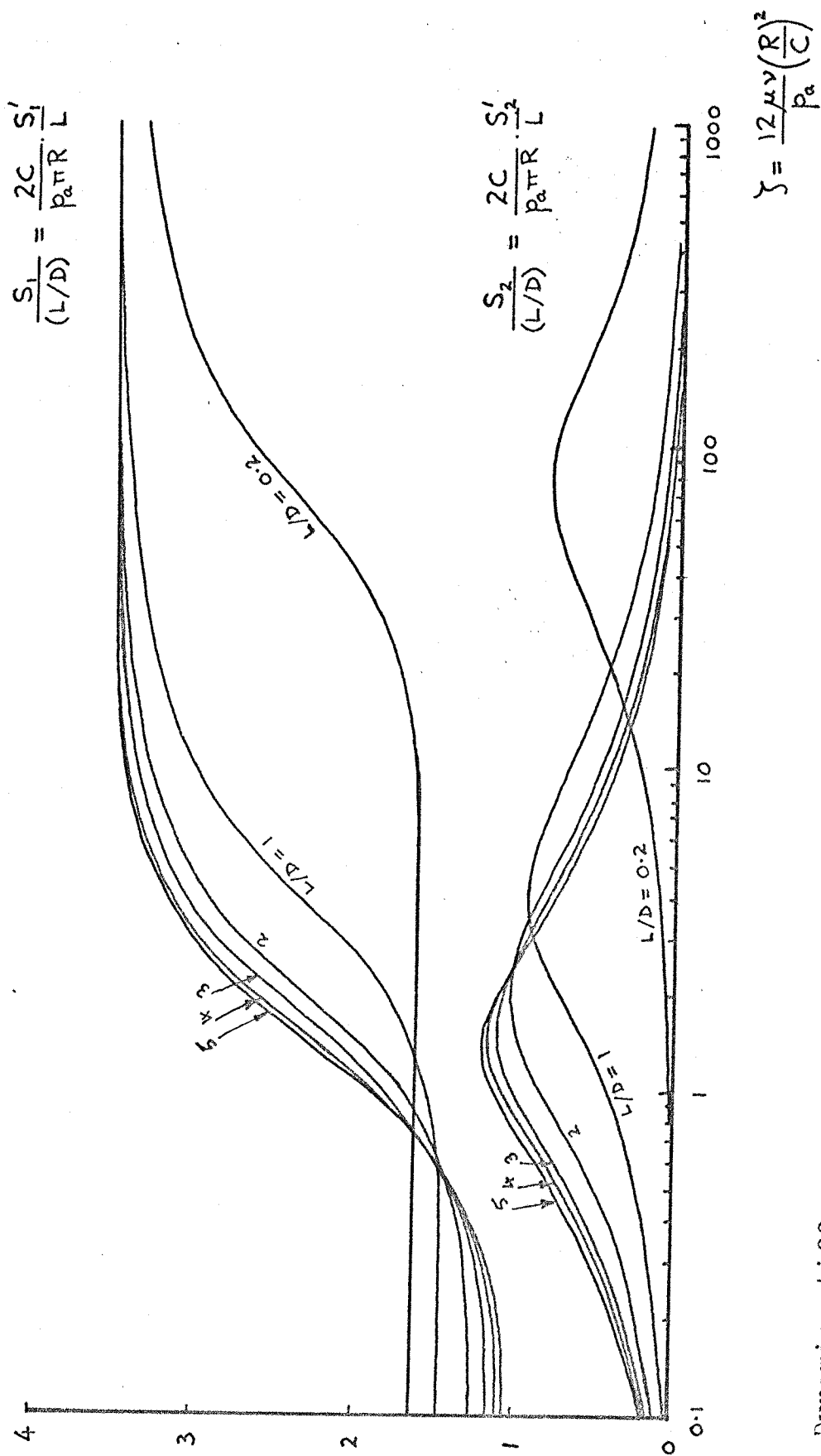
Fig.41   Dynamic stiffness components per unit length in finite length journal bearings

when $c_1 = 0.5$

Fig.42

$$\zeta = \frac{12\mu\nu}{p_a}\left(\frac{R}{C}\right)^2$$

$\dfrac{\delta_1}{\delta_1(\zeta=0)}$
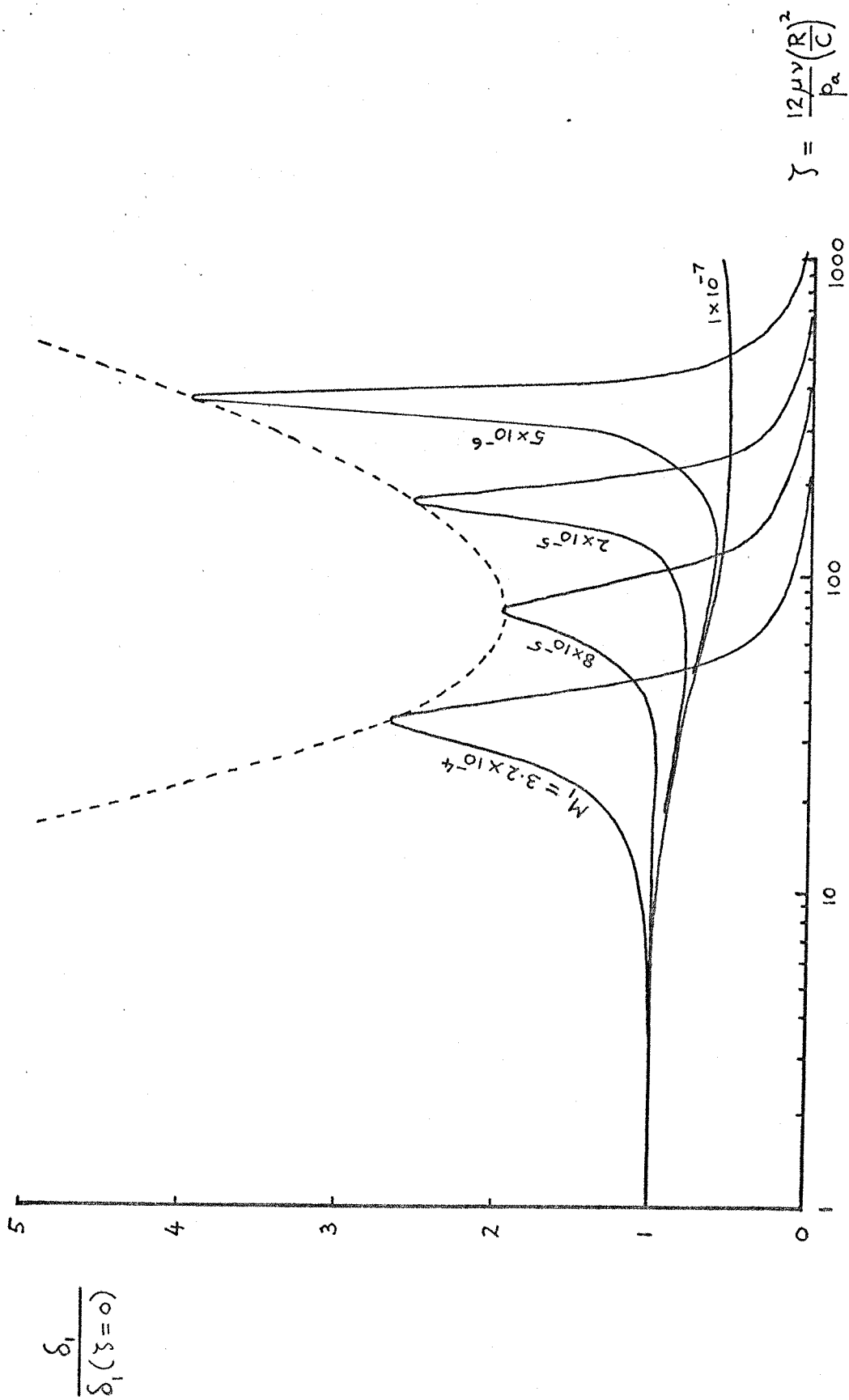
Fig.42   Dynamic compliance in a finite length journal bearing with L/D = 0.2 and e_1= 0.5

Fig.43

The y-axis is labelled $\dfrac{\delta_1(\zeta = \zeta_{res})}{\delta_1(\zeta = 0)}$ with values 0, 1, 2, 3, 4.

The x-axis is labelled $M_1 = \dfrac{m p_a}{72 \pi \mu^2} \left(\dfrac{L}{D}\right)\left(\dfrac{c}{R}\right)^5$ with values 10^{-5}, 10^{-4}, 10^{-3}, 10^{-2}, 10^{-1}, 10^{0}, 10^{1}, 10^{2}.

Curves labelled $L/D = 0.2$, $L/D = 1$, $L/D = 2$, $L/D = 3$, $L/D = 4$, $L/D = 5$.
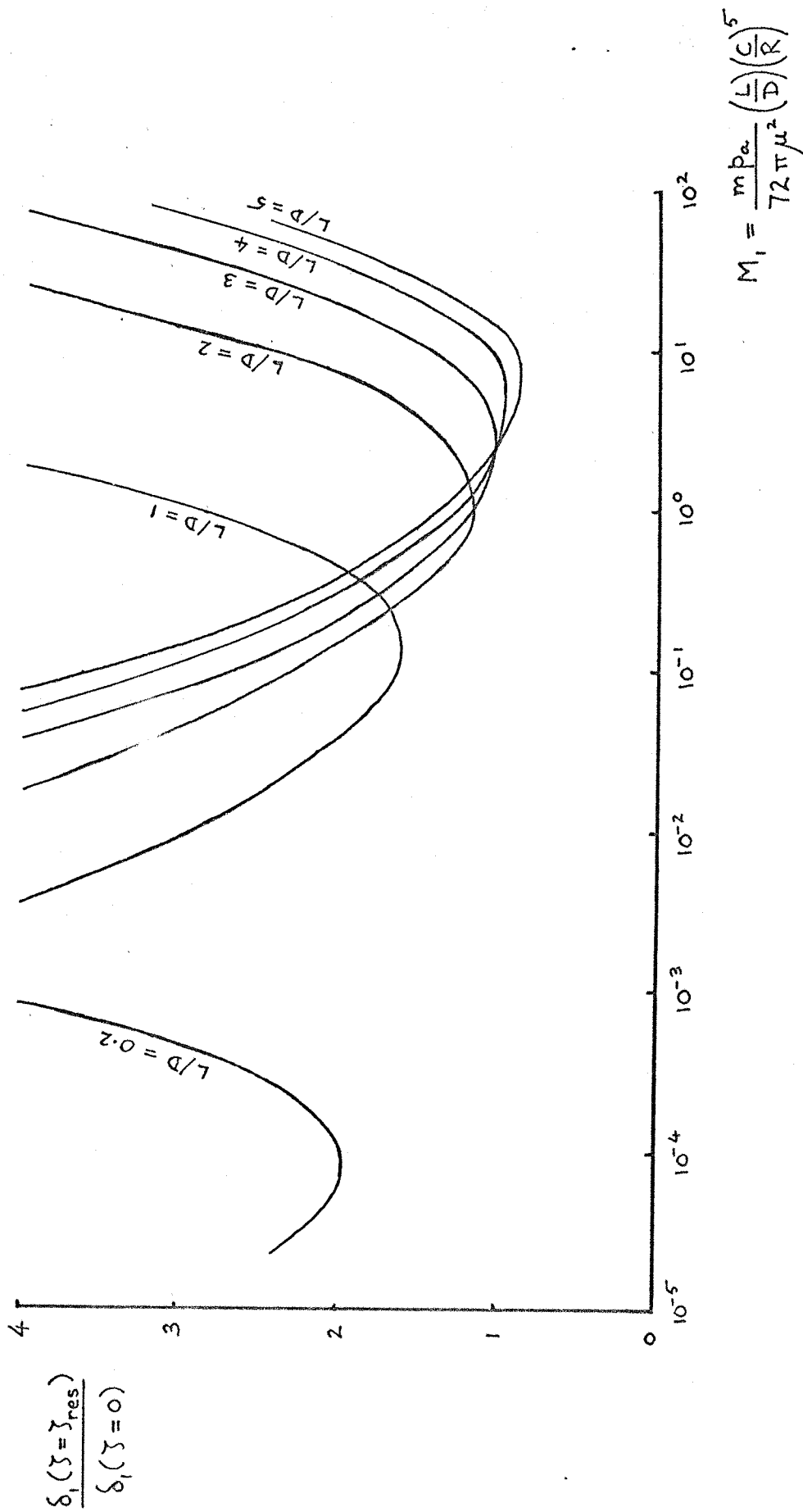
Fig.43   Peak dynamic compliance as a function of mass per unit length in finite

length journal bearings when $e_1 = 0.5$

Fig. 44

$$M_1 = \frac{m p_a}{72 \pi \mu^2} \left(\frac{L}{D}\right)\left(\frac{C}{R}\right)^5$$
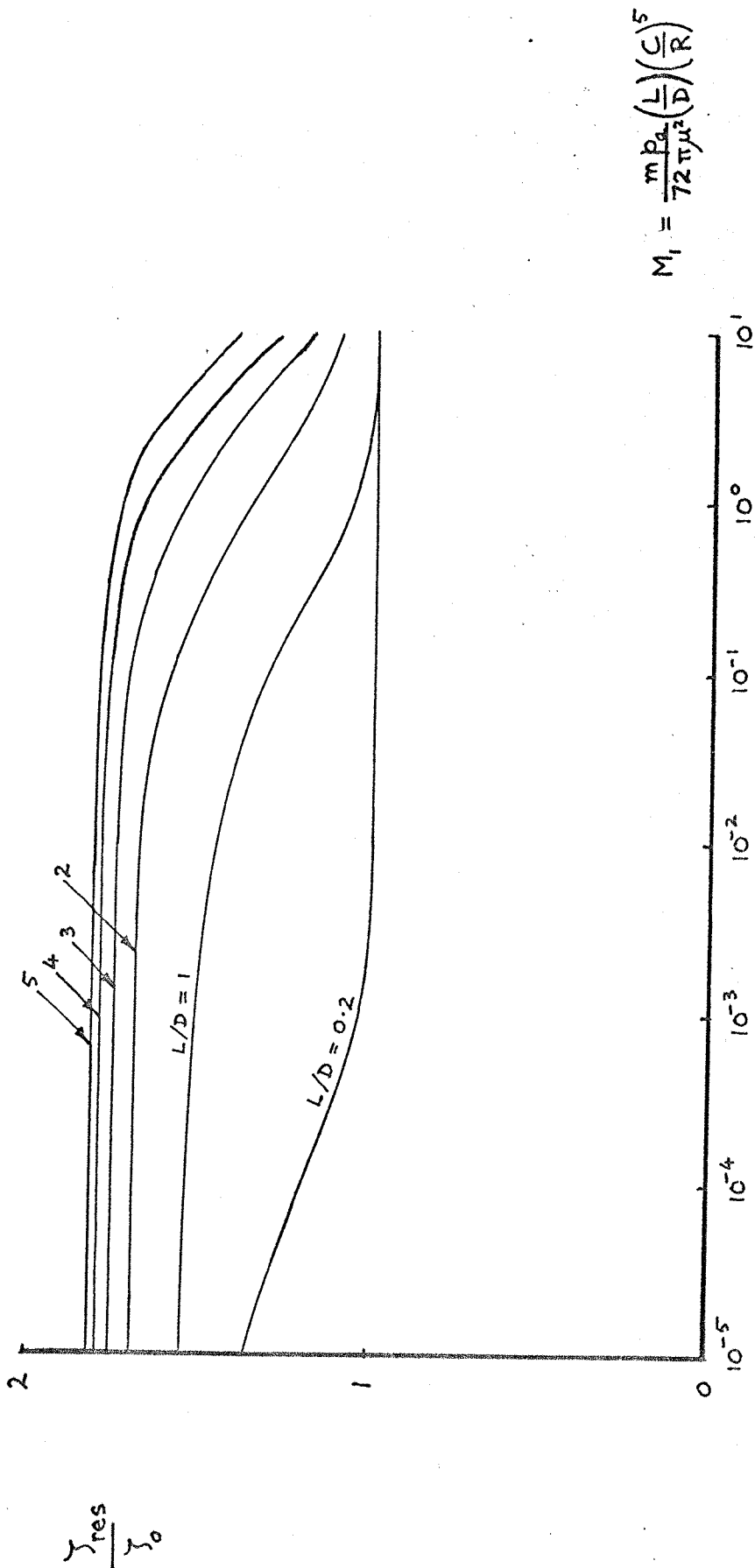
Fig. 44 Variation of resonance frequency with mass per unit length in finite length
journal bearings when $c_1 = 0.5$

Fig.45

$$\dfrac{\left(\dfrac{S_o}{\ell/D}\right)\Big|_{\ell/D\to 0}}{\dfrac{S_o}{(L/D)}}$$
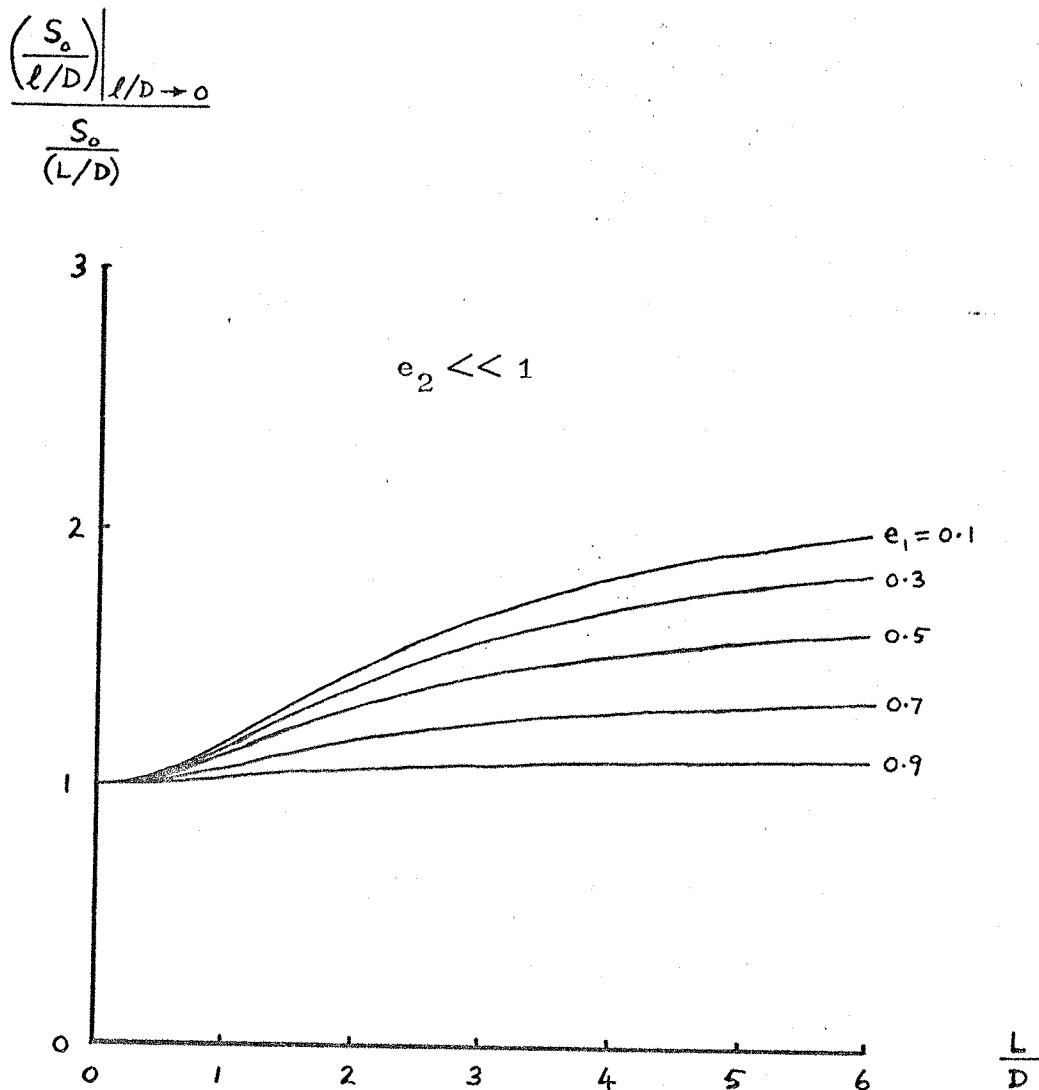
Fig.45   Static stiffness per unit length as a function
         of L/D in circumferentially grooved journal
         bearings with $\ell/D \to 0$ for various values of c_1
         normalised with respect to the ungrooved bearing

Fig. 46

$$\dfrac{\left(\dfrac{S_o}{\ell/D}\right)\Big|_{\ell/D \to 0}}{\dfrac{S_o}{(L/D)}}$$
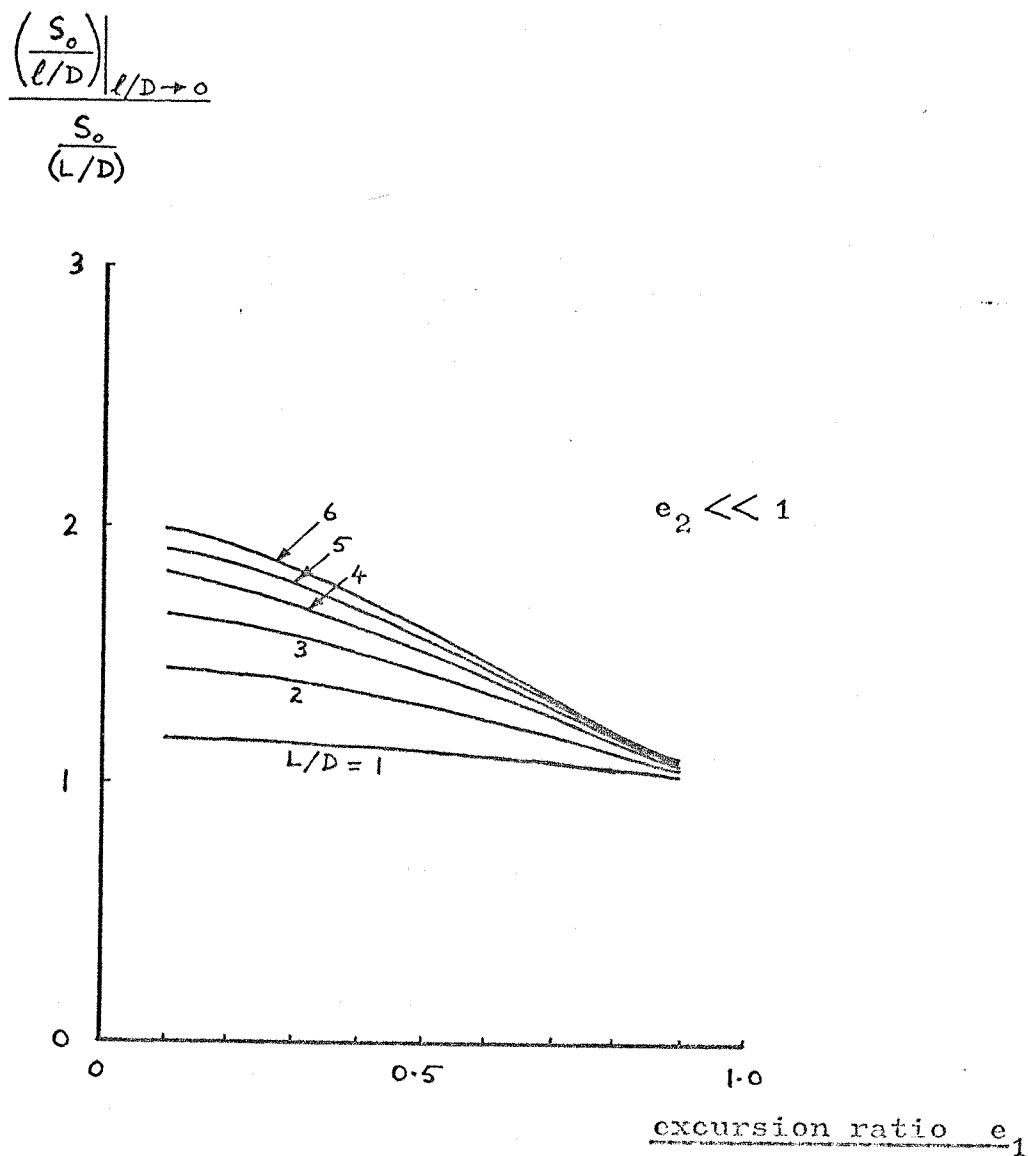
Fig. 46   Static stiffness per unit length as a function of excursion ratio in circumferentially grooved journal bearings for various values of L/D, normalised with respect to the ungrooved bearing
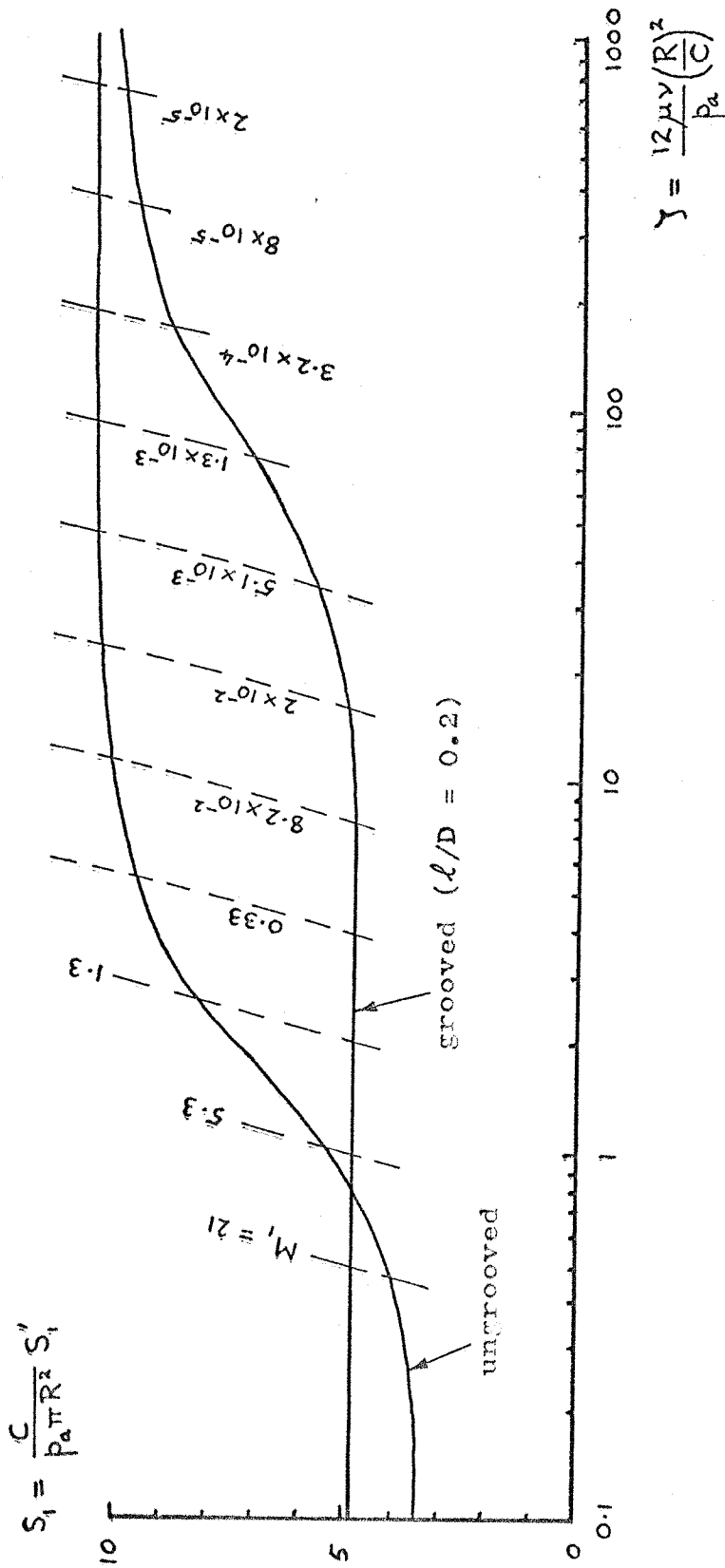
Fig. 47   Dynamic stiffness in ungrooved and circumferentially grooved journal bearings

with L/D = 3 and e_1 = 0.5

Fig.48

$$S_2 = \frac{C}{p_a \pi R^2} S_2'$$

grooved ($\ell/D = 0.2$)

ungrooved

$$\zeta = \frac{12 \mu \nu}{p_a} \left(\frac{R}{C}\right)^2$$
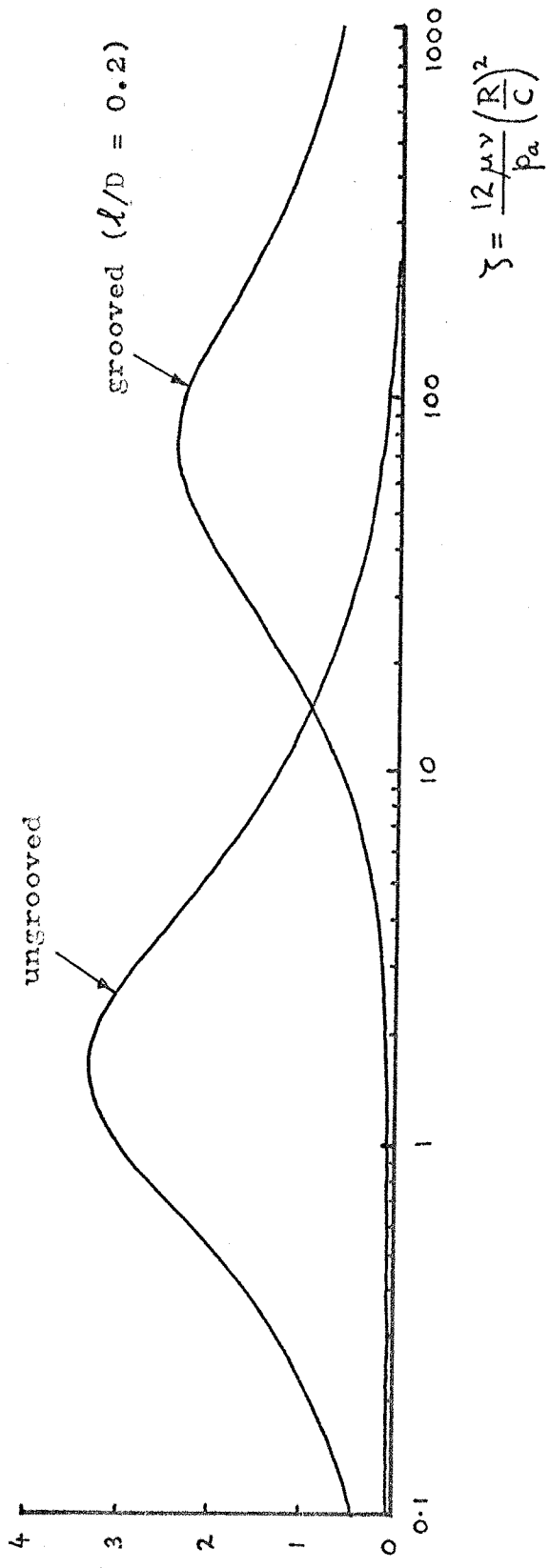
Fig.48   Dynamic 'damping' in ungrooved and circumferentially grooved journal bearings

with $L/D = 3$ and $e_1 = 0.5$
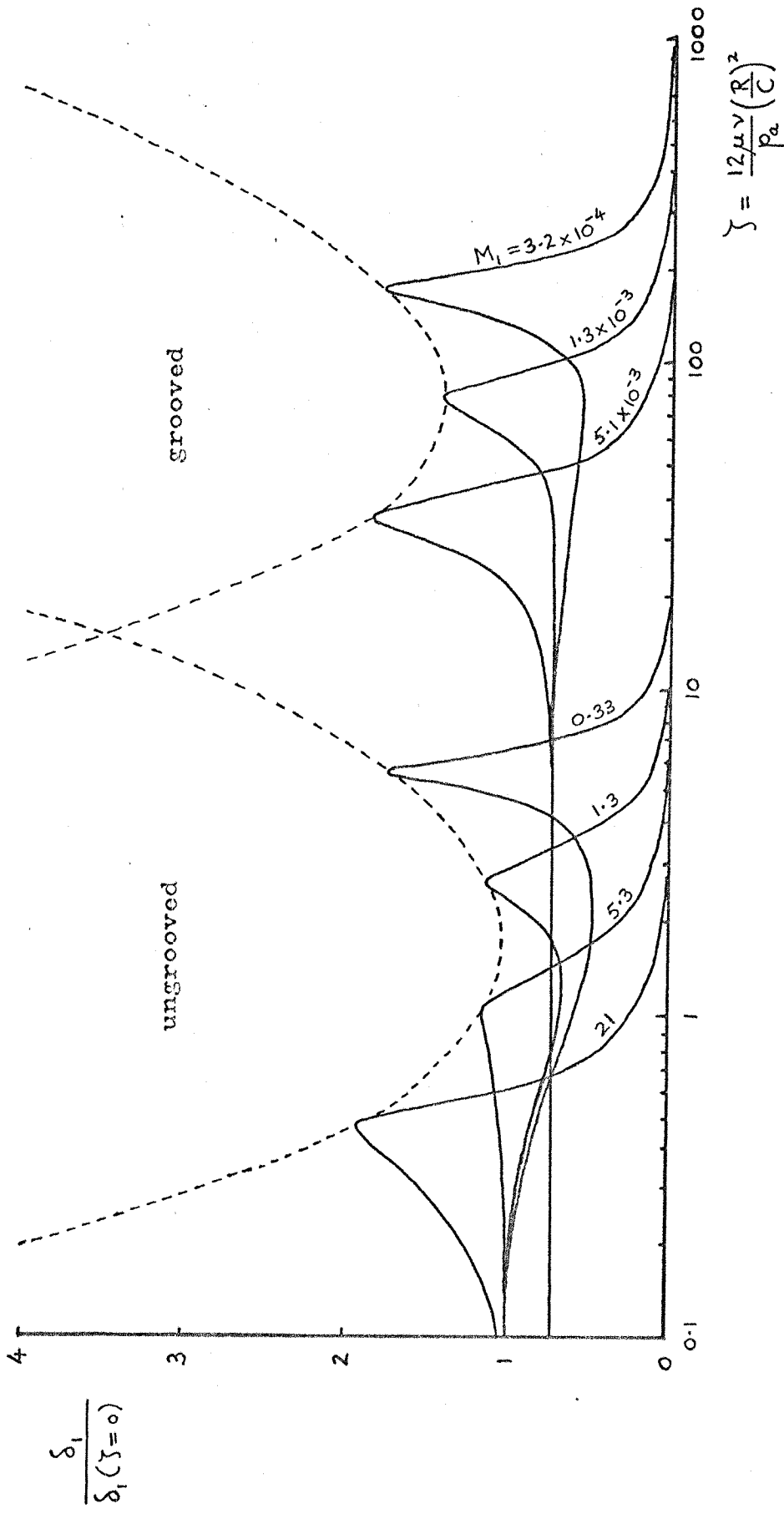
Fig.49

Fig. 49   Effect of circumferential grooving on dynamic compliance in a journal bearing

with L/D = 3 when c_1 = 0.5
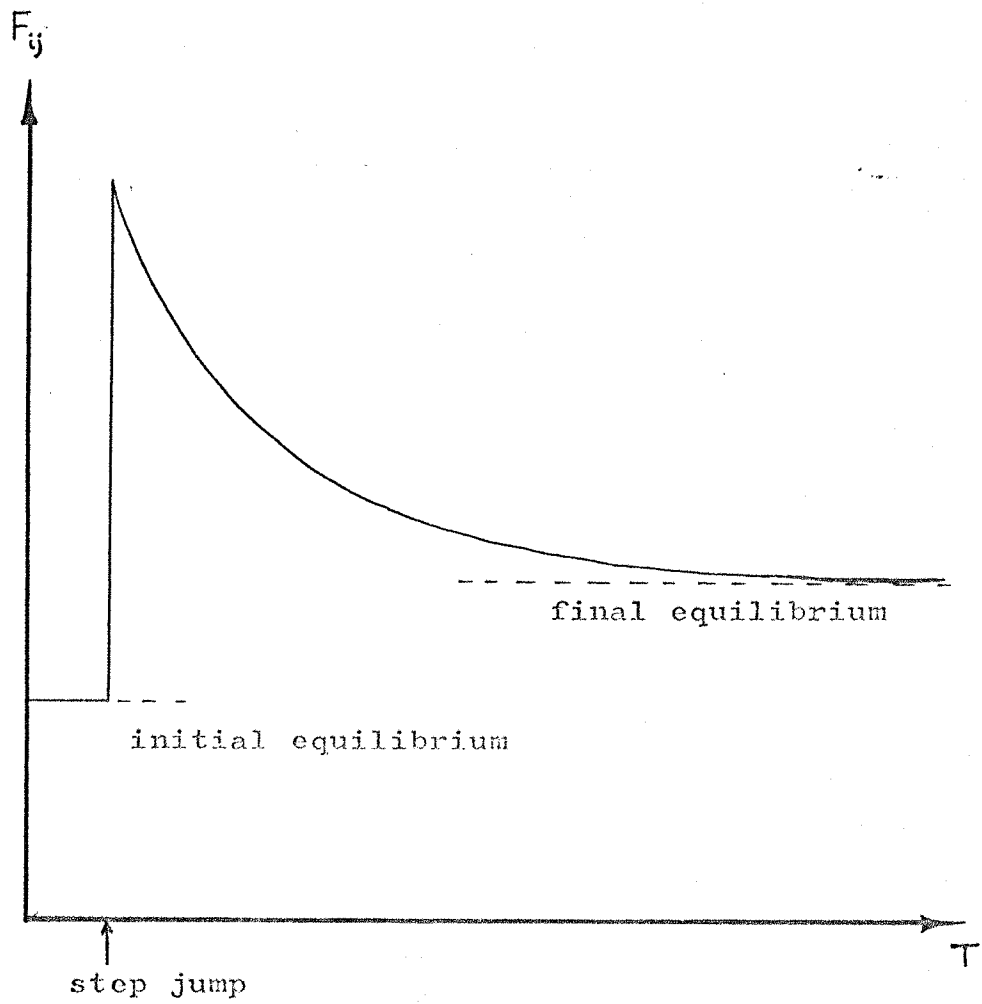
Fig.50

Fig.50   Typical step-jump response curve

Fig.51

$n = 9$

$m = 13$

$e_1 = 0.5$

$\zeta = 10$

$L/D = 1$

initial eccentricity $e_2 = 0$

step jumps $\delta \bar{x}_i = \delta \bar{x}_j = 0.08$

$F_{ij} = F_{ji} = 0$

$\left\{ \begin{matrix} F_{ii} \\ -F_{jj} \end{matrix} \right.$

$T = \nu t$
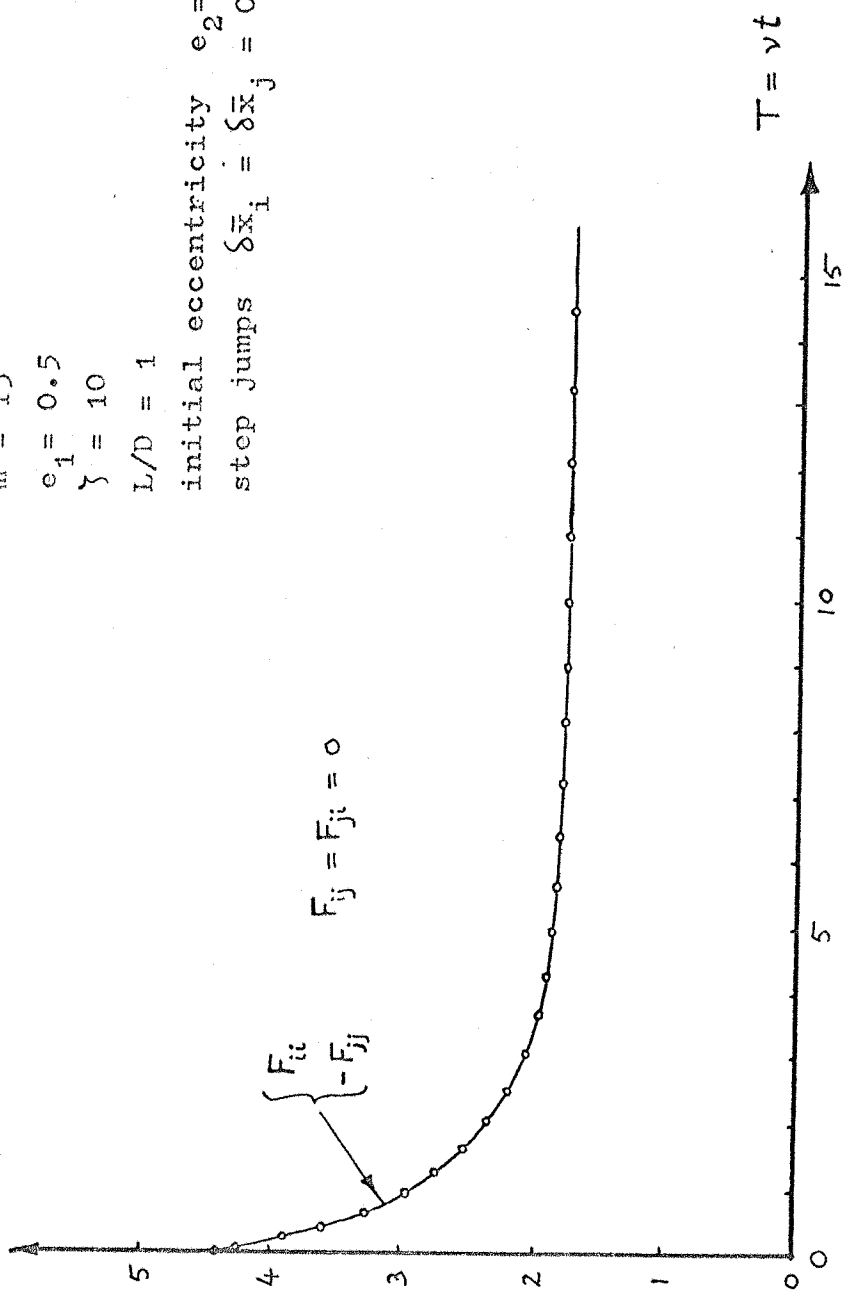
Fig.51   Set of response curves using a square law time grid spacing following step jumps
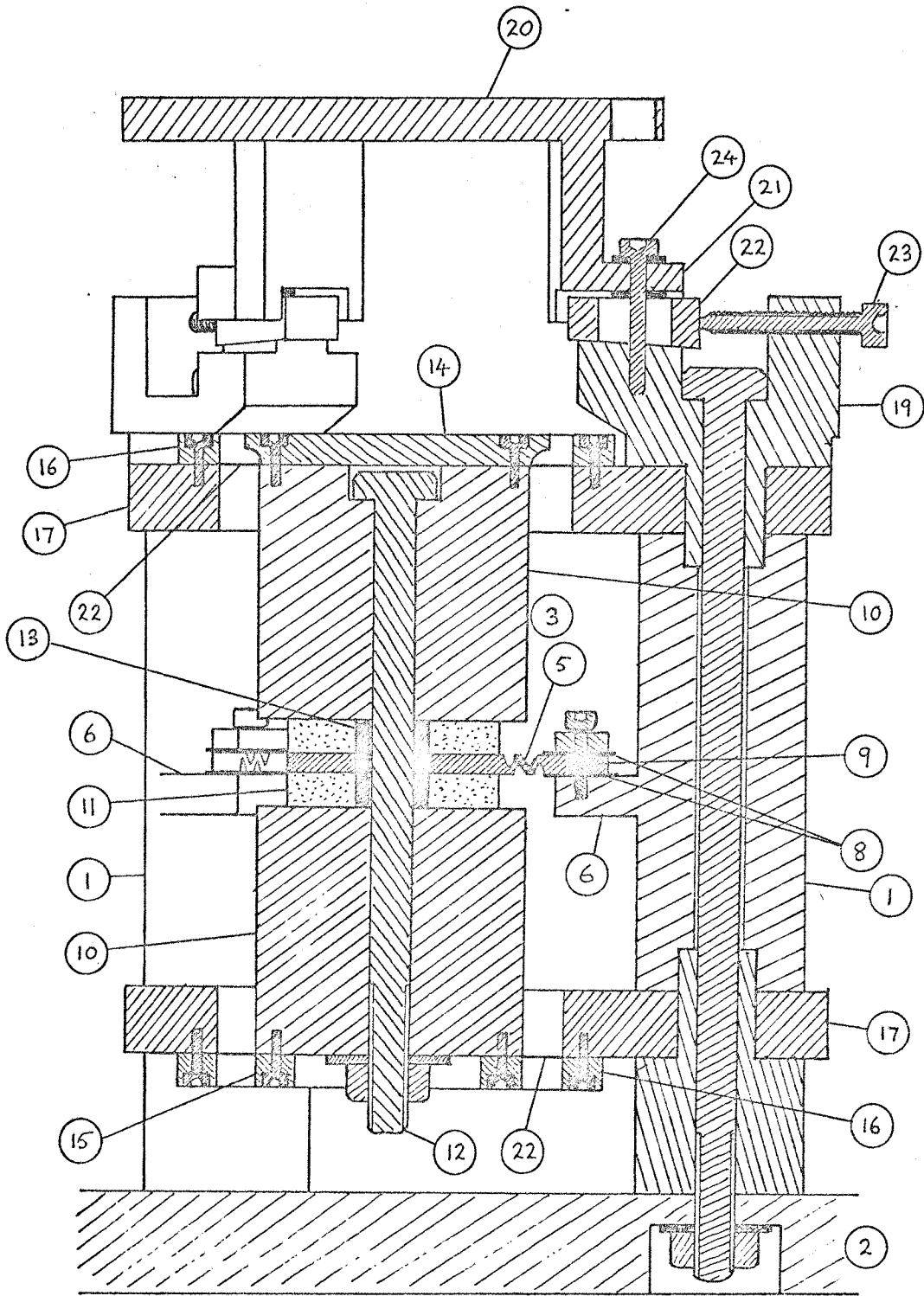
Fig.52

Fig.52   Section through thrust bearing rig
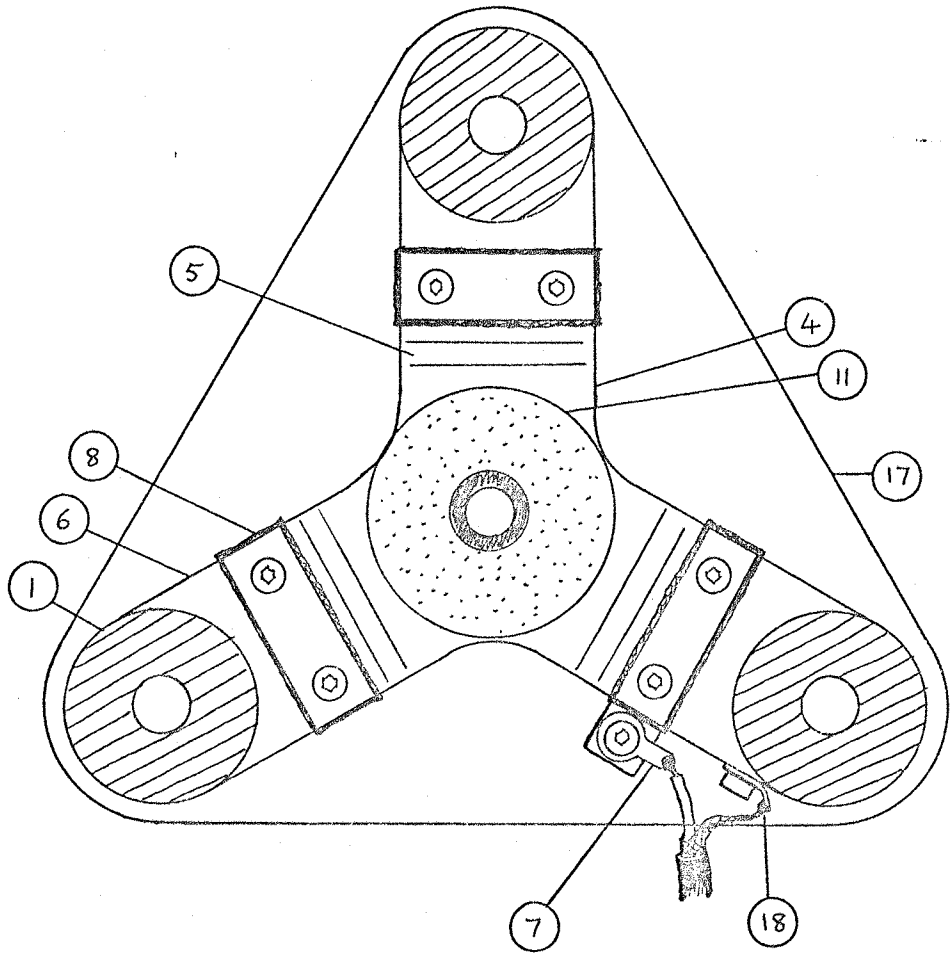
Fig.53

Fig.53 Scrap view looking down on centre electrode

assembly
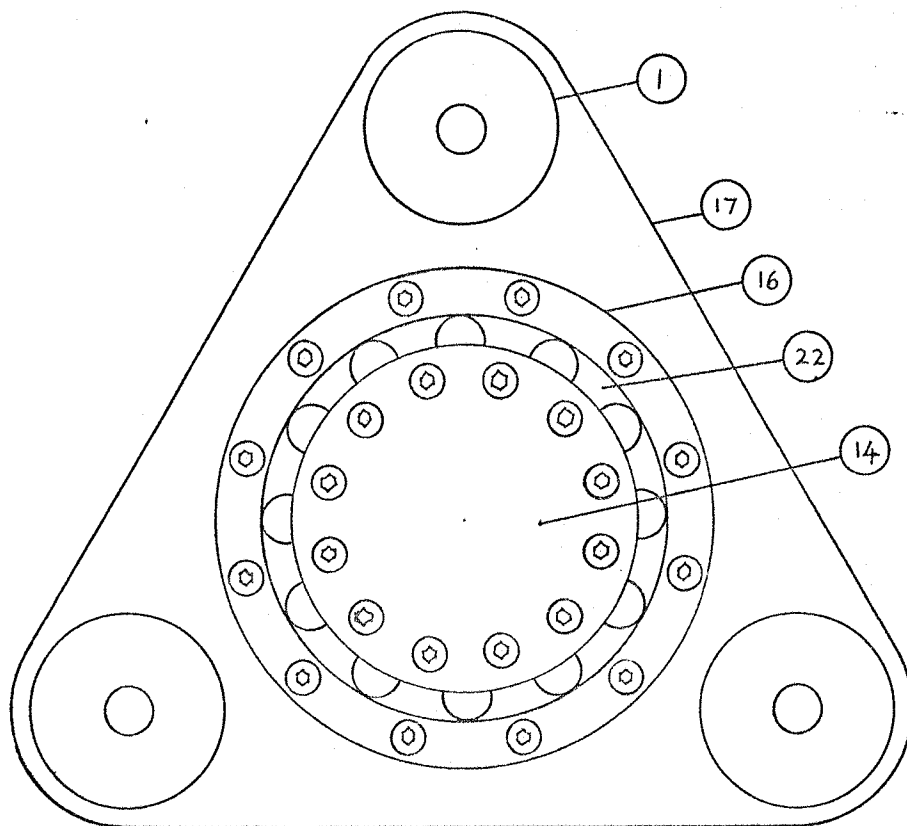
Fig.54

Fig.54 View looking down on the lower bearing plate
with the probe tripod and feet removed
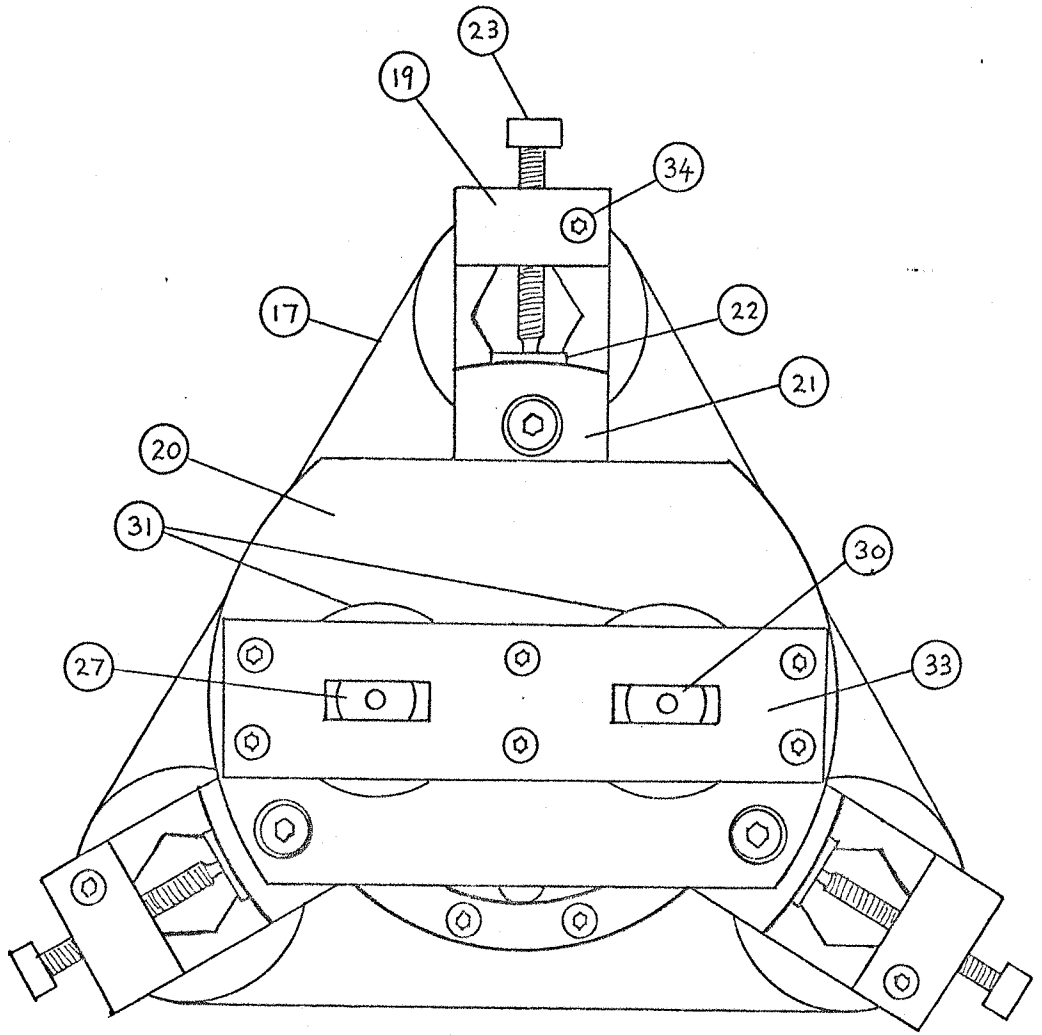
Fig.55

Fig.55   Plan view of thrust bearing rig
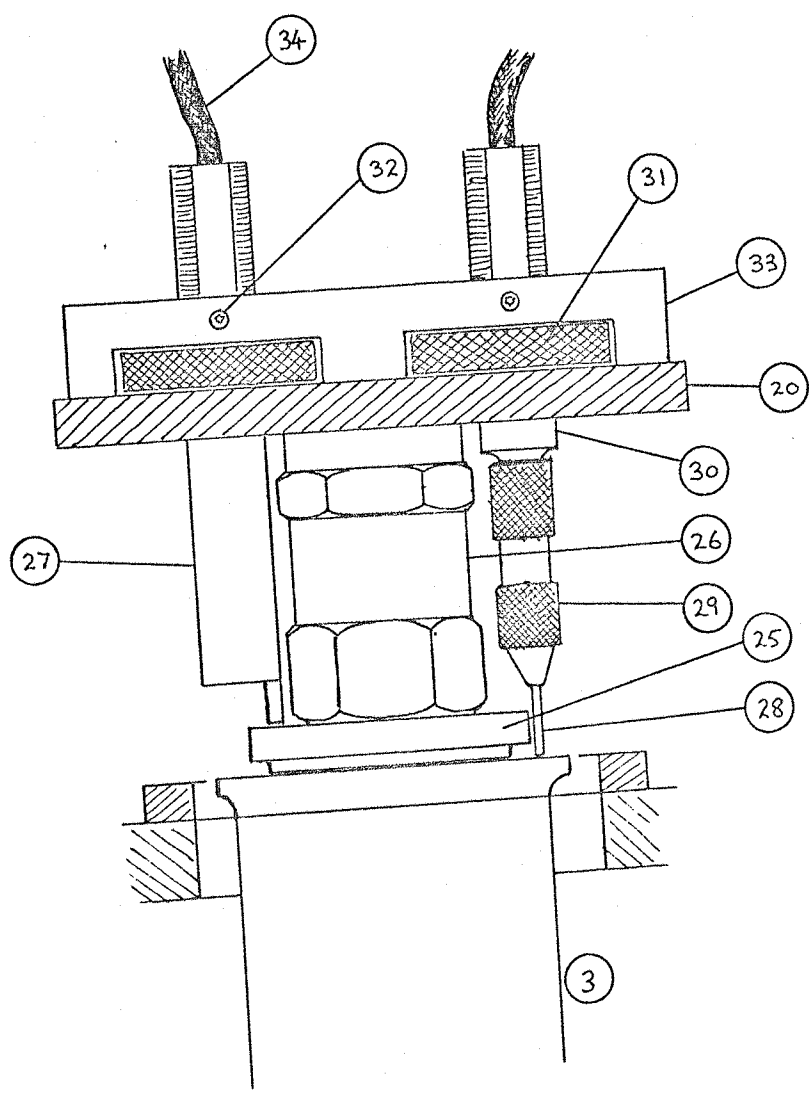
Fig.56

Fig.56 Scrap view of assembly carried by the probe tripod
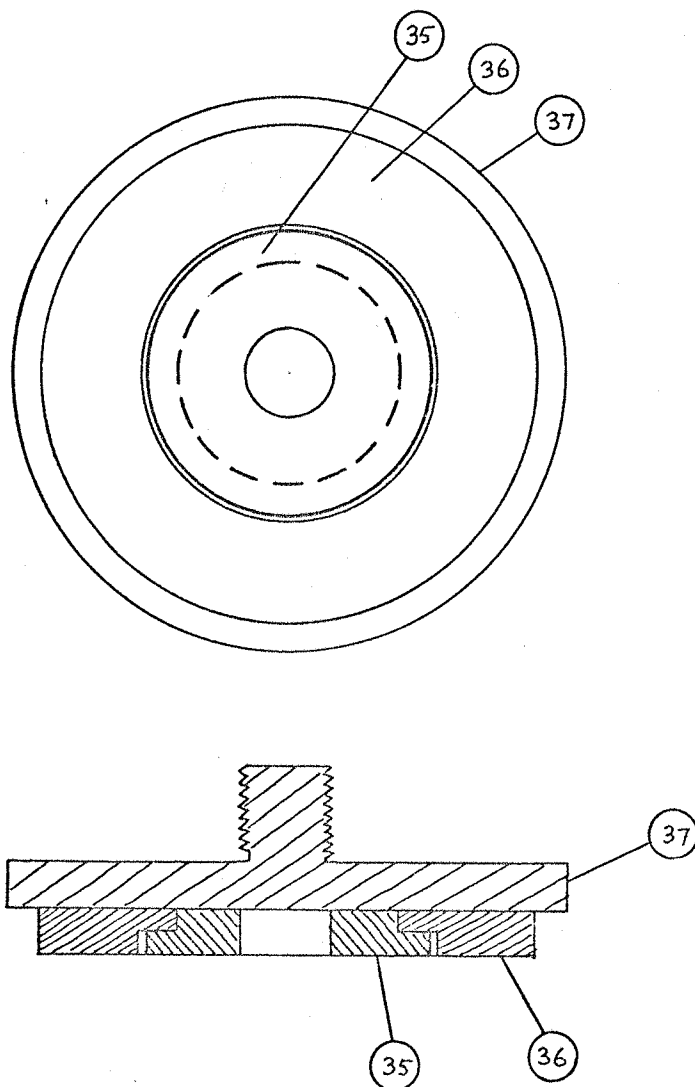
Fig.57

Fig.57 Upper bearing plate for investigating the effect of groove cross-section
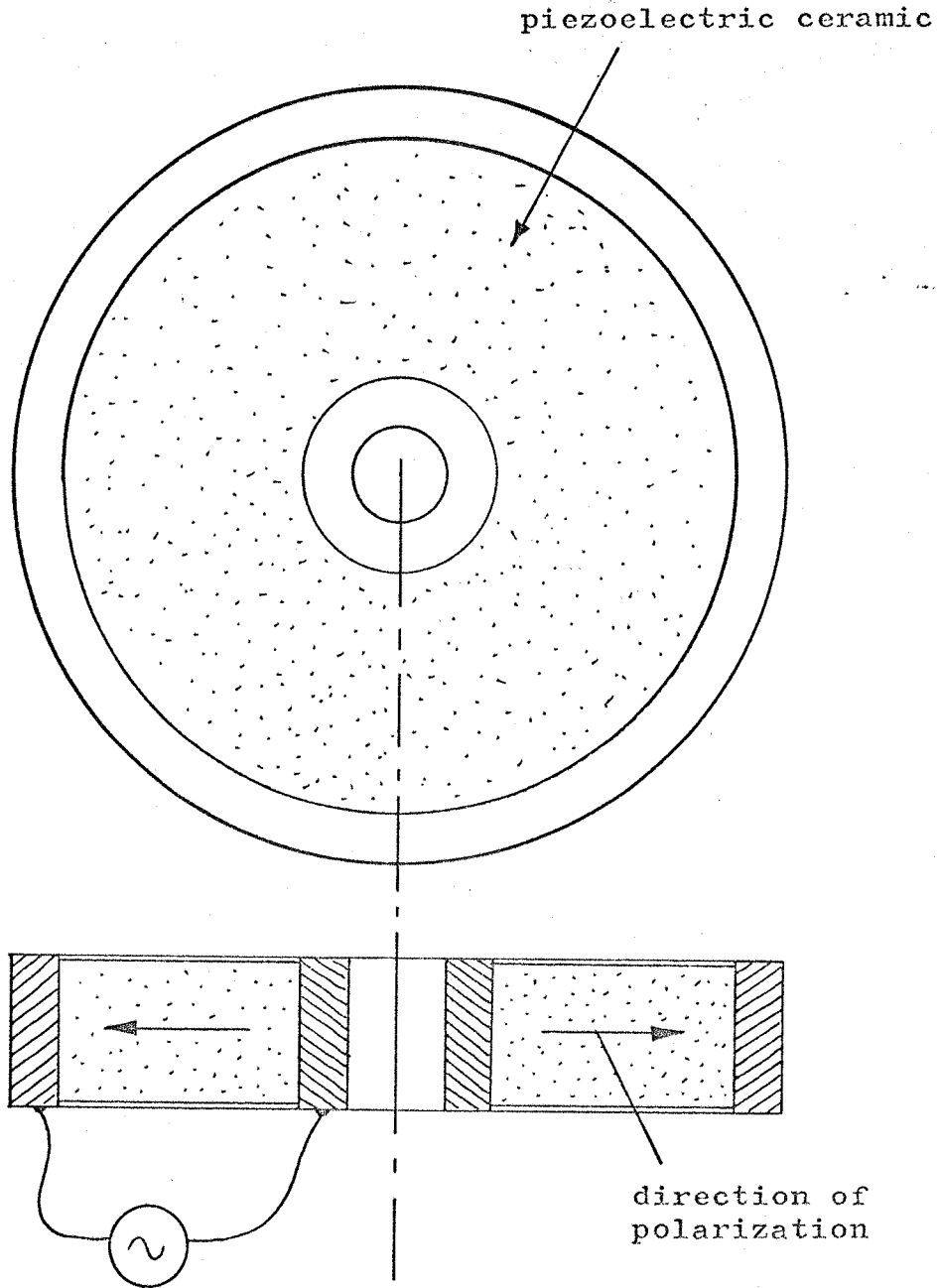
Fig.58

Fig.58   Piezoelectric transducer module
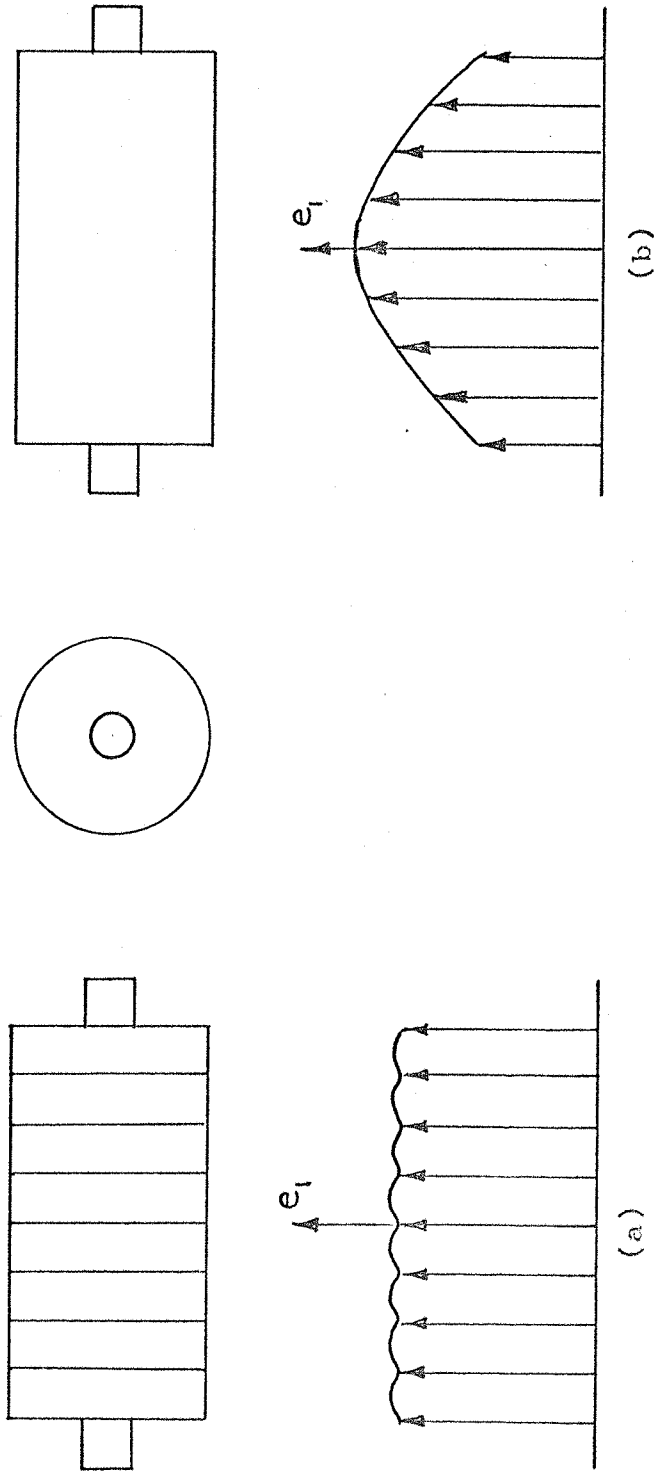
Fig.59

Fig.59 Typical excursion profiles in (a) segmented, and (b) unsegmented, cylindrical bearing transducers

Fig.60

platinum ink,
screen printed

tape of un-fired
piezoelectric material
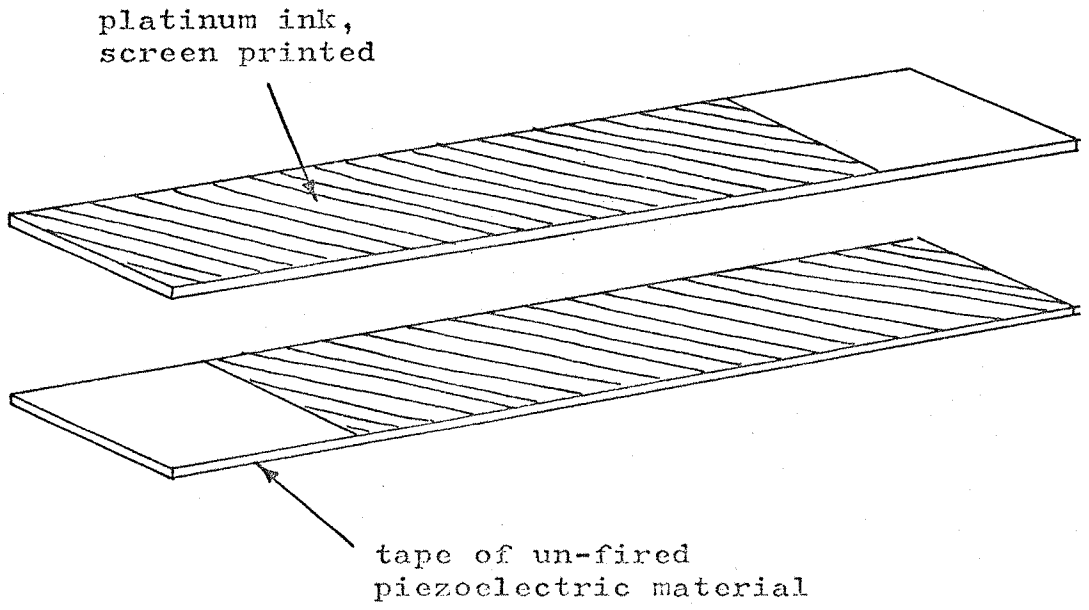
Fig.60   Piezoelectric tapes before coiling

Fig.61


metal sleeves

piezoelectric
double spiral
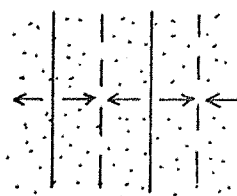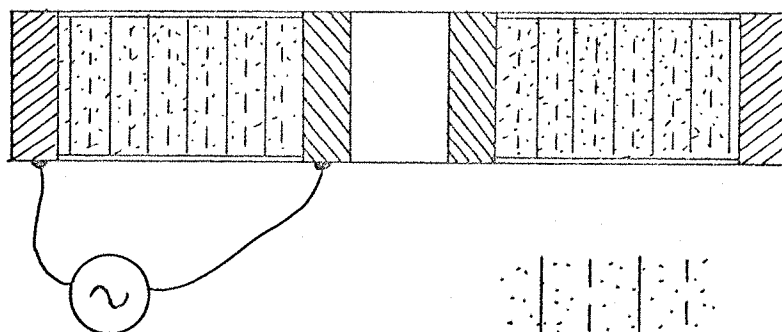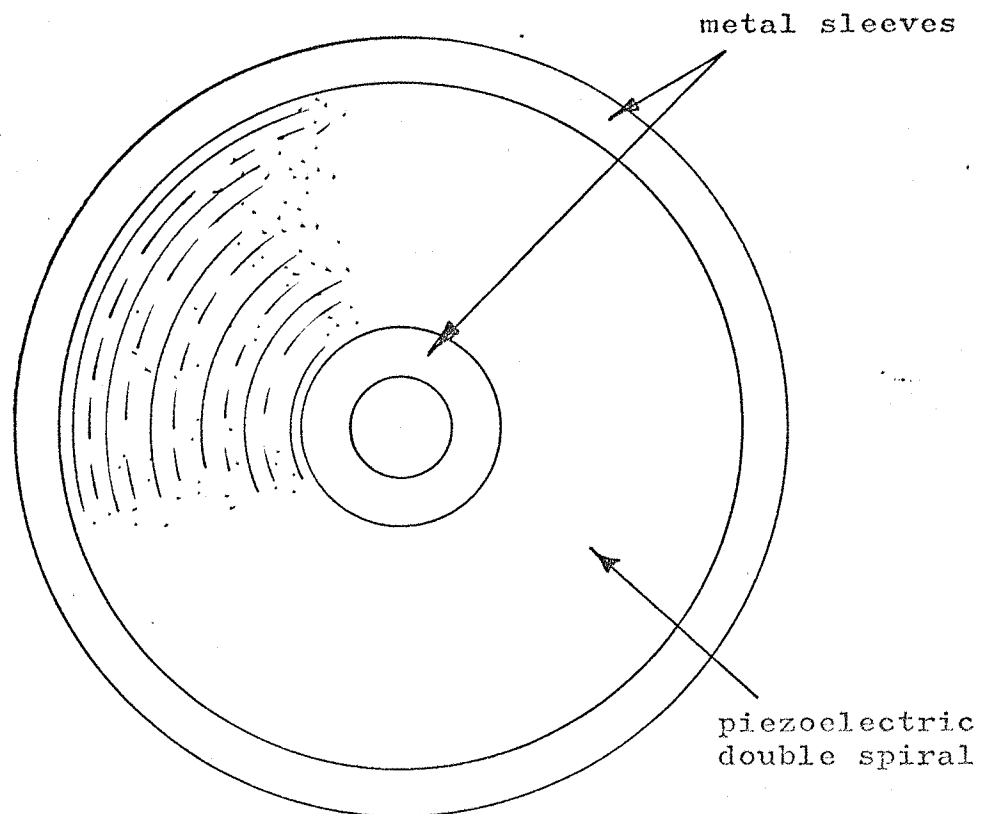
direction of polarization
within laminations

Fig.61   Transducer module with twin spiral laminations
of piezoelectric material

Fig.62

Fig.62   Plan view of journal bearing rig for static

stiffness measurements
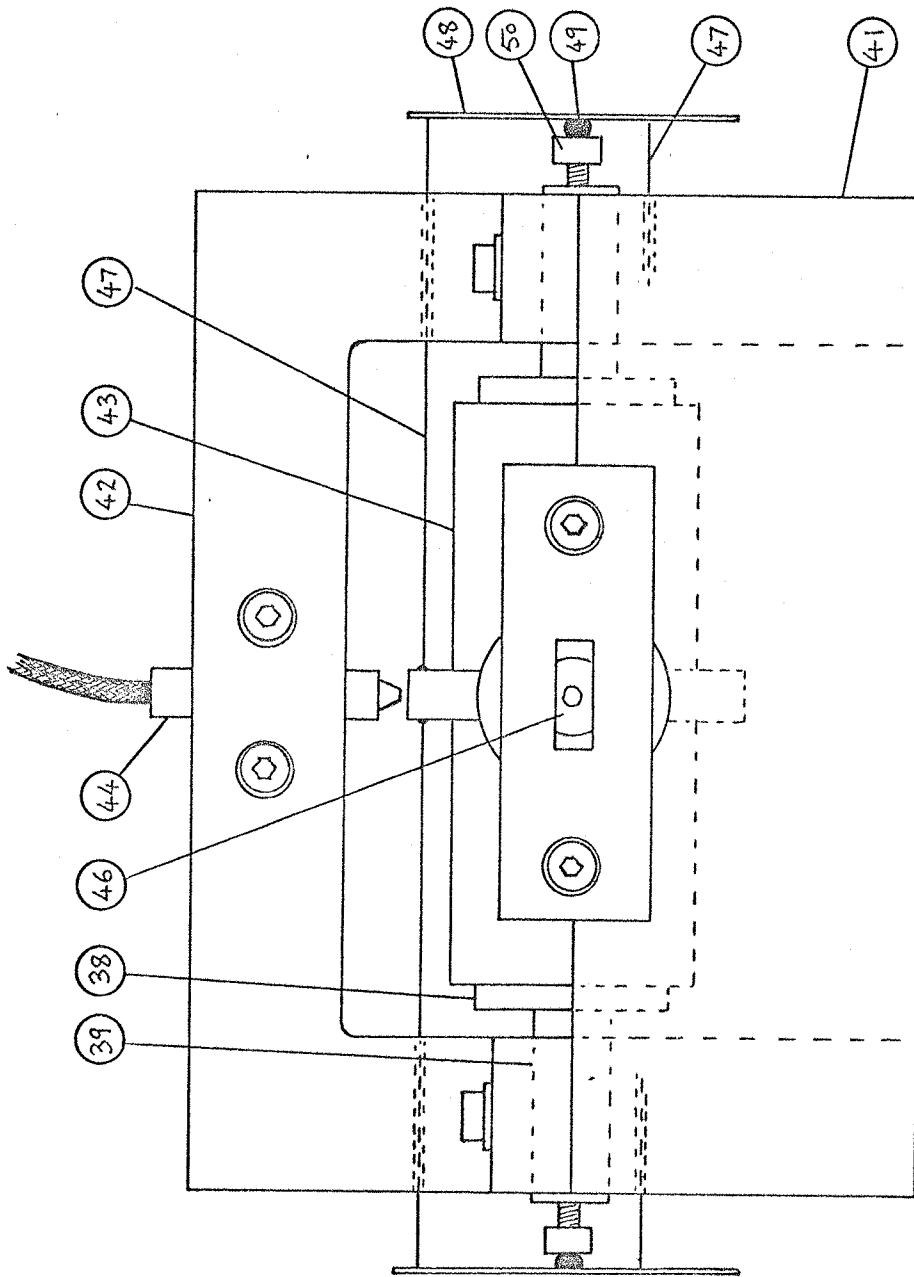
Fig.63   Front elevation of journal bearing rig for static stiffness measurements
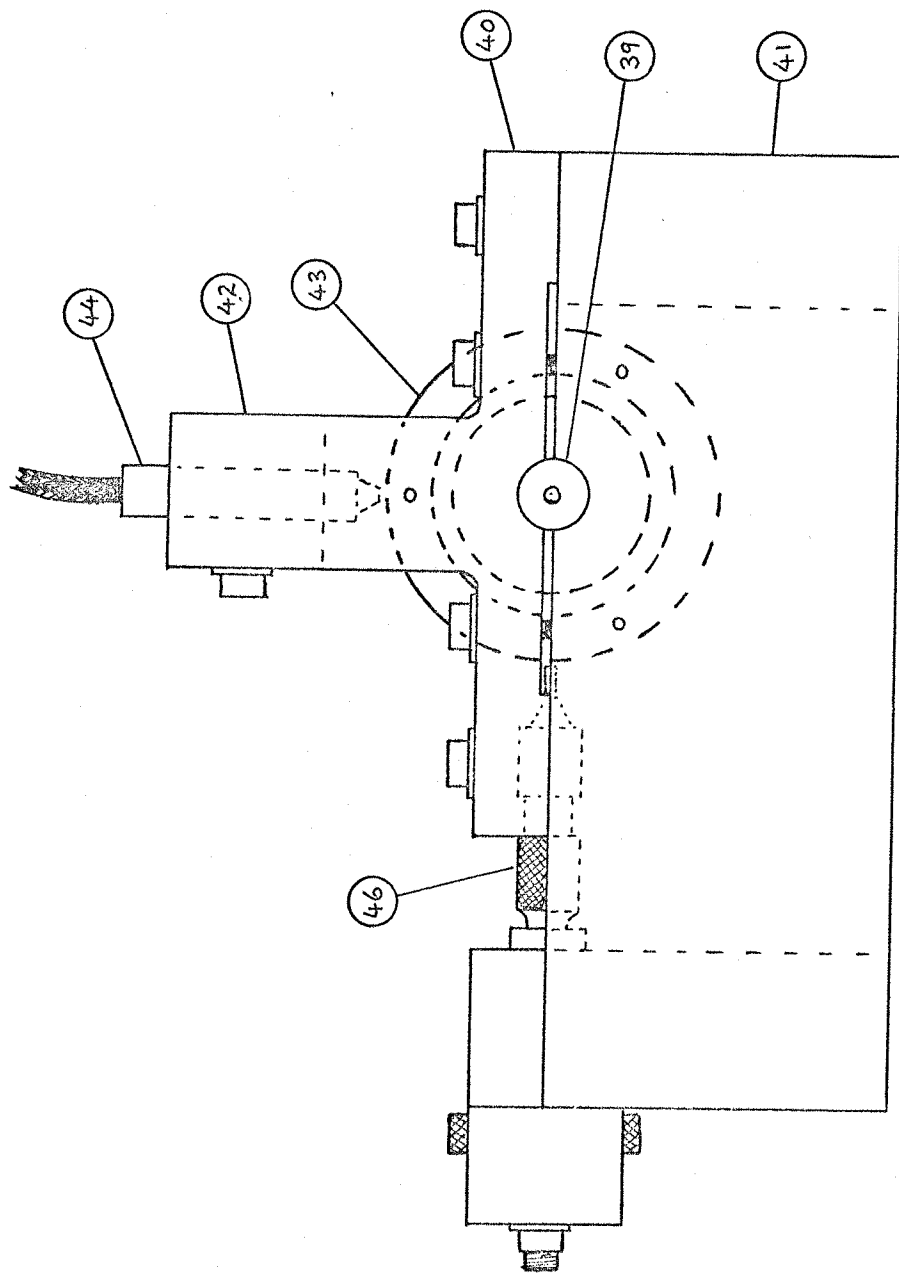
Fig.64   Side elevation of journal bearing rig

Fig.64